Food security and climate change:
Responses of rice with altered stomatal development to heat stress

By:

Lígia Tereza Bertolino

A thesis submitted in partial fulfilment of the requirements for the degree of
Doctor of Philosophy

The University of Sheffield
Faculty of Sciences
Department of Molecular Biology and Biotechnology

November 2020

<u>Acknowledgements</u>

Abstract

Rice is a major staple food in developing countries, but changes in climate are expected to have detrimental impacts on its future production. Regions where rice is cultivated are likely to be exposed to damaging elevated temperatures that, particularly during flowering, can result in sterility and substantial yield losses. This work investigated whether the manipulation of stomatal development could be a viable approach towards producing thermotolerant rice cultivars. More specifically, it was hypothesised that a targeted increase in stomatal density might enhance rice transpiration rates and evaporative cooling capacity, helping plants to overcome heat stress by reducing tissue temperatures. In addition, a local increase in stomatal density in floral organs could be of particular interest in improving heat tolerance over the sensitive flowering stage. Since little is known about the stomata on rice florets, a detailed investigation of the distribution and development of floral stomata was conducted. This study found that although the stomata on florets have a different morphology, they develop in a similar manner to leaves, following the same cell lineage transitions and being regulated by the same molecular signalling components. Altered stomatal densities were observed in florets of transgenic rice lines overexpressing either *OsEPFL9a* or *OsEPF1* (respectively a positive and a negative regulator of stomatal development in leaves), but these changes did not seem to have an impact on plant fertility. The characterization of *OsEPFL9a* overexpressing lines revealed that, although these plants had significant increases in leaf stomatal density in early vegetative stages and in floral organs, the increment in the number of stomata on flag leaves was not substantial. Under high temperature conditions during the flowering stage, OsEPFL9a-oe lines did not have an increased evaporative cooling response, and as consequence, showed similar yield losses to the control plants. Although more work is needed to fully understand the consequences of changing rice stomatal densities, the findings of this study suggest that altering stomatal development in rice leaves and florets through the overexpression of *OsEPFL9a* is not an effective approach to improve evaporative cooling and alleviate yield declines caused by heat stress. Finally, to begin to understand the function of the stomata on the floral organs of rice and the consequences of altering their development, an experiment was carried out to compare the transcriptomes of developing floral tissues from control and *OsEPF1* overexpressing plants, which produce very few floral stomata. This experiment revealed that differences in floret expression profile between rice lines were more pronounced when floral stomata

were maturing or recently matured, and that several biological processes might be affected by the manipulation of stomatal development, in particular, the expression patterns of genes with function in pollen development were significantly altered or delayed in plants with reduced stomatal density in floral organs.

Table of Contents

X

Chapter 1

General Introduction

Predicted changes in climate patterns due to global warming are likely to have negative impacts on global crop production and food security (Deryng et al., 2014; IPCC, 2014; Zhao et al., 2016). Agricultural ecosystems are highly vulnerable to fluctuations in environmental conditions, and as observed in past decades, increases in average temperatures have already caused significant yield losses for important cereal crops (Lobell et al., 2011; Lobell and Field, 2007). According to the Fifth Assessment Report (AR5) of the Intergovernmental Panel on Climate Change (IPCC), the Earth's mean surface temperature is projected to continue rising under various greenhouse gas emission scenarios, possibly reaching a 4.8 °C increase by 2100 (Figure 1.1). This forthcoming warming is expected to cause further and long lasting changes in the climate system, including shifts in precipitation patterns and increases in the frequency of extreme drought, floods and heat wave events (IPCC, 2014).
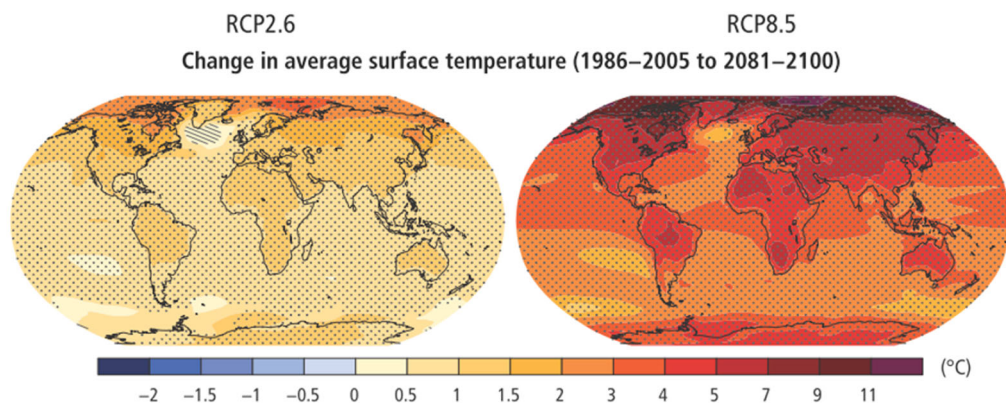
Figure 1.1. Change in average surface temperature based on multi-model projections for 2081-2100 relative to 1986-2005 under two of the Representative Concentration Pathways (RCPs) considered by the Intergovernmental Panel on Climate Change (IPCC). RPC2.6 (left) is representative of optimistic scenarios in the literature leading to very low levels of greenhouse gas concentration in the atmosphere by 2100. RPC8.5 (right) represents pessimistic scenarios leading to higher greenhouse gas concentration levels by 2100 (image reproduced from AR5, IPCC 2014). Colour scale represents the projected temperature increase in °C.

Rice is one of the crops that will be negatively impacted by the predicted increase in temperatures, raising concerns about food security (Lobell et al., 2008; Zhao et al., 2016, 2017). This cereal is considered one of the most important food crops in the world, being the staple food for more than 3 billion people (GRiSP, 2013). Rice is produced in an area of about 158 million ha, spread across at least 114 countries. The environmental

conditions of rice cultivation differ widely between locations, which include different altitudes in tropical, subtropical and temperate climates. Humidity conditions are also highly diverse, varying from very wet (e.g. areas in the Philippines and in the Myanmar's Arakan Coast) to arid environments (e.g. areas in Egypt and Pakistan). Rice growing ecosystems are in general classified according to the water source (irrigated or rainfed) and altitude (lowland or highland). Currently most of the global rice production (~75 %) is based on irrigated lowland systems (Figure 1.2), mainly located in warm and temperate regions of Asia, Africa, and Latin America (GRiSP, 2013; Mohanty, et al., 2013; Rao et al., 2017)

The optimal temperature conditions for rice cultivation may vary according to the variety, nonetheless, daytime temperatures above 33 °C are in general associated with reduced yields (Arshad et al., 2017). High night temperatures are also considered detrimental, with each 1 °C increase in minimum average temperature leading to productivity losses of about 10% (Peng et al., 2004). Although in most rice growing regions day temperatures are currently close to the optimal (27 °C to 32 °C day), they occasionally exceed the critical limit for appropriate plant development (Shah et al., 2011). With climate models projecting that 120 million ha of the rice agricultural areas will be susceptible to further high temperature episodes between 2071 and 2100 (Teixeira et al., 2013), the development of strategies to overcome the negative effects of heat stress in rice yields is an important concern for current crop science research.

Figure 1.2. Rice paddy fields in the Philippines. **(A)** Lowland irrigated area in Los Baños. **(B)** Upland rice terrace in Banaue. In paddy fields rice is grown under continuously flooded conditions.

1.1. The reproductive phase and heat stress

Plants exposed to above optimal temperatures undergo physiological and biochemical changes that can lead to irreversible damages to their development, limiting growth and productivity. For instance, high temperatures can increase the production of reactive oxygen species (ROS), change membrane fluidity, damage protein structures, reduce carbon assimilation, as well as cause the shortening of developmental phases (as reviewed in Shah et al., 2011; Wahid et al., 2007; Zinn et al., 2010). The severity and the extent of damage induced by these changes might vary substantially according to the growth stage at which plants are subjected to heat stress, in addition to the intensity and the duration of exposure. During the vegetative phase (Figure 1.3), rice plants can withstand daytime temperatures of ~35 °C without substantial negative impacts; however, exposure to temperatures beyond this limit often causes poor seedling growth, as well as reductions in plant tillering and height. At the reproductive stage of development, however, exposure to temperatures above 33 °C for short periods lead to severe spikelet infertility levels, directly affecting grain production. Likewise, plants experiencing equivalent temperatures during seed ripening stages may produce low quality grains, with reduced weight and high chalkiness (reviewed in Shah et al., 2011; Wassmann et al., 2009).
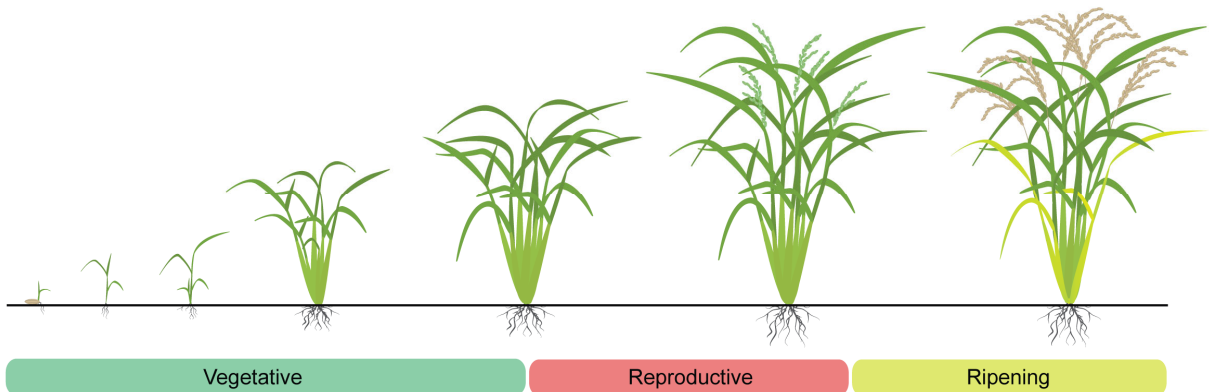
Figure 1.3. Representation of the growth phases of a rice plant. In summary, the vegetative phase starts with seedling development, includes the gradual emergence of leaves and an increase in the number of tillers. The reproductive phase comprises of panicle primordia initiation inside the flag leaf sheath, the progression of panicle development until emergence, flowering and fertilization. After flowers are fertilized, the ripening phase starts including the gradual filling and maturation of the grains.

In general, the reproductive phase is recognized as the most vulnerable to heat stress in rice, as well as in other cereals crops (Arshad et al., 2017; Barnabás et al., 2008; Jagadish, 2020; Shah et al., 2011; Wahid et al., 2007). This phase typically starts 55 to 85 days after germination and lasts approximately 45 days, depending on the rice variety. It

consists of the period from panicle development initiation until the start of grain development (Figure 1.3), comprising crucial processes for seed setting. The initiation of the panicle primordia coincides with the start of internode elongation and the ceasing of tillering. The panicle develops at the uppermost node within a tiller, inside the developing flag leaf sheath. As its primordium differentiates, an immature panicle (~ 2 mm) becomes visible to the naked eye, anticipating the start of the booting stage of the reproductive development. Booting lasts approximately 15 to 20 days. It comprises further differentiation of the panicle, the progressive bulging of the leaf sheath and a rapid internode elongation. This stage is highly nutrient demanding and includes important events in the development of the male and female gametes, such as meiosis (GRiSP, 2013; Hardke, 2018; Saichuk, 2014).

As the panicle development continues, the emergence of the flag leaf occurs, subsequently, the final internode elongation causes the emergence (or heading) of the mature panicle from inside the flag leaf sheath. Panicle heading progresses gradually, being followed by flowering (or anthesis), which refers to a series of events between the opening and closing of rice spikelets. As the top part of panicles emerge, flowering starts in individual spikelets positioned at this portion. First, palea and lemma start to open and stamen filaments to elongate. As the spikelets opening continues, the tip of the stigma becomes visible and the filaments elongate further, causing anthers to emerge from inside the spikelets. Subsequently, palea and lemma close, leaving the anthers outside. This cycle lasts around 1 to 2.5 hours, taking approximately 7 days to all panicles on a plant completely flower. Anther dehiscence typically occurs shortly before anthesis or just after the spikelets start to open. Therefore, pollen falls directly onto the stigma, leading to a high self-pollination frequency. The viability of rice pollen grains declines rapidly after leaving the anthers, while pistils can still be fertilized from 3 to 7 days after flowering takes place. Once stigma is pollinated, pollen germination starts, and the pollen tube grows towards the ovule. Double fertilization is generally completed up to 6 hours after pollination, then, the ovary will develop into the rice grain (GRiSP, 2013; Hardke, 2018; Saichuk, 2014).

From all the processes taking place during rice reproductive development, flowering and, to a lesser extent, microsporogenesis (during pollen development) are considered the most sensitive to heat stress (Figure 1.4). Flowering takes place over the hottest period of the day (around noon), when panicles are already subjected to the environment at the top part of the plants (after heading). During this process, the exposure to temperatures of ~33 °C for a period as short as 1 hour can lead to reductions in seed set, which become

more severe under higher temperatures (Jagadish et al., 2007). High levels of sterility after heat stress during flowering are primarily associated with poor anther dehiscence and pollination. It has been suggested that high temperatures cause restrictions on the swelling of the pollen grains, inhibiting anther septum rupture and proper anther dehiscence, consequently leading to insufficient deposition of pollen on stigmas (Jagadish et al., 2010; Matsui, 1999; Matsui et al., 2000; Satake and Yoshida, 1978). In addition, heat stress during the flowering days also seems to limit pollen germination, pollen tube growth and stigma receptivity (Shi et al., 2018; Wu et al., 2019b; Zhang et al., 2018).
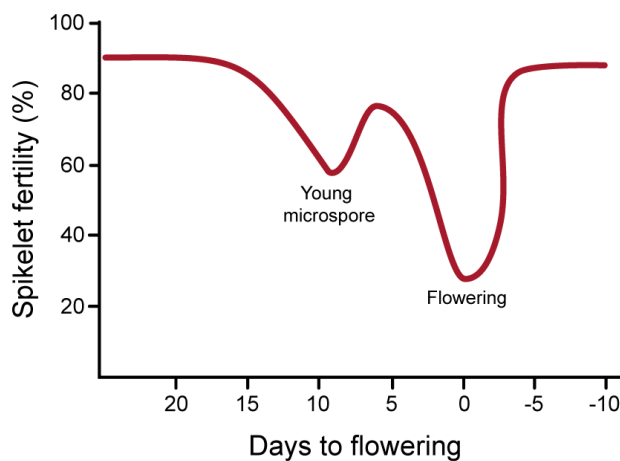
Figure 1.4. Spikelet fertility trend in an Indica rice variety subjected to 35 °C day temperature for 8 hours during 5 consecutive days, at different periods of the reproductive phase of plant life cycle. Figure redrawn with publisher's permission, Satake and Yoshida (1978). X-axis shows number of days prior to flowering from the middle date of temperature treatment. Rice plants were more sensitive to the treatment at flowering, and nine days before flowering (around the microsporogenesis stage).

The second most affected process, microsporogenesis, occurs within the anthers during booting. In summary, during the initiation of the stamen primordia, the mitotic division of archesporial cells gives origin to parietal cells (that will form the different anther layers) and to sporogenous cells (which will develop into microspores, later producing mature pollen). Microsporogenesis is the initial phase in pollen development. During this process the diploid sporogenous cells differentiate into pollen mother cells, subsequently dividing by meiosis to produce tetrads of haploid microspores. The microspore tetrads are held together by a callose wall, which is then degraded, releasing the individual microspores into the anther locule. After microsporogenesis, the microgametogenesis phase of pollen development starts. The free microspores go through two rounds of mitotic division and the pollen wall synthesis continues to form mature pollen (Gómez et al., 2015; Wilson and Zhang, 2009). Exposure to above optimum temperatures during the formation of the microspores can cause severe decreases in yield (Figure 1.4), which have been associated with a decline in the ability of pollen grains to adhere to the stigma and germinate, as well as, lower pollen viability (Endo et al., 2009; Jagadish et al., 2015; Satake and Yoshida, 1978). Other stages of the reproductive

development are also vulnerable, in panicle initiation, for instance, heat stress can impact on the differentiation of secondary branches, reducing the number of spikelets per panicle (Wu et al., 2019b).

1.2. Thermotolerance and evaporative cooling in rice

Heat tolerance refers to the ability of a plant to endure above optimal temperatures and produce economic yield, despite the experienced adverse conditions (Wahid et al., 2007). In rice, as in other crop species, the degree of heat tolerance differs greatly between varieties (Cheabu et al., 2018; Jagadish et al., 2010; Matsui and Osama, 2002; Sailaja et al., 2015; Wu et al., 2019a). This can be illustrated by the study of Jagadish et al (2010), that investigated the fertility of plants after exposure to 38 °C during flowering. Whilst the japonica variety Moroberekan had only 18% of fertility after stress treatment, the indica cultivar IR64 displayed 48% fertility, and the aus cultivar N22 78%. Such divergent responses may be associated to differences in adaptative mechanisms, for instance the accumulation of heat shock proteins (Jagadish et al., 2010; Sailaja et al., 2015), greater membrane thermostability (Sailaja et al., 2015) and longer basal pore length in anther dehiscence (Matsui et al., 2007; Matsui and Hasegawa, 2019) have been linked to superior performance of some rice cultivars under heat stress.

Additionally, mechanisms associated with heat escape or avoidance (such as early-morning flowering and tissue temperature regulation) can also be effective to overcome heat damage (Jagadish, 2020; Jagadish et al., 2015; Julia and Dingkuhn, 2012, 2013; Matsui et al., 2007). In certain regions, an efficient evaporative cooling process can help rice fields to remain productive, even after experiencing above optimum temperatures during the reproductive development. This avoidance mechanism is driven by an increase in plant transpiration rates. As water evaporates from the leaf surface it promotes the loss of heat, helping to maintain plant tissue temperatures below damaging thresholds, and avoiding heat stress.

The transpiration capacity and the ability to substantially increase transpiration rates under high temperatures seem to differ across different genotypes (Sailaja et al., 2015; Yang et al., 2020), additionally, the levels of evaporative cooling are closely related to the ambient relative humidity (RH). As transpiration from the plant canopy is driven by the difference in water vapour concentration between the leaf air spaces and the atmosphere surrounding the plant, the atmospheric vapour pressure deficit (VPD, a combined function of temperature and RH, representing the atmospheric desiccation

strength) influences the rate of water loss from plant surfaces. Transpiration typically increases under high VPD conditions, therefore under environments where high temperature is coupled with low humidity, evaporative cooling can be strongly intensified, as long as sufficient water is also provided (Grossiord et al., 2020; Wassmann et al., 2009). Rice production in hot and dry regions/seasons is, therefore, facilitated by an effective evapotranspiration (Jagadish et al., 2015; Wassmann et al., 2009). This effect was studied in Riverina (Australia), where at times temperatures can be extremely hot (~ 40 °C) and humidity very low (~ 20%). Matsui et al. (2007) showed that in this region the temperature of rice panicles was maintained between 4°C and 6.8°C lower than the ambient air in paddy fields, avoiding heat damage. A similar response was observed for different rice cultivars grown in the hot and dry (~ 20% minimum RH) season in Senegal. Under these conditions, an effective evaporative cooling process allow panicles to reduce tissue temperatures to up to 9.5 °C lower than air temperature. In contrast, under the hot and humid (~ 85% RH) conditions in the Philippines, the same rice cultivars did not show a successful heat avoidance response (Julia and Dingkuhn, 2013). The influence of relative humidity in this avoidance mechanism is also supported by studies under controlled conditions; Weerakoon et al (2008) showed that, for a group of Indica and Japonica rice cultivars exposed to 34 °C and 36 °C, panicle temperature and heat induced sterility are substantially reduced under 60% RH in comparison to 85% RH.

Although at regular temperature conditions (~30 °C) rice plants are normally highly productive under high RH, the low VPD in very humid areas or seasons can be a disadvantage for the use of evaporative cooling as an avoidance mechanism. In such environments, the development/selection of varieties with other heat tolerance traits, in addition to changes in cropping management, will be essential to maintain yields as temperature rises. In irrigated areas in the Philippines, for example, farmers already adjust the planting calendar to prevent heat stress at the reproductive phase, nonetheless, in rainfed areas this might not be possible, due to the rainfall patterns and the risk of water shortage (Manigbas et al., 2014). In irrigated warm areas that experience low to moderate RH, however, improving cultivars evapotranspiration responses can be one of the strategies used to reduce heat damage.

1.3. Water loss from leaves is regulated by stomatal pores

Although plant transpiration relies on the water vapour gradient between the leaf air spaces and the atmosphere, the movement of water from the leaf to the atmosphere is also

dependent on the diffusional resistances of the transpiration pathway. Because the waxy cuticle that covers leaf epidermis is an efficient barrier to water loss, most of the water that is pulled from the xylem to the mesophyll cell walls evaporates into the mesophyll airspaces and moves out the leaf via a low resistance pathway offered by stomatal pores (Figure 1.5), later diffusing through the boundary layer (a thin film of still air at the leaf surface) to reach the atmosphere (Taiz and Zeiger, 2010).
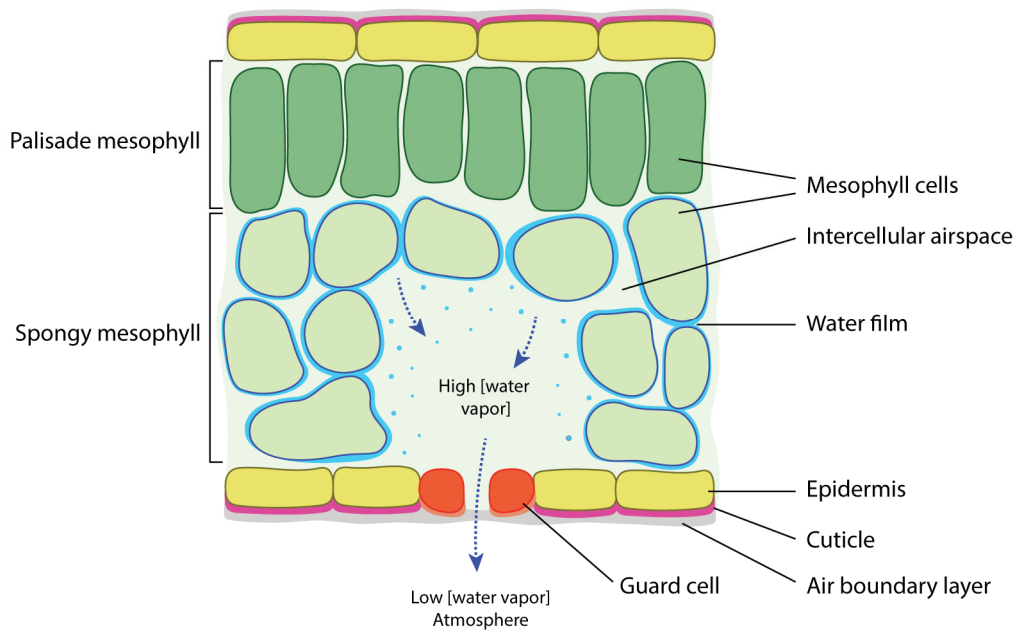
Figure 1.5. Water diffusion from mesophyll airspaces to the atmosphere. Dotted arrows show the water vapour path. Water evaporates from the surface of the mesophyll cells, then water vapour diffuses through the leaf airspaces, leaving the leaf through the stomatal pore and crossing the boundary layer of still air to reach the atmosphere.

Stomatal pores are present in the epidermis of most plants. These structures are formed by a pair of specialized guard cells that surround a microscopic pore (Figure 1.6), and in some species, such as rice, also includes subsidiary cells (Hetherington and Woodward, 2003). By providing a pathway to the mesophyll, stomata mediate the exchange of gases between the leaf interior and the atmosphere, playing an important role in regulating water vapour loss for transpiration and also CO_2 uptake for photosynthesis. The diffusion of gases through stomata, termed stomatal conductance (g_s), can be regulated by adjustments in guard cell turgor pressure leading to changes in guard cell shape and, consequently, in the degree of openness (Figure 1.7) (Franks and Farquhar, 2001, 2007; Lawson and Matthews, 2020). The osmoregulation of the guard cells is a dynamic process and changes can rapidly be triggered by multiple internal and external stimuli. This allows a fine regulation of the trade-off between water use and carbon gain in response to

environmental signals, including changes in temperature, light intensity, concentration of atmospheric CO_2, soil moisture and air relative humidity (Assmann and Jegla, 2016; Farquhar and Sharkey, 1982; Grossiord et al., 2020; Kostaki et al., 2020; Lawson and Matthews, 2020). Increases in temperature are usually associated with increases in stomatal apertures and consequently in conductance rates, although this response is also dependent on the interaction with other environmental factors, such as VPD and water availability (Kostaki et al., 2020; Urban et al., 2017). While transpiration rates are typically intensified with VPD increases, stomatal aperture tends to decrease, minimizing water loss. However, sensitivity to VPD changes is variable and can differ between species, cultivars or even within leaves of the same plant (Grossiord et al., 2020; Streck, 2003; Urban, et al., 2017).
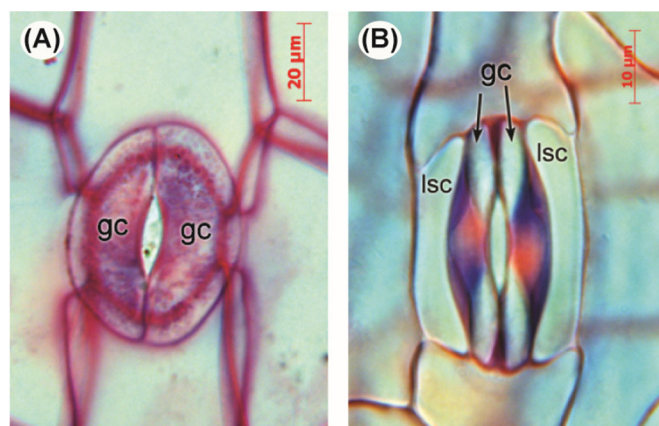
Figure 1.6. Stomata on the epidermis of **(A)** *Zygadenus venenosus* (Liliales), comprising a pair of guard cells (gc) and of **(B)** *Flagellaria indica* (Poales), comprising a pair of guard cells (gc) and lateral subsidiary cells (lsc). Reproduced with publisher's permission, (Rudall et al., 2017).
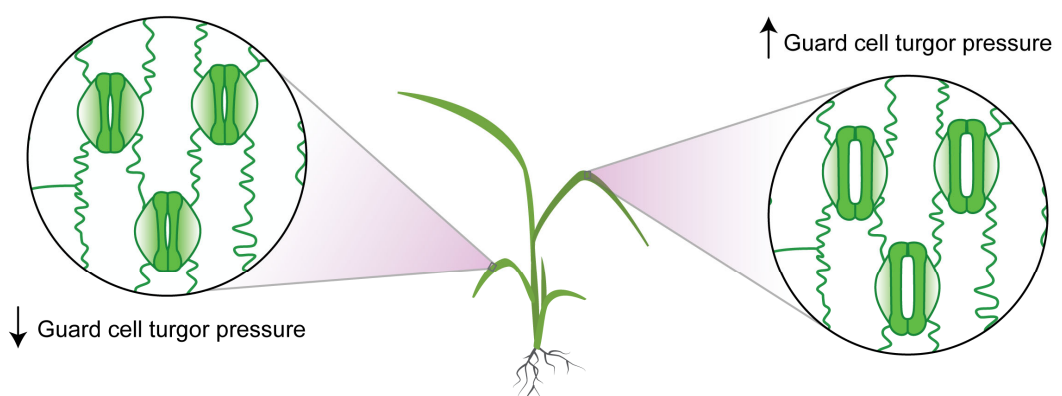
Figure 1.7. Stomatal conductance rates can be regulated by adjustments in the size of stomatal pore apertures. Changes in guard cell turgor pressure alter the shape of guard cells, leading to increases in the degree of stomatal opening (higher turgor pressure) or decreases in pore aperture (lower turgor pressure). Diagram represents stomata on the epidermis of rice plants.

Moreover, the magnitude of the dynamic adjustments in stomatal conductance is constrained by developmental pathways that control the number and the size of stomata formed in the leaf epidermis. These anatomical traits determine the leaf maximum stomatal conductance (g_{smax}), which is the theoretical maximum g_s level in a state where all stomata are fully open (Dow et al., 2014a; Franks and Beerling, 2009). Despite gas exchange rates being normally much lower than the theoretical maximum capacity, actual g_s positively correlates with its estimated g_{smax}. Indeed, stomata are thought to operate in a turgor pressure range that provides optimal sensibility of guard cells responses, at least under typical environmental conditions (Dow and Bergmann, 2014; Franks et al., 2015). Therefore, increases in g_{smax} allow plants to adjust their operating gas exchange range while maintaining optimum control of stomatal aperture (Figure 1.8). Although stomatal traits are not the only factor influencing leaf gas exchange, changes to stomatal density and size can impact on plant carbon assimilation and water use (reviewed in Bertolino et al., 2019; Dow and Bergmann, 2014; Harrison et al., 2020), making stomatal development an interesting target in order to manipulate transpiration rates and maximize plant evaporative cooling capacity.
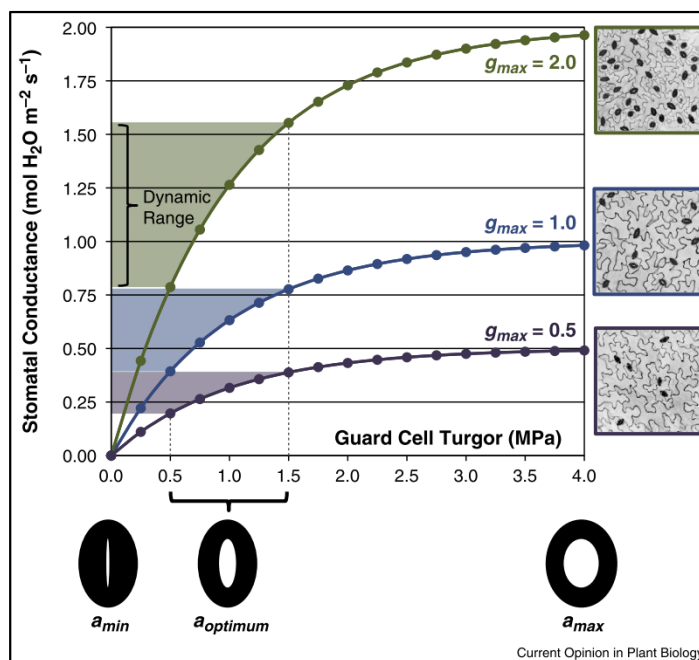
Figure 1.8. Maximum stomatal conductance (g_{max}) impacts on optimum operating g_s (figure reproduced with publisher's permission, Dow and Bergmann, 2014). Stomata tend to operate in a range where changes in turgor pressure have an efficient control of stomatal aperture ($a_{optimum}$, optimum turgor pressure range), therefore, developmental changes in g_{max} can alter the dynamic range of g_s while maintaining optimum stomatal response.

Adjustments in the density and/or size of stomata have been reported in plastic developmental responses to changes in the environment and also during evolution, with a negative correlation between these stomatal traits being often observed (Casson and Gray, 2008; de Boer et al., 2016; Dilcher et al., 2000; Dittberner et al., 2018; Fanourakis et al., 2015; Franks and Beerling, 2009; Lake et al., 2001; Sun et al., 2014; Woodward, 1987). Evolutionary adaptations towards higher g_{smax} in Angiosperms seem to be closely linked to increases in stomatal density and decreases in stomatal size, alongside increases in vein density (de Boer et al., 2016; Franks and Beerling, 2009). This relationship is believed to have conferred improved water movement and operational gas exchange ranges during the evolution of angiosperms, while minimizing the leaf space allocated for stomata (de Boer et al., 2012; McElwain et al., 2016). There also appear to be constraints associated with how stomata are distributed in the epidermis. The clustering of stomatal pores, for example, can be detrimental to stomatal functioning by either impairing the control of guard cell movement or by creating interference between diffusion shells (Dow et al., 2014b; Franks and Casson, 2014; Harrison et al., 2020).

Changes in stomatal density and size associated with developmental responses to changes in environment can be variable, suggesting a species-specific response in g_{smax} adjustments in response to particular abiotic factors. For example, Arabidopsis plants grown under high temperature display decreases in stomatal density without alterations in stomatal size. Nonetheless, these plants have an improved evaporative cooling in comparison to plants grown under normal temperature conditions, which is most likely related to changes in plant architecture observed under high temperature growth, promoting better water diffusion rates (Crawford et al., 2012). On the other hand, rice IR64 plants grown under high temperature invested in increasing g_{smax} by increasing stomatal density without significant changes in stomatal size (Caine et al., 2019).

1.4. Stomatal development – from Arabidopsis to grasses

Although little is known about the genetic mechanisms controlling stomatal size, significant advances have been made in understanding the molecular pathways regulating stomatal patterning and density (reviewed in Buckley et al., 2019; McKown and Bergmann, 2020; Zoulias et al., 2018). Most of this knowledge is derived from research on the eudicot *Arabidopsis thaliana*, nonetheless, recent studies have begun to also unravel the genetic pathways underlying stomatal differentiation in monocot grass species

(Lu et al., 2019; Raissig et al., 2016, 2017; Wu et al., 2019c; Yin et al., 2017), paving the way for the manipulation of stomatal traits in important cereal crops.

Grasses show substantial differences in stomatal morphology and patterning to those of eudicots (Nunes et al., 2019; Rudall et al., 2017; Stebbins and Shah, 1960). In Arabidopsis, the stomatal complexes are formed by a pair of kidney-shaped guard cells. These structures have a dispersed distribution, with heterogenous orientation on the leaf epidermis. Their development occurs in a proximal-distal gradient, and although the stomatal lineage is primarily initiated at the base of the leaf, stomatal development progresses in a scattered manner, and cells at different developmental stages can be observed across the epidermis (summarized in Figure 1.9 A-B, reviewed in Buckley et al., 2019; Pillitteri and Dong, 2013; Zoulias et al., 2018). In contrast, in rice and other grasses, stomata are formed by a pair of dumbbell-shaped guard cells, flanked by a pair of subsidiary cells. These stomatal complexes are evenly distributed into cell rows organized longitudinally along the leaf, adjacent to leaf veins. Stomatal development in grasses also occurs in a proximal-distal mode; however, there is a more noticeable developmental gradient with earlier stages typically observed basally, followed by a longitudinal expansion and differentiation of cells towards the tip of the leaf (summarized in Figure 1.10, reviewed in Hepworth et al., 2018; McKown and Bergmann, 2020; Nunes et al., 2019).

(A)

(B)
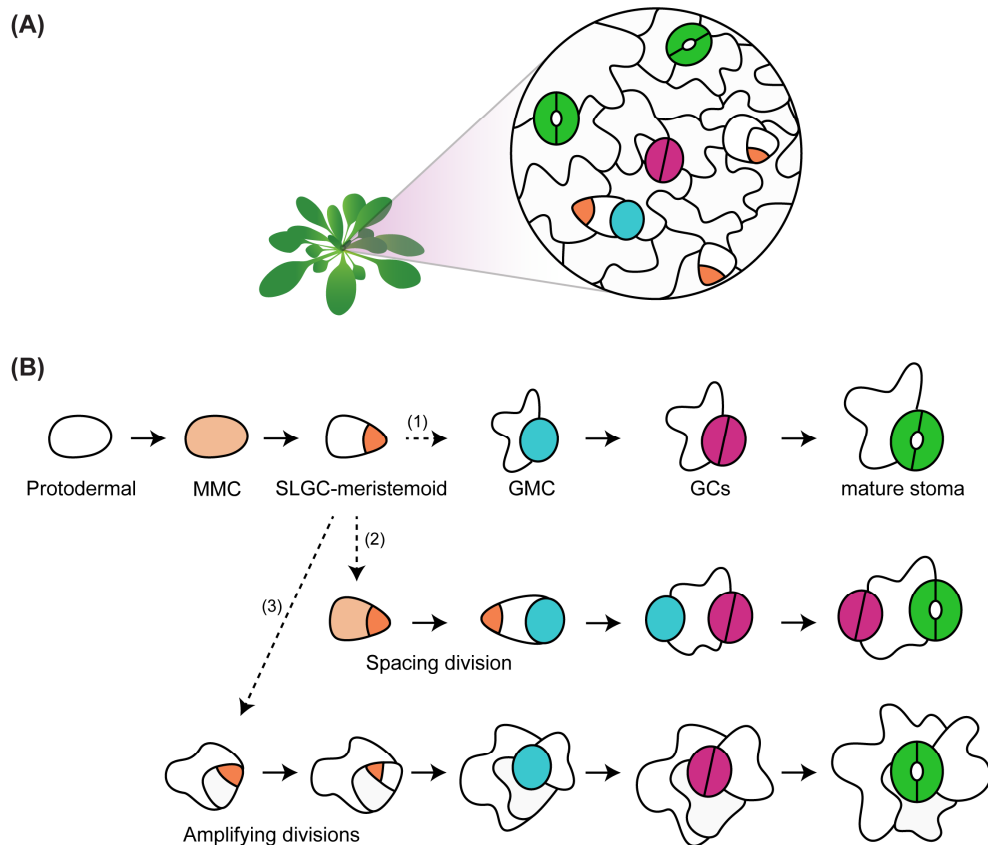
Figure 1.9. Stomatal development in Arabidopsis. **(A)** The stomatal cell lineage is initiated in dispersed epidermal cells of new developing leaves, producing stomatal complexes with irregular orientation. **(B)** To produce mature stomata a series of cell divisions and successive cell-state transitions occur. In the model species *Arabidopsis thaliana*, stomatal development is initiated by a protodermal cell that differentiates into a meristemoid mother cell (MMC, light orange). The MMC undergoes an asymmetric entry division, forming a small meristemoid (orange) and a larger cell, known as a stomatal lineage ground cell (SLGC). The meristemoid and the SLGC have distinct behaviours and can follow multiple fates (dotted arrows 1-3). The SLGC can directly differentiate into a pavement cell (arrow 1); alternatively, it might undergo an asymmetric spacing division to produce a satellite meristemoid (arrow 2), which will be separated from the first meristemoid by a pavement cell, ensuring that future stomata have at least one cell space from one another. Meanwhile, the meristemoid might directly become a rounded guard mother cell (GMC, arrow 1), or undergo amplifying divisions (arrow 3), producing more SLGCs. After the differentiation into a GMC, a symmetrical division produces two precursor guard cells (GCs, pink) that will undergo a final differentiation, producing a mature stoma (green) (reviewed in Buckley et al., 2019; McKown and Bergmann, 2020; Pillitteri and Dong, 2013; Qu et al., 2017; Zoulias et al., 2018).

13
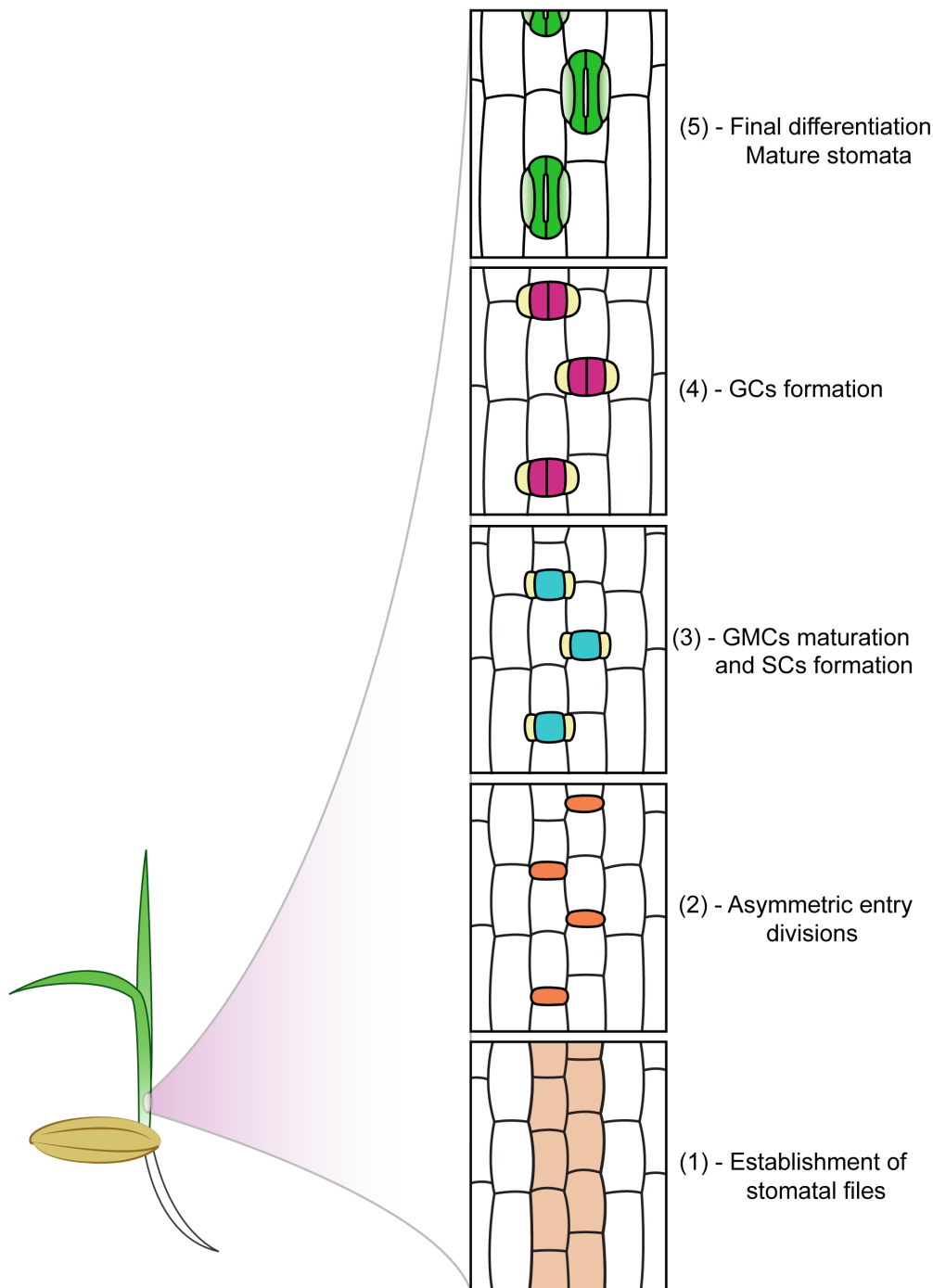
Figure 1.10. Stomatal development in grasses. The development of grass stomata is restricted to the base of the next developing leaves and follows a proximal-distal gradient through the following stages: **(1)** Some cell rows adjacent to veins acquire the capacity to develop stomata (light orange) and start to divide more rapidly than the adjacent rows. **(2)** The stomatal lineage is initiated through the asymmetric division of protodermal cells in the stomatal rows, originating a larger cell and a small (orange) cell, that is not capable of self-renewing. **(3)** The larger daughter will differentiate into a pavement cell, while the smaller cell expands and differentiates into a guard mother cell (GMC, blue) fate. The GMC induces the transition of a pair of lateral neighbour cells into subsidiary mother cells, which then undergo a longitudinal asymmetric division to produce subsidiary cells (SCs, in yellow). **(4)** Subsequently, the GMC divides symmetrically to form two guard cell (GC, pink) precursors, and **(5)** the four-celled complex expands and differentiates to produce a mature stomatal complex (green) (reviewed in Buckley et al., 2019; McKown and Bergmann, 2020; Nunes et al., 2019).

Despite the differences in stomatal morphology and development, recent findings in Brachypodium, rice, and maize demonstrate that several components of the molecular pathway regulating stomatal development are shared between grasses and Arabidopsis (Liu et al., 2009; Lu et al., 2019; Raissig et al., 2016, 2017; Wu et al., 2019c). Indeed, sequence analyses suggest that the core regulators of stomatal development are highly conserved across land plants (Chater et al., 2017; Qu et al., 2017). Five basic helix-loop-helix (bHLH) transcription factors, named SPEECHLESS (SPCH), MUTE, FAMA, SCREAM2 (SCRM2) and ICE1 function at different sequential stages of Arabidopsis stomatal development, controlling the major cell fate transitions from entry to the stomatal lineage to final differentiation of stomatal complexes. In short, AtSPCH promotes the differentiation of protodermal cells into MMCs and their asymmetric entry divisions. Additionally, AtSCPH drives meristemoid amplifying divisions. AtMUTE is then required to terminate meristemoid divisions and promote their differentiation into GMCs. This is followed by regulation of the symmetric division of GMCs and GC maturation by AtFAMA. To function in these cell fate transitions, AtSPCH, AtMUTE and AtFAMA require heterodimerisation with either AtICE1 or AtSCRM2, which are functionally redundant and expressed in all stomatal-lineage cells (Kanaoka et al., 2008; MacAlister et al., 2007; Ohashi-Ito and Bergmann, 2006; Pillitteri et al., 2007).

Orthologs of these core transcriptional regulators are also present in grass species, with a duplication in SPCH (Chater et al., 2017; Qu et al., 2017). Although some level of functional divergence has been observed, many of the grass homologs regulate similar developmental events (Figure 1.11). The initiation of stomatal development in grasses occurs as stomatal cell files are specified close to the vasculature. This positioning appears to be regulated by the transcription factors SHORTROOT1-2 (SHR1, SHR2) and SCARECROW1-2 (SCR1, SCR2) (Kamiya et al., 2003; Schuler et al., 2018). Subsequently, the two SPCH homologs (SPCH1-2) act to establish stomatal lineage fate and induce asymmetric entry divisions. Although SPCH1 and SPCH2 have overlapping functions, SPCH2 appears to have a more prominent role (Raissig et al., 2016; Wu et al., 2019c). The differentiation into GMCs is then promoted by MUTE, which in grasses has been co-opted for the recruitment of neighbour SMCs and establishment of SCs (Raissig et al., 2017; Wu et al., 2019c). Following these events, symmetric GMC divisions occurs. Although the function of FOUR LIPS (FLP) is not fully understood in grasses, evidence suggests that in rice it might play a role in regulating the division of GMCs (Wu et al., 2019), whilst FAMA regulates cell fate and GC maturation (Liu et al., 2009; Wu et al.,

2019c). During these transitions, the grass homologs of either AtICE1 or AtSCRM2 are required. Although some distinction between their functions in Brachypodium and rice has been observed, it seems that ICE1 is the primary regulator during stomatal initiation, and at least in Brachypodium, SCRM2 acts in later during stomatal maturation steps (Raissig et al., 2016; Wu et al., 2019c).

1.5. Altering stomatal development

The cell fate transitions outlined above, are tightly controlled during stomatal development. This is particularly important for the optimization of stomatal function, allowing the modulation of stomatal density and ensuring proper spacing between stomatal complexes. In Arabidopsis, the cysteine-rich signalling peptides AtEPF1 (Epidermal Patterning Factor 1), AtEPF2 and AtEPFL9 (AtEPF-like 9) act to mediate intercellular communication and regulate stomatal patterning (reviewed in Buckley et al., 2019; Zoulias et al., 2018). AtEPF1 and AtEPF2 negatively regulate stomatal development. AtEPF2 limits stomatal lineage initiation and meristemoid amplifying divisions, whereas, AtEPF1 prevents the formation of a stoma next to another (one cell spacing rule) (Hara et al., 2007; Hunt and Gray, 2009). In turn, AtEPFL9 (also known as STOMAGEN) is a positive regulator of stomatal development produced by mesophyll cells, that promotes stomatal lineage entry by competing with AtEPF1-2 for the same receptor complex (Sugano et al, 2010; Hunt et al., 2010; Lee et al., 2015). The binding of these EPF/EPFL peptides to their cognate receptor regulates a downstream mitogen-activated protein kinase (MAPK) cascade, culminating in the modulation of AtSPCH activity (Lampard et al., 2008; Lee et al., 2015). The genetic manipulation of this signalling pathway results in alterations in Arabidopsis stomatal density, as well as in g_{smax}, and has been a valuable tool to investigate how changes in the number of stomata affect plant physiology in this model species (Doheny-Adams et al., 2012; Franks et al., 2015; Hepworth et al., 2015; Tanaka et al., 2013). Changes in stomatal density in Arabidopsis resulted in alterations in plant cooling (Doheny-Adams et al., 2012), moreover, a study in plants overexpressing AtEPFL9 showed that the substantial increase in stomatal density caused by this genetic manipulation resulted in higher stomatal conductance and transpiration rates (Tanaka et al., 2013).

Functional orthologs of the EPF family members are present in grass species, and likewise, changes in their expression through both gene knock-out, knockdown or ectopic overexpression, leads to changes in stomatal densities (Caine et al., 2019; Dunn et al.,

2019; Hughes et al., 2017; Lu et al., 2019; Mohammed et al., 2019; Yin et al., 2017). Although the mechanism through which these peptide signals act in grasses is not fully understood, it is clear that the homologues of AtEPF1 and AtEPF2 function to regulate GMC fates in grasses, inhibiting the stomatal cell lineage progression and negatively regulating stomatal density (Figure 1.11). Moreover, two homologs of AtEPFL9 are present in grasses, EPFL9a and EPFL9b. Studies in rice have shown that OsEPFL9a shares more similarities with the sequence of AtEPFL9, than OsEPFL9b (Hepworth et al., 2018; Lu et al., 2019). Although both genes seem to act in promoting stomatal development, when overexpressed in Arabidopsis OsEPFL9a plays a major role regulating stomatal density, whilst OsEPFL9b shows a tissue-specific stomatal clustering phenotype (Lu et al., 2019).
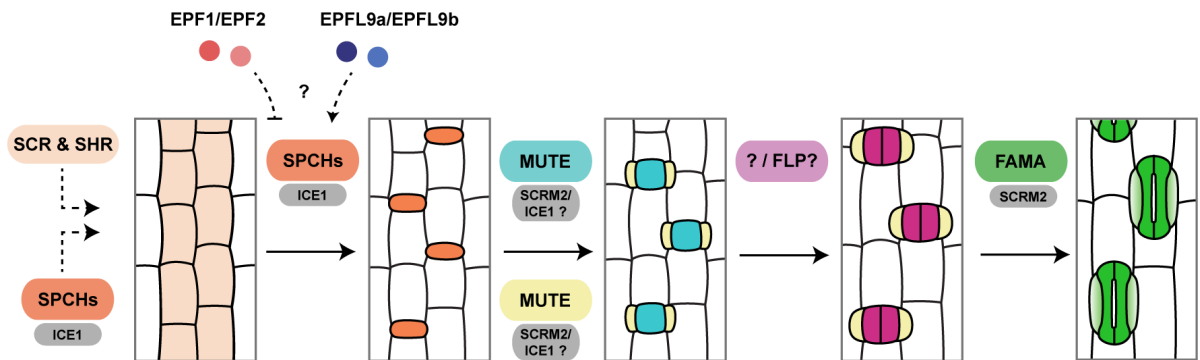
Figure 1.11. Model of the stomatal development regulation in grasses. The positioning of stomatal rows is determined by SHRs and SCRs. A heterodimer between SPCH and, most likely, ICE1 promotes the establishment of stomatal fate in specified rows and subsequent asymmetric entry divisions. MUTE induces guard mother cell (GMC) differentiation and the formation of lateral subsidiary cells (SCs) from neighbour cells, potentially partnering with ICE1 or SCRM2. The regulation of the symmetric division of GMCs is still unknown, with a potential role for FLP in this process. The maturation of the stomatal complex is regulated by FAMA, possibly through heterodimerization with SCRM2. EPF and EPFLs act to inhibit or promote stomatal development during the early stages by modulating the level of SPCH activity, nonetheless how and in which additional stages this regulation takes place is still to be fully determined.

Engineered alterations in stomatal density through the manipulation of EPF/EPFL expression levels has been investigated in multiple cereal crops, in particular to produce decreases in g_{smax} (Caine et al., 2019; Dunn et al., 2019; Hughes et al., 2017; Mohammed et al., 2019). In rice, a reduction of up to 90% in stomatal density was achieved by CRISPR knockout of OsEPFL9a (Yin et al., 2017). Studies on the physiological consequences of decreasing the number of stomata showed that a more moderate change (~ 58% decrease), observed in transgenic rice plants overexpressing OsEPF1, can improve plant water use efficiency and drought tolerance (Caine et al., 2019; Mohammed

et al., 2019). Changing stomatal densities in the opposite direction, targeting an increase in the number of stomata, has been less explored in crops. The overexpression of OsEPFL9a in Nipponbare rice resulted in a more modest (~28%) increase in leaf stomatal densities during early vegetative development. Despite increases in g_{smax}, this change did not seem to significantly affect plants operational gas exchange rates under typical environmental conditions (Mohammed et al., 2019). Similar results were obtained by targeting the overexpression of SCR (Schuler et al., 2018).

Although the physiological responses of these rice plants with increased stomatal densities did not change significantly under optimal conditions, their capacity to promote a greater evaporative cooling effect and avoid heat stress is yet to be investigated. Under conditions that promote greater stomatal apertures, such as high temperatures and moderate to high VPD, plants with higher g_{smax} have the potential to increase their transpiration rates beyond those reached by plants with regular number of stomata, promoting a greater cooling effect. As mentioned in previous sections, such mechanism may help rice plants to remain productive under heat stress periods, providing that enough water is available to maintain stomatal conductance rates. Therefore, altering stomatal densities might be an interesting strategy to tackle rice yield losses under predicted climate change conditions in certain cropping areas.

Whereas further studies on rice plants with altered stomatal densities are necessary to understand whether this approach will indeed be beneficial to improve thermotolerance in rice, the trade-off between plant cooling and water use needs to be considered. As plants with higher g_{smax} could be less water use efficient, the manipulation of the stomatal densities could be particularly interesting if targeted to the reproductive tissues or to the reproductive stage of the rice life cycle, avoiding excessive water loss throughout the growing season, but tackling heat stress during the most sensitive phase of rice development. Studies in Arabidopsis showed that the overexpression of AtEPFL9 also causes increases in stomatal densities in floral organs (Sugano et al., 2010), nonetheless this potential is yet to be investigated in rice. In fact, despite being present in different organs of the rice florets (Ebenezer et al., 1990), not much is known about rice floral stomata, their function or contribution to evaporative cooling. Investigations in this area could be beneficial for understanding whether it is possible to target changes to the density of stomata present on rice florets, and if this could be an effective tool to protect the heat sensitive floral tissues and enhance heat stress tolerance during the reproductive development of rice plants.

1.6. Thesis aims

The aims of this thesis were to investigate (1) whether the manipulation of stomatal development by altering the expression of Epidermal Patterning Factors could prove a useful and novel way to enhance evaporative cooling and heat stress tolerance during the rice reproductive phase; (2) the presence, position and development of stomata on rice floral organs; and (3) the potential consequences of altering floral stomata development through a comparison of rice lines with different stomatal densities.

To address these objectives the following investigations were conducted:

- Transgenic rice lines ectopically overexpressing the gene *OsEPFL9a* were characterized during the vegetative and the reproductive phases of plant development. Subsequently, their physiological responses and productivity were investigated under high temperature stress during the flowering stage.
- In parallel, the presence and distribution of stomata on floral organs was characterized in rice plants of the lowland Indica cultivar IR64, and then investigated in genetically modified IR64 lines ectopically overexpressing either of the Epidermal Patterning Factors *OsEPFL9a* or *OsEPF1*;
- The development of floral stomata was studied, with a focus on rice lemma and palea. Gene expression in rice florets was investigated during the different stages of stomatal lineage fate transition in IR64 and in *OsEPF1* overexpressing plants.

Chapter 2

Materials and Methods

2.1. Plant material

2.1.1. IR64 rice variety

IR64 is a high yield and high quality semidwarf Indica rice variety developed by the International Rice Research Institute (IRRI) in the Philippines and released in 1985. IR64 was developed for irrigated rice production and due to its wide adaptation to tropical lowland conditions, it became extensively grown in South and Southeast Asia (Mackill and Khush, 2018), being also well adapted to regions of West Africa (Julia and Dingkuhn, 2013). Although grown in tropical areas, IR64 is considered sensitive to heat stress. In this variety, tissue temperatures of above 29.6 °C for up to 1 hour during flowering can cause a 7% reduction in fertility, per 1 °C increase (Jagadish et al., 2007). Due to its superior grain quality and popularity, IR64 has been used in rice breeding programs. As a result, it has been substituted by newer varieties with similar quality, but improved traits. IR64 is widely used as a recipient for new genes in marked-assisted crossing and genetic transformation, in QTL mapping and in fundamental studies on tropical lowland rice (reviewed in Mackill and Khush, 2018). In this study, IR64 rice plants that were genetically modified to overexpress either *OsEPFL9a* or *OsEPF1* were investigated.

2.1.2. Transgenic rice lines overexpressing *OsEPFs*

All transgenic rice lines used in this study were produced by the group of Professor William Paul Quick at the International Rice Research Institute (IRRI), in the Philippines. To generate genetically modified rice, *Agrobacterium tumefaciens* mediated transformation was conducted using IR64 rice immature embryos, followed by explant regeneration by tissue culture (Hiei and Komari, 2008). An initial characterization of T_0 and T_1 generation plants was conducted by collaborators at IRRI. Only T_2 and T_3 generation plants were used in this study. A summary of the rice lines investigated is presented in Table 2.1.

- Rice overexpressing *OsEPFL9a*

OsEPFL9a-oe-2 (ID: IR64-IRS1079-012-08) and OsEPFL9a-oe-3 (ID: IR64-IRS1079-028-14) are independent transgenic Indica IR64 rice lines that were genetically

modified to overexpress the gene *OsEPFL9a* (Os01g0914400) under the control of the maize ubiquitin promoter. According to analysis from collaborators at IRRI, T_0 generation of OsEPFL9a-oe-2 had multiple copies of the transgene (6 copies), whereas OsEPFL9a-oe-3 T_0 had a single copy of the transgene.

- Rice overexpressing *OsEPF1*

The lines OsEPF1-oe-W (ID: IR64-IRS1080-029-27) and OsEPF1-oe-S (ID: IR64-IRS1080-031-16) are Indica IR64 rice genetically modified to overexpress the gene *OsEPF1* (Os04g0637300) under the control of the maize ubiquitin promoter. These lines were previously characterized in Caine et al. (2019), OsEPF1-oe-W is a single copy line, whilst T_0 of OsEPF1-oe-S had 6 copies of the transgene.

- Control line

Plants of the Indica IR64 cultivar went through the same transformation and tissue regeneration procedure as transgenic lines without the presence of agrobacterium, therefore, do not contain a transgene. These plants will be referred as either IR64 or IR64-control (ID: IR64-C-IRS1080-002-06). Only T_2 and T_3 generation plants were used here.

Table 2.1. Summary of rice lines investigated.

Rice line name	IRRI ID	Overexpression construct	Transgene copies (T_0)
OsEPFL9a-oe-2	IR64-IRS1079-012-08	*ZmUBQ$_{pro}$:OsEPFL9a*	6
OsEPFL9a-oe-3	IR64-IRS1079-028-14	*ZmUBQ$_{pro}$:OsEPFL9a*	1
OsEPF1-oe-W	IR64-IRS1080-029-27	*ZmUBQ$_{pro}$:OsEPF1*	1
OsEPF1-oe-S	IR64-IRS1080-031-16	*ZmUBQ$_{pro}$:OsEPF1*	6
IR64-control	IR64-C-IRS1080-002-06	None	-

2.2. Plant growth

Rice seeds were placed in sealed transparent magenta pots containing RO water (water purified by reverse osmosis system) at ~1 cm level, and were kept in a Sanyo growth chamber (12h photoperiod, 26 °C/ 24 °C day/night temperature, 200 µmol m^{-2} s^{-1} light) for germination. After 7 to 10 days seedlings were transferred to pots with soil saturated with water. Soil mix consisted of 71% Kettering loam, 23.5% John Innes No. 3 compost, 5% sand and 0.5% Osmocote extract standard slow-release fertilizer (v/v). For most experiments in this study plants were grown in pots of 0.88 L. However, for the seedling thermal imaging experiment (in Chapter 3) plants were grown in pots of either 120 mL or 7 mL, and for the flowering stage heat experiment (in Chapter 4) plants were grown in 2.4 L pots. After transplanting, plants were grown in Conviron controlled-environment

growth cabinets or in Conviron controlled-environment walk in growth rooms (Figure 2.1) under optimal conditions for rice, unless stated otherwise. Plant pots were kept in trays with a constant supply of water to the pot base and were also watered from the top twice a week. From the 4th growth week, plants were fertilized in intervals of two weeks with Chempak High Nitrogen Feed No. 2.

2.2.1. Optimal growth conditions

- Conviron growth cabinets (Chapters 3 and 5): 12h photoperiod, ~30 °C/ 24 °C day/night temperature, ~60% relative humidity, ~850 µmol m^{-2} s^{-1} PAR (at canopy level), CO_2 concentration was not controlled.

- Conviron walk in chamber (Chapters 3 and 4): 12h photoperiod, ~30 °C/ 24 °C day/night temperature, ~60-70% relative humidity, ~1200 µmol m^{-2} s^{-1} PAR (at canopy level), CO_2 concentration was not controlled.

2.2.2. High temperature treatment at seedling stage (Chapter 3)

To investigate leaf temperature under rising temperature conditions, seedlings were grown under optimal conditions in a Conviron cabinet and later exposed to the following temperature treatment during a day. The light period was onset at 7am, and temperature was initially kept at 30 °C until 12pm; then temperature was slowly raised to 32.5 °C from 12h to 12:30pm; kept at 32.5 °C from 12:30 to 1pm; raised to 35 °C from 1h to 1:30pm; kept at 35 °C from 1:30 to 2pm; then raised to 37.5 °C from 2h to 2:30pm; kept at 37.5 °C from 2:30 to 3pm; and finally decreased to 30 °C from 3pm (temperature ramp was 5 °C/h), ~60% relative humidity at all times, ~850 µmol m^{-2} s^{-1} PAR (at canopy level).

2.2.3. High temperature treatment at flowering stage (Chapter 4)

Plants were grown in a Conviron walk in chamber under optimal conditions until the flowering stage, when a subset of plants was transferred to a similar Conviron walk in chamber, with the same 12h photoperiod and light intensity, and were kept for 8 days under the following heat treatment: during the light period (from 7 am) the temperature was slowly increased to reach 37 °C by 9:30 am. Temperature was kept at 37 °C for 5 hours (from 9:30 am to 3:30 pm), afterwards, temperature was slowly returned to 30°C (reached at 4:30 pm), and kept at this level until the end of the light period (at 7 pm). During the night period temperature was kept at 24 °C. Moisture content (specific humidity) was ~ 0.018 kg/kg day and ~ 0.013 kg/kg night, CO_2 concentration was not

controlled, varying from ~ 350-500 ppm. Plants were well watered all the times (more details about this experiment are described in Chapter 4).
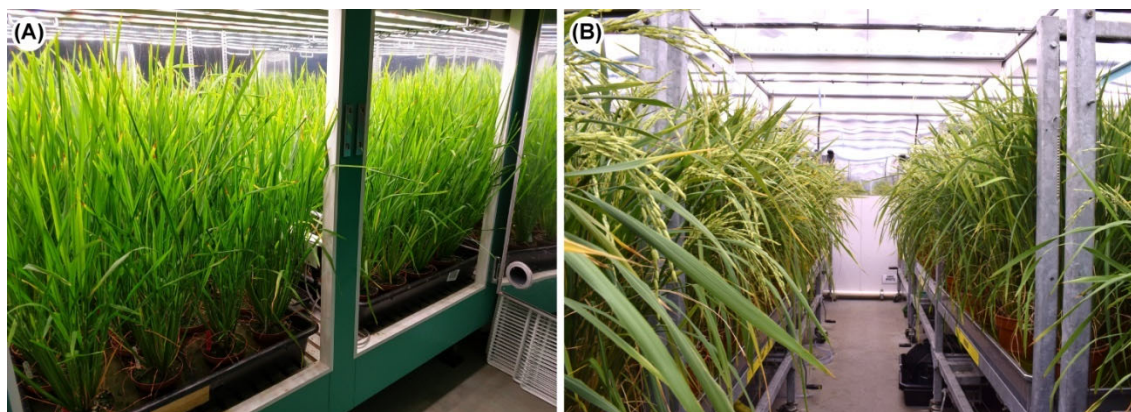
Figure 2.1. Plants growing in **(A)** Conviron controlled-environment growth cabinet and in **(B)** Conviron controlled-environment walk in growth rooms.

2.3. Plant genotyping

2.3.1. Genomic DNA isolation

DNA was isolated using a protocol adapted from Ikeda et al. (2001). Fresh leaf material (about 1 cm^2) was collected and ground in a 1.5 mL tube with 200 µL of TE buffer (10mM Tris-HCl, 1mM EDTA, pH 8.0) using a micropestle. The tube was placed in a heat block at 100 °C for 15 minutes, subsequently, more 800 µL of TE buffer were added to the tube and mixed. The tube was centrifuged for 3 minutes at 14,000 rpm, the supernatant was recovered and used as template in PCR reactions.

2.3.2. PCR reactions

PCR reactions were assembled using One *Taq* Quick-Load 2x Master Mix with Standard Buffer (Biolabs) according to manufacturer's instructions, using 1.5-2.5 µL of DNA as template. An initial denaturation step of 94 °C for 30s was followed by 35 amplifications cycles (94 °C for 15 s; annealing temperature for 60 s; 68 °C for 60 s) and a final extension step of 68 °C for 5 min. To amplify only the overexpression constructs a forward primer complementary to a region of the maize ubiquitin promoter was used with a reverse primer complementary to a region in the coding sequence of the relevant gene.

Primers used to amplify the *OsEPFL9a* overexpression construct: FW - 5'CTGC TAGCGTTCGTACACGG3' and RV - 5'TGCATATTTGGGGCAGCCTCTCC3'. Annealing temperature: 60 °C. Fragment size: 674bp.

Primers used to amplify the *OsEPF1* overexpression construct: FW - 5'CTGCTAG CGTTCGTACACGG3' and RV - 5'TTGAAGCTCACCATGACGCGGTTG3'. Annealing temperature: 60 °C. Amplicon size: 784bp.

2.3.3. Agarose gel electrophoresis

Agarose gels were prepared by dissolving 1% agarose (w/v) in TAE buffer (40mM Tris, 20mM acetic acid, and 1mM EDTA). Ethidium bromide was added to a final concentration of ~0.5μg/ml. Gels were run at 90-110V.

2.4. Analysis of *OsEPFL9a* overexpression levels

2.4.1. RNA purification and quantification

RNA was extracted from the shoot of 8-day-old rice seedlings. The plant material was frozen in liquid nitrogen, ground to a fine powder, and RNA was extracted using the Spectrum Plant Total RNA Kit (Sigma-Aldrich), according to the manufacturer's instructions. Total RNA was treated with DNA-free DNA removal Kit (Thermo Fisher Scientific) to remove traces of genomic DNA from samples. RNA quantification was performed with NanoDrop 8000 Spectrophotometer (Thermo Scientific), using 1 μL of sample. RNA integrity was checked in a TAE agarose gel as, described in section 2.3.1.

2.4.2. RT-qPCR

For first-strand cDNA synthesis, 1μg of RNA was added as template in reactions with oligo (dT)$_{18}$, using the M-MVL Reverse Transcriptase (Invitrogen) according to the manufacturer's instructions. The single stranded cDNA was then used as template in a real-time quantitative PCR analysis using the Rotor-Gene SYBR Green PCR Kit (Qiagen) in a Corbett Rotor-Gene 6000 Real Time PCR machine. Each reaction was assembled with 5 μL of 2x Rotor-Gene SYBR Green Master Mix, 1 μL forward primer (10 μM working concentration), 1 μL reverse primer (10 μM), 2 μL template cDNA (total of 10 ng) and 1 μL nuclease-free water. qPCR conditions were: initial denaturation at 95 °C for 10 min, followed by 35 amplifications cycles (95 °C for 10 s; 60 °C for 55 s) and a final melting curve (steps of 1 °C increase, from 55 °C to 90 °C, 5 s in each temperature step). qPCR reactions were assembled to amplify either the *OsEPFL9a* (target) or the housekeeping gene *OsPROFILIN2* (Os06g0152100), three technical replicates and three biological replicates were performed. Relative expression analysis were conducted by normalizing take-off values and amplification efficiencies of the target gene relative to the housekeeping gene and to the control line (Pfaffl, 2001).

Primers used to amplify *OsEPFL9a*: Fw - 5'CATGGCAGCATCTCAGGTACAG3' and Rv - 5'-TGCATATTTGGGCAGCCTCTCC-3'.

Primers used to amplify *OsPROFILIN2*: Fw - 5'GGTTGTCATCCGAGGAAAGAA GGG3' and Rv - 5'ACGACAGGCCAGTCTTCTTGAC3'

2.5. Microscopy imaging

2.5.1. Plant material collection and preparation

Epidermal surfaces of rice floral organs and leaves were imaged using freshly collected tissue or fixed material. To collect developing rice spikelets, panicles were removed from inside flag leaf sheaths and spikelets were isolated. Fully expanded rice spikelets were collected at heading stage. For fresh tissue visualization, spikelets were dissected under a stereo microscope to separate the different floral organs, which were subsequently visualized and imaged under appropriate microscope. Otherwise, whole spikelets were fixed in a solution of ethanol and acetic acid (3:1). Immersed samples were vacuum infiltrated for 40 minutes at room temperature, and then kept at 4 °C for at least 48h. Afterwards the fixative solution was replaced by 70% ethanol (v/v) and the samples stored at 4 °C. On the day of visualization, samples were washed for 10 minutes in 50% ethanol and in water twice. After the second wash in water, samples were cleared in a chloral hydrate (2 g/mL) 20% glycerol (v/v) solution for 10 minutes to 1 hour (depending on the floret developing stage, young florets needed less clearing time). Then, spikelets were dissected under stereo microscope in 20% glycerol (v/v), and floral organs were mounted in the same solution.

2.5.2. Light microscopy

Rice floral organs were imaged using an Olympus BX51 microscope equipped with an Olympus DP71 camera and Cell B software. Observations were conducted using either fresh tissue mounted in water, or fixed tissue as described in 2.5.1.

2.5.3. Scanning electron microscopy (SEM)

Fresh tissue of rice floral organs and leaves were visualized using Hitachi TM30303Plus benchtop SEM equipped with a DEBEN Specimen Cooling Unit. Dissected fresh tissue was mounted in 9 mm flat stubs, using double-sided carbon adhesives pads (Agar Scientific) or cryo-gel embedding medium (Agar Scientific). Samples were visualized on a cooled stage (-20 °C) under 15kV.

2.6. Measurements of stomatal traits

2.6.1. Stomatal density of rice leaves

Stomatal densities from rice leaves were estimated by counting stomata from nail varnish impressions. Light, fast set vinyl polysiloxane impression material (ImpressionPLUS Wash, Perfection Plus) was applied to the surface of fully expanded rice leaves at the central portion of the blade to create a negative impression of the leaf epidermis. Once the material was set, it was removed from the leaf surface, and a coat of transparent nail varnish was applied to the impression. After nail varnish set, a transparent sellotape piece was laid on top of it, being removed afterwards, carrying the nail varnish epidermal impression with it. The piece of tape was then affixed to a glass slide and observed under a Nikon light microscope. Stomatal counts were taken from fields of ~0.26 mm^2. For leaf 2 and leaf 6 analyses, stomata were counted from 5-6 fields of view per replicate, whilst for flag leaves analyses, 3 fields of view were counted from 3 different leaves per plant (total of 9 fields of view per plant).

2.6.2. Stomatal size and maximum anatomical stomatal conductance (g_{smax})

To investigate stomatal size and g_{smax} leaf impressions were taken from the abaxial and adaxial epidermis of fully expanded leaf 6 and stomatal densities were assessed (as described in section 2.6.1). Then pictures of the epidermal impressions were taken under 400x magnification using an Olympus BX51 microscope equipped with an Olympus DP71 camera. Using ObjectJ plugin in ImageJ 1.50i (Fiji), measurements of guard cell length, guard cell width and stomatal pore length were taken from 35 stomata per leaf surface (abaxial and adaxial, a total of 70 stomata per plant). Anatomical g_{smax} was calculated using the double end-correction equation described by Franks and Farquhar (2001):

$$\textit{Anatomical } g_{smax} \quad = \frac{d.D.a_{max}}{v.\left(l+\left(\frac{\pi}{2}\right).\sqrt{\left(\frac{a_{max}}{\pi}\right)}\right)}$$

where a_{max} is the maximum stomatal pore aperture (μm^2, calculated as an ellipse of major axis equal to the measured stomatal pore length and minor axis equal to half pore length); l is stomatal pore depth (μm, estimated as equal guard cell width at middle of stomata); d is the diffusivity of water in air (m^2 s^{-1}); v is the molar volume of air (m^3 mol^{-3}); D is stomatal density (mm^{-2}) and π is a mathematical constant (~3.142). The values used for diffusivity of water vapour in air and the molar volume of air at 30 °C were 0.0000259 m^2 s^{-1} and 0.0249 m^3 mol^{-3}, respectively, as described in Caine et al. (2019). G_{smax} values

were estimated independently for the abaxial and adaxial leaf epidermis and then added to calculate total anatomical g_{smax}.

2.6.3. Stomatal density in rice floral organs

Stomatal densities were estimated from inner epidermis of lemma and connective tissue of anthers, using fully expanded spikelets. Tissue of rice spikelets were collected, fixed and cleared, as described in section 2.5.1, then visualized under an Olympus BX51 microscope. Three florets per plant were examined. Stomatal density was estimated in the upper region of adaxial lemma, using two fields of view of $0.985mm^2$ each, per lemma. Stomatal densities were also estimated in the folding area of lemma, by counting stomata in an area of $0.985mm^2$ in the lemma adaxial middle portion. Three anthers per spikelet were visualized (nine anthers in total per plant), stomatal were counted from one side of the connective tissue of each anther, and stomatal density was calculated relative to the connective tissue length. To measure connective tissue length, anthers were imaged as described in and 2.5.2, and the connective tissue was measured using ImageJ 1.50i (Fiji).

2.7. Gas exchange analysis

Leaf stomatal conductance, net carbon assimilation and transpiration rates were evaluated using an infrared gas analyser (IRGA; LI-6800 Portable Photosynthesis System, LI-COR Biosciences, Lincoln, NE, USA) coupled with a $6 cm^2$ leaf chamber fluorometer (6800-01A, LI-COR Biosciences). Measurements were taken from young fully expanded leaf blades of intact plants, starting at least 2 hours after the onset of the light period and ceasing before the last three hours of the photoperiod.

2.7.1. Steady-state measurements

Leaf chamber conditions were controlled at flow rate of $300 \, \mu mol \, s^{-1}$, 80% fan speed, 10% blue light, 90% red light and CO_2 set to reference. Temperature, relative humidity, light intensity and CO_2 concentration varied according to each experiment, and are detailed in the relevant chapters. After environmental condition were set in the leaf chamber, the leaf was clamped, and IRGAs were matched a few minutes later. The leaf was left to acclimate to the experimental conditions until g_s and carbon assimilation rates were stable (~20-30 min). Then, measurements were logged for 5 minutes, every 30 seconds.

2.7.2. Light-response curves

Leaf chamber conditions were set as described in 2.7.1, additionally, leaf temperature was controlled at 30 °C, reference CO_2 concentration at 480 ppm and RH at 60%. Decreasing light levels of 2000, 1500, 1200, 1000, 800, 600, 480, 340, 200, 150, 100, 75, 50, 25, 0 µmol m^{-2} s^{-1} PAR were applied. Light intensity was first set to 2000 µmol m^{-2} s^{-1} when leaf was clamped. After few minutes IRGAs were matched, and leaf was left to acclimate to the experimental conditions until g_s and carbon assimilation rates were stable (~20-30 min). Between each light intensity change, leaves were allowed 5-7 minutes stabilization time. Measurements in each light step were logged for 5 minutes, with 30 seconds intervals.

2.7.3. Temperature-response analysis

Leaf chamber conditions were controlled at 275 µmol s^{-1} flow rate, 80% fan speed, sample CO_2 concentration of 480ppm, 2000 µmol m^{-2} s^{-1} PAR with 10% blue light and 90% red light. Increasing air temperature steps of 30, 32.5, 35 and 37.5 °C were applied. Leaf was clamped and left to acclimate to the experimental conditions at 30 °C until g_s and carbon assimilation rates were stable (~20-30 min). IRGAs were matched before measurements started and after each temperature step change. Leaves were allowed 20 minutes stabilization time after each change in temperature, afterwards, measurements were taken every 1 minute for a total of 10 minutes. When an unstable series of measurements were taken, data was removed from analysis.

2.8. Chlorophyll fluorescence

Photosystem II (PSII) dark and light-adapted chlorophyll fluorescence were investigated using a FluorPen (FP100, Photon Systems Instruments, Brno, Czech Republic). Measurements were taken from the middle blade of young fully expanded flag leaves. For dark-adapted quantum yield measurements (Fv/Fm), data was collected before the onset of the light period, whereas, light-adapted measurements (Fv'/Fm') were conducted ~5h into the light period.

2.9. Thermal imaging

Thermal imaging analyses were conducted using an infrared (IR) thermal imaging camera FLIR T650SC (FLIR Systems Inc., Boston, MA, USA). All images were taken

inside the growth chamber where plants were being grown. Emissivity was set to 0.95 and other parameters were in default settings.

2.9.1. Seedling temperature analysis

In Chapter 3, thermal images of rice seedlings were captured during the course of a high temperature treatment (section 2.2.2). The IR camera was positioned either above or in front of plants, capturing images of all seedlings being analysed. Treated or transgenic plants were routinely imaged alongside an appropriate control plant. After chamber doors were closed, an image was taken every 1 minute. Temperature treatment started approximately 45 minutes after chamber doors were closed. Each temperature step transition took 30 minutes and was followed by 30 minutes of stable temperature. Data was collected from the last 10 minutes of each stable temperature step. Images were analysed using the researchIR software (FLIR Systems, Inc.), average temperature of each replicate was estimated from spot measurements of similar position in leaves.

2.9.2. Flowering stage temperature analysis

In Chapter 4 thermal images were taken of rice plants at the flowering stage with the camera positioned in front of the plants, at approximately 2 meters distance. As plants were large, only two plants were captured per image (a pair of a control and a transgenic plant). Each pair of plants were imaged twice in opposite positions. Images were analysed with the FLIR Tools software (FLIR Systems, Inc.), and the average temperature of each replicate was estimated from spot measurements of equivalent areas of leaves.

2.10. Floret temperature using thermocouples

Floret temperature was measured using type K thermocouple probes of 0.25 mm diameter, connected to a 4-channel thermometer datalogger SDL200 (Extech Instruments, Nashua, NH, USA). Thermocouple probes were inserted between the lemma and palea edges (Figure 2.2 A) of florets of equivalent position in plants. Thermocouple leads were fixed to the base of the flag leaf with a tape to prevent falling of the probes (Figure 2.2 B). Temperatures from 3 florets (1 of each genotype) and ambient air temperature were recorded simultaneously. After thermocouple probes were adjusted, a time was allowed until floret temperatures were stabilized (~5 minutes), then temperature values were logged for 5 minutes, in 5 second intervals. A total of 6 florets per plants were analysed.
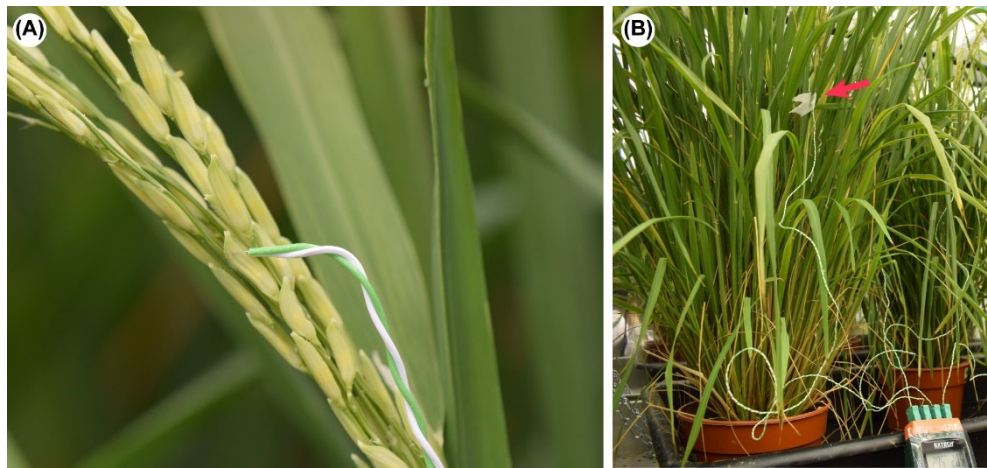
Figure 2.2. Floret temperature was measured with thermocouple probes. **(A)** Thermocouple probe inserted in a floret through lemma and palea edges. **(B)** Red arrow shows a thermocouple lead fixed with a tape to the base of the panicle and flag leaf.

2.11. Pollen viability

Pollen viability was assessed using MTT (thiazolyl blue tetrazolium bromide, Sigma-Aldrich) staining (Khatun and Flowers, 1995; Rodriguez-Riano and Dafni, 2000). Mature spikelets were collected prior to anthesis, anthers were removed from florets and placed in 1.5mL tubes with 40μL of 0.5% MTT (w/v), 50% sucrose (w/v) solution. Anthers were gently broken and mixed using a pipette (with the tip cut) to release pollen grains. After 6-8 minutes at room temperature pollen grains were stained, being subsequently placed on slides with coverslips. Slides were observed under a Nikon Labophot microscope, and 200 pollen grains were counted per slide. Purple stained pollen was considered viable, non-stained pollen was considered non-viable, and black stained pollen was considered to be in the process of degeneration, therefore non-viable (Figure 2.3). Anthers from 3 florets from different panicles were analysed per plant. Prior to analysis this protocol was tested in samples of freshly collected and heated pollen (15 minutes at 90°C), confirming that dead pollen was not stained using MTT.
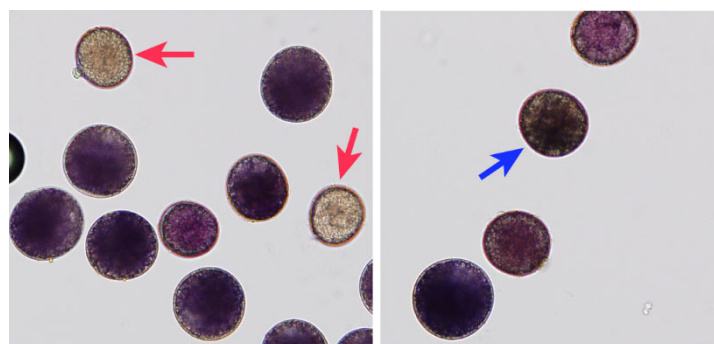
Figure 2.3. Pollen sample stained with MTT. Red arrows indicate dead pollen (non-stained) and blue arrow indicates pollen in degeneration (black-stained).

2.12. Inflorescence and spikelet morphology

Inflorescence and spikelet morphology were investigated in Chapter 3. Measurements of inflorescence length were taken from five fully extended panicles per plant using a ruler. Inflorescences were measured from the base of the rachis to the tip of the uppermost floret. The length of 30 spikelets per plant was assessed, the uppermost spikelets of three different exerted panicles were collected prior to anthesis (10 spikelets per panicle). Spikelet length was measured from the base of the lower glume to the floret tip, using a pair of calipers. The average number of spikelets per panicle in a plant was determined by counting the spiklets of five panicles per plant.

2.13. Plant growth and yield analysis

Components of plants growth and yield were analysed in Chapter 4 in mature plants, after the exposure to temperature treatment.

2.13.1. Biomass dry weight

Aboveground biomass, vegetative shoot biomass and number of panicles were estimated in mature plants at the end of the ripening stage (~ 130 days after sowing). When seeds were ready to harvest, plants were left without water supply for 2 days to reduce seed moisture and start drying the leaves and tillers. Then, all panicles were collected to avoid loss of seeds, and were kept in paper envelopes to dry further. The vegetative shoot was collected only after all tillers were dry and was also later kept in paper bags. The weight of the vegetative shoot (leaves and tillers) and the reproductive parts (panicles and seeds) were measured using portable balances. Dry weight of total above ground biomass was calculated by adding these values.

2.13.2. Number of panicles and spikelet fertility

After panicles were collected as described above, the number of panicles per plant was counted. Spikelet fertility was estimated in 10 panicles per plant, for this purpose the total number of filled and unfilled spikelets per panicle was counted. Spikelet fertility per panicle was estimated as the proportion of seeds produced to the total spikelets developed.

2.13.3. Total grain yield

Total grain yield per plants was estimated by separating all the seeds produced in a plant from their panicles and weighing them with a portable balance.

2.13.4. Seed weight

Seed weight was estimated by counting 100 seeds per plant, removing their husks manually and weighing on a portable balance. The average weight per seed was calculated for each plant by dividing the total weight of 100 seeds by 100.

2.14. Statistical analyses of phenotypic and physiological data

All statistical analyses in Chapters 3 and 4 were performed using R v3.6.1 (R Core Team, 2019). ANOVA was used to test for differences between genotypes and interaction effects between factors, when appropriate. If significant differences were found, the analysis of variance was followed by a multiple comparisons Tukey post-hoc test (Tukey's HSD). Before performing an ANOVA, data were tested for the normality assumption by analysing the linear model residuals, using QQ plots and the Shapiro-Wilk test. The homogeneity of variances assumption was checked using the Levene's test. When both assumptions were not met, a non-parametric Kruskal-Wallis followed by a post-hoc Dunn test were performed. For data in which only the homogeneity of variances could not be assumed, a Welch one-way test followed by a Games-Howell were performed. To investigate the relationship between variables, analyses of multiple linear regression were carried out.

2.15. Collection of developing florets for RNA-seq analyses

2.15.1. Establishment of floret stages according to stomatal development

The spatiotemporal distribution of the stomatal lineage cells was characterized during the development of IR64 florets. For this purpose, developing panicles were removed from inside flag leaf sheaths during the booting stage, and florets in different development stages were collected, fixed and cleared as described in section 2.5.1. Floret length was measured with a ruler under a stereo microscope, then florets were dissected, and floral organs placed in slices for visualization under an Olympus BX51 microscope (Olympus Corporation, Tokyo, Japan). Multiple lemmas and paleas of different sizes florets (from 1 to 8 mm length, with 0.5 mm intervals) were examined. A qualitative description of stomatal development with a focus on how stomata develop in the internal epidermis of lemma was produced, allowing the classification of florets into 5 stages that reflect the stomatal development progress, using florets length as a marker: Stage 1 - from ~0.5 to 1 mm florets; Stage 2 - from ~1.1 to 2 mm florets, Stage 3 – from ~2.5 to 3.5 mm florets, Stage 4 – from ~4 to 5 mm florets, Stage 5 – from ~5.5 to 6.5 mm florets.

2.15.2. Material collection

Three subsets of plants were sown sequentially, one week apart from each other, and grown in cabinets under optimal growth conditions (as in 2.2.1). Developing florets of stages 1 to 5 collected ~75-85 days after sowing, and mature florets were collected collected after panicle heading, but prior to anthesis (~ 95 days after sowing). Developing florets were isolated and measured under a stereo microscope, then placed in tubes with liquid nitrogen, being sampled per plant and according to their size/stage (as stated in 2.14.21). All samples were kept at -70 °C.

2.16. RNA purification and quality control for RNA-seq analysis

Floret samples of individual plants were ground to a fine powder in liquid nitrogen using a micropestle, and RNA was extracted using the Spectrum Plant Total RNA Kit (Sigma-Aldrich), with the On-Column DNase I Digest step, according to the manufacturer's instructions in protocol A. RNA was eluted in 50 µL of elution buffer. RNA purity and concentration were analysed in a NanoDrop 8000 Spectrophotometer (Thermo Scientific) and in a Qubit 4 Fluorometer (Invitrogen), using the Qubit RNA BR Assay Kit (Thermo Scientific), according to the manufacturer's instructions. RNA integrity was assessed by electrophoresis in 0.5x TBE 1.2% agarose gels. Agarose gels were prepared by dissolving 1.2% agarose (w/v) in 0.5x TBE buffer (49 mM Tris-borate, 1mM EDTA). Ethidium bromide was added to a final concentration of ~0.5µg/ml. Gels were run with 0.5x TBE buffer at 90-100V for 40-50 minutes. Subsequently, RNA extracted from developing floret samples (stages 1 to 5) of three individual plants were mixed, in proportional RNA quantities. Each biological replicate for developing florets comprised RNA from three different rice plants. Three biological replicates per stage, per genotype were sent for RNA sequencing in Novogene facilities in China. Prior to library preparation and sequencing, quality control checks were also performed by Novogene, including analyses using an Agilent 2100 Bioanalyzer. All samples had RIN (RNA integrity number) values above 8.5 and passed quality control.

2.17. Library preparation and RNA sequencing

Library preparation and RNA sequencing were performed by Novogene (China). According to information provided by the company, mRNA enrichment was conducted by poly(A) mRNA isolation method, using the NEBNext Poly(A) mRNA Magnetic Isolation Module (Biolabs), and library preparation was performed using the NEBNext

Ultra RNA Library Prep Kit (Biolabs). Library quality control consisted in preliminary concentration tests using Qubit 2.0, insert size tests using Agilent 2100 and precise quantification of library concentration using qPCR. Subsequently, sequencing was performed in an Illumina Nova-seq 6000 platform to produce paired-end reads with read length of 150 bp. A minimum of 30 million pairs of reads per sample were generated.

2.18. Processing of RNA-seq reads

All bioinformatic processing of RNA-seq data was performed using the ShARC HPC cluster of the University of Sheffield.

2.18.1. Quality assessment and filtering of raw reads

Quality control of raw reads was initially assessed using FastQC 0.11.8 (Babraham Bioinformatics). Then, raw reads were subjected to quality trimming and adapter filtering to remove adapter contamination and low-quality sequences using Trimmomatic 0.38 (Bolger et al., 2014). Trimmomatic was set to identify specific adapter sequences in the palindrome mode, searching for seed matches of 16 bases, with a maximum of 2 base mismatches. Extended paired-end seeds of alignment score of 30 or higher (~ 50 bases), with a minimum adapter length of 8 bases, were clipped and pairs were kept. For quality trimming, any trailing sequence of quality lower than 10 (Phred score) were removed and the first 12 bases of the reads were cropped. Reads were scanned with a 4-base sliding window and were cut if the average quality per base was lower than 15. After these steps, reads with less than 60 bases long or unpaired were discarded. Quality of trimmed reads were then checked again using FastQC 0.11.8.

2.18.2. Mapping to a reference genome

Trimmed paired-end reads were mapped to the Nipponbare IRGSP 1.0 genome assembly (Kawahara et al., 2013), using the genome annotation available on the Rice Annotation Project Database (RAPDB, https://rapdb.dna.affrc.go.jp) (Sakai et al., 2013). Mapping of reads was performed with HISAT2 v2.1.0 (Kim et al., 2015). First, a genome index was built with *hisat2-buid* indexer, including splicing sites and exon list information from RAPDB. Then reads were mapped to the genome using the default settings of HISAT2 paired-end mode. The SAM files produced during mapping were converted to sorted BAM files and indexed BAM files using SAMtools-1.9 (Li et al., 2009). Read alignment results were examined using Qualimap2 v2.2.1 (Okonechnikov et al., 2016).

2.18.3. Mapped reads quantification

Reads successfully mapped to the Nipponbare IRGSP 1.0 genome were quantified using the function featureCounts from the R package Subread 2.0.0 (Liao et al., 2014). Quantification was performed at gene level, considering only DNA fragments bookended by a pair of reads that were mapped to exonic regions. FeatureCounts was run at default settings for pair-ended reads. Multi-mapping and multi-overlapping reads were not counted.

2.19. RNA-seq counts quality assessment

After the quantification of mapped reads, library sizes (number of counts assigned per sample), counts distribution and variation between samples were examined in R. For the principal component analysis and distance matrices, count data were normalized and log-transformed using the functions *rlog* or *vst* from the R package DESeq2 (Love et al., 2014).

2.20. Differential expression analysis

Differential expression analyses were conducted using the R package DESeq2. DESeq2 pipeline performs hypothesis testing using the Likelihood Ratio Test (LRT) or the Wald Test, with the Benjamini-Hochberg adjustment of p-values. The pipeline models data following a negative binomial distribution and normalizes raw counts by size factor (median-of-ratios method) to account for differences in library depth. Three analyses were run in this study. First, an LRT was performed to identify genes that show expression changes across the developing stages 1 to 5 in IR64-control florets, using an adjusted p-value cut-off of 0.001 (full model = ~ Stage, reduced model = ~ 1). Second, a LRT was conducted to identify genes that change expression in a genotype-specific manner across the stages 1 to 5 comparing two different genotypes, considering an adjusted p-value threshold of 0.05 (full design = ~ Genotype + Stage + Genotype:Stage, reduced model = ~ Genotype + Stage). Finally, pairwise comparisons were performed to identify genes that were up or down-regulated in specific stages between two different genotypes. A null hypothesis of $\log_2$ fold change (LFC) equals 0 (no difference in expression) was tested using a Wald test, with an adjusted p-value cut-off of 0.05 (design = ~ Genotype_Stage).

2.21. GO term analyses

Gene ontology (GO) term analyses were performed using the *enricher* function of the R package ClusterProfiler (Yu et al., 2012). The GO term annotation used in the analyses was the version 48 osativa_eg_gene for *Oryza sativa* Japonica Group genes (IRGSP-1.0) downloaded from Ensembl Plants (https://plants.ensembl.org). Long GO term result lists were summarized using REVIGO (Supek et al., 2011), or alternatively, redundancy was manually removed in short result lists.

2.22. Visualization of RNA-seq results

Graphs, including heatmaps, MA plots, gene expression level comparisons and cluster plots were produced in R v3.6.1 (R Core Team, 2019). Heatmaps were produced using data that was normalized and log-transformed using the *vst* function from the R package DESeq2. MA plots were produced with shrunken LFC values, and normalized log-transformed count values (*vst*) in DESeq2. Gene clusters were identified using the function *degPatterns* from the R package DEGreport. Individual gene counts were normalized by size factor for visualization.

Chapter 3

Changing stomatal density in rice leaves and floral organs

3.1. Introduction

The reproductive phase of rice life cycle is highly susceptible to heat stress, with the exposure to above optimum temperatures, in particular during microsporogenesis and flowering, leading to great yield losses (Jagadish et al., 2007, 2015; Satake and Yoshida, 1978). In irrigated or flooded rice growing areas, high levels of water loss through stomata can be an effective mechanism to maintain plant temperatures below a damaging threshold (Julia and Dingkuhn, 2013; Matsui et al., 2007). Therefore, the improvement of rice evaporative cooling capacity could prove useful for overcoming heat stress and protect rice yields.

Transpiration from leaves largely results from water vapour diffusion through stomatal pores, or stomatal conductance (g_s), which is regulated by controlling stomatal pore aperture. Adjustments in the opening degree of guard cells are achieved in short term responses to environmental conditions, including changes in temperature (Farquhar and Sharkey, 1982; Kostaki et al., 2020). Nonetheless, the maximum g_s capacity is limited by leaf anatomy traits (Franks et al., 2009; Franks and Farquhar, 2001). Potentially, higher g_s levels can be promoted by adjustments in the number and size of stomata that develop in the epidermis, leading to an increase in the anatomical maximum rate of stomatal conductance (g_{smax}) (Dow and Bergmann, 2014). Variation in these stomatal traits may occur due to growth under different environmental conditions, but also due to genetic factors. Although it is not known whether the pathways regulating stomatal size and density are connected, a negative correlation has often been observed between these traits, with various studies reporting increases in stomatal density coupled with decreases in stomatal size, and vice versa (de Boer et al., 2012; Dittberner et al., 2018; Doheny-Adams et al., 2012; Franks and Beerling, 2009; Sun et al., 2014).

3.1.1. Altering stomatal development

Studies on stomatal development have shown that it is possible to manipulate the number of stomata that develop in the epidermis by altering the expression of Epidermal Patterning Factors (EPFs). In Arabidopsis, the cysteine-rich signalling peptides, AtEPF1,

AtEPF2 and AtEPFL9, regulate stomatal patterning by acting as ligands to members of the ERECTA family of receptors (AtER, AtERL1 and AtERL2) and to the receptor-like protein AtTMM (Lee et al., 2015). In association with somatic embryogenesis receptor kinases (SERKs), this complex regulates a mitogen-activated protein kinase (MAPK) cascade that culminates in the modulation AtSPCH function (Lampard et al., 2008; Lee et al., 2015; Meng et al., 2015). AtEPF2 acts to prevent stomatal lineage entry and meristemoid amplifying divisions, whereas, AtEPF1 acts later enforcing at least one cell spacing between stomata (Hara et al., 2007; Hunt and Gray, 2009; Kumar Jewaria et al., 2013). In contrast, AtEPFL9 promotes stomatal development by competing for the same receptors as AtEPF1 an AtEPF2 (Lee et al., 2015). Consequently, the overexpression of *AtEPF1* or *AtEPF2* leads to a decrease in stomatal density (Hara et al., 2007; Hunt and Gray, 2009), while the overexpression of *AtEPFL9* causes an increase in stomatal density and also in the formation of stomatal clusters (Hunt et al., 2010; Sugano et al., 2010). Studies in Arabidopsis with altered expression of EPFs and substantial increases in stomatal density revealed that, despite decreases in stomatal size, these plants have a higher g_{smax} and an associated increase in operational g_s (Franks et al., 2015; Tanaka et al., 2013). In addition, analyses under different CO_2 concentrations suggested a potential improved evaporative cooling in these plants (Doheny-Adams et al., 2012).

Functional orthologs of these EPF family members are present in grass species, and likewise, changes in their expression lead to changes in stomatal densities (Caine et al., 2019; Dunn et al., 2019; Hughes et al., 2017a; Lu et al., 2019; Mohammed et al., 2019). Recently, the potential to improve water use efficiency and drought tolerance in barley, wheat and rice, by overexpressing the *AtEPF2* ortholog (denominated *EPF1* in grasses), has been explored with encouraging results (Caine et al., 2019; Dunn et al., 2019; Hughes et al., 2017b). In transgenic rice plants, a moderate reduction in leaf stomatal density (~58%) improves water conservation without negative impacts on photosynthesis or grain yield (Caine et al., 2019; Mohammed et al., 2019). The physiological consequences of enhancing stomatal densities in grasses have been less fully explored. A study of rice overexpressing *OsEPFL9a* produced plants with up to ~28% increase in the number of stomata in leaves (Mohammed et al., 2019). Likewise, in Schuler et al. (2018), rice plants with similar increases in stomatal density were produced by expanding the expression domain of *SHORTROOT2*, and thereby promoting the development of additional stomatal files. Both studies showed that the development of more stomata in the leaf epidermis did not result in improved operational gas exchange rates. Nonetheless, the responses of these

plants were analysed under optimal conditions, and it is yet to be investigated if they show an advantageous response under heat stress.

Whilst increases in stomatal density might improve transpiration-mediated cooling, the trade-off of a less efficient use of water must be considered, as heat and drought stresses often occur simultaneously. Greater yield declines are observed when rice plants experience above optimal temperatures during the reproductive phase. Therefore, targeting the increase in evaporative cooling capacity to this phase of the rice life cycle would avoid an unnecessary increase in water use during the vegetative growth. The presence of stomata was previously reported in rice florets (Ebenezer et al., 1990) yet, little is known about their distribution and function in the different rice floral organs, or whether they contribute to transpiration-mediated cooling of rice florets.

3.1.2. Objectives

In this chapter, an initial characterization of plants of the IR64 lowland rice cultivar overexpressing the *OsEPFL9a* gene was conducted. Stomatal traits and gas exchange capacity of two independent transgenic lines were investigated, with a focus on their potential for an increased stomatal conductance and evaporative cooling. To investigate the possibility of enhancing evaporative cooling in the heat-sensitive rice florets, the occurrence of stomata in different floral organs was characterized in IR64 control plants. This was followed by stomatal density analyses in anthers and lemma of transgenic plants overexpressing either *OsEPFL9a* or *OsEPF1*.

3.2. Results

3.2.1. Stomatal density in leaves of rice plants overexpressing *OsEPFL9a*

In order to produce rice plants with increased number of stomata, the International Rice Research Institute in the Philippines (IRRI) genetically modified plants of the *Indica* rice cultivar IR64 to ectopically overexpress the gene *OsEPFL9a* under the control of the maize ubiquitin promoter. The overexpression construct was transformed into rice via *Agrobacterium tumefaciens*-mediated transformation using immature embryos, with subsequent regeneration of transformed material by tissue culture methods (Hiei and Komari, 2008). Two of the independent transgenic lines produced at IRRI, designated OsEPFL9a-oe-2 and OsEPFL9a-oe-3, were characterized in this study using either T_2 or T_3 generation plants. PCR was used to check that transformed plants carried the *OsEPFL9a* overexpression construct (as described in Methods Section 2.3). Control IR64 plants that had been through the same tissue regeneration process, but without agrobacterium infection (therefore do not contain a transgene), were included in each experiment. In this study, they will be referred as either IR64 or IR64-control.

RT-qPCR analyses of *OsEPFL9a* transcript levels in leaves of 8-day old seedlings confirmed that both transgenic lines overexpressed *OsEPFL9a* (Figure 3.1 A). The line OsEPFL9a-oe-2 showed the highest expression levels, in average 10 times higher than the control, whilst OsEPFL9a-oe-3 showed a 4.5-fold increase in *OsEPFL9a* expression. To investigate if this increase in *OsEPFL9a* expression led to changes in stomatal development, the stomatal density of the transgenic rice lines was compared to the IR64-control plants. Measurements were taken from resin impressions of the abaxial epidermal surface of fully expanded leaves in different plant growth phases: seedling stage (leaf 2, first leaf to emerge after the coleoptile, ~8-day-old seedling), early vegetative growth (leaf 6, fifth leaf after coleoptile, ~21-day-old plant) and reproductive stage (flag leaf, ~ 90-day-old plant). The transgenic line OsEPFL9a-oe-2 showed a significant increase in stomatal density in all leaves analysed (Figure 3.1 B-D). OsEPFL9a-oe-3 rice plants showed a statistically significant higher stomatal density only in leaf 6; however, a trend towards an increase was also observed in leaf 2 and in flag leaves (Figure 3.1 B-D).

The number of stomata present in the fully expanded leaf epidermis was much higher in flag leaves than in leaves of earlier growth phases, such as leaf 2 and 6. In leaf 2 of IR64-control, there were an average of 125.2 stomata per mm^2, in leaf 6 this number increased to 188, whilst in flag leaves, an average of 778 stomata were found in the same

leaf area (Figure 3.2). The increase in the number of stomata per mm^2 in the transgenic lines seems to be similar in the different leaves; in OsEPFL9a-oe-2 there was an average increase of approximately 30-55 stomata per mm^2 and in OsEPFL9a-oe-3 there was an increase of approximately 20-40 stomata per mm^2. Therefore, the proportion of increment is higher in the earlier growth phases analysed. In leaf 2, OsEPFL9a-oe-2 and OsEPFL9a-oe-3 showed an enhancement in mean stomatal density of 25% and 18%, respectively, in comparison to controls. In leaf 6 the average increase was of 29% and 21%, however in flag leaves, an increase of only 7% and 4% was observed. In all IR64-control leaves analysed, a minimum of one pavement cell separated stomata in the same epidermal files, and there were no indications of a change in this spacing regulation in the transgenic plants, therefore stomatal clustering was not quantified.
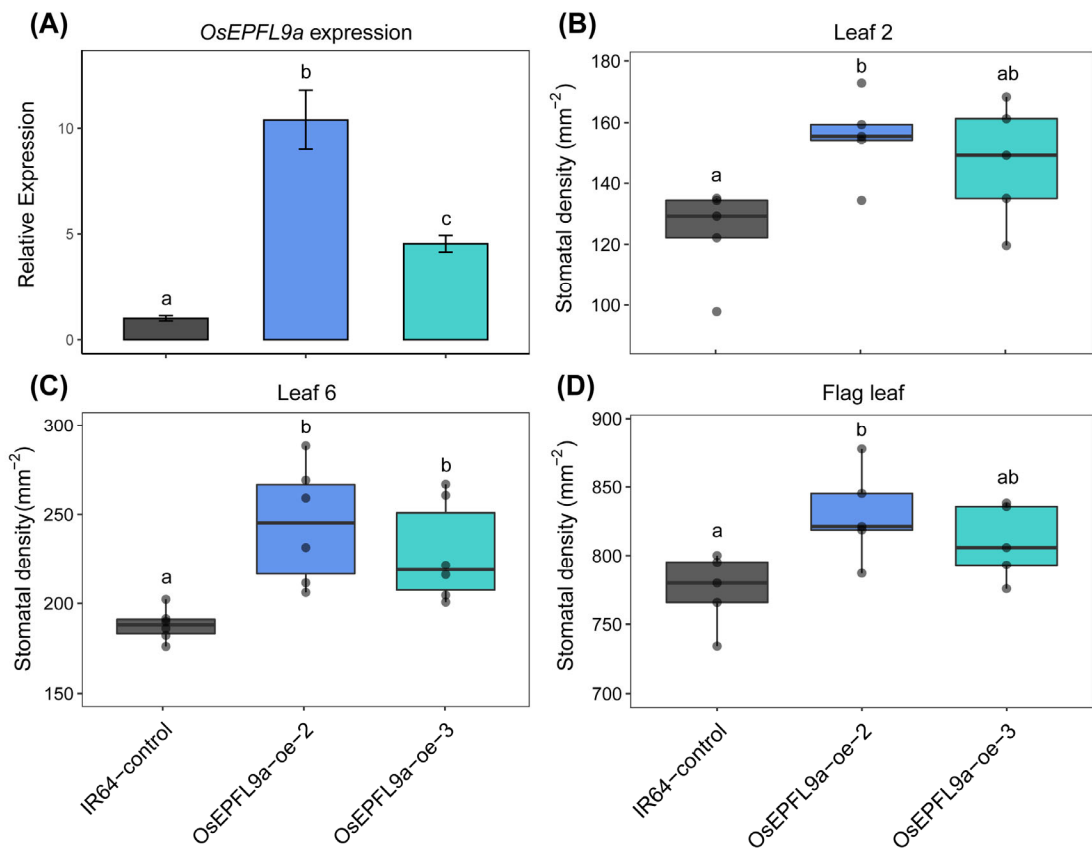
Figure 3.1. Overexpression of *OsEPFL9a* and abaxial stomatal densities of transgenic rice lines in comparison to control. **(A)** Expression levels of *OsEPFL9a* relative to IR64-control plants, error bars represent the standard error of the mean, n = 3 plants. **(B-D)** Boxplots of stomatal densities in abaxial leaf epidermis; individual points show the average value for each biological replicate, boxes limits display the first and the third quartiles, and the horizontal bars in the boxes represent the medians. **(B)** Leaf 2, n = 5 plants; **(C)** Leaf 6, n = 6 plants; **(D)** Flag leaf, n = 5 plants. **(A-D)** Different letters represent significant different groups (p-value < 0.05). **(A, B and D)** One-way ANOVA and a post hoc Tukey's test were performed to evaluate differences between groups. **(C)** Due to a non-homogenous variance in the data, Welch one-way test and the Games-Howell post hoc test were performed.
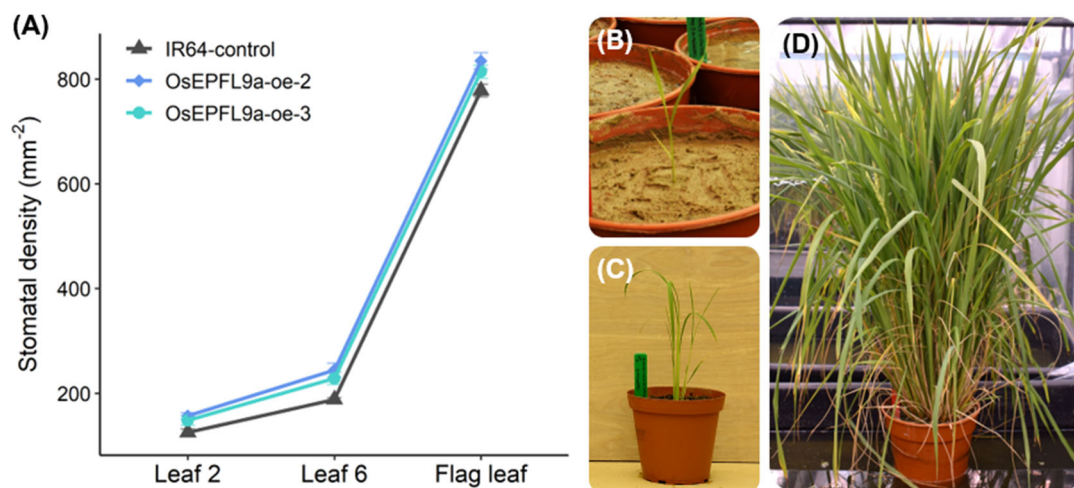
Figure 3.2. Leaf stomatal density varies in different growth phases. **(A)** Stomatal density in each rice genotype varies between different leaves. **(B-D)** Representative pictures of each of the growth phases in which stomatal density was analysed, **(B)** seedling, **(C)** early vegetative growth and **(D)** reproductive growth.

3.2.2. Stomatal size and g_{smax} in leaf 6 of rice lines overexpressing *OsEPFL9a*

Often adjustments to stomatal density are linked to changes in stomatal size. These anatomical traits influence leaf maximum stomatal conductance capacity, having an impact on operational gas exchange rates. To investigate if OsEPFL9a-oe rice lines showed differences in stomatal size, measurements of guard cell length and width were taken from resin impressions of the abaxial and adaxial epidermal surfaces of fully expanded leaf 6. These values were then used to estimate guard cell pair area. Additionally, measurements of pore length, stomatal density and guard cell width (taken from the same plants, from both adaxial and abaxial leaf surfaces) were used to calculate the theoretical leaf maximum stomatal conductance (g_{smax}), which is an estimate of the maximal potential gas exchange in a state where all stomata are fully open.

Despite the increase in stomatal density of leaf 6 in OsEPFL9a-oe-2 and OsEPFL9a-oe-3 rice lines, no statistically significant changes in guard cell area or in stomatal pore length were detected (Figures 3.3 A, B and E). Measurements of guard cell length and width revealed that OsEPFL9a-oe-3 plants had significant shorter stomatal cells than the IR64 control, whereas a trend towards an increase in guard cells width and a decrease in length was observed in OsEPFL9a-oe-2 (Figure 3.3 C and D). The estimate of g_{smax} indicated that the rice lines overexpressing *OsEPFL9a* had an average increase of ~ 23-29% in anatomical stomatal conductance capacity (Figure 3.3 F), which was mainly

driven by the increment in stomatal numbers in the leaf epidermis. With regards to variation between abaxial and adaxial epidermis of leaf 6 in each genotype, no differences were observed in stomatal density, however small differences were found in other anatomical measurements, resulting in a g_{smax} that was 7 to 10 % higher in the adaxial surface in all genotypes (data not shown).
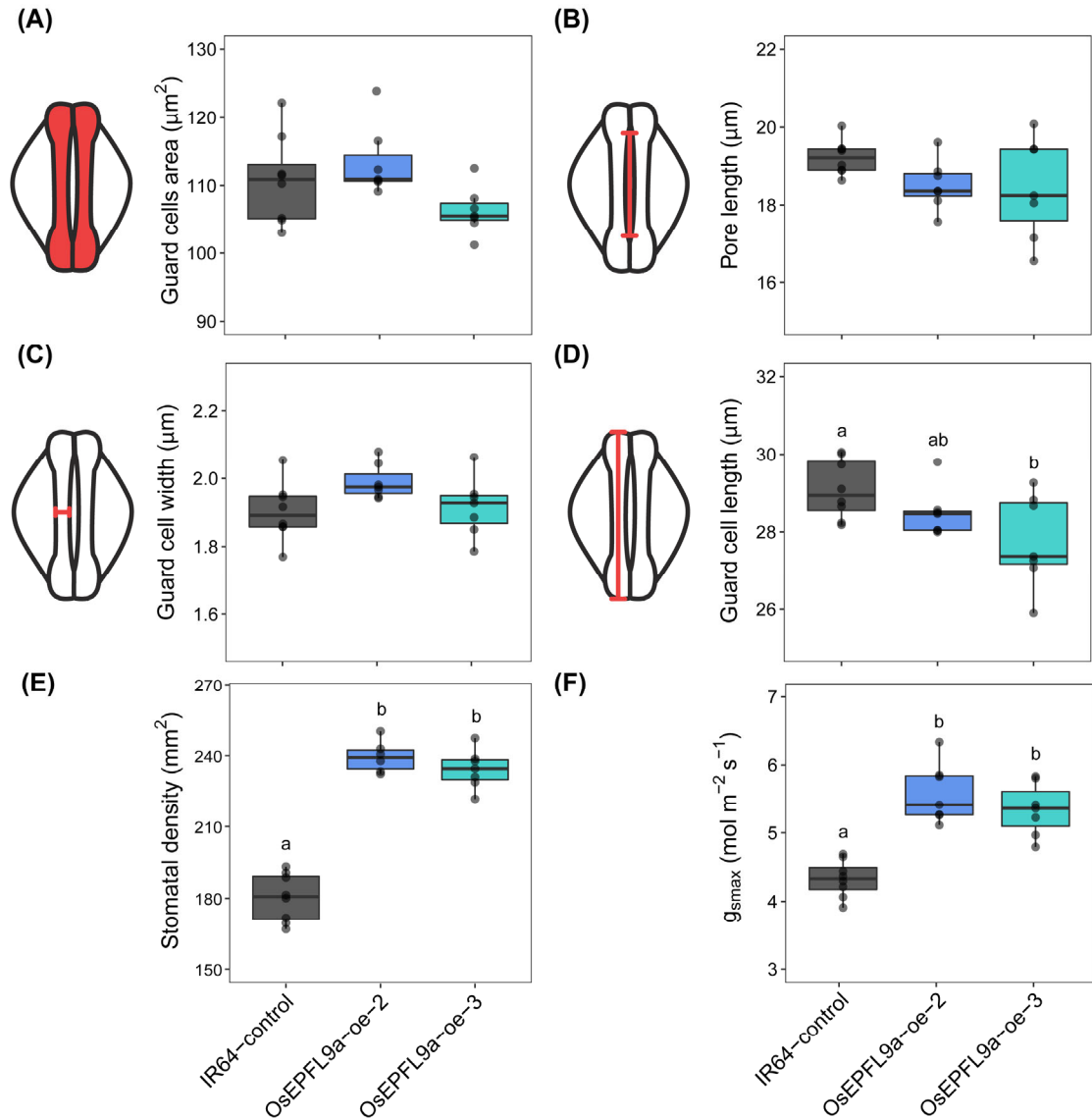
Figure 3.3. Anatomical data of stomata and estimated g_{smax} in leaf 6 of OsEPFL9-oe lines in comparison to IR64-control. **(A-D)** Anatomical data from combined abaxial and adaxial epidermal surfaces of leaves. **(A)** Guard cell pair area; calculated by using guard cell length and width data. **(B)** Pore length. **(C)** Guard cell width. **(D)** Guard cell length. **(E)** Stomatal density. **(F)** Maximum stomatal conductance values estimated for each line. **(D-F)** Different letters represent significant different groups, n = 7-8 plants, (E-F) $p < 0.001$, (D) $p < 0.05$. **(A-C)** There were no significant differences between groups ($p > 0.05$), n = 7-8 plants. **(A, C-F)** One-way ANOVA and a post hoc Tukey's test were performed to evaluate differences between groups. **(B)** Due to a non-homogenous variance in the pore length data, Welch one-way test was performed to evaluate differences between groups.

3.2.3. Stomatal conductance and carbon assimilation of lines overexpressing OsEPFL9a under different light intensities

To test whether the enhanced theoretical g_{smax} of OsEPFL9a-oe-2 and OsEPFL9a-oe-3 was translated into an increased operational stomatal conductance, gas exchange rates of these transgenic lines were experimentally investigated. Analyses were conducted on fully expanded leaf 6, using an infrared gas analyser (IRGA) (LI-6800, LI-COR Biosciences). Plants were grown under a 12h photoperiod, at 30 °C/ 24 °C day/night temperature, 850 μmol m^{-2} s^{-1} light (at canopy level), 60% relative humidity and CO_2 concentration of ~ 450-480 ppm (not controlled). The infrared gas analyser leaf chamber was set to conditions similar to the growth room (60% RH, 480 ppm CO_2) and leaf temperature was maintained at 30 °C. Steady-state measurements were taken under 2000 μmol m^{-2} s^{-1} PAR, whilst a light-response curve analysis was conducted under decreasing light intensity: 2000, 1500, 1200, 1000, 800, 600, 480, 340, 200, 150, 100, 75, 50, 25 and 0 μmol m^{-2} s^{-1} PAR (refer to Methods 2.7 for more details).

Despite showing a greater theoretical g_{smax}, the gas exchange analysis suggested that the lines overexpressing *OsEPFL9a* had similar stomatal conductance (g_s) rates to those of the IR64-control plants under the conditions tested (Figure 3.4 A). Although OsEPFL9a-oe-3 rice showed an increasing trend over the different light intensities, the g_s levels observed were quite variable between plants. This is better illustrated in Figure 3.4 B, where individual leaf stomatal densities are compared to the g_s measurements under steady-state conditions. A linear regression analysis indicated that there was no association between stomatal density and g_s rates in this dataset (Figure 3.4 B). In addition to that, analysis of the carbon assimilation levels showed that the transgenic lines responded very similarly to the control under different light intensities, being able to reach equivalent photosynthetic rates (Figure 3.4 C).
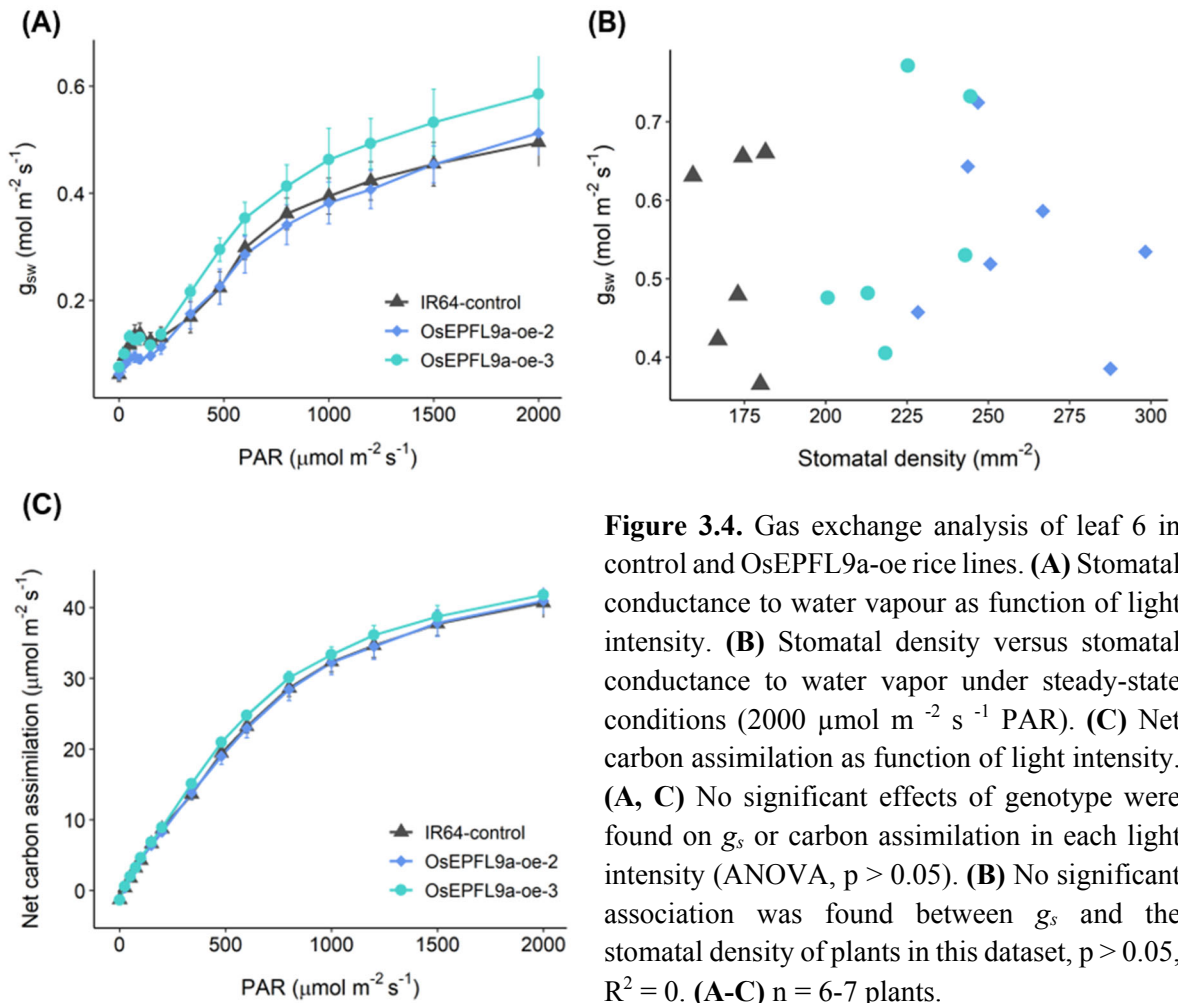
Figure 3.4. Gas exchange analysis of leaf 6 in control and OsEPFL9a-oe rice lines. **(A)** Stomatal conductance to water vapour as function of light intensity. **(B)** Stomatal density versus stomatal conductance to water vapor under steady-state conditions (2000 μmol m^{-2} s^{-1} PAR). **(C)** Net carbon assimilation as function of light intensity. **(A, C)** No significant effects of genotype were found on g_s or carbon assimilation in each light intensity (ANOVA, $p > 0.05$). **(B)** No significant association was found between g_s and the stomatal density of plants in this dataset, $p > 0.05$, $R^2 = 0$. **(A-C)** n = 6-7 plants.

3.2.4. Gas exchange response to increased temperatures in lines overexpressing *OsEPFL9a*

To further investigate whether rice plants overexpressing *OsEPFL9a* can achieve greater stomatal conductance, gas exchange analyses were performed under increased temperature conditions. An infrared gas analyser (LI-6800, LI-COR Biosciences) was used to measure gas exchange on fully expanded leaf 6 of rice plants. The same set of plants were used in this experiment as for the g_{smax} estimation presented in section 3.2.2. Plants were grown under a 12h photoperiod, at 30 °C/ 24 °C day/night temperature, 850 μmol m^{-2} s^{-1} light (at canopy level), 60% relative humidity and ~ 450-480 ppm CO_2 (not controlled). Measurements were taken with the IRGA chamber set to 2000 μmol m^{-2} s^{-1}, 60% RH, 480 ppm CO_2 and increasing air temperatures of 30, 32.5, 35 and 37.5 °C (for more details refer to Method 2.7.3).

The data analysis revealed that stomatal conductance increased with the rise in temperature, and that this response was similar for all genotypes (Figure 3.5). In this

experiment, the line OsEPFL9a-oe-3 showed an overall higher stomatal conductance, compared to both OsEPFL9a-oe-2 and to IR64-control, despite a large variation in g_s rates between plants of the same genotype. No differences were found between OsEPFL9a-oe-2 and IR64-control, although this transgenic line showed the greater increase in stomatal density. Similar results were observed for the transpiration rates (Figure 3.6 A). In terms of photosynthesis, the changes in temperature did not have a significant impact on its rates (Figure 3.6 B). However, a significant difference was found between the two transgenic lines, but not between transgenics and controls.

Since the IRGA chamber was set to adjust air temperature in this experiment (not leaf temperature, as set for the light curve experiment), the leaf temperature data was analysed to check if there was any variation between the rice genotypes. All lines responded in a similar way to the increase in temperature, however, both transgenic lines showed a significantly lower temperature in comparison to the control (Figure 3.6 C). Although statistically significant, this difference was small, especially for OsEPFL9a-oe-2. In this transgenic line, the leaf temperature average was 0.2-0.36 °C lower than the IR64-control, depending on the temperature treatment. For OsEPFL9a-oe-3 rice plants, the difference in average leaf temperature was larger, with a decrease of 0.57-0.86 °C, depending on the temperature treatment.
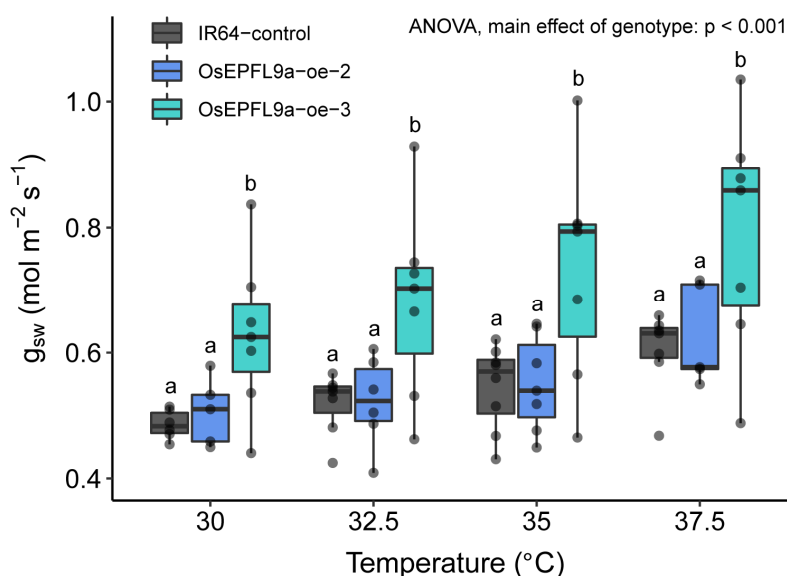
Figure 3.5. Stomatal conductance of leaf 6 in control and OsEPFL9a-oe rice lines under different temperatures. A two-way ANOVA was conducted to test for the effects of the factors genotype and temperature on g_s. A significant interaction between the effects of both factors on g_s was not found (p > 0.05). Main effect analysis showed that genotype (p < 0.001) and temperature (p < 0.0001) impacted independently on g_s. Tukey's multiple comparisons test indicated a significant difference between OsEPFL9a-oe-3 and the other two genotypes (p < 0.0001). Letters in the plot represent Tukey's test result for the factor genotype. Number of plants per genotype: 30 °C n = 7-8; 32.5 °C n = 7-8, 35 °C n = 7-8, 37.5 °C n = 5-7 plants.

(A)

(B)

(C)
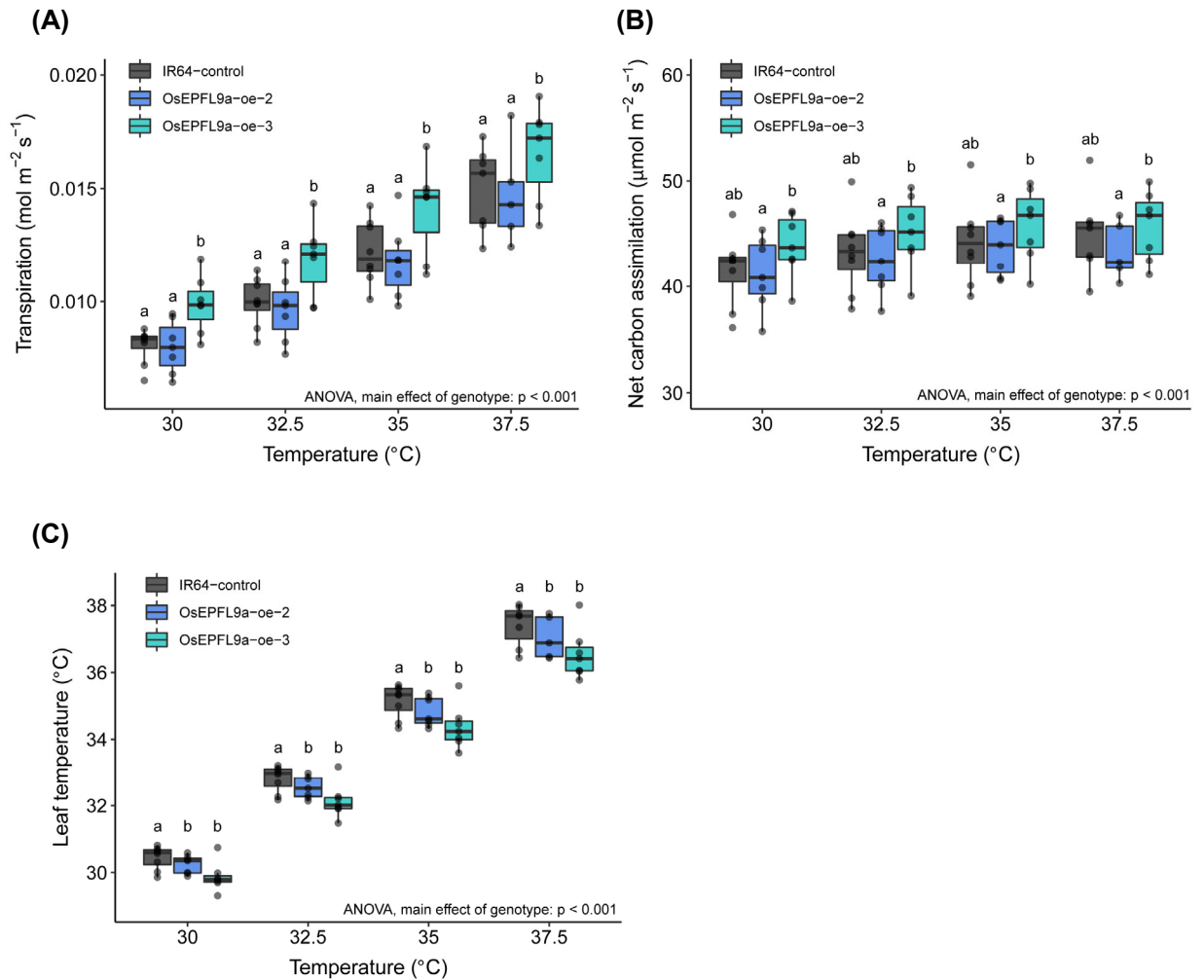
Figure 3.6. (A) Transpiration rates, **(B)** Net carbon assimilation and **(C)** leaf temperature in control and OsEPFL9a-oe rice lines under different temperatures. A two-way ANOVA was conducted to examine the effects of the factors genotype and temperature on the physiological variables. **(A)** There was not a statistically significant interaction between the effects of both factors on transpiration ($p > 0.05$). Main effect analysis showed that genotype ($p < 0.001$) and temperature ($p < 0.0001$) impacted independently on transpiration rates. Tukey's multiple comparisons test indicated a significant difference between OsEPFL9a-oe-3 and the other two genotypes ($p < 0.0001$). Letters in the plot represent Tukey's test result for the factor genotype. **(B)** There was not a statistically significant interaction between the effects of both factors on net carbon assimilation ($p > 0.05$). Main effect analysis detected a significant impact of the rice genotype ($p < 0.05$), but not of temperature ($p > 0.05$), on carbon assimilation rates. Post-hoc Tukey's test indicated a significant difference between OsEPFL9a-oe-2 and OsEPFL9a-oe-3 ($p < 0.05$). **(C)** There was not a significant interaction between the effects of genotype and temperature ($p > 0.05$). Main effect analysis showed that genotype ($p < 0.001$) and temperature ($p < 0.0001$) impacted independently on leaf temperature. Tukey's test indicated a significant difference between OsEPFL9a-oe-2 and IR64-control ($p < 0.01$), and between OsEPFL9a-oe-3 and IR64-control ($p < 0.0001$). Letters in the plot represent Tukey's test result for the factor genotype. **(A-C)** Plants per genotype: 30 °C n = 7-8 plants; 32.5 °C n = 7-8 plants, 35 °C n = 7-8 plants, 37.5 °C n = 5-7 plants.

3.2.5. Leaf temperature of *OsEPFL9a* overexpressing lines

To further evaluate the differences on leaf temperature, preliminary investigations were conducted using a thermal imaging camera (FLIR T650SC) under standard and increased growth room temperature. Control and transgenic rice lines were grown at 30 °C (other conditions were equivalent to those described above) and imaged at increasing growth room temperatures, with steps of 30, 32.5, 35 and 37.5 °C (for more details refer to Methods 2.2.2 and 2.9.1). Two different methods were used to perform this analysis. In the first approach (here designated Setup 1), 15 rice seedlings were grown in the same small pot. Each pot had only plants of a specific rice genotype, which was considered as a biological replicate. Four pots per line were used and plants were imaged 15 days after sowing. In Setup 1, the camera was positioned above the plant pots. In the second approach (Setup 2), plants were grown in individual pots, and each plant was treated as a biological replicate. Plants were imaged from their side, 17 days after sowing (leaf 4 stage). Two experiments were conducted using each Setup.

The results varied between experiments. In Setup 1, the first experiment showed that there were no differences in leaf temperature between rice lines (Figure 3.7 A). However, results from the second experiment (performed in the same way), suggested that temperature was significantly lower in the transgenic lines, although differences were small (Figure 3.7 B). To minimise potential variation caused due to differences in the way the multiple plants grew in each pot, and also to improve the standardization between measuring spots in the thermal images, two experiments were performed using Setup 2. Results differed again in these experiments. In the first attempt (Figure 3.8 A), both transgenic lines had a significant lower temperature compared to the IR64-control plants. However, in the second experiment (Figure 3.8 B), only the rice line OsEPFL9a-oe-3 showed lower leaf temperature in comparison to the control. This variation in the results obtained, might indicate that if a difference in leaf temperature indeed exists between the different genotypes, this is not consistent or large enough to be always detected in the conditions here tested.
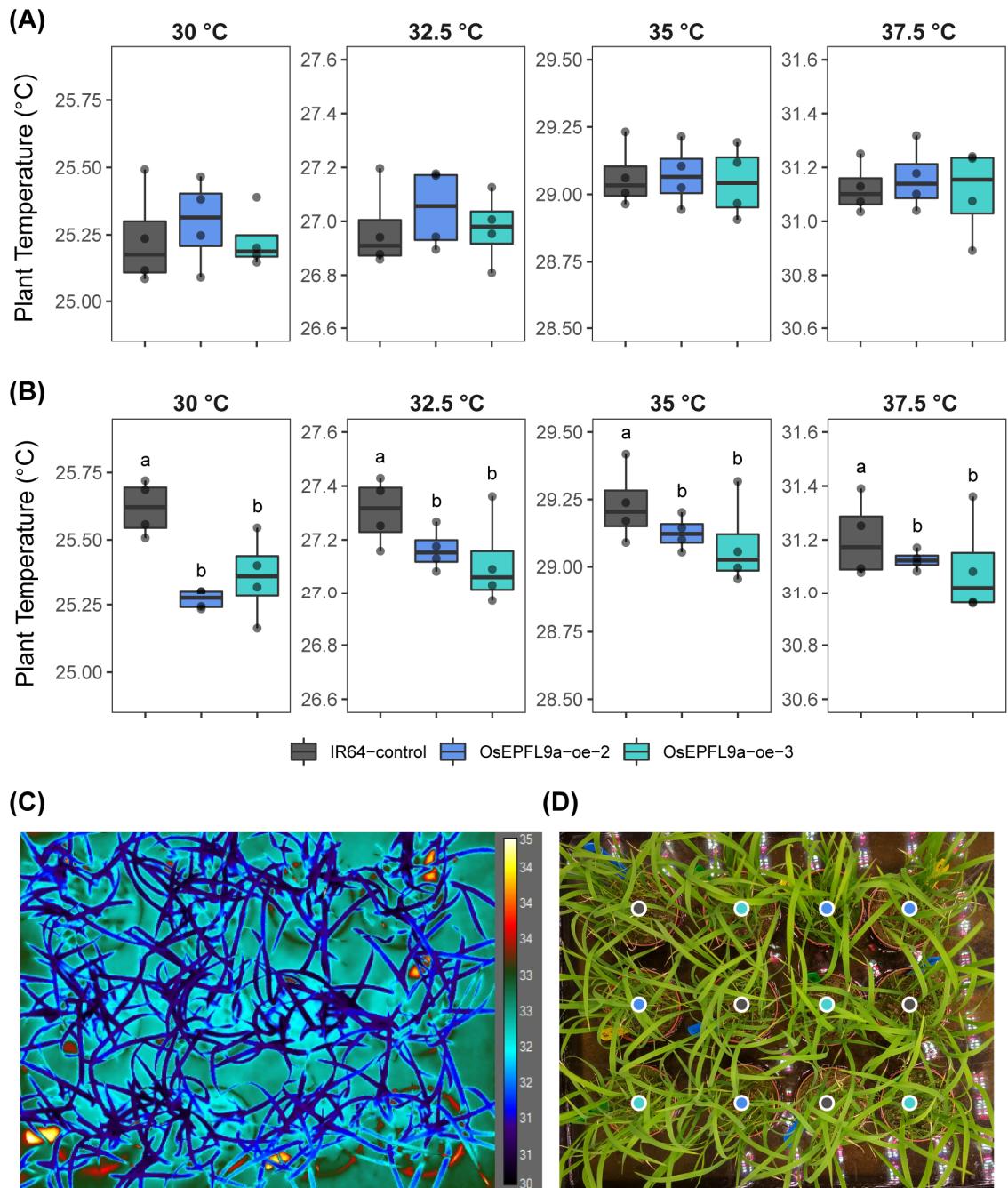
Figure 3.7. Thermal imaging analysis using Setup 1. **(A)** Experiment 1. **(B)** Experiment 2. **(A-B)** Growth room temperature is shown on top of each plot in both panels. Y-axis scale varies between plots. A Two-way ANOVA was performed for each experiment to test the effects of genotype and room temperature on leaf temperature. Four biological replicates per genotype, per experiment. **(A)** No significant differences were found (p-value > 0.05). **(B)** There was not a significant interaction between the effects of genotype and growth room temperature (p > 0.05). The main effect analysis showed that genotype (p < 0.01) and growth room temperature (p < 0.001) impacted independently on leaf temperature. Post hoc Tukey's test indicated a statistically significant difference between both transgenic lines and the IR64-control (p < 0.05). Letters in the plot represent Tukey's test result for the factor genotype. **(C)** Representative thermal image of Setup 1 at 37.5 °C. **(D)** Picture corresponding to thermal imaging in C, coloured circles on each plant pot indicate the rice genotype. Grey – IR64-control, Blue – OsEFL9a-oe-2, and Green - OsEFL9a-oe-3.

(A)

(B)

IR64−control   OsEPFL9a−oe−2   OsEPFL9a−oe−3

(C)

(D)
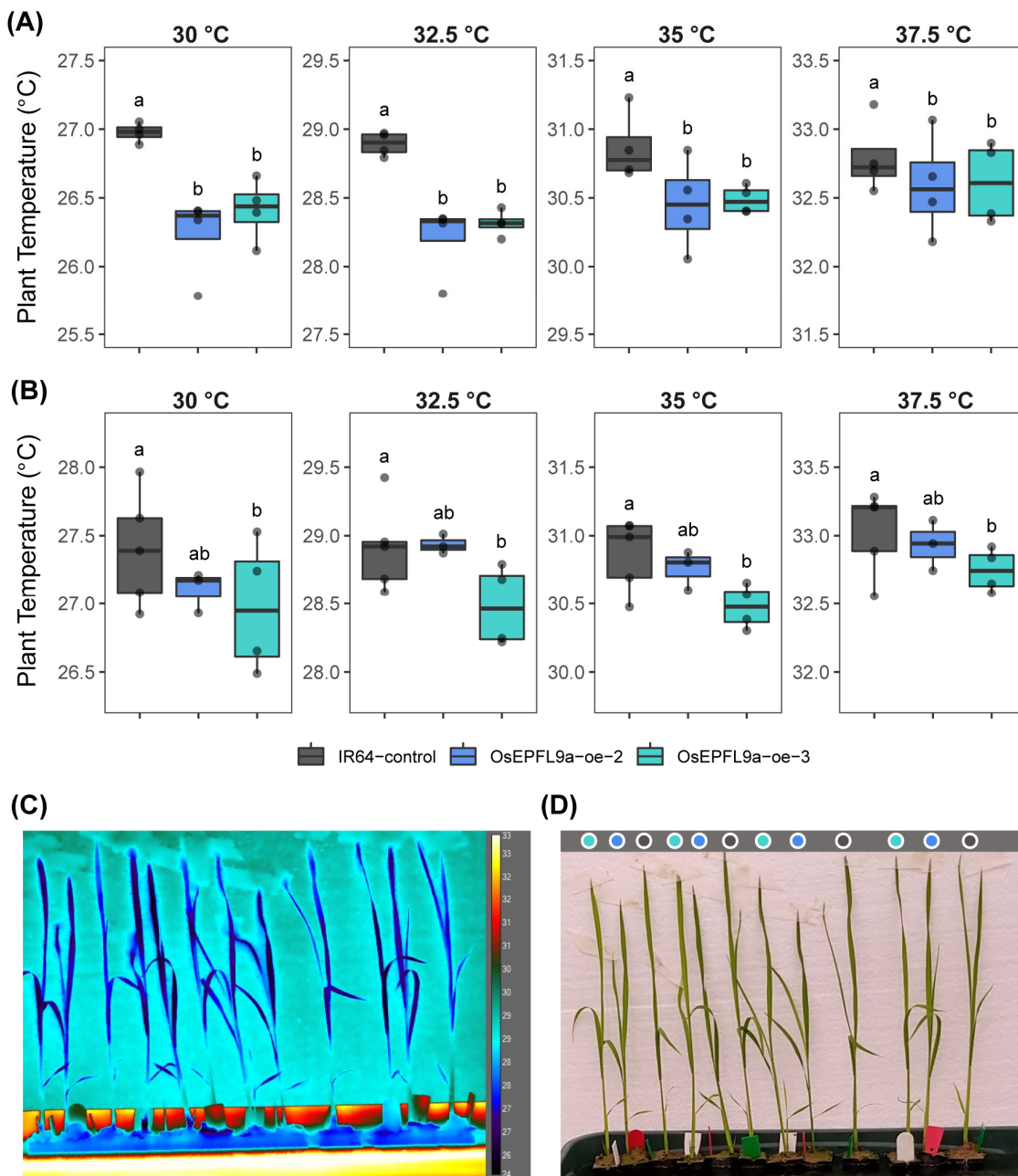
Figure 3.8. Thermal imaging analysis using Setup 2. **(A)** Experiment 1, n = 4 plants per line. **(B)** Experiment 2, n = 3-4 plants per line. **(A-B)** Growth room temperature is shown on top of each plot in both panels. Y-axis scale varies between plots. A two-way ANOVA was performed for each experiment to test the effects of the factors genotype and room temperature on leaf temperature. **(A)** A significant interaction between the effects of both factors was not found ($p > 0.05$). The main effect analysis showed that genotype ($p < 0.001$) and growth room temperature ($p < 0.001$) impacted independently on leaf temperature. Post hoc Tukey's test indicated a statistically significant difference between both transgenic lines and the IR64-control ($p < 0.001$). **(B)** A significant interaction between the effects of genotype and growth room temperature was not found ($p > 0.05$). The main effect analysis showed that genotype ($p < 0.01$) and growth room temperature ($p < 0.001$) impacted independently on leaf temperature. Tukey's test indicated a statistically significant difference between OsEPFL9a-oe-3 and the IR64-control ($p < 0.01$). **(C)** Representative thermal image of Setup 2 at 30 °C. **(D)** Picture corresponding to thermal imaging in C, coloured circles on top of each plant indicate rice plant genotype. Grey – IR64-control, Blue – OsEFL9a-oe-2, and Green - OsEFL9a-oe-3.

3.2.6. Characterization of stomatal distribution on rice florets

Rice and other grasses have a floral architecture very distinct from that of eudicot species. In rice, the inflorescence, also known as panicle, is formed by a rachis with around ten or more primary branches. From the primary branches, spikelets and secondary branches are formed. The spikelet, comprising glumes and florets, is the primary unit of the grass inflorescence (Figure 3.9 A). The number of florets in a spikelet varies among species. In rice, each spikelet comprises only one floret, which is formed by a pair of grass specific bract-like organs (called lemma and palea), lodicules, stamens and a carpel (Figure 3.9 B) (Ikeda et al., 2004; Yoshida and Nagato, 2011). To understand whether it might be possible to locally enhance the evaporative cooling of the heat-sensitive reproductive organs in rice plants by altering the stomatal density on these tissues, the presence of stomatal pores in rice florets was first investigated in IR64-control plants.

Using light and scanning electron microscopy (SEM), stomata were identified in different organs of IR64 rice florets (Figure 3.10). Stomatal complexes, comprising a pair of guard cells and a pair of subsidiary cells were found on both abaxial (outer) and adaxial (inner) epidermis of lemma and palea, and in different areas of the anthers; however, they were absent in pistils. Analysis of fresh tissue of fully expanded florets (prior to panicle heading) allowed the visualization of stomatal pores showing different aperture degrees (Figure 3.10 G-H). A functional analysis to investigate whether the floral stomata are able to control their aperture in response to environmental clues was not conducted.
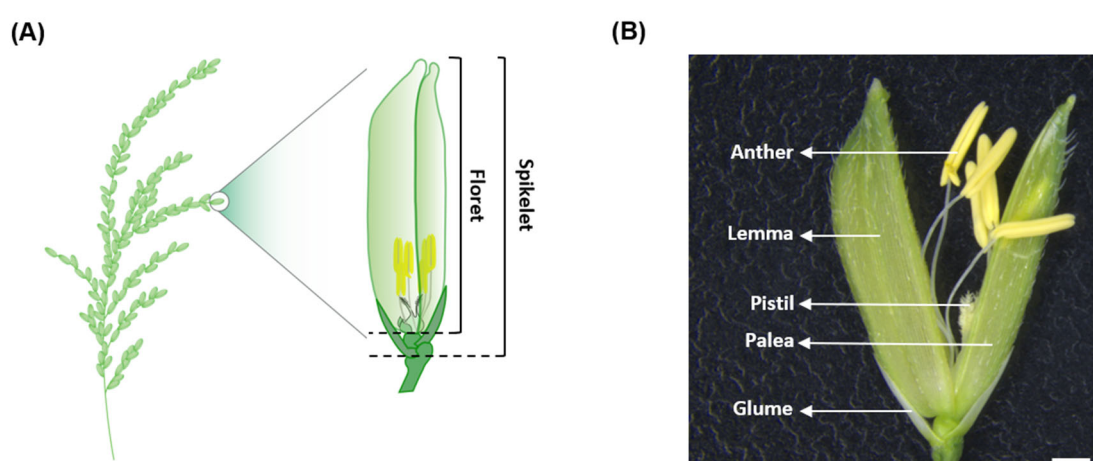
Figure 3.9. Floral architecture in rice. **(A)** Diagram showing a rice panicle and a zoom of a rice spikelet with one floret. **(B)** Image of a rice spikelet and its parts. Lodicules cannot be viewed in this image. Scale bar = 1 mm.
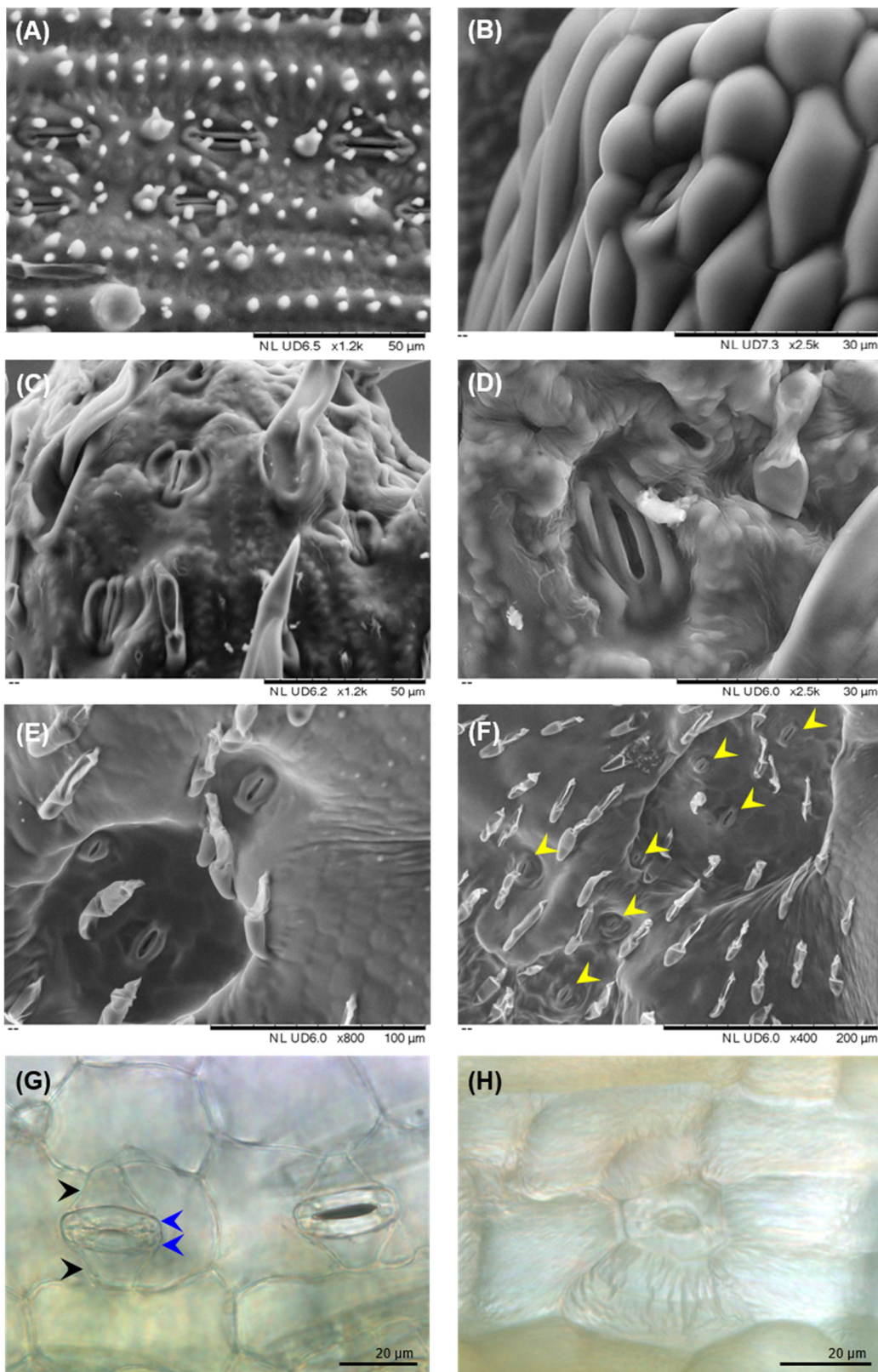
Figure 3.10. SEM **(A-F)** and light microscopy **(G-H)** images of stomata on the surfaces of various rice organs. **(A)** Rice leaf 6. **(B)** Rice anther. **(C-D)** Abaxial epidermal surface of lemma. **(E-F)** Adaxial epidermal surface of lemma, yellow arrowheads in (F) point to stomata. **(G)** Image from fresh tissue of lemma (adaxial), showing two stomatal pores with different aperture sizes. Black arrowheads indicate subsidiary cells and blue arrowheads indicate guard cells, 1000x magnification. **(H)** Image from fresh tissue of rice anther showing a stomatal complex, 1000x magnification.

To further characterize the spatial distribution of the stomata in the IR64 florets, a careful examination of rice lemma, palea and anthers was conducted. This analysis revealed that stomata were not uniformly distributed through the epidermis of these floral organs. Furthermore, where stomata were present, they were less abundant than normally observed on the epidermal surfaces of rice leaves. To summarize the observed pattern of stomatal distribution in the rice florets, representative diagrams were produced (Figures 3.11 and 3.12). As shown in the diagrams, stomata were found in very few areas of the abaxial (inner) surfaces of lemma and palea. In abaxial lemma, stomatal pores were observed at the tip and on the edges (close to the margins dividing abaxial and adaxial epidermis), whilst on abaxial palea, they were found only at the tips (Figures 3.11 A and 3.13 A-C). In contrast, on the adaxial (inner) surfaces of lemma and palea, stomata were found following the vasculature from base to top, being apparently more numerous towards the middle and upper regions. Although stomata were more abundant in the inner epidermal surfaces of the lemma and palea, their density was not comparable to that of rice leaves. In adaxial lemma, they were mainly found along the lateral, the central and the folding area (Figures 3.11 B and 3.13 D-F). In adaxial palea, stomata were also observed close to the lateral margins and along the folding region (Figures 3.11 B and 3.13 G-H). In the anthers, stomata were observed along the area between the two locules of the same thecae (close to the stomium region), and on the connective tissue between the two distinct thecae (Figures 3.12 and 3.14).

The shape and distribution of the stomatal pores in IR64 florets was noticeably distinct from that observed in leaves (Figure 3.10 A). Leaf stomatal complexes show a very regular contour in rice. They are formed by a pair of roughly triangular subsidiary cells that flank a pair of characteristic narrow dumbbell-shaped guard cells (Itoh et al., 2005). Stomata are usually present at high numbers in leaves, and are observed in specific rows of epidermal cells, and this organization within cell files is very pronounced. In contrast, in the rice florets, subsidiary cells had a quite variable format. This was particularly observed in anthers (Figure 3.14), however, the subsidiary cells of lemma and palea were also less homogeneous in shape than that normally seen in rice leaves (Figure 3.13). Moreover, guard cells of floral stomata had a more rounded shape compared to that of leaves. Although floral stomata were roughly vertically organized, the identification of epidermal cell files was difficult, since the pavement cells showed a large variation in size and shape (Figure 3.13).
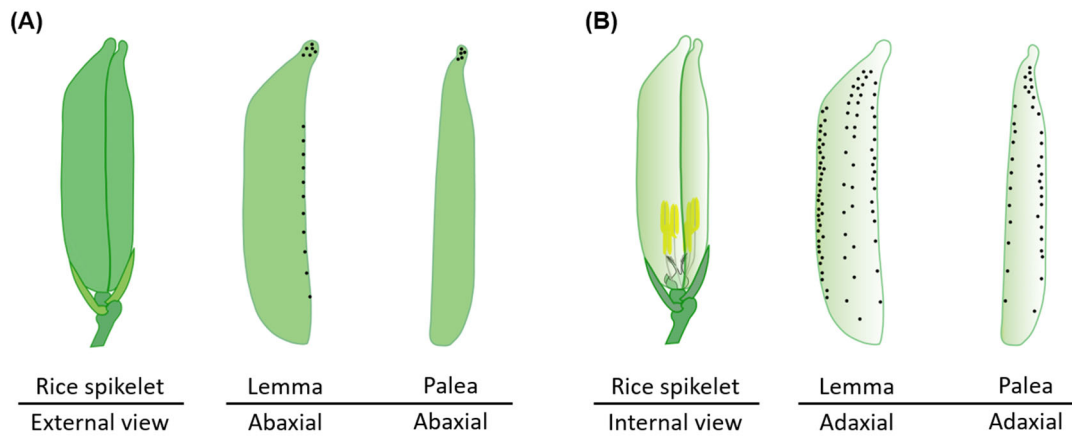
Figure 3.11. Distribution pattern of stomata on IR64 lemma and palea. **(A)** Diagram of a rice spikelet; and the individual representations of abaxial epidermal surfaces of lemma and palea, showing the distribution pattern of stomata on these floral organs. Black dots indicate the presence of stomata. **(B)** Diagram of the internal view of a rice spikelet; individual representations of adaxial epidermal surfaces of lemma and palea, showing the distribution of stomata on organ. Black dots indicate the presence of stomata, they indicate location but do not directly correlate to stomatal quantity.
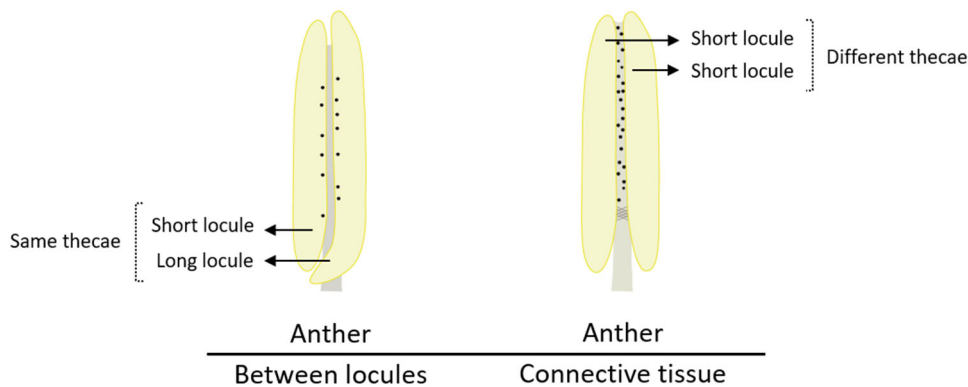
Figure 3.12. Distribution pattern of stomata in IR64 rice anthers. Black dots represent stomatal distribution. Rice anthers are composed by two thecae linked by a connective tissue. Each thecae has two locules, a long and a short one, connected by septum and stomium (Matsui et al., 1999). Stomatal pores were found between locules (close to the stomium area) and in the connective tissue that separates the two thecae. Black dots indicate location but do not direct correlate to stomatal quantity.
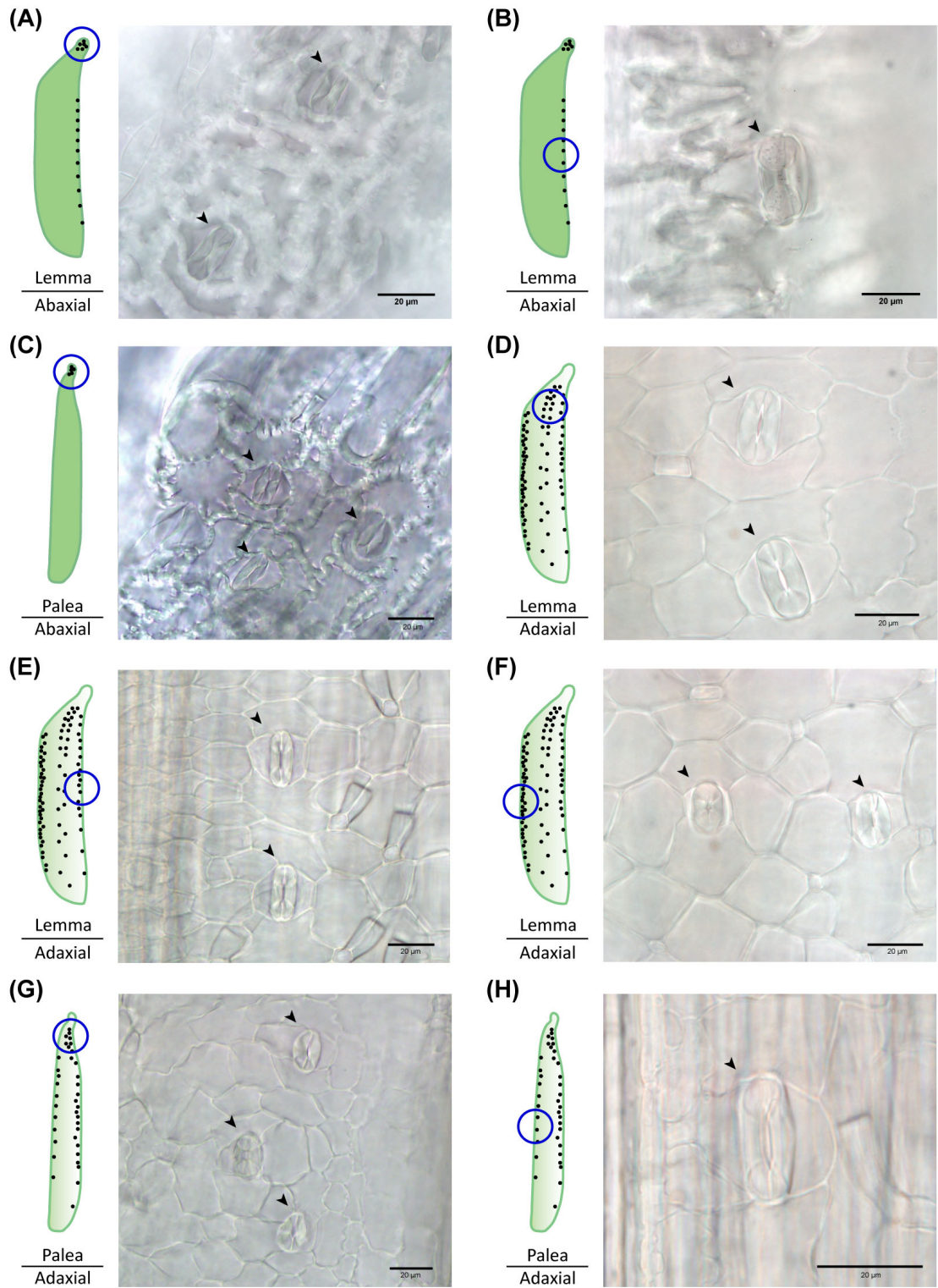
Figure 3.13. Light microscopy images of stomata on lemma and palea. Fully expanded florets were fixed in a solution of ethanol and acetic acid, then cleared in a chloral hydrate solution. **(A-B)** Abaxial epidermis of lemma. **(C)** Abaxial epidermis of palea. **(D-F)** Adaxial epidermis of lemma. **(G-H)** Adaxial epidermis of palea. **(A-H)** Blue circles on diagrams indicate the areas corresponding to each picture. Black arrowheads indicate stomata. Scale bars = 20 μm.
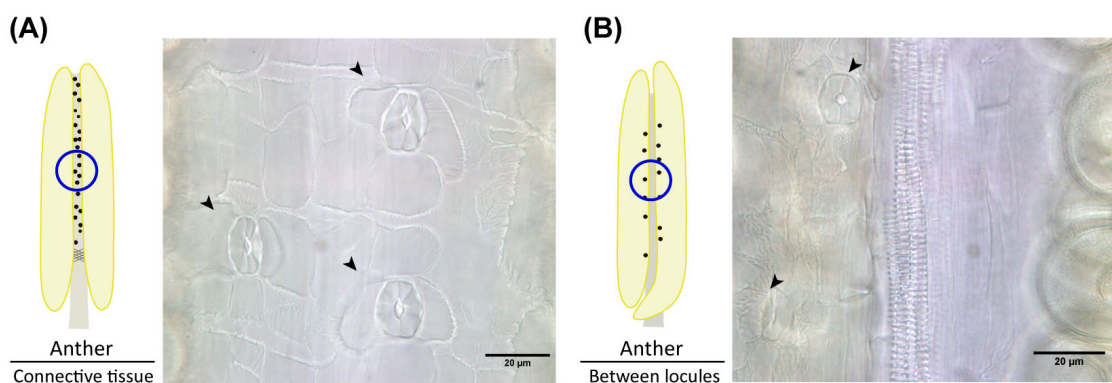
Figure 3.14. Light microscopy images of stomata on anthers. Fully expanded florets were fixed in a solution of ethanol and acetic acid, then cleared in a chloral hydrate solution. **(A)** Connective tissue between anther thecae. **(B)** Region between locules of the same thecae. Blue circles on diagrams indicate the areas corresponding to each picture. Black arrowheads indicate stomata. Scale bars = 20 µm, 1000x magnification.

3.2.7. Stomatal density in florets of rice lines overexpressing *OsEPFs*

To investigate whether the manipulation of *OsEPFs* expression could affect stomatal development in rice florets, the stomatal density of lemma and anthers was analysed in IR64-control and in transgenic rice lines overexpressing two different *OsEPF* genes. This analysis included two rice lines overexpressing *OsEPFL9a* (OsEPFL9a-oe-2 and OsEPFL9a-oe-3, described above in this chapter), in addition to two transgenic lines overexpressing the gene *OsEPF1*. Rice lines overexpressing *OsEPF1*, designated OsEPF1-oe-S and OsEPF1-oe-W, ectopically overexpress this gene under the control of the maize ubiquitin promoter, in the same Indica rice background (IR64). Both lines show strong reductions in leaf stomatal density and were previously characterized in Caine et al. (2019).

Analyses were conducted using tissue from fully expanded flowers, which were fixed and cleared as described in Methods section 2.5.1 and 2.5.2. Stomata were counted from two specific regions of adaxial epidermal surface of lemma, one in the upper area and another in the folding area (Figure 3.15 A-B). In anthers, all stomata present on one side of the connective tissue were counted (Figure 3.15 C). All transgenic lines investigated showed altered number of stomata on rice florets compared to IR64-control rice. The genotypes overexpressing *OsEPFL9a* had a significant increase in stomatal density in all areas investigated (Figures 3.16 and 3.17). In the upper area of the adaxial epidermis of the lemma, an average increase of ~ 126% and 72% were observed in OsEPFL9a-oe2 and OsEPFL9a-oe-3, respectively. This increase was of ~ 141% and 76% in the folding area of lemma and of ~ 90% and 94% in the connective tissue of anthers. Although stomatal

density was increased in the florets in OsEPFL9a-oe lines, the spatial distribution of stomata followed the same pattern as that described for IR64 floral organs, and stomata did not develop in additional areas of transgenic florets. In contrast, in the OsEPF1-oe lines stomata were absent from all anthers and folding area of lemmas analysed (Figure 5.16). In the upper area of lemma, stomata were also absent from the majority of fields viewed in plants overexpressing *OsEPF1*, but occasionally, a sole stomate was found. In this area of the lemma, the average stomatal density was 15.19 stomata per mm^2 in IR64-control plants, whilst in OsEPF1-oe-S and in OsEPF1-oe-W this number was reduced to, respectively, 0.3 and 0.06 stomata per mm^2.
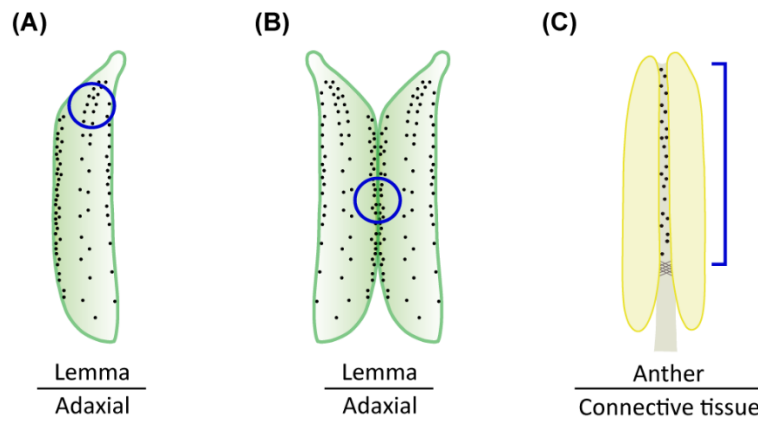
Figure 3.15. Diagrams indicating (in blue) the areas from which stomatal density measurements were taken. **(A)** Upper area of adaxial lemma epidermis, two equivalent field of views of 0.98 mm^2 were visualized per floret. **(B)** Folding area of adaxial lemma epidermis, a field of view of 0.98 mm^2 were visualized per floret. **(C)** Connective tissue of anther, all stomata were counted. Counts were normalized by the length of the connective tissue.
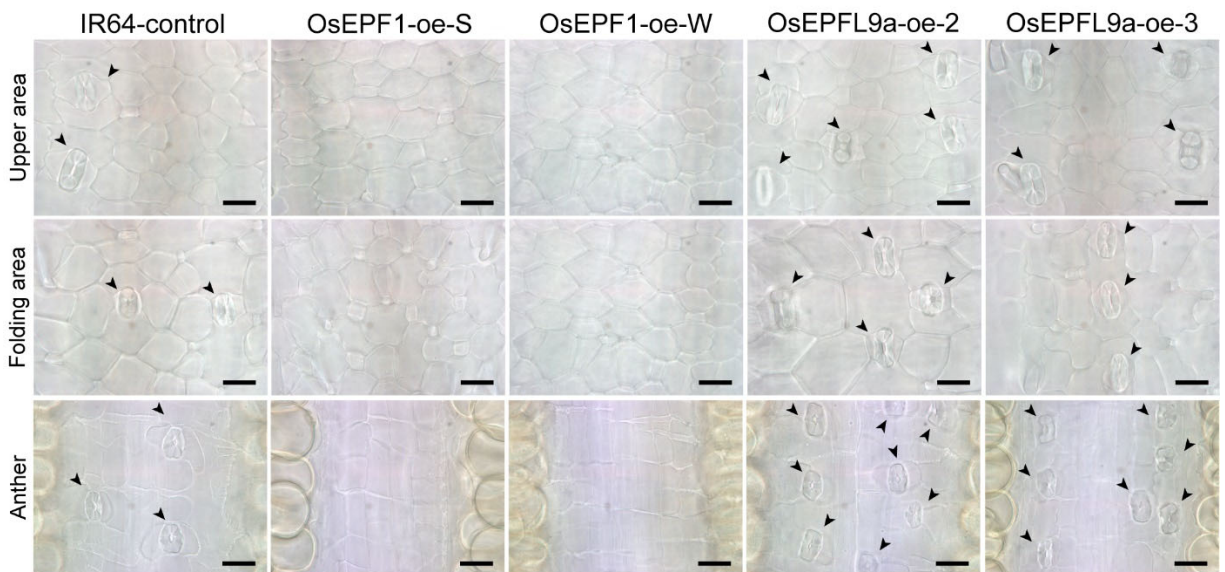
Figure 3.16. Representative microscopy images of lemma and anthers highlighting the differences in stomatal density between IR64-control and transgenic rice. Black arrowheads show stomatal complexes. Scale bars = 20 μm. 1000x magnification.
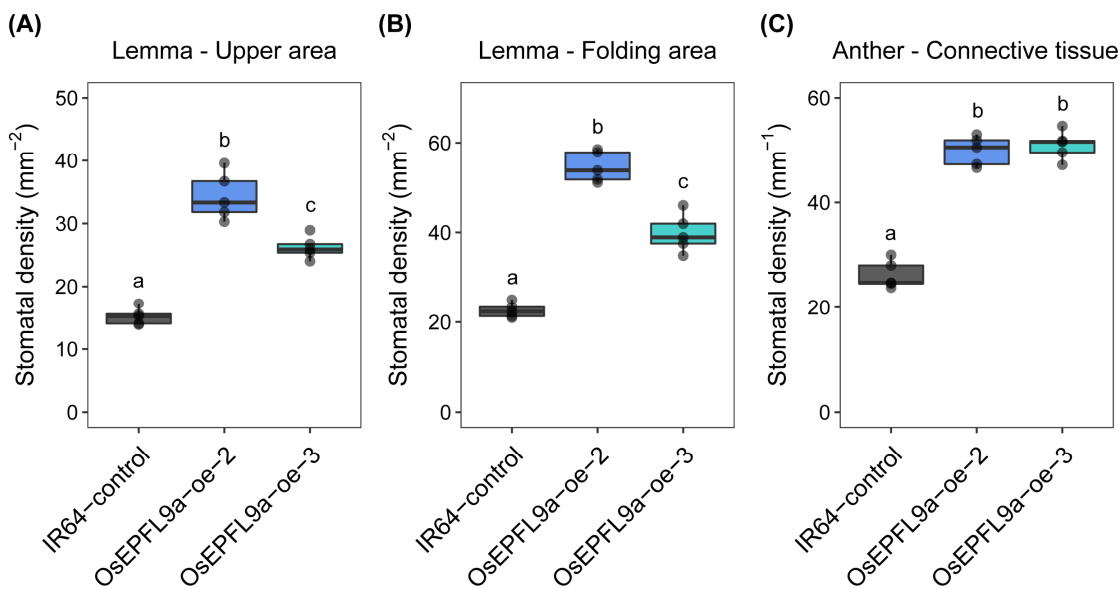
Figure 3.17. Stomatal densities of different parts of florets of IR64-control and *OsEPFL9a* overexpressing lines. (A) Upper area of adaxial epidermis of lemma. (B) Folding area of adaxial epidermis of lemma. (C) Connective tissue of anther. (A-C) One-way ANOVA and post hoc Tukey's test were performed to evaluate differences in mean stomatal density across the different genotypes. Different letters represent significant different groups ($p < 0.001$), n = 5 plants per line.

3.2.8. Pollen viability and panicle traits in rice lines overexpressing *OsEPFs*

To investigate if the altered stomatal density in florets of the transgenic rice lines were impacting on pollen development or survival, pollen viability of IR64-control and rice lines overexpressing the two *OsEPFs* was evaluated. Pollen grains from mature anthers prior to dehiscence were collected and stained using MTT (thiazolyl blue). Similar levels of pollen viability were observed in all genotypes analysed (Figure 3.18 A). Indeed, there was no noticeable indication of a potential reduction on spikelet fertility. Although grain yield was not quantified in this experiment, a careful examination of these plants in the grain ripening stage revealed that all genotypes successfully produced seeds. Several panicle traits with potential to impact on rice yields, such as panicle size, number of spikelets per panicle and spikelet size were also investigated. This analysis showed that OsEPF1-oe-S and OsEPFL9a-oe-2 rice lines had a small reduction in panicle length (Figure 3.18 B). Nonetheless, this did not lead to a statistically significant reduction in the number of spikelets per panicle in these rice genotypes (Figure 3.18 C, E). Moreover, both transgenic lines overexpressing *OsEPFL9a* gene showed a slight reduction on spikelet size (Figure 3.18 D, E).
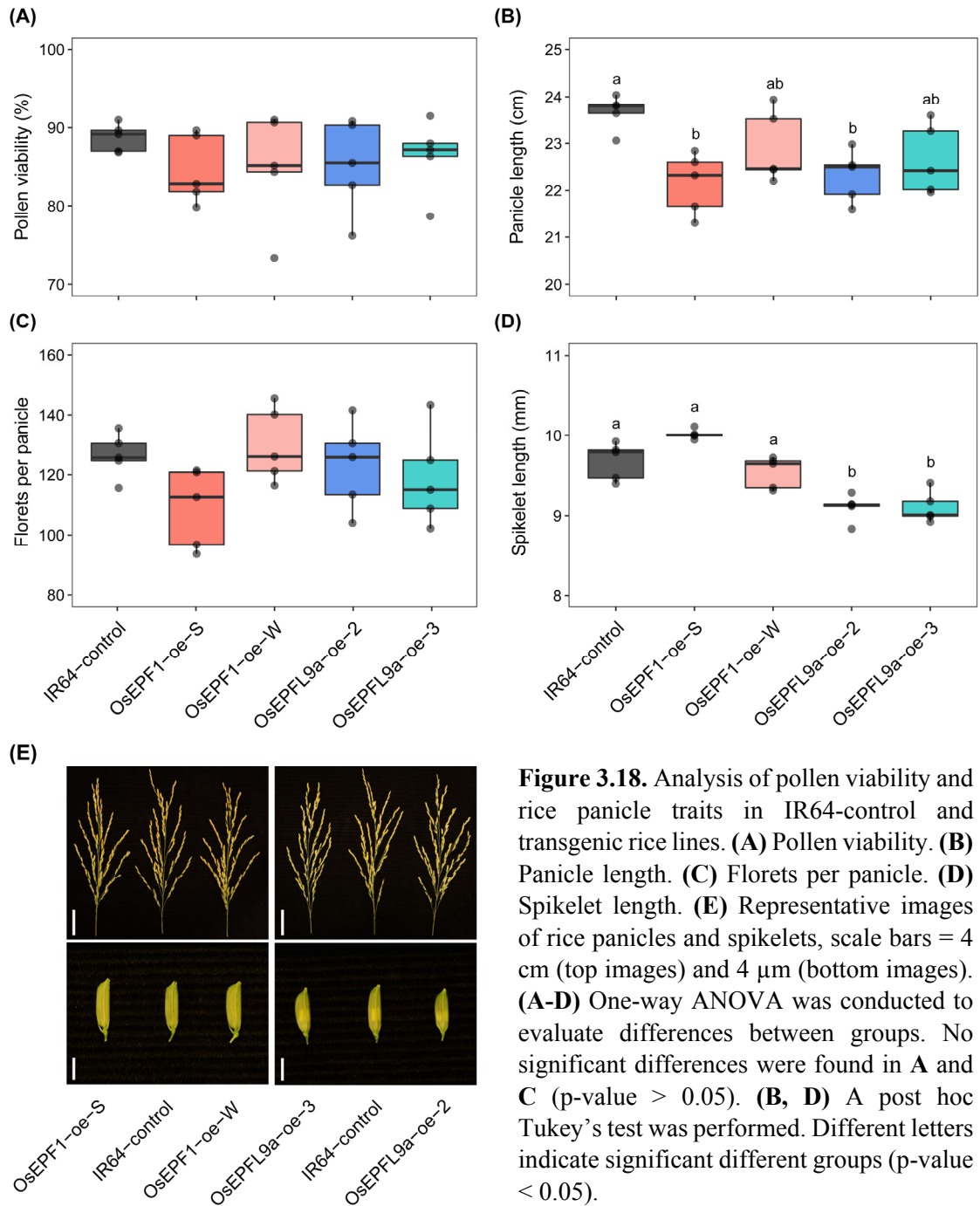
Figure 3.18. Analysis of pollen viability and rice panicle traits in IR64-control and transgenic rice lines. **(A)** Pollen viability. **(B)** Panicle length. **(C)** Florets per panicle. **(D)** Spikelet length. **(E)** Representative images of rice panicles and spikelets, scale bars = 4 cm (top images) and 4 μm (bottom images). **(A-D)** One-way ANOVA was conducted to evaluate differences between groups. No significant differences were found in **A** and **C** (p-value > 0.05). **(B, D)** A post hoc Tukey's test was performed. Different letters indicate significant different groups (p-value < 0.05).

3.3. Discussion

3.3.1. The overexpression of *OsEPFL9a* changes stomatal patterning in IR64 rice leaves

The overexpression of *OsEPFL9a* led to an increase in the stomatal densities of leaves of the Indica rice cultivar IR64, consistent with previous work where leaf 6 of the japonica cultivar Nipponbare was investigated (Mohammed et al., 2019). However, the examination of leaves that emerged at different phases of plant growth (seedling – leaf 2; early vegetative – leaf 6; and reproductive – flag leaf) revealed that this increase was not proportional across the different leaves (Figures 3.1 and 3.2). In IR64 leaves with naturally lower stomatal densities (leaf 2 and leaf 6) the increment in the number of stomata per leaf area varied from 18% to 29%, whilst in flag leaves, which have a much higher number of stomata, the increase observed was of 7% or less. This difference might be related to a variation in the expression levels of the transgene in the different growth stages. In an alternative hypothesis, this could indicate that an upper limit in the number of stomata was achieved in the flag leaves, and that perhaps, during leaf development, other mechanisms ensured that a maximum proportion of the epidermis was allocated for stomata, regardless of *OsEPFL9a* expression levels. Indeed a coordination with the development of other structures, such as veins and mesophyll airspace is crucial for promoting an optimal gas exchange capacity (Bergmann, 2004; de Boer et al., 2012; Schuler et al., 2018; Zhang et al., 2018). Furthermore, close proximity between stomatal complexes can lead to impairment of guard cell movement and also to interferences between diffusion shells (de Boer et al., 2016; Dow et al., 2014b; Franks and Casson, 2014; Harrison et al., 2020). In the transgenic rice analysed here, the one cell spacing between stomatal complexes in the same epidermal cell rows was maintained. To understand the constraints that led to differences in the stomatal density increments between leaves in the OsEPFL9a-oe plants additional work is needed. For instance, a detailed analysis of the transgene expression during leaf development at different growth stages, and a further investigation of the leaf anatomy would be necessary to address this question.

3.3.2. Stomatal size was not affected in leaf 6 of transgenic plants

Although the OsEPFL9a-oe lines showed between 21-29% increase in leaf 6 stomatal density, the average area occupied by a pair of GCs in these transgenic lines was not

significantly different to that of control plants (Figure 3.3). These results differ from those previously reported for Nipponbare rice overexpressing *OsEPFL9a*, which showed a decrease in GC area (Mohammed et al., 2019). Other studies in rice also reported adjustments in stomatal size due to the genetic manipulation of stomatal numbers. In the cultivar IR64, the overexpression of *OsEPF1* led to reductions in stomatal density and size (Caine et al., 2019), whereas in Nipponbare plants overexpressing the same gene and showing similar density phenotype, larger stomata were observed (Mohammed et al., 2019). In Schuler et al., (2018), an increase in leaf 6 stomatal density was achieved by expressing *ZmSHR1* in the japonica rice Kitaake. In these plants, only one out of three transgenic lines analysed showed a decrease in guard cells area (Schuler et al., 2018). Taking together, these studies suggest that stomatal size and density might be regulated by different pathways and/or that stomatal size might be regulated in distinct ways in different rice cultivars.

Although changes in guard cell area and in stomatal pore length were not statistically significant between the lines investigated here, the analysis of the guard cells length showed that stomata were shorter in OsEPFL9a-oe-3 rice in comparison with IR64-control. A similar trend towards shorter guard cells was observed in OsEPFL9a-oe-2, which also showed wider guard cells in comparison with the other rice lines (although not significant). Whereas smaller stomata have been associated with faster aperture responses in closely related species, due to their higher cell surface area to volume ratio (Drake et al., 2013; McAusland et al., 2016), other aspects, such as cell wall thickness, composition, interaction with neighbour cells and the proportion between guard cell length and diameter can also interfere in the stomatal opening mechanism (Franks and Farquhar, 2007; Woolfenden et al., 2018; Yi et al., 2019). For instance, it was suggested that narrower guard cells can be more easily deformed laterally than the wider ones (Yi et al., 2019). Although the changes observed in the geometric proportions of stomata between the rice lines analysed here were small, it is important to highlight that a potential effect of these alterations in each individual stoma would be amplified at the leaf level, possibly impacting in plants gas exchange rates. Nonetheless, more investigations are necessary to understand whether the observed changes in guard cells shape could be affecting stomatal function across the rice lines analysed here.

3.3.3. Operational stomatal conductance does not correlate with g_{smax} in OsEPFL9a-oe rice lines

The maximum anatomical stomatal conductance (g_{smax}) in leaf 6 of rice lines overexpressing *OsEPFL9a* was estimated to be 23-29% higher than in control plants due to a significant increase in stomatal density. To understand how this increment in g_{smax} was translated in terms of operational stomatal conductance (g_s), gas exchange analyses were performed under steady-state conditions and in a light response curve. Levels of g_s were lower than that predicted by the anatomical measurements, and this is indeed expected, as plants do not normally operate in their upper gas exchange limit (Dow et al., 2014a; Fanourakis et al., 2015; McElwain et al., 2016). However, stomatal conductance levels were not significantly increased in transgenic lines compared to IR64-control, although OsEPFL9a-oe-3 plants showed a trend towards an increased g_s (Figure 3.4). Previous studies in transgenic rice with similar stomatal density phenotype also found that g_s rates were not enhanced under typical environmental conditions (Mohammed et al., 2019; Schuler et al., 2018). And while genetically modified Arabidopsis with higher stomatal density showed a greater g_s, these plants had a much more substantial increment (100% or more) in the number of stomata (Franks et al., 2015; Tanaka et al., 2013).

To investigate if OsEPFL9a-oe lines are able to increase their g_s to higher rates in conditions that promote wider stomatal apertures, and potentially improve evaporative cooling, gas exchange responses were investigated under high light intensity and cumulative temperature increases. All plants responded to the rise in temperature by opening stomata and increasing g_s and transpiration, but no significant difference was found in the proportion of this response between transgenics and controls (Figure 3.5). In this experiment, the line OsEPFL9a-oe-3 showed significantly higher g_s and transpiration rates in comparison to IR64-control and to OsEPFL9a-oe-2 (the transgenic line with greater stomatal density and g_{smax}). It appears unlikely that this increase in g_s in just one transgenic line is due to the increased stomatal density, but it is possible that the number of stomata in OsEPFL9a-oe-3 is optimal for conductance and the higher number of stomata in OsEPFL9a-oe-2 is above optimum, limiting stomatal function. Alternatively, differences in stomatal geometry (discussed in the previous section) or in leaf structure such as the formation of veins and mesophyll airspaces between lines could be leading to this difference. Analyses of genetically modified Arabidopsis (Dow et al., 2017), wheat (Lundgren et al., 2019) and rice (Schuler et al., 2018) with altered stomatal traits identified some level of change in the mesophyll structure. However, it is yet not known

if the transgenic plants analysed here show consistent changes in the mesophyll. Further anatomical analysis could elucidate whether the coordination between mesophyll airspace and stomatal development was disrupted in rice lines overexpressing *OsEPFL9a*. Moreover, the investigation of gas exchange responses under low CO_2 levels or with more extreme temperatures or light intensity could determine whether the transgenic plants indeed have potential to increase gas exchange to rates beyond of those of IR64-control plants.

3.3.4. Can OsEPFL9a-oe plants promote a greater evaporative cooling?

The examination of the leaf temperature data obtained from the infrared gas analyser suggested that the transgenic plants, in particular the line OsEPFL9a-oe-3, had lower leaf temperature than the IR64-controls (Figure 3.6 C) which is in line with the finding that it has elevated transpiration. However, the results of subsequent thermal imaging analysis of leaf surface temperature were not conclusive, and therefore could not confirm the temperature reduction in OsEPFL9a-oe-3 (Figures 3.7 and 3.8). Temperature data were quite variable, especially for the transgenic line OsEPFL9a-oe-2. Although the line OsEPFL9a-oe-3 showed lower leaf temperature more consistently, it is still uncertain if the level of increase in conductance in this line is due to an increase in stomatal densities, and if it could lead an enhancement of evaporative cooling in the early vegetative stage. The variability in the recorded temperatures could be associated with technical challenges in the thermal imaging experiments. For instance, the variation in the positioning of the narrow rice leaves complicates the measurement of comparable areas, which is compounded by the air flow inside the growth chamber that moves the leaves. Alternatively, it is possible that any differences in temperature were simply not large enough to be detected in the conditions tested here, which might indicate that the transgenic plants are not able to promote a more effective cooling. It would be interesting to investigate whether a more substantial difference in leaf temperature might be seen in other growth stages, when plants are actively tillering and a denser canopy is formed, providing an additive effect of an increased g_s in all leaves.

3.3.5. The overexpression of *EPFs* changes stomatal densities in rice florets

Heat stress can cause damage to rice development in different growth phases, however, negative impacts in yield are more pronounced when plants experience elevated temperatures during the reproductive phase (Jagadish et al., 2015; Matsui et al., 2000;

Satake and Yoshida, 1978). Therefore, it was hypothesised that a local increase in the stomatal density in rice florets could prove useful for enhancing evaporative cooling and protecting these heat-sensitive structures. The examination of stomatal distribution in IR64 plants showed that stomatal complexes were present in palea, lemma and anthers of the rice florets (Figures 3.10 to 3.12). In the bract-like organs, stomata were mostly present in the inner epidermis, along the vasculature; in turn, only few stomata were found in the outer epidermis of the floret. This spatial arrangement of stomata on the inner surfaces of the lemma and palea suggests that these pores might not primarily function on floret evaporative cooling, as during the rice reproductive development florets remain closed, opening only during flowering, which usually takes 1-2.5 hours, and then closing again (Yoshida, 1981). The presence of stomata on flowers has been reported in various angiosperms (Clement et al., 1997; Ebenezer et al., 1990; Hew et al., 1980; Roddy et al., 2016; Wei et al., 2018; Zhang et al., 2018), however, their role during flower and seed development is not fully understood. It is likely that the importance of floral stomata varies across plant species. These structures might contribute to water and nutrient uptake, but could also be associated with photosynthesis and cooling, or in helping to keep optimum water and humidity conditions for either pollen development or for facilitating dehydration during anther dehiscence (Clement et al., 1997; Keijzer et al., 1987; Lugassi et al., 2020; Nelson et al., 2012; Roddy et al., 2016; Wei et al., 2018).

Plants overexpressing *OsEPFL9a* showed a significant increase in the density of stomata in the floral organs, however the distribution boundaries of stomata were not expanded (Figure 3.17). Under optimal growing conditions, these transgenic plants showed pollen viability rates equivalent to those of IR64-controls, and no obvious impacts on fertility were observed. Although the position of the stomata in the rice lemma and palea suggests that the increased stomatal density in OsEPFL9a-oe might not promote an effective increase in evaporative cooling, in particular during floret development or ripening (when florets are closed), these additional stomata could play a role during flowering. In this stage rice spikelets open, anther dehiscence is completed promoting pollination, and spikelets close again. Studies have shown that the exposure to high temperatures during this sequence of events leads to spikelet sterility in various rice cultivars, and that this disruption in fertilization is mainly associated with a defective anther dehiscence (Jagadish et al., 2010; Matsui et al., 2000; Rang et al., 2011; Satake and Yoshida, 1978). It would be interesting to test whether OsEPFL9a-oe plants could keep their floral tissues cooler during flowering, and if this would prevent heat-induced infertility. Furthermore, studies in some non-grass monocots and in Arabidopsis have

suggested that the presence of stomata in anthers might facilitate anther dehiscence (Keijzer et al., 1987; Wei et al., 2018); similarly, in mosses stomata are important for timely sporophyte capsule dehiscence (Chater et al., 2016). In the rice lines overexpressing OsEPF1-oe analysed here, stomata were virtually absent in the floral organs, yet no noticeable impacts on fertility were observed either in this study or reported in previous work (Caine et al., 2019). Whether or not the increase or absence of stomata in floral organs could affect anther dehiscence or tissue temperature differently under optimum or under stress conditions is yet to be investigated. Furthermore, the use of transgenic plants overexpressing either *OsEPFL9a* or *OsEPF1* tissue specific manner during the development of the floral organs could be a useful tool to study and the function of stomata in rice florets.

3.3.6. Conclusion

The findings presented in this chapter showed that the overexpression of *OsEPFL9a* in rice promoted increases in leaf stomatal density, and that these were proportionally less pronounced in flag leaves. Although an increase in stomatal conductance and a decrease in leaf temperature were observed in one of the transgenic lines analysed, these were not consistently achieved under the conditions tested here. Nonetheless, the physiological responses of these transgenic lines in other developmental stages are yet to be investigated. It remains possible that the increase in stomatal number in rice floral organs of OsEPFL9a-oe plants might prove beneficial to protect florets under heat stress, but if so the level of protection is not likely to be substantial. Additionally, the detailed characterization of the spatial distribution of stomata in rice floral organs described here provides the basis for future functional studies on the role of floral stomata during floret and seed development.

Chapter 4

Response of rice overexpressing *OsEPFL9a* under heat stress conditions during the flowering stage

4.1. Introduction

4.1.1. Heat stress during flowering

Rice is usually cultivated as an annual crop, with a growth duration that varies from 3 to 6 months depending on the variety and environmental conditions. Rice growth cycle can be divided into three general phases: vegetative, reproductive and ripening (summarized in Figure 4.1 A). Traits such as tillering capacity, number of tillers producing panicles, panicle branching and number of spikelets per panicle determine rice yield potential. However, actual yield also relies on seed set, and is ultimately constrained by the success of fertilization and proper grain filling. Flowering (also referred as anthesis) and to a lesser degree, microsporogenesis during booting, are the processes most susceptible to heat stress in rice (Endo et al., 2009; Satake and Yoshida, 1978). Flowering begins after panicles start to emerge from the flag leaf sheath (Figure 4.1 B-C) and involves a series of short events, including floret opening, filament elongation, anther dehiscence, pollination and floret closure. Flowering commonly occurs between 10 am to 1 pm in tropical environments, and progresses gradually as panicle heading continues, taking approximately 7 days to all panicles on a plant completely emerge and flower (GRiSP, 2013; Jagadish, 2020). Previous studies have established that the exposure to temperatures above 32 °C during the reproductive phase is associated with reduced fertility in certain genotypes, and that even short periods of more extreme temperatures (>35 °C) can lead to substantial yield losses (Arshad et al., 2017; Jagadish et al., 2007, 2010, 2015; Rang et al., 2011; Satake and Yoshida, 1978). Rice heat-induced infertility is often caused by a restriction in pollen swelling, which is an important driving force for rice anther dehiscence (Matsui et al., 1999). The disruption of this process leads to poor shedding and insufficient deposition of pollen on stigmas, reducing spikelet fertility rates (Jagadish et al., 2010; Matsui et al., 1999, 2000; Satake and Yoshida, 1978; Wilson et al., 2011). In addition, changes in the ability of pollen to germinate after pollination or in sustaining pollen tube development have been reported in rice exposed to heat stress

during flowering, which might impair fertilization even when sufficient number of pollen grains land on the stigma (Jagadish et al., 2010; Shi et al., 2018; Tang et al., 2008).
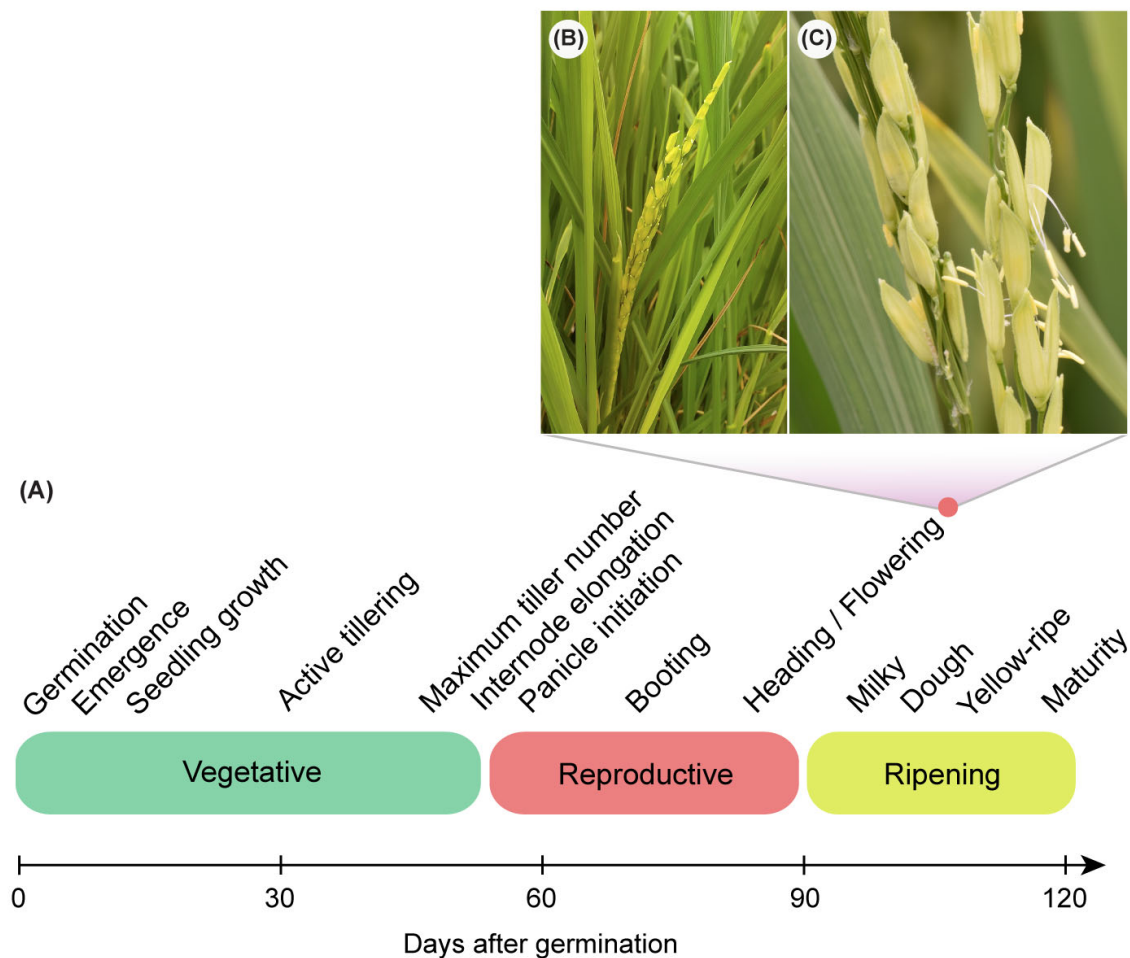
Figure 4.1. (A) Main stages in the growth of a 120-day rice variety, in a tropical environment (GRiSP, 2013). The vegetative phase comprises the growth and development of the plant from germination to panicle initiation in the main stem. This phase is characterized by a gradual increase in plant height, tillering, and leaf emergence at regular intervals. The transition to the reproductive phase begins at the onset of internode elongation as flag leaves start to develop. The reproductive growth phase includes panicle primordia initiation, booting (including microsporogenesis), heading and flowering. After fertilization, ripening starts with the gradual filling of the grains by the accumulation of carbohydrates in the pistils. Grain formation can be divided in milky, dough and yellow-ripe stages based on grain texture and colour. Finally, as carbohydrates stop to be translocated to panicles, grains loss moisture and maturity is reached (GRiSP, 2013; Saichuk, 2014). **(B)** Panicle emerging from the flag leaf sheath in IR64 rice heading stage. **(C)** Anthesis of florets during the flowering stage in IR64 rice.

4.1.2. Avoiding heat stress

Heat stress triggers multiple biological processes to avoid or alleviate damage. In addition to molecular and biochemical changes (such as expression of heat shock proteins, accumulation of osmo-protectants and increased membrane lipid saturation) (Janni et al.,

2020), maintaining a cooler canopy through increased evapotranspiration is recognized as an effective strategy for overcoming heat stress in crops cultivated in well-irrigated conditions (Jagadish, 2020). Although levels of evapotranspiration can be affected by abiotic factors, the ability to substantially increase and sustain transpiration rates under high temperatures differs between different rice cultivars (Sailaja et al., 2015; Yang et al., 2020). Water loss from leaves are influenced by the plant's cuticle characteristics and boundary layer resistance. Additionally, as this process largely results from water vapour diffusion through stomatal pores, stomatal resistance is a major factor governing transpiration rates (Grossiord et al., 2020; Meinzer, 1993; Sheriff, 1984). This study hypothesised that by increasing stomatal gas exchange capacity, an improved evaporative cooling range might also be achieved. The results presented in Chapter 3 of this thesis showed that rice plants overexpressing *OsEPFL9a* developed a greater number of stomata in leaves and florets. Increases in stomatal density were found to be less marked in flag leaves, possibly limiting the potential for an enhanced stomatal-mediated evaporative cooling during flowering. However, it is possible that the presence of more stomatal pores inside rice florets could also help in keeping spikelet temperatures lower during anthesis, or even help to promote more effective anther dehiscence, improving responses to high temperatures.

4.1.3. Objectives

To understand whether the increase in number of stomata in leaves and florets has the potential to enhance the evaporative cooling capacity and thermotolerance of rice plants during the flowering stage, the physiological responses of IR64-control plants and of two transgenic rice lines overexpressing *OsEPFL9a* were investigated under control and high temperature conditions at the peak flowering time.

4.2. Results

4.2.1. Evaluating the responses of transgenic rice overexpressing *OsEPFL9a* under heat stress during flowering

OsEPFL9a-oe-2 and OsEPFL9a-oe-3 are independent transgenic rice lines that ectopically overexpress the gene *OsEPFL9a* in the IR64 cultivar background. As described in Chapter 3, these lines have increased stomatal density in leaves and in floral organs in comparison to IR64-control. In the experiments described in this Chapter, it was evaluated whether OsEPFL9a-oe-2 and OsEPFL9a-oe-3 plants are able to maintain higher levels of transpiration-mediated cooling and avoid heat stress during the flowering stage. For this purpose, T_2 generation OsEPFL9a-oe-2, OsEPFL9a-oe-3 and IR64-control rice plants were exposed to either heat stress or control conditions, specifically during the flowering time, allowing the investigation of plant physiological responses and yield.

- *Experiment overview*

Three subsets of plants were sown sequentially one week apart from each other. Plants were maintained in a walk-in growth room under optimal growth conditions for rice until the flowering stage. Each plant was grown in soil in an individual 2.4 L pot. Pots were stood in trays that were kept topped up with water (Figure 4.2 A-B). As plants reached the flowering stage (with the start of panicle emergence, ~ 90 days after sowing), part of them were moved to an equivalent walk-in chamber to be exposed to a heat stress treatment for 8 days (Figure 4.2 D). During this period measurements of leaf gas exchange, leaf temperature, pollen viability and chlorophyll fluorescence were taken from plants under both heat and control conditions. Material for assessing stomatal density was also collected. After the 8-day treatment, plants under heat stress conditions were moved back to the control chamber (Figure 4.2 E). All plants were then kept under optimal conditions until seed set was completed (Figure 4.2 C). Seeds and dried above ground biomass from all plants were collected to evaluate yield components (detailed methodology is described in Chapter 2).

- *Treatment conditions:*

Control treatment: 12h photoperiod, ~1200 µmol m^{-2} s^{-1} light (at canopy level), 30 °C day temperature, 24 °C night temperature, 70% day relative humidity (~ 0.018 kg/kg absolute humidity), 70% night temperature (~ 0.013 kg/kg specific humidity). Relative humidity was set to 60%, however moisture built up naturally in the chamber as plants

grew, reaching 70% during reproductive development. Plants were kept well-watered at all times. CO_2 concentration was not controlled.

Heat treatment: 12h photoperiod, ~1200 μmol m^{-2} s^{-1} light (at canopy level). During the light period (from 7 am) the temperature was slowly increased to reach 37 °C by 9:30 am. Temperature was kept at 37 °C for 5 hours (from 9:30 am to 3:30 pm, the period when most of anthesis and pollination was believed to occur), afterwards, temperature was slowly returned to 30°C (reached at 4:30 pm), and kept at this level until the end of the light period (at 7 pm). During the night period temperature was kept at 24 °C (same as the control treatment). As the walk in growth rooms were not able to keep high relative humidity under 37 °C, the specific humidity (rather than the relative humidity) of the heat stress treatment was set to levels equivalent to those of the control chamber (~ 0.018 kg/kg, ~ 45% RH during the day and ~ 0.013 kg/kg, ~70% RH at night), CO_2 concentration was not controlled, and plants were kept well-watered at all times.

* Experimental conditions were affected by failure events in systems of the University plant growth facility in March 2018, during the reproductive phase of plants development. For one day, humidity was 10% lower than expected in the heat chamber, due to a failure in the RO water system. In a second incident, both chambers experienced temperatures above the originally set (+4-6 °C) for 2 hours due to a failure in the chilling system. In addition, a break down event left the control chamber switched off for few hours.
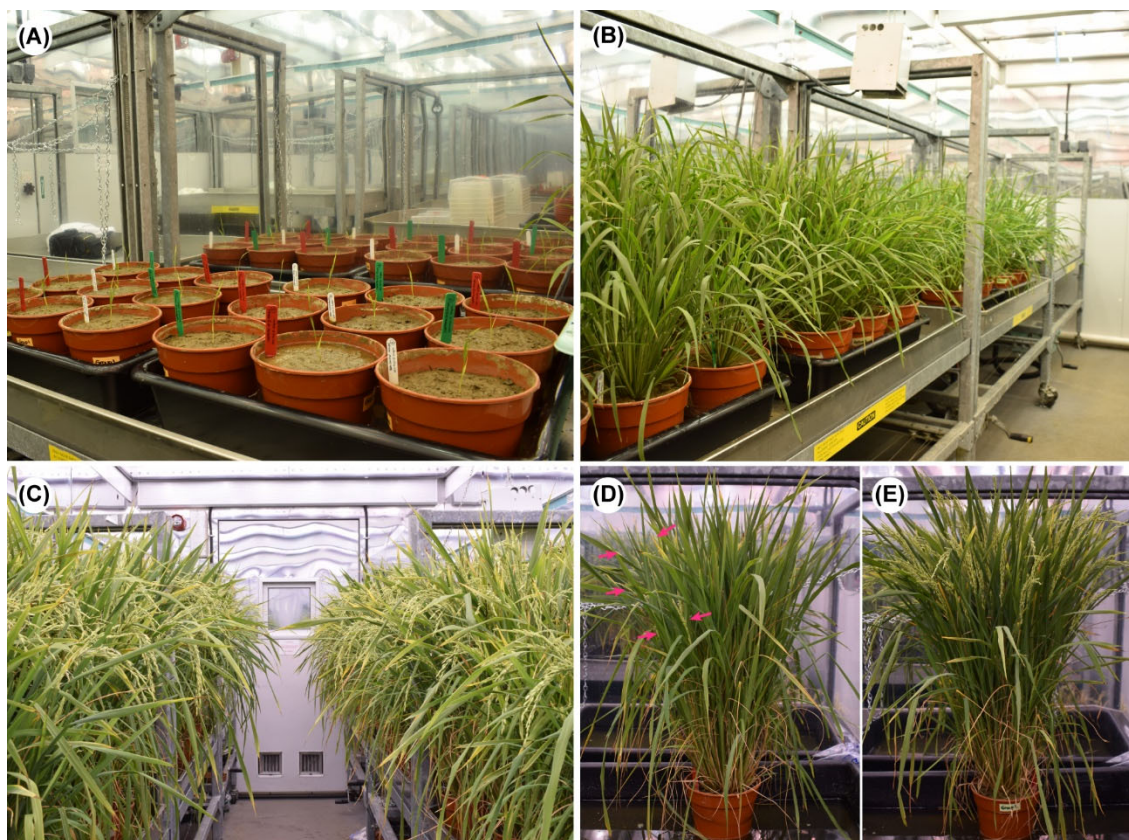
Figure 4.2. Plant growth during the heat stress experiment. **(A)** Seedlings growing in pots with soil placed inside trays filled with water. **(B)** Plants in mid-vegetative stage under control conditions. **(C)** Plants in the grain filling stage under control conditions. **(D)** Representative image of plants in early flowering stage (start of heat treatment), red arrows indicate panicles emerging from flag leaves sheath. **(E)** Representative image of plant 8 days later (after heat treatment), most panicles were completely emerged and spikelets were pollinated.

4.2.2. Stomatal density phenotype

To verify that transgenic plants had an increased number of stomata, as described in Chapter 3, stomatal density was assessed in the abaxial epidermis of flag leaves and in the adaxial epidermis of the upper lemma. Stomatal densities in both OsEPFL9a-oe-2 and OsEPFL9a-oe-3 were significantly higher than in IR64-control (Figure 4.3). In lemma, average increases of ~ 124% and 74% were observed in OsEPFL9a-oe2 and OsEPFL9a-oe-3, respectively. Whereas in the flag leaf, an average increase of around 10-11% was found in both transgenic lines, which is slightly higher than what was found in Chapter 3. In addition, PCR confirmed that all transgenic plants carried the *OsEPFL9a* overexpression construct (data not shown).
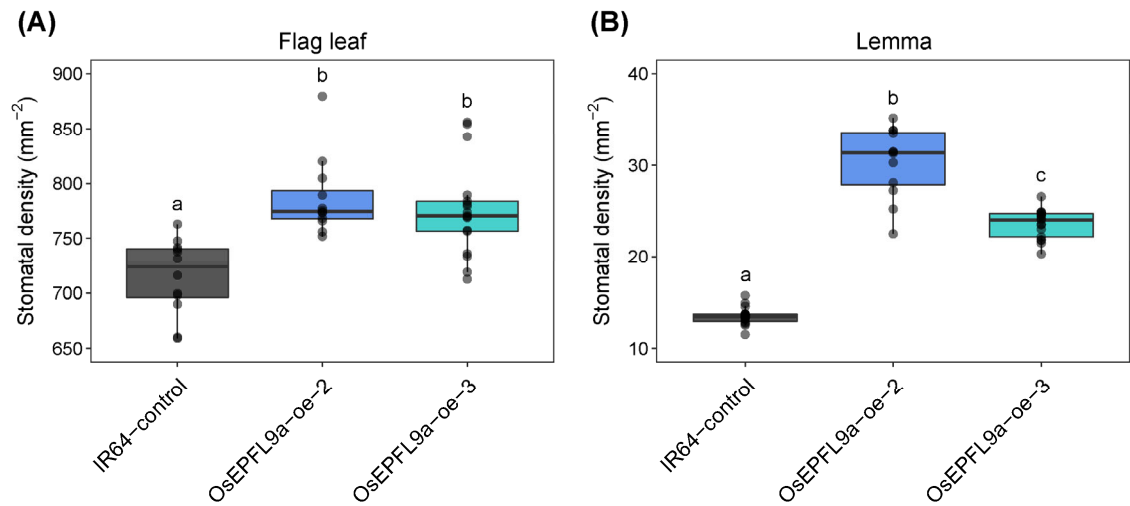
Figure 4.3. Stomatal densities of transgenic rice lines in comparison to control. **(A)** Abaxial flag leaf blade. **(B)** Upper area of inner lemma epidermis. **(A)** One-way ANOVA and post hoc Tukey's test were performed to evaluate differences between genotypes, $p < 0.0001$. **(B)** Kruskal-Wallis and post-hoc Dunn test were performed to evaluate differences between genotypes, $p < 0.0001$. **(A-B)** n = 12-16 plants per genotype. **(A-B)** Different letters indicate significant different groups according to post-hoc analysis.

4.2.3. Gas exchange responses under heat treatment

Leaf gas exchange responses during temperature treatments were evaluated under steady-state conditions in fully expanded flag leaves, using infrared gas analysers (LI-6800, LI-COR Biosciences). Analyses were conducted in parallel in plants exposed to heat (37 °C) and to control (30 °C) conditions, between the 2nd and the 4th day after temperature treatment started. IRGA leaf cuvettes were set to conditions that matched the temperature and humidity of each corresponding treatments, at 1300 µmol m^{-2} s^{-1} PAR, 300 µmol s^{-1} flow rate and 400 ppm CO_2 concentration. Results revealed differences in gas exchange rates between plants exposed to control and high temperatures (Figure 4.4), however, transgenic lines and IR64-control showed similar gas exchange rates, and no significant differences were found between genotypes in either of the temperature treatments. Plants overexpressing *OsEPFL9a* had a more evident drop in photosynthetic and stomatal conductance rates under high temperature (Figure 4.4 A-B), which contrasts to results observed in Chapter 3 (section 3.2.4) that showed an increase in g_s and photosynthesis under increasing temperatures. This difference is probably related to the lower RH levels and consequent increased vapour pressure deficit experienced under the heat conditions tested here. Despite lower levels of stomatal conductance, transpiration rates were significantly higher for all genotypes analysed under heat stress, compared to the control treatment (Figure 4.4 C). Nonetheless, OsEPFL9a-oe-2 and OsEPFL9a-oe-3

plants did not show enhanced transpiration in comparison to IR64-control plants, suggesting that an increased evaporative cooling effect under heat stress was not achieved, despite the significant increases in stomatal density shown by *OsEPFL9a* overexpressing lines.

(A)

(B)

(C)
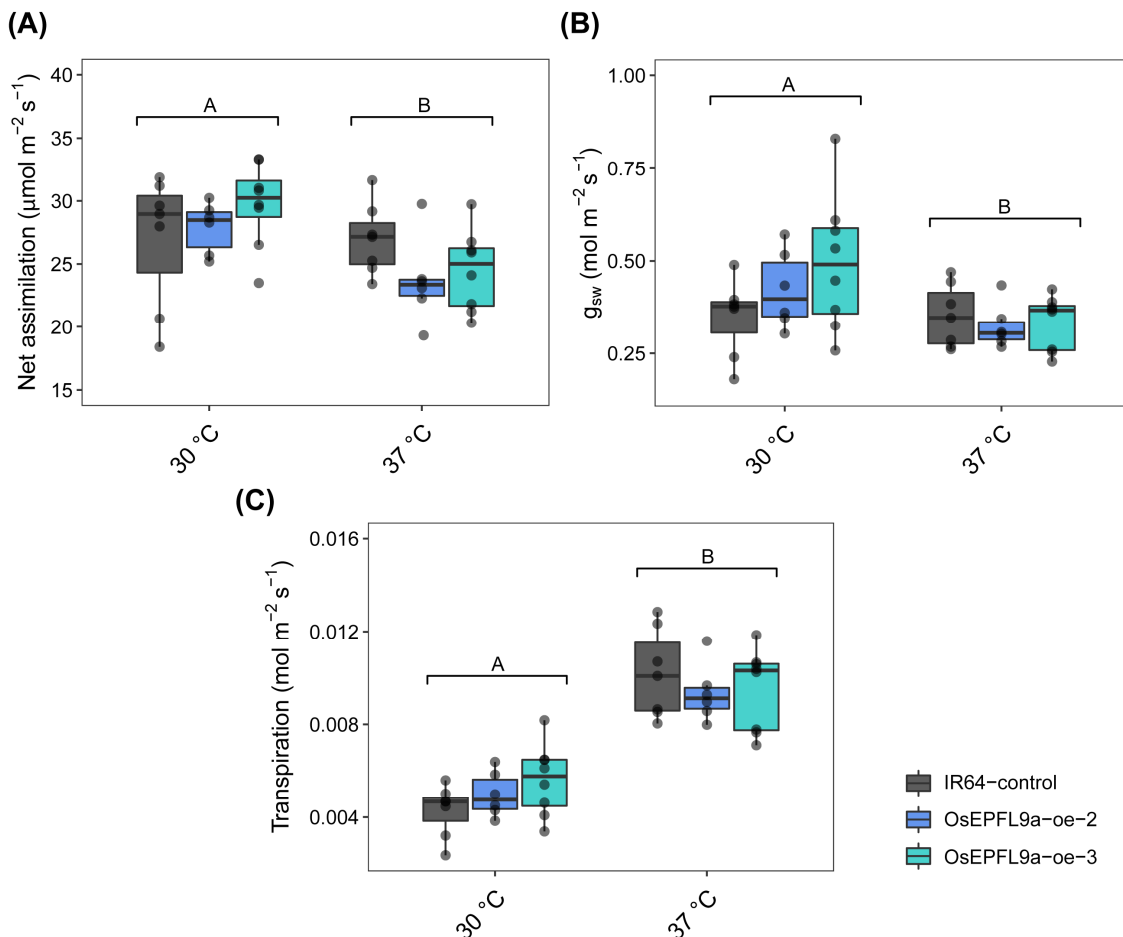
Figure 4.4. Rice overexpressing *OsEPFL9a* showed gas exchange responses similar to IR64-control under different temperature treatments during flowering. **(A)** Carbon assimilation, **(B)** stomatal conductance and **(C)** transpiration rate of flag leaves under control (30 °C) and heat (37 °C) treatment. **(A-C)** Two-way ANOVA was conducted to test for the effects of the factors genotype and treatment on each physiological parameter (n = 6-8 plants per genotype, per treatment). Main effect analysis showed that treatment impacted on all parameters tested (**A**- $p < 0.01$; **B**- $p < 0.05$; **C**- $p < 0.001$). No significant interaction between the effects of genotype and treatment was not found ($p > 0.05$). No differences between genotypes were found ($p > 0.05$). Letters in the plots represent differences for the main effect of the factor treatment.

4.2.4. Effect of temperature treatments on photosystem II activity

To evaluate whether the exposure to elevated temperature would affect the activity of photosystem II (PSII), dark and light-adapted chlorophyll fluorescence measurements were taken from IR64-control and transgenic plants. Maximum quantum yield of three

fully expanded flag leaves per plant was estimated using a FluorPen (FP100, Photon Systems Instruments). For dark-adapted measurements (Fv/Fm), data were collected around 6 am, before chamber lights were switched on (pre-dawn), whereas light-adapted measurements (Fv'/Fm') were conducted at noon. No significant difference between transgenics and IR64-control plants were observed, and there was no indication of a negative impact of the heat treatment on photosystem II activity (Figures 4.5 and 4.6); indeed plants from both control and heat treatments looked healthy. Fv'/Fm' was reduced on day 8, in comparison to day 1, however this response was equally observed in both temperature treatments, being potentially related to a developmental process rather than differences in temperature.
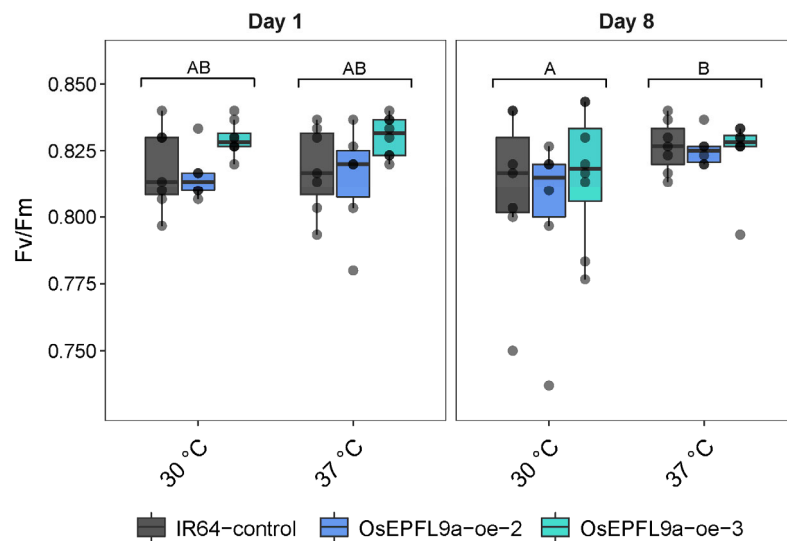
Figure 4.5. Dark-adapted maximum quantum efficiency of flag leaves PSII at day 1 and day 8 of temperature treatments. A three-way ANOVA was conducted to test for the effects of the factors genotype, treatment and day on Fv/Fm (n = 6-8 plants per genotype, per treatment). No significant effects of genotype were found ($p > 0.05$). A significant interaction between the factors day and treatment was found ($p < 0.05$). Post-hoc Tukey's test indicated that Fv/Fm values for plants exposed to 30 °C at day 8 were significantly different than those of plants exposed to 37 °C at day 8 ($p < 0.05$). Letters in the plot represent Tukey's test results for the interaction between day and treatment.
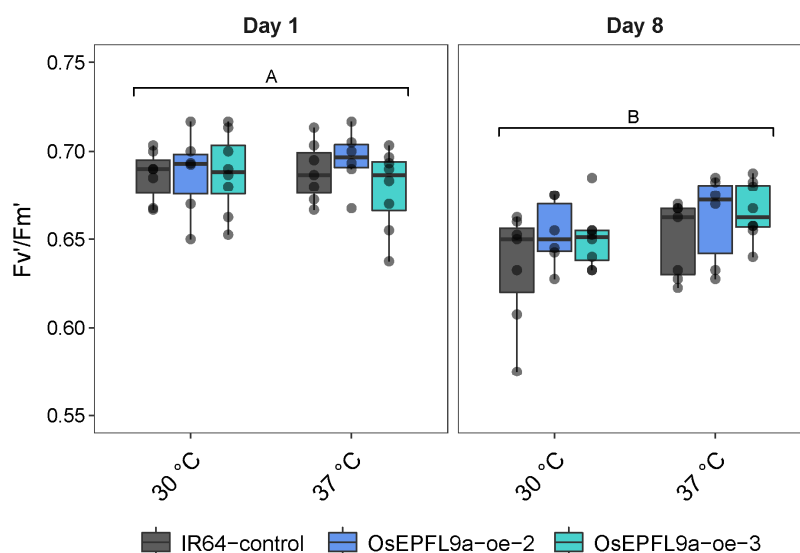
Figure 4.6. Light-adapted maximum quantum efficiency of flag leaves PSII at day 1 and day 8 of temperature treatments. A three-way ANOVA was conducted to test for the effects of the factors genotype, treatment and day on Fv'/Fm' (n = 6-8 plants per genotype, per treatment). No significant interactions or main effects of genotype or treatment were found (p > 0.05). A significant impact of the factor day on Fv'/Fm' was found (p < 0.001), which is represented by the different letter in the plot.

4.2.5. Differences in plant temperature under heat and control treatments

To investigate whether the transgenic lines with increased densities of stomata in florets and leaves were able to keep their tissue temperature lower than that of IR64-control plants during the flowering stage, the temperature of leaves and spikelets of plants exposed to control and heat treatments was evaluated.

- *Leaf temperature*

Leaf temperature was investigated with a thermal imaging camera (FLIR T650sc) between the 6th and the 7th day of treatment. Quantification of temperature was performed using the software FLIR TOOLS, and data was collected from equivalent areas of mature leaves. As it was possible to capture the image of only two large plants at the same time, each transgenic line was independently compared to an IR64-control in this analysis. Lines overexpressing *OsEPFL9a* and IR64-control had similar increases in leaf temperature when exposed to the heat treatment (Figures 4.7 and 4.8). Despite showing levels of stomatal conductance and transpiration that were equivalent to the IR64-control, OsEPFL9a-oe-3 plants had overall a lower leaf temperature in comparison to IR64-control plants (average of ~0.4 °C lower). No significant differences were found in leaf temperature between OsEPFL9a-oe-2 plants and the IR64-control.
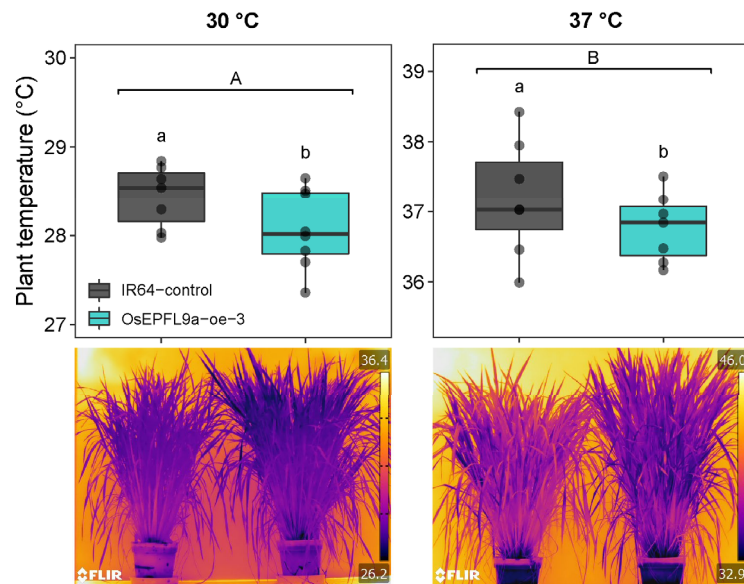
Figure 4.7. Leaf temperature of OsEPFL9a-oe-3 and IR64-control plants under control (30 °C) and heat (37 °C) treatment. Two-way ANOVA was conducted to test for the effects of the factors genotype and treatment on leaf temperature (n = 7 plants per genotype, per treatment). No significant interaction between the effects of factors was found (p > 0.05). Main effect analysis showed that genotype (p < 0.01) and treatment (p < 0.0001) impacted independently on leaf temperature. Letters in the plot represent results for the main effect analysis. Representative thermal images of OsEPFL9a-oe-3 and IR64-control in each temperature treatment are shown below the graphs.
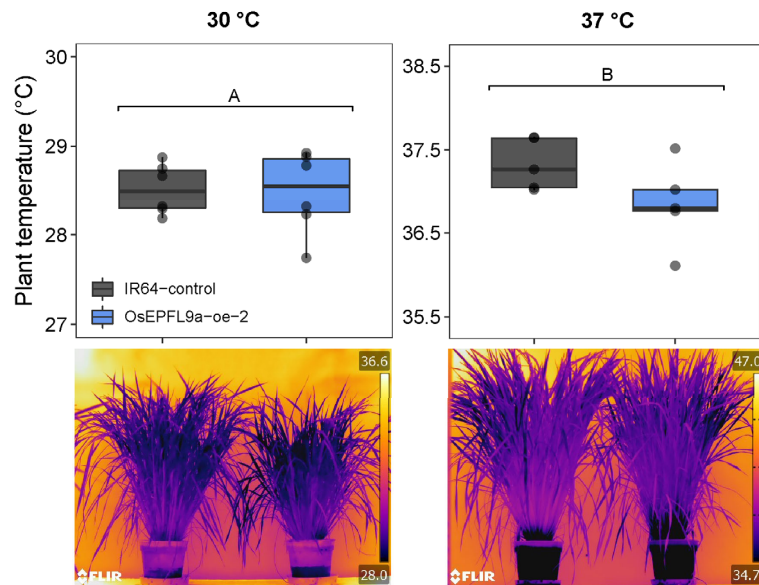
Figure 4.8. Leaf temperature of OsEPFL9a-oe-2 and IR64-control plants under control (30 °C) and heat (37 °C) treatment. Two-way ANOVA was conducted to test for the effects of the factors genotype and treatment on leaf temperature (n = 5-6 plants per genotype, per treatment). No significant interaction between the effects of factors was found (p > 0.05). Main effect analysis showed that treatment (p < 0.0001) impacted on leaf temperature, which is represented by different letters in the plot. No significant difference between genotypes was found (p > 0.05). Representative thermal images of OsEPFL9a-oe and IR64-control in each temperature treatment are shown below the graphs.

- *Floret temperature*

The temperature of mature florets was investigated prior to anthesis on days 5-6 after treatment started. For this analysis, thermocouple sensors connected to a datalogger were inserted in florets, between the lemma and palea edges (Figure 4.9 A). Spikelets of equivalent positioning in the plants were chosen, and data from the different rice genotypes was collected simultaneously. As expected, the temperature from plants under heat treatment was higher than plants under control treatment. Although the mean temperatures of the transgenic lines were slightly lower than that of IR64-controls, no significant differences were found between either the transgenic and control line (Figure 4.9 B), suggesting that the increased stomatal density in rice florets had no impact on improving the evaporative cooling of floral tissues, or at least not while florets were still closed.
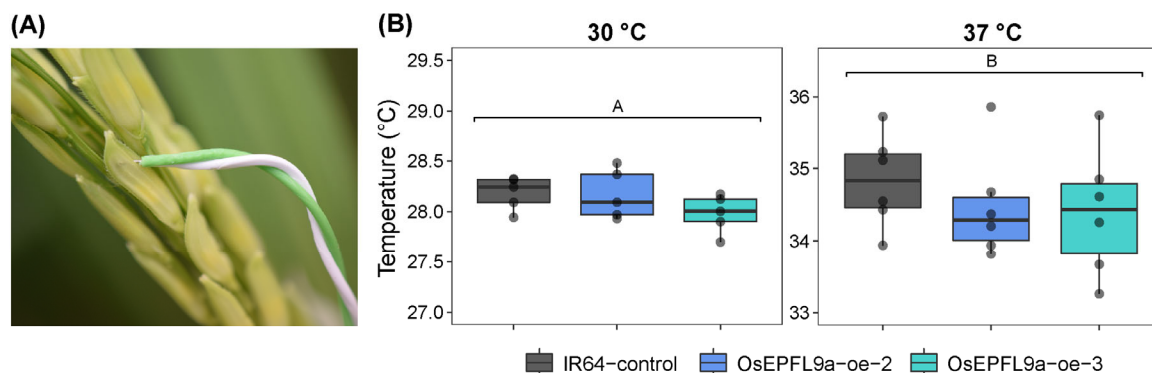
Figure 4.9. Floret temperatures of rice overexpressing *OsEPFL9a* and in IR64-controls were analysed using thermocouple thermometers. **(A)** Picture of a thermocouple sensor placed inside a rice floret for data collection. **(B)** Plots showing floret temperature under control (30 °C) and heat (37 °C) treatment. Two-way ANOVA was conducted to test for the effects of the factors genotype and treatment on floret temperature (n = 5-6 plants per genotype, per treatment). No significant interaction between the effects of factors was found ($p > 0.05$). Main effect analysis showed that treatment ($p < 0.0001$) impacted on leaf temperature, which is represented by different letters in the plot.

4.2.6. Pollen viability

To investigate if the heat treatment had a negative impact on pollen in IR64-controls or in plants overexpressing *OsEPFL9a*, pollen viability was estimated between the 6th and the 8th day of temperature treatment. Pollen grains from mature anthers were collected prior to dehiscence and stained using MTT (thiazolyl blue). Similar levels of pollen viability were observed in all genotypes analysed, and no significant differences were found between plants exposed to different temperature treatments (Figure 4.10).
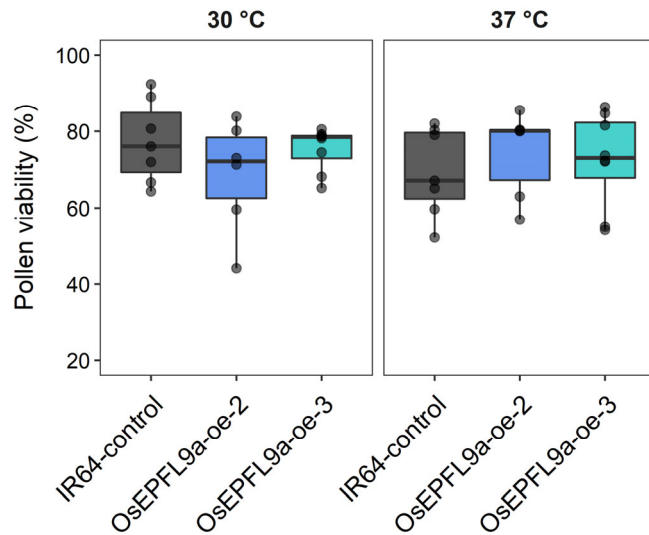
Figure 4.10. Pollen viability rates of IR64-control and transgenic lines exposed to control (30 °C) and heat treatment (37 °C). A two-way ANOVA was conducted to evaluate the effects of temperature treatment and genotype on pollen viability. No significant differences were found ($p > 0.05$, n = 6-8 plants per genotype per treatment).

4.2.7. Plant biomass and panicle production in transgenic and control lines

After the 8-day heat treatment during flowering, all plants were kept in the control growth room until the end of the grain ripening phase, which took a further 5-6 weeks (ripening follows fertilization and includes grain filling and maturity; Figure 4.11). Plants were harvested after reaching maturity (~ 130 days after sowing) and analyses of plant biomass and yield components were conducted. The dry weight of vegetative shoots and the number of panicles per plants were assessed to understand whether there was variation in the development of these plants that could result in yield differences. Additionally, the total above ground biomass was also measured. No differences were found in vegetative shoot dry weight; however, a significant variation was observed in the number of panicles produced in each line. Independently of the temperature treatment, OsEPFL9a-oe-2 produced fewer panicles compared to OsEPFL9a-oe-3 and to IR64-control (Figure 4.12 A and C), furthermore, a trend towards a higher number of panicles was be observed in OsEPFL9a-oe-3, although there was not a significant difference between this line and the control. The number of panicles is determined by the number of tillers (grain-bearing branches in monocots), suggesting that OsEPFL9a-oe-2 plants had a reduced tillering/branching capacity during vegetative development. OsEPFL9a-oe-2 also showed an overall significant reduction in above ground biomass when compared to OsEPFL9a-oe-3 (Figure 4.12 B).

Figure 4.11. Ripening in rice. **(A)** Grain filling stage after fertilization. **(B)** Grain maturity stage is reached when grain filling stops and moisture is lost.
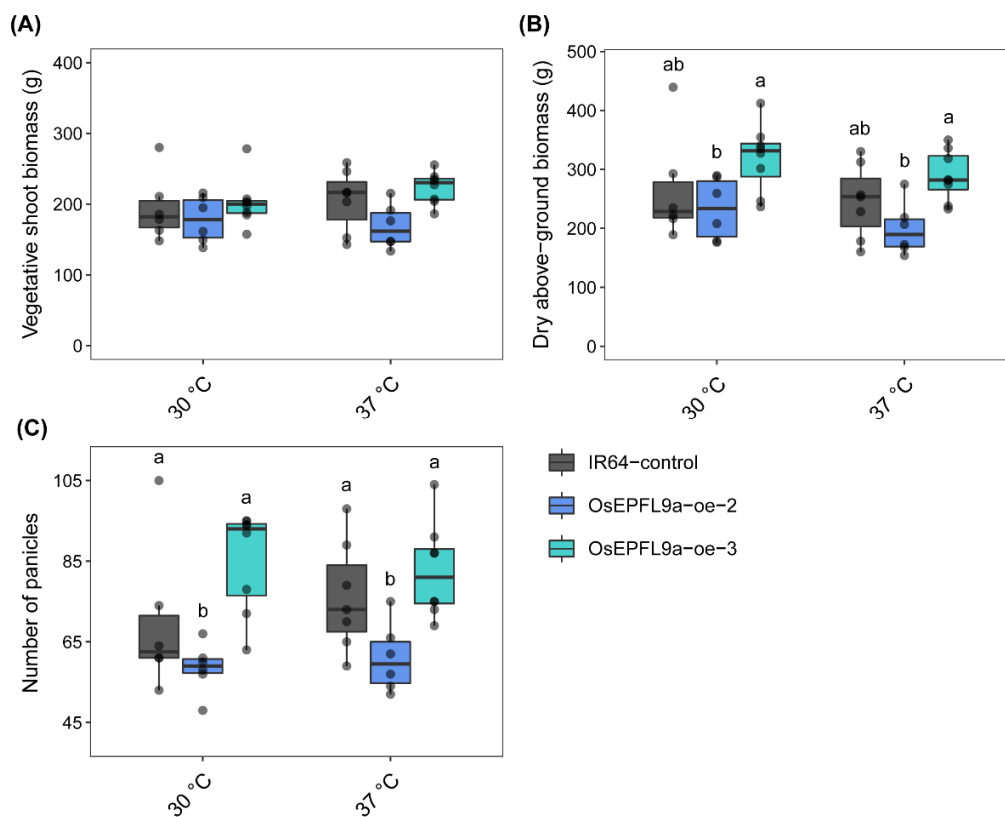
Figure 4.12. Dry biomass weight and number of panicles per plant of transgenic and IR64-control rice exposed to control (30 °C) or heat (37 °C) treatment. **(A)** Vegetative shoot dry weight. **(B)** Above-ground biomass dry weight. **(C)** Number of panicles per plant. **(A-C)** Two-way ANOVA was conducted to test for the effects of the factors genotype and treatment on each variable (n = 6-8 plants per genotype, per treatment). **(A)** No significant differences were found ($p > 0.05$). **(B)** Main effect of the factor genotype was significant ($p < 0.05$), Tukey's post-hoc test indicated a difference between OsEPFL9a-oe-2 and OsEPFL9a-oe-3 ($p < 0.05$), which is represented by letters in the plot. No interaction between the effects of both factors, nor main effect of treatment were found ($p > 0.05$). **(C)** Main effect of the factor genotype was found ($p < 0.05$), Tukey's post-hoc test indicated a significant difference in the number of panicles in OsEPFL9a-oe-2 compared to OsEPFL9a-oe-3 ($p < 0.0001$) and to IR64-control ($p < 0.05$). Letters in the plot represent Tukey's post-hoc results. No interaction between the effects of both factors nor main effect of treatment was found ($p > 0.05$).

4.2.8. Yield and fertility under control and heat treatment

To investigate how the high temperature treatment at flowering impacted on plants yield, the weight of all grains produced per plant was evaluated. Differences in grain filling were also investigated by weighing 100 seeds of each plant. Lines showed great variation in yield per plant, and a substantial negative impact of the heat treatment was observed (Figure 4.13 A). Reductions in grain yield were similarly found across all genotypes investigated. Nonetheless, OsEPFL9a-oe-3 rice had, overall, greater yields in comparison to the IR64-control and the OSEPFL9a-oe-2 line (Figure 4.13 A). This increased yield in OsEPFL9a-oe-3 did not correlate with the increase in stomatal density of either leaves or flowers (Figure 4.13 C-D). Since both lines overexpressing *OsEPFL9a* had similar stomatal density phenotypes, this might be associated with other characteristics observed in this transgenic rice line. For instance, the yield data showed a significant correlation with the number of panicles produced by each plant (Figure 4.13 E). Moreover, the OsEPFL9a-oe-3 rice also had an overall greater seed weight when compared to IR64-control plants (Figure 4.13 B).

To further understand how the heat treatment impacted the flowering process in the rice lines, plant fertility rates were estimated by analysing the proportion of filled versus unfilled spikelets in 10 panicles per plant (Figure 4.14). In line with the grain yield results, fertility rates were strongly reduced by the heat treatment, and whereas no significant interaction between the effects of rice genotype and treatment was found, OsEPFL9a-oe-3 rice showed significantly greater fertility rates in comparison to the IR64-control and to OsEPFL9a-oe-2 (Figure 4.15 A). Although an enhanced fertility was observed in OsEPFL9a-oe-3, similar negative impacts were observed across all lines (Figure 4.15 B), suggesting that rather than having an increased tolerance to high temperatures, this transgenic rice line was in general more productive than the others analysed here. Fertility rates rely on successful pollination and male/female gametophyte viability. Although no differences in pollen viability were detected using a staining technique, it is still possible that the heat treatment impacted on the ability of pollen grains to germinate, in addition to diminish pollination due to anther indehiscence, a commonly observed impact of heat stress during flowering in rice. As these processes were not investigated here, further analyses are needed to understand which mechanisms were specifically impacted, causing the fertility reductions observed, and also the overall difference in fertility rates between lines.

(A)

(B)

(C)

(D)

(E)
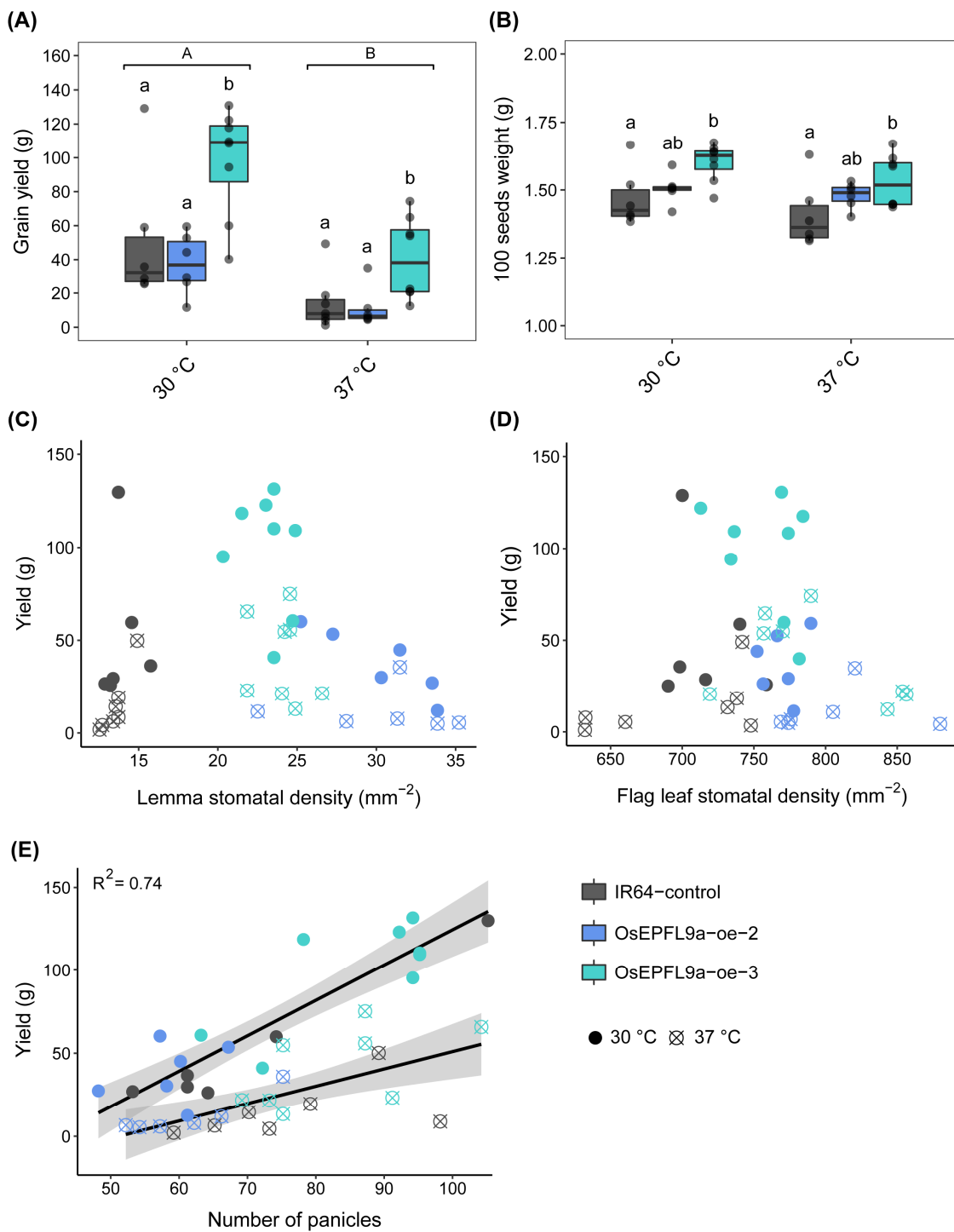
Figure 4.13. Productivity of transgenic and IR64-control rice exposed to control (30 °C) and heat (37 °C) treatment. **(A)** Grain yield. **(B)** Weight of 100 dehulled seeds per plants. **(A-B)** Two-way ANOVA was conducted to test for the effects of the factors genotype and treatment on each variable (n = 6-8 plants per genotype, per treatment). **(A)** No interaction between the effects of both factors was found ($p > 0.05$). Main effect analysis indicated that treatment ($p < 0.001$) and genotype ($p < 0.001$) impacted independently on yield. Tukey's post-hoc test indicated a significant difference in yields of OsEPFL9a-oe-3 compared to OsEPFL9a-oe-2 and to IR64-control ($p < 0.001$). Differences due to main effect of treatment and genotype are represented by the letters in the plot. **(B)** No interaction between the effects of both factors, or main effect of treatment were found ($p > 0.05$). Main effect of genotype ($p < 0.01$) impacted on seed weight. Tukey's post-hoc test indicated a significant difference between OsEPFL9a-oe-3 and IR64-

control (p < 0.01). Differences due to main effect of genotype are represented by the letters in the plot. **(C-D)** Grain yield as function of (C) lemma stomatal density and (D) flag leaf stomatal density; no significant association between variables was found in a multiple linear regression (p > 0.05). **(E)** Grain yield as function of number of panicles; a multiple linear regression was carried out, approximately 74% of the variation in yield data can be explained by a model including number of panicles and treatment ($R^2 = 0.7443$, p < 0.001), shaded area shows confidence interval (95%).

Figure 4.14. Differences in spikelet fertility. **(A)** Rice panicle at maturity, with most spikelets empty. **(B)** Rice panicle at maturity, with most spikelets producing seeds.
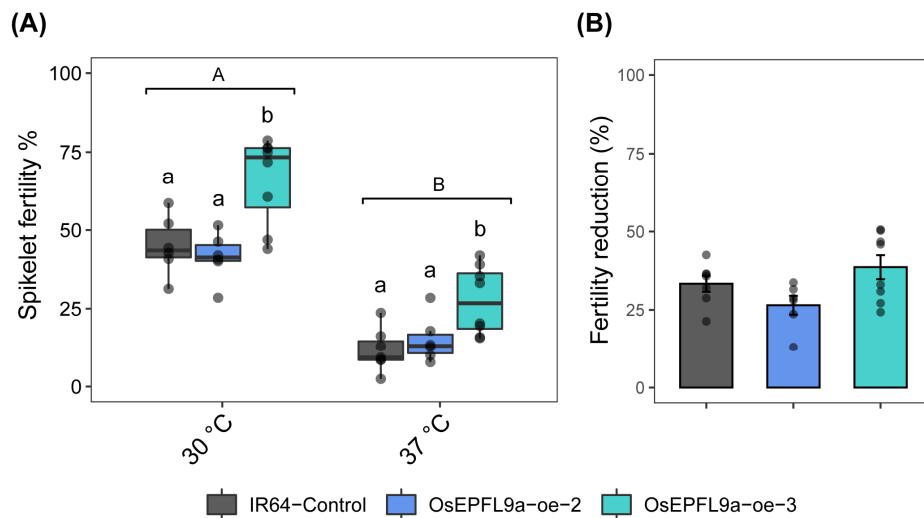
Figure 4.15. Spikelet fertility of transgenic and IR64-control rice exposed to control (30 °C) and heat (37 °C) treatment. **(A)** Percentage of filled spikelets per panicle, two-way ANOVA was conducted to test for the effects of the factors genotype and treatment on fertility (n = 6-8 plants per genotype, per treatment). No interaction between the effects of both factors was found (p > 0.05). Main effect analysis indicated that treatment (p < 0.001) and genotype (p < 0.001) impacted independently on fertility. Tukey's post-hoc test indicated a significant difference in fertility rates of OsEPFL9a-oe-3 compared to OsEPFL9a-oe-2 and IR64-control (p < 0.001). Differences due to main effect of treatment and genotype are represented by the letters in the plot. **(B)** Bar chart to compare the percentage reduction in fertility rates due to high temperature during flowering in each rice genotyped analysed.

4.3. Discussion

4.3.1. Rice overexpressing *OsEPFL9a* does not show improved stomatal conductance or transpiration rates at high temperature during flowering

In Chapter 3, when the response of leaf 6 to rising temperatures was analysed, a behaviour consistent with the opening of stomatal was observed for all genotypes. Additionally, g_s and transpiration rates were higher in OsEPFL9a-oe-3 plants. In the current Chapter, gas exchange measurements were compared between the flag leaves of flowering rice plants exposed to different temperature conditions (control: 30 °C, and heat stress: 37 °C), after growth at control temperature (30 °C). Throughout the temperature treatments all plants analysed looked healthy and did not exhibit obvious signs of stress. PSII quantum yield data showed that the heat treatment did not lead to photoinhibition (Figure 4.5); however, analysis of the gas exchange rates indicated differences between plants exposed to different temperature conditions. The average transpiration rates of flag leaves increased under high temperature, whilst g_s declined. This indicates that a reduction in stomatal apertures possibly minimized a potentially stronger evapotranspiration response and caused a decline in photosynthesis (Figure 4.4). Previous studies have established that when the effect of temperature is isolated stomata tend to open with the rising of leaf temperature. This response is, nonetheless, constrained by other factors, such as water availability and VPD (vapour pressure deficit), which is the atmospheric desiccation strength (Grossiord et al., 2020; Kostaki et al., 2020; Urban et al., 2017; Yang et al., 2020). For a range of species transpiration rates increase and remain high under high VPD, but this increased water loss is often minimized by a decline in g_s (Franks and Farquhar, 1999; Medina et al., 2019; Urban et al., 2017). Responses to VPD can vary between cultivars and even between leaves within a plant, depending on their specific function during the plant life cycle (Streck, 2003). In the experiment conducted in this Chapter, although plants were well watered, relative humidity (RH) was substantially lower during the heat treatment. Due to technical limitations, absolute rather than relative humidity was matched between the two growth rooms, which accentuated the VPD difference between temperature treatments, possibly inducing reductions in stomatal aperture. Regardless of the temperature treatment, no significant differences in water loss were identified between flag leaves of IR64-control and the transgenic plants (Figure 4.4), indicating that OsEPFL9a-oe lines did not have an improved

evapotranspiration. This could be a consequence of the rather small increase in the flag leaf stomatal density observed in these plants ($\sim$ 10%).

4.3.2. Increased stomatal density in leaves and floral organs does not impact on plant temperature

Analysis of flag leaf and floret temperature did not suggest that the stomatal density phenotype in plants overexpressing *OsEPFL9a* had an impact in plant cooling (Figures 4.7 to 4.9). Although leaf temperature was lower in OsEPFL9a-oe-3 compared to IR64-control ($\sim$ 0.4 °C lower on average), this result was not consistent across both transgenic lines. Additionally, as transpiration and g_s rates were similar between all genotypes under heat treatment, it is unlikely that temperature differences arose as a direct effect of changes in the number of stomata. The slight reduced temperature in OsEPFL9a-oe-3 leaves could be associated with other characteristics, for instance, plant architecture and shape can affect plant cooling (Bridge et al., 2013; Crawford et al., 2012). Although this study did not focus on such traits, OsEPFL9a-oe-3 had a trend towards a higher number of panicles (Figure 4.12), which suggests differences in tillering, and therefore in plant architecture.

Despite the high increments in floral stomatal density ($\sim$ 124% and 74%), no significant differences in floret temperature were found between genotypes before anthesis (Figure 4.9). As stomata are mainly distributed on the inner surfaces of the palea and lemma, and on anthers (as described in Chapter 3), it was unlikely that plants overexpressing *OsEPFL9a* would have a significantly increased evaporative cooling in floral tissues while rice florets were closed. Taking appropriate temperature measurements of open spikelets using either the thermal imaging camera or the thermocouples was not possible in this work. Capturing focused thermal images of panicles attached to plants at a close enough distance to allow the identification of open spikelets within the panicle was difficult, and it was made more challenging by the movement of the panicles caused by the air flow inside the growth room. Likewise, thermocouple measurements are compromised if these are not correctly positioned and still. Perhaps taking measurements with a highly sensitive spot infrared thermometer could be an easier and appropriate method for assessing floret temperature during anthesis. Nonetheless, as spikelet fertility results did not suggest that the presence of a greater number of stomata led to an improved thermotolerance, no further investigations were conducted with regards to floret temperature in this study.

4.3.3. Altered stomatal density did not prevent heat-induced infertility

Although the unexpected failure events in the growth rooms during the reproductive phase of plants might have had a negative impact on seed set, IR64-control and transgenic plants subjected to heat (37 °C) had similar decline in yield and spikelet fertility when compared to plants subjected to control treatment (30 °C) (Figures 4.13 and 4.15). As discussed in the previous sections, there were no indications that mature OsEPFL9a-oe-2 and OsEPFL9a-oe-3 plants were able to keep an improved evaporative cooling effect under either temperature treatments imposed. Furthermore, although floret temperature was not investigated during anthesis, yield and fertility results suggest that if a cooling effect was achieved due the increased stomatal density in rice florets, this was not sufficient to alleviate heat damage, at least not under the conditions tested here.

Despite having similar levels of heat-induced sterility, OsEPFL9a-oe-3 had a strikingly improved total grain yield when compared to the OsEPFL9a-oe-2 and IR64-control, regardless of the temperature conditions. Multiple factors might be contributing to the greater yield observed in OsEPFL9a-oe-3, such as its greater number of panicles and tillers, heavier grains and high spikelet fertility (Figures 4.13 and 4.15). Further analyses are needed to understand the causes of the differences observed between these transgenic lines. Tillering capacity, for example, can be determined by genetic factors, although the total number of tillers in a plant is also affected by environmental conditions (Jiang et al., 2019; Wang and Li, 2005). Many genes identified as regulators of tillering in rice have been linked to the signalling pathway of strigolactones, which inhibit tiller bud outgrowth. There is also evidence that other phytohormones, such as auxin, cytokinin and brassinosteroid are involved in tillering regulation (Fang et al., 2020; Wang and Li, 2011; Xu et al., 2005; Yeh et al., 2015). Analyses of gene expression and phytohormone levels could reveal whether the molecular control of tillering is being differentially impacted in plants overexpressing *OsEPFL9*.

Results in Chapter 3 also revealed distinctions between the two transgenic lines studied here. OsEPFL9a-oe-3 had slightly smaller stomata in comparison to OsEPFL9a-oe-2, although this difference was not significant (Figure 3.3). Additionally, OsEPFL9a-oe-3 showed a trend towards a higher g_s in leaf 6, while OsEPFL9a-oe-2 and the control line had similar gas exchange rates (Figures 3.4 and 3.5). As previously discussed, analyses of leaf anatomy could determine whether there are differences in the formation of mesophyll airspaces between the transgenic lines, and an investigation on the speed of the stomatal responses could reveal differences in stomatal behaviour.

As the overexpression of *OsEPFL9a* in OsEPFL9a-oe-2 is more than twice as high as OsEPFL9a-oe-3 (Figure 3.1), it is also possible that the distinct levels OsEPFL9a led to the divergent phenotypes observed. Pleiotropic effects could be considered; in Arabidopsis *AtEPFL9* is expressed in roots (Sugano et al., 2010), nonetheless, in two Nipponbare rice lines overexpressing *OsEPFL9a* no significant differences were found in root structure (Mohammed et al., 2019). It is also likely that these differences between lines resulted from somaclonal variation induced during the tissue culture process, and subsequent inbreeding of lines. The investigation of a third independent transgenic line could have helped in the understanding of the distinctions observed.

4.3.4. Conclusions

This investigation showed that transgenic rice lines with increased stomatal densities in leaves and florets were not able to overcome the damages caused by the exposure to high temperature during the flowering stage. The increase in flag leaf stomatal density observed in the transgenic lines was modest (~ 10%), therefore it is still possible to speculate that a greater increase in the number of stomata could have been effective. Although the problems with the growth rooms conditions experienced during this study could have had an impact in the yield data, there were no indications of an improved evaporative cooling process nor protection of seed yields in the lines overexpressing *OsEPFL9a* under the conditions tested. Therefore, this hypothesis was not further investigated in this study.

Chapter 5

Stomatal development and gene expression in rice florets

5.1. Introduction

The importance of stomata to plant water and carbon relations has led to in depth research into the functioning and development of these structures. However, most of what is known about stomata comes from studies of leaves (and cotyledons), which are the primary photosynthetic organs and tend to have high densities of veins and stomata (Zhang et al., 2018). In flowers, the presence of stomata varies according to the species and to the floral organ in question (Mathew et al., 1981; Patiño and Grace, 2002; Roddy et al., 2016), and in most cases, their function and development are poorly characterized. In contrast to mature leaves, flowers are an important sink for water, carbon and nutrients, and essential for sexual reproduction. The research described in this chapter aimed to characterize stomatal development and function in the floral organs and to add to our understanding of the physiological processes associated with maintenance of flowers from early development to anthesis.

5.1.1. The presence and development of stomata in floral organs is variable

Floral stomata have been reported in different plant groups, including monocots (Azad et al., 2007; Clement et al., 1997; Ebenezer et al., 1990; Hew et al., 1980; Teare et al., 1972), eudicots (Gupta et al., 1965; Lugassi et al., 2020; Patiño and Grace, 2002; Roddy et al., 2016; Watson, 1962; Wei et al., 2018), Austrobaileyales (Roddy et al., 2016; Zhang et al., 2018) and magnoliids (Roddy et al., 2016; Zhang et al., 2018). Although observations in a variety of monocot species suggest that stomatal ontogeny is similar between different organs in the same plants (Stebbins and Khush, 1961), species with variable stomatal development modes across different organs are also described in the literature (Gupta et al., 1965; Mathew et al., 1981). In these plants, floral organs might display mature stomata with a different number of subsidiary cells in comparison to leaves. Additionally, variation in the temporal patterning of floral stomata can also be observed. At early stages of flower development in citrus plants, for example, stomata were found on anthers, styles, and sepals, but not on ovaries, where stomata were observed only after anthesis (Lugassi et al., 2020).

The genetic pathway that drives stomatal development has not been directly studied in flowers, however it is well characterized in leaves, in particular for the eudicot model *Arabidopsis thaliana*. Although leaf stomatal ontology and architecture varies across plant groups, functional analyses suggest that the stomatal development pathway is regulated by the same key bHLH transcription factors in different species from mosses to angiosperms (for a detailed description of the current stomatal development model, see Chapter 1) (Chater et al., 2017; Qu et al., 2017). Additionally, analysis of Arabidopsis mutants for either AtICE1 or AtEPFL9 reported alterations in stomatal development in anthers as well as leaves, suggesting a common regulatory pathway between different organs (Sugano et al., 2010; Wei et al., 2018).

5.1.2. Floral stomata might be involved in diverse functions

The role and ability of floral stomata to function might vary according to species and floral organ (Azad et al., 2007; Feild et al., 2009; Hew et al., 1980; Huang et al., 2018; Lugassi et al., 2020). Stomata found on anthers have been associated with the dehiscence process, as the evaporation from these pores can facilitate anther dehydration after anthesis (Keijzer et al., 1987; Nelson et al., 2012; Wei et al., 2018). Similarly, stomata in the sporophyte of *Physcomitrella patens* assist in dispersal of spores, and stomata-less phenotypes show a delayed capsule dehiscence (Chater et al., 2016). In petals, a study in tulip showed that stomata present on these floral organs adjust their aperture in response to temperature changes, coinciding with the opening and closing cycle of the corolla. Interestingly, an inverse relationship was observed between stomatal aperture in outer and inner surfaces of petal during this cycle (Azad et al., 2007). In gerbera sepals, stomata have been shown to be responsive to stimuli, adjusting their apertures in response to light/dark and ABA treatments (Huang et al., 2018). However, environmental responsiveness is not universally observed, and stomata present on flowers are considered non-functional in some plants, as in tropical orchids (Hew et al., 1980). Floral tissues might also contribute to carbon assimilation, although photosynthetic rates tend to be lower than in leaves, and also vary between floral organs and species (reviewed in Brazel and Ó'Maoileídigh, 2019). Studies in grasses, including wheat, rice and barley, suggest that inflorescence photosynthesis is an important contributor to grain filling in these crops, but that respiratory CO_2 is a significant proportion of the photosynthetic carbon source (Araus et al., 1993; Bort et al., 1996; Chang et al., 2020; Molero and Reynolds, 2020).

5.2.3. Stomata in rice florets

In rice plants, the presence of stomata on floral organs has been previously reported (Ebenezer et al., 1990; Wu et al., 2014), and the distribution of floral stomata in the Indica cultivar IR64 was characterized in detail in the present study. Results described in Chapter 3 showed that in this rice variety stomata are mainly found in the internal epidermis of the palea and lemma, and also in the connective tissue of anthers. These stomata are formed by a pair of SCs and a pair of GCs, but their shape is distinct from that of leaf stomata, perhaps as a result of a developmental variation. Results from the present study also showed that stomatal development in rice florets is altered by the overexpression of the Epidermal Patterning Factors *OsEPF1* and *OsEPFL9a*, which function in leaf stomatal development. Additionally, seed set was not affected in transgenic rice plants with a strong reduction in the number of floral stomata, suggesting that the presence of stomata in rice florets might not be essential for floral development and successful plant reproduction. Yet, there is still much to learn about floral stomata in rice. A characterization of the patterning and timing of development of these structures might be a starting point for further investigations. Additionally, a more detailed analysis of plants with a reduction or absence of stomata on floral organs might provide insights regarding processes affected by floral stomata.

5.1.4. Objectives

To improve the current understanding of how stomata develop in rice floral organs, the progression of stomatal development was studied in IR64 rice florets, with a focus on the spatiotemporal gradient observed in lemma. Based on this investigation, a transcriptomic analysis was performed in different stages of early developing florets, allowing the characterization of gene expression profiles over the course of stomatal development. Moreover, to investigate the potential consequences of stomatal density reductions on biological processes associated with floret development and physiology in rice, the expression profile of IR64 developing and mature florets was compared to that of transgenic rice overexpressing *OsEPF1*.

5.2. Results

5.2.1. Stomatal development in rice florets

As shown in Chapter 3, the stomatal pores present on the florets of IR64 rice had a less structured and more discontinuous distribution than the regular stomatal patterning characteristic of rice leaves. The shape of subsidiary and guard cells in the florets were also slightly different than those of leaves. In addition, in the internal epidermal surfaces of fully expanded florets, pavement cells surrounding the stomatal complexes were more variable in shape and size, making it frequently difficult to identify the epidermal cell files. The analysis of lemma of young rice florets, however, revealed that the development of stomatal complexes in this organ was similar to that previously observed in rice leaves. A detailed examination of the internal surface of developing lemmas showed that cells proliferated in distinct files. As cells were pushed up, asymmetric divisions were observed in specific cell rows, originating either guard mother cells (GMCs) or trichome precursor cells (Figure 5.1 A). As development progressed, subsidiary mother cells (SMCs) were formed next to GMCs, as result of asymmetric divisions in neighbour files (Figure 5.1 B-C). A longitudinal symmetric division of the GMCs led to the formation of two guard cells (GCs) (Figure 5.1 D). Then, the stomatal complex matured (Figure 5.1 E), achieving its total size in fully expanded florets (Figure 5.1 F). As stomatal cells entered the maturation stage, pavement cells were also differentiating, acquiring a more variable shape and losing the noticeable distribution in rows.
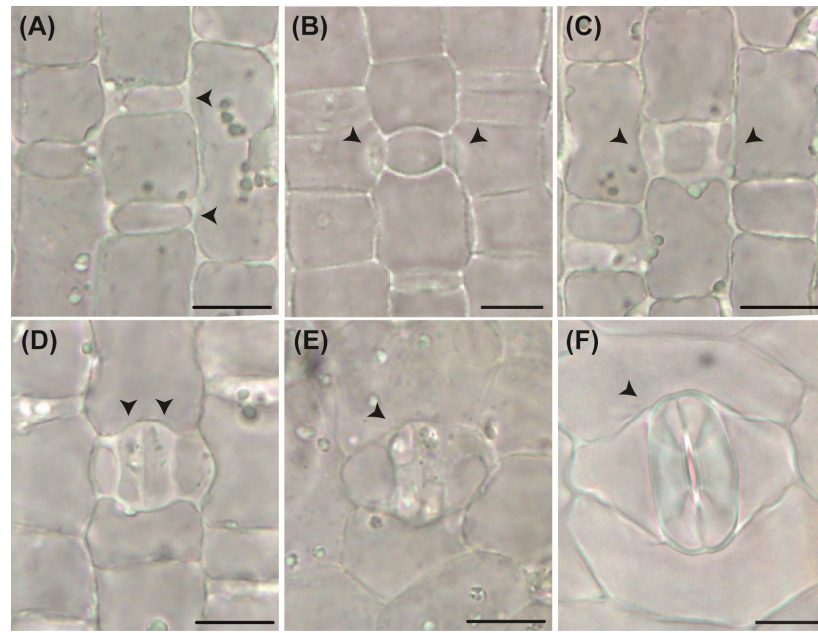
Figure 5.1. Stomatal development in lemma of IR64 rice florets. (A-F) Light microscopy images of developing rice lemma epidermis, showing the progression of stomatal development in its internal surface. Scale bars = 10μm, 1000x magnification. **(A)** Asymmetric divisions in specific cell files resulted in small GMCs. **(B-C)** Following asymmetric divisions led to the formation of SMCs next to a GMC. **(D)** Symmetric division of GMC formed two GCs. **(E)** The stomatal complex entered a maturation stage and cells started to expand. **(F)** Fully mature and expanded stomatal complex. Black arrowheads indicate stomatal complexes or relevant stomatal lineage cells.

5.2.2. Spatiotemporal gradient of stomatal development in IR64 lemma

To characterize the spatiotemporal progress of the stomatal lineage cells during the development of IR64 florets, developing panicles were removed from inside the flag leaf sheath, and florets at different developmental stages were analysed by light microscopy. By examining the internal epidermis of lemma in developing florets of various sizes (starting at a stage when florets were approximately 0.75 mm in length), a qualitative description of stomatal development in lemma was produced. As detailed in Figure 5.2, in 1 mm florets, a few GMCs that had originated from asymmetric divisions could be identified in the upper portion of lemma. In 1.5 mm florets, SMCs had begun to form at the upper, or distal, end of the lemma, and GMCs resulting from asymmetric entry divisions could be observed in the middle portion of the lemma. Then, in slightly larger florets, the distal region of lemma contained recently divided immature GC pairs, with earlier lineage events in lower, proximal, areas. This spatiotemporal gradient, with earlier stages of stomatal development being observed on the basal area of lemma and moving up as development of stomata and floret progresses, was observed until all the stomatal complexes were fully differentiated with mature GCs and SCs, in florets of approximately

6.5 mm length. After this stage, final expansion of stomatal complexes occurred as florets grew. There were, however, exceptions to this pattern and, in some instances, new stomatal files were being initiated whilst most other stomata were advanced in their development. These delayed stomatal files were generally found in lateral and folding areas of lemma.
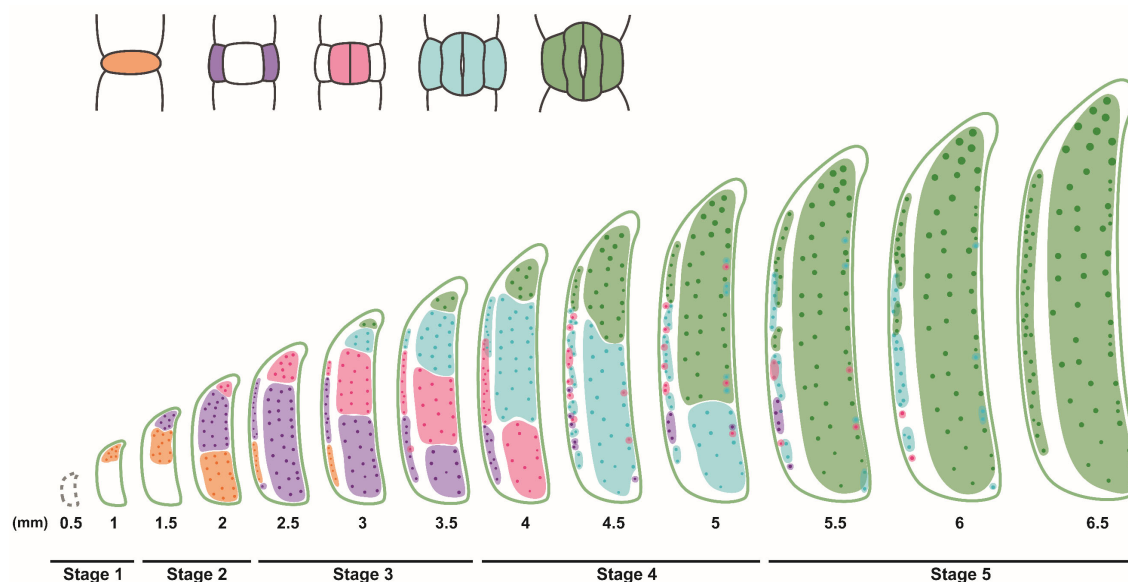
Figure 5.2. Diagram of the stomatal development gradient in the adaxial epidermis of the lemma of IR64 rice florets. Top left: coloured-coded stomatal lineage cells: GMC (orange), SCs (purple), recent divided GCs (pink), stomatal complex in maturation process (blue) and differentiated stomatal complex (green). Main: representation of lemmas from different floret sizes (length of floret in mm is shown below each lemma). Coloured shadows on lemmas correspond to coloured-coded stomatal lineage cells on the top left, showing regions where the specific stomatal lineage cells can be mainly found. Stage division of floret development used for subsequent RNA-seq analysis is indicated at the bottom. Dots indicate location but do not direct correlate to stomatal quantity.

Although this study primarily investigated lemma, observations of palea showed that stomatal development follows a similar pattern in this floral organ (not shown). Therefore, based on the results described above, this floret development window was broken down into five stages (shown in Figures 5.2 and 5.3) that represent the course of stomatal development in the bract like organs of the rice florets: **Stage 1** – proliferation and initiation of entry asymmetric divisions (~0.5-1 mm florets); **Stage 2** – entry divisions continue, SMC establishment and divisions initiate (1.1-2 mm florets); **Stage 3** – symmetric divisions of GMCs begin to produce GCs (2.5-3.5 mm florets); **Stage 4** – Most asymmetric divisions cease and stomatal complexes begin to mature (4-5 mm florets); **Stage 5** – Most stomatal complexes are differentiated (5.5-6.5 mm florets). This stage classification using floret length as marker facilitated the subsequent study of gene

expression in rice flowers during stomatal development, alongside the study of fully mature florets (Fig 5.4). Florets were considered mature after heading of the panicle, but prior to anthesis and anther dehiscence. At this stage, florets had approximately 8.5 to 9.5 mm.

Figure 5.3. Rice spikelets with increasing floret sizes, from 0.5mm to 6.5mm. Stage division used in this studied for gene expression analysis are indicated.
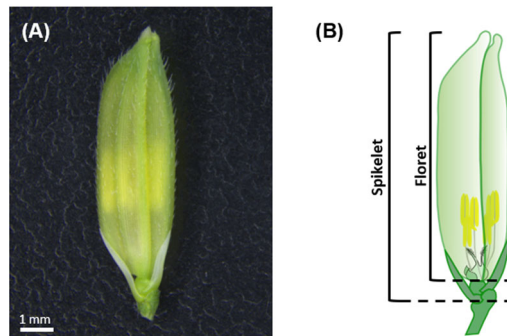
Figure 5.4. (A) Mature rice spikelet. **(B)** Diagram showing the difference between spikelet and floret length. Only florets were used in this study.

5.2.3. RNA-sequencing - Reads processing and quality control

To characterise gene expression during the stomatal development in IR64 florets, as well as to identify potential differences between florets of IR64 and transgenic plants with a reduction in stomatal density, a RNA-sequencing analysis was conducted. This analysis included florets in the developing stages 1 to 5 and mature from IR64 and OsEPF1-oe-S rice plants. OsEPF1-oe-S rice was first characterised in Caine et al. (2019), this transgenic rice line ectopically overexpresses the gene *OsEPF1* and shows a strong reduction in leaf stomatal density. As previously described in Chapter 3, this transgenic line also showed

a strong reduction in stomatal density (near absence) in the floral tissues. To confirm that the OsEPF1-oe-S plants included in this RNA-seq analysis had the expected phenotype in the flowers, their stomatal density was evaluated in lemma (not shown). Results were similar to those found in Chapter 3; IR64 plants had in average 15.60 stomata per mm^2, while OsEPF1-oe-S plants showed in an average of 0.22 stomata per mm^2 in the upper area of adaxial epidermis of lemma.

Three biological replicates of florets from each of the developing stages 1 to 5 (Figures 5.2 and 5.3) were collected between the 11th and the 12th week after sowing of IR64 and OsEPF1-oe-S rice plants, while mature flowers (Figure 5.4 A) were collected around the 14th week after sowing. Each biological replicate from developing florets comprised RNA from three different plants, whilst for mature flowers, a biological replicate comprised only one plant. RNA samples were purified using the Spectrum Plant Total RNA Kit (Sigma-Aldrich) and sent to Novagene facilities (in China), where library preparation and RNA sequencing were conducted. The Illumina platform Nova-seq 6000 was used to produce paired-end reads, with read length of 150 bp (for more details on sample/library preparation and sequencing see Methods sections 2.14 to 2.16).

Sequencing depths varied from 31.5 to 79.4 million pairs of reads, which were subjected to quality trimming, adaptor filtering and, were successfully mapped to the reference genome (summary in Table A1 in Appendix). Overall, alignments rates were between 94-96%, with 86-89% of reads aligned uniquely. The Nipponbare IRGSP 1.0 genome (Kawahara et al., 2013) was used as reference in this study due to its high assembly and annotation quality, however, attempts to align this data to other available genomes, such as the rice pangenome (Wang et al., 2018) and the IR64 assembly (Schatz et al., 2014) were also conducted (not shown). Pairs of reads that were concordantly aligned to unique exonic regions of the reference genome were subsequently used to estimate gene-level abundance. Due to initial variation in sequencing depth, the number of counts assigned to genes varied considerably between samples, however, all samples had more than 20 million counts assigned to genes (Figure 5.5) and showed very similar count density distribution (Figure 5.6) (for details on the bioinformatics procedures, see Methods sections 2.17 and 2.18).

A principal component analysis (PCA) on the count data revealed a clear separation between samples according to developmental stage (Figure 5.7 A). The principal component 1 (PC1) mainly separated younger developmental stages from mature florets, indicating that the expression profile of mature florets is particularly different from those of other samples. Differences between lines (IR64 or OsEPF1-oe-S) did not appear to be

an important source of variation. To further investigate dissimilarities between developing florets of stages 1 to 5, a PCA including only these samples was performed (Figure 5.7 B). Samples were clearly separated by stage in the PC1 axis, indicating that developmental stage is the major source of variation between samples. Similar results were found in a clustering analysis based on the Euclidean distance matrix of all samples (Figure 5.8). In this analysis, the mature flowers formed a distinct group, whilst stages 1 to 5 were placed together in a separated cluster, in which stages 1, 2 and 3 formed well-defined subgroups, and stages 4 and 5 were included in the same subgroup. In addition, count data confirmed that all OsEPF1-oe-S samples overexpress *OsEPF1* in comparison to the non-transgenic IR64 samples (Figure 5.9). The expression level of *OsEPF1* declined as non-transgenic IR64 florets matured but, as expected, was maintained at a relatively high level in the mature OsEPF1-oe florets.
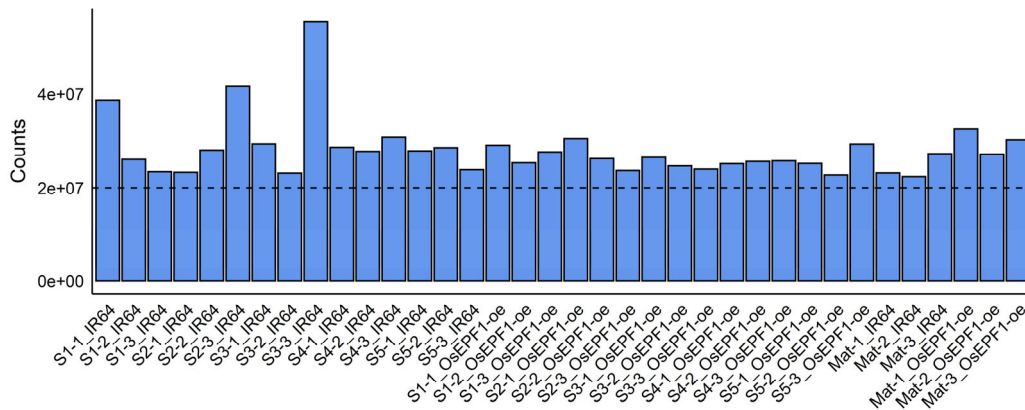
Figure 5.5. Number of counts assigned to genes in each sample. Samples were named according to their stage (e.g. S1: Stage 1, Mat: Mature), followed by -replicate number (1, 2, or 3), and _rice genotype
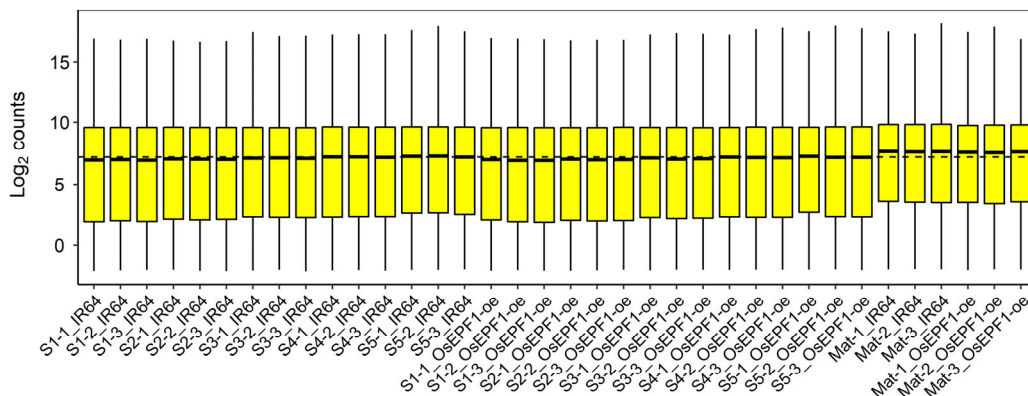
Figure 5.6. Count density distribution per sample. Counts were transformed to $\log_2$ scale and normalized by sample size (number of counts per sample) using regularized log transformation (rlog) function from DESeq2 (Love et al., 2014).

(A)

(B)
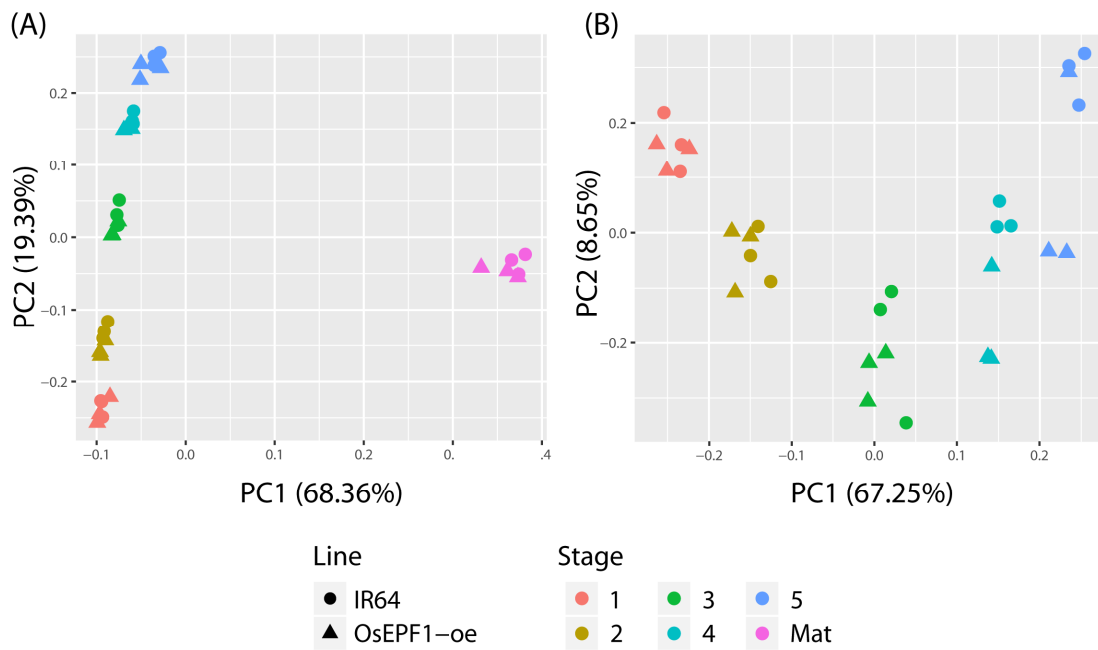
Figure 5.7. PCA plots. Data was transformed to $\log_2$ scale and normalized by sample size (number of counts per sample) using variance-stabilizing transformation (vst) (Love et al., 2014). **(A)** PCA including samples of developmental stages 1 to 5 and mature florets of IR64 and OsEPF1-oe-S plants. **(B)** PCA including samples of stages 1 to 5 of IR64 and OsEPF1-oe-S plants.
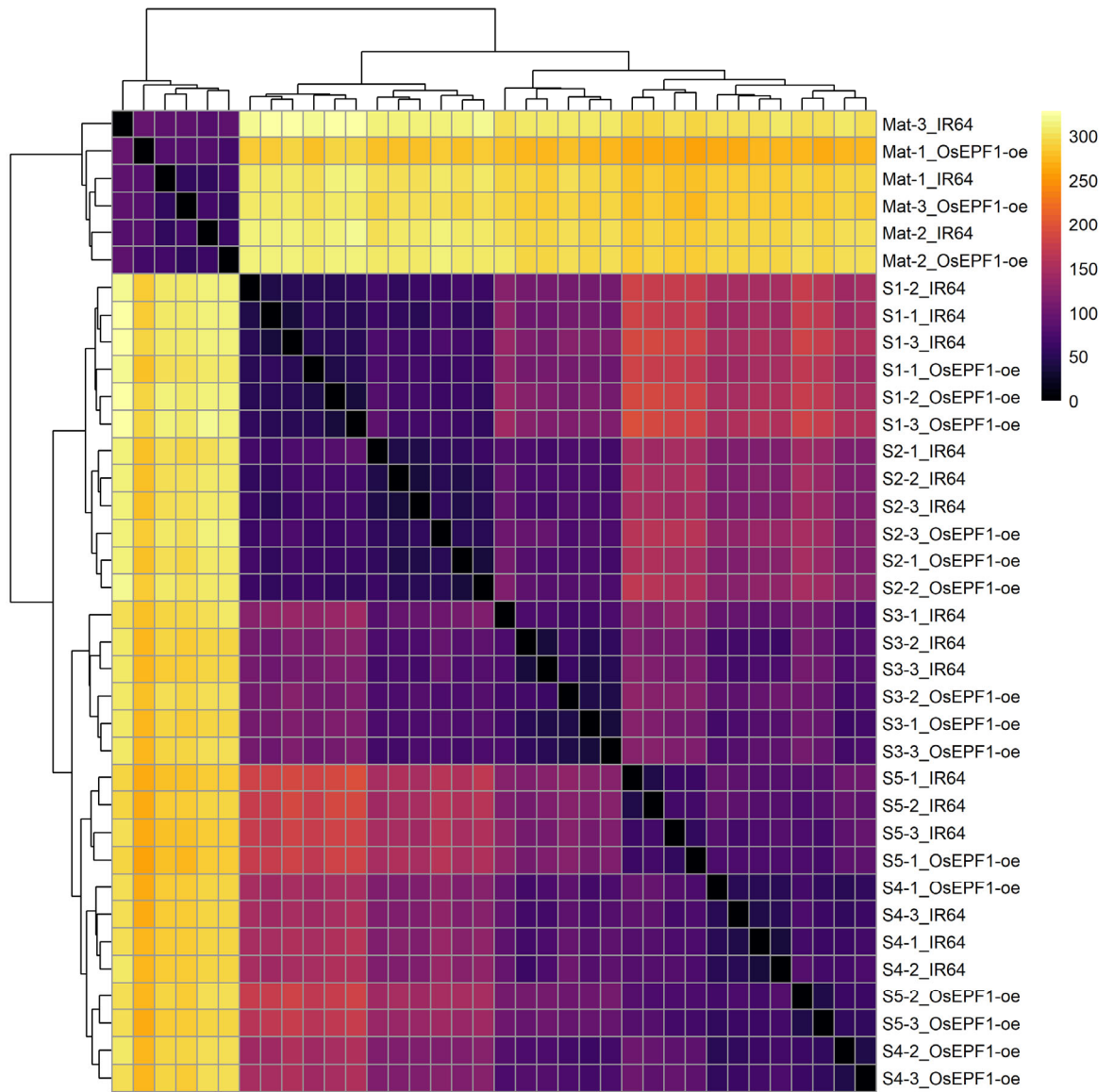
Figure 5.8. Heatmap of sample to sample distances. Variance stabilizing transformation (vst) of count values (Love et al., 2014) was performed, and a matrix of Euclidean distances between samples was produced. Sample identity is indicated on the right-hand side. Scale - values are proportional to level of dissimilarity between samples, zero indicates least dissimilar.
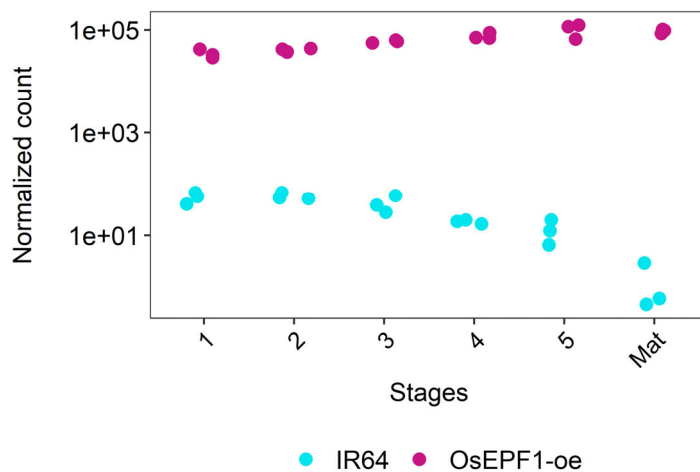
Figure 5.9. Expression levels of *OsEPF1* across all samples. Counts were normalized by size factor and a pseudo count of 0.5 was added. Y-axis is transformed to log scale.

5.2.4. Stomatal development series in IR64 florets – Analysis of florets stages 1 to 5

To characterize the overall changes in gene expression in IR64 florets during stomatal development, a differential expression analysis was conducted using the R package DESeq2 (Love et al., 2014). This analysis included floret stages 1 to 5 of IR64 plants. A likelihood ratio test (LRT) comparing gene expression across this developmental series reported 13,279 differentially expressed genes (DEGs) from a total of 31,017 expressed genes analysed, considering an adjusted p-value < 0.001 (Benjamini-Hochberg correction). Hierarchical clustering analyses using the 250 most significant genes (Figure 5.10) revealed two major sample subgroups, one comprising stages 1 and 2, and a second, grouping stage 3 to 5. Likewise, considering the changes in expression across all the sample levels, the 13,279 DEGs were grouped in 21 significant gene clusters according to their expression pattern (Fig 5.11). The two major gene clusters identified, cluster 1 and 2, comprised genes with opposite expression patterns. These genes showed higher expression levels, respectively, at stages 1 or 5, and were gradually switched off (cluster 1) or on (cluster 2) across the developmental time-course. Other expression patterns, with smaller groups of genes showing higher expression levels in stages 1 and 5 were also identified, as well as groups peaking in stages 2, 3 and 4.
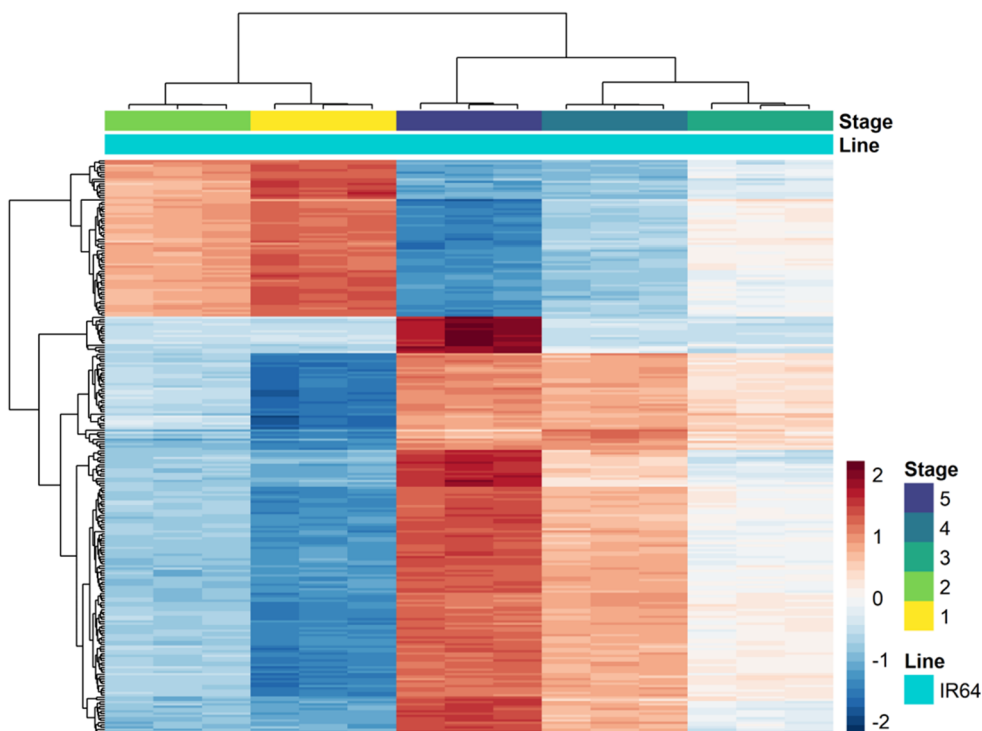
Figure 5.10. Hierarchical clustering analysis with the 250 most significant DEGs found in the IR64 floret developmental time-series. Heatmap scale shows row z-score of vst-transformed values across samples. Rows correspond to genes. Columns correspond to samples.
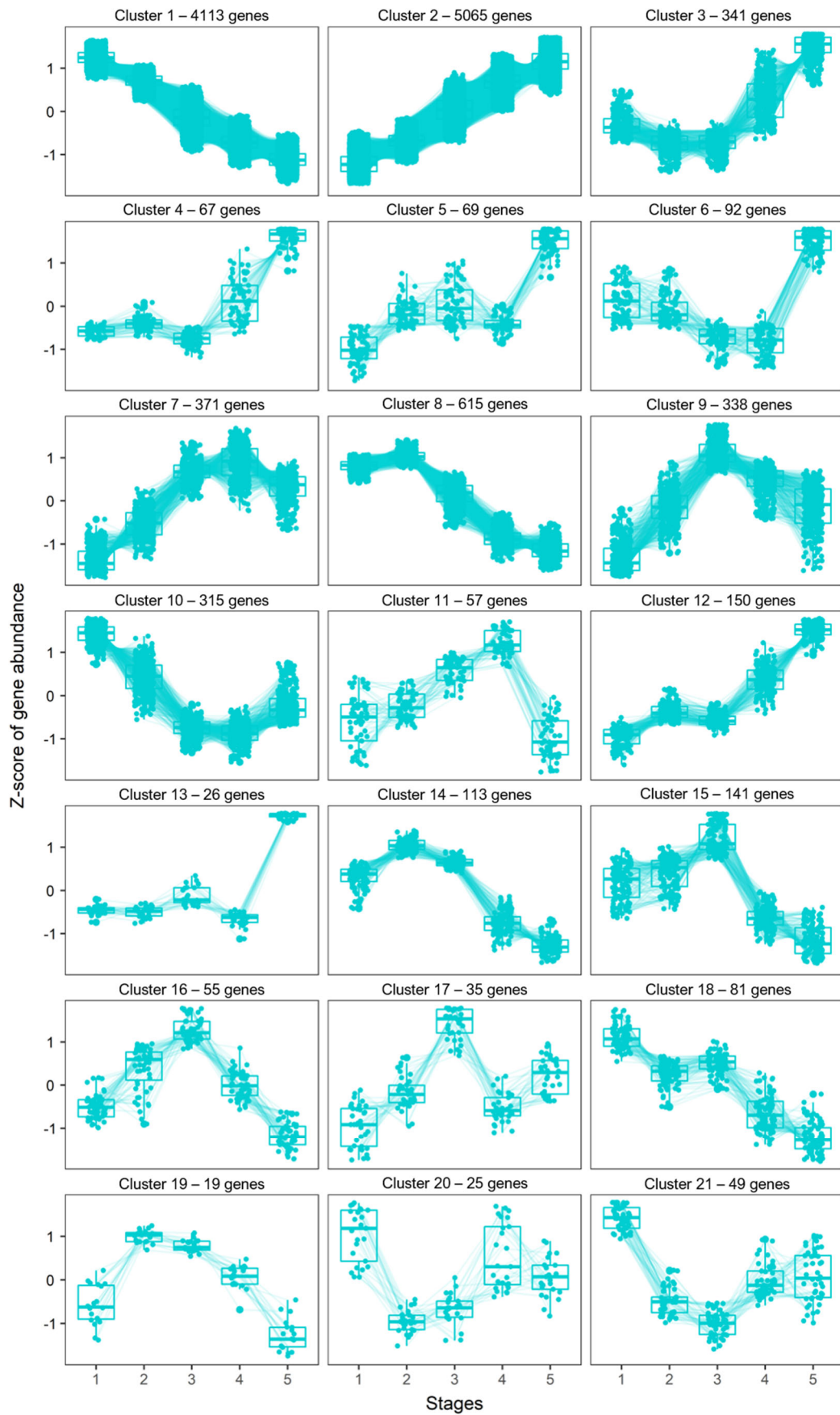
Figure 5.11. Expression patterns of DEGs across the stomatal development series in IR64 plants. Using a hierarchical approach, genes were grouped into 21 significant clusters according to their expression patterns.

- *Functional profile of DEGs*

To identify the potential biological processes in which these DEGs are involved, a functional enrichment analysis was performed. The genes identified in the expression pattern clusters (Fig 5.11) were grouped according to their peak of expression (Table 5.1), then, each gene set was tested for over-representation of Gene Ontology (GO) terms, according to the annotation available for *Oryza sativa* on Ensembl Plants (https://plants.ensembl.org). The analysis revealed that genes with higher expression in stage 1 were mainly linked to cell division, RNA processing and plant organ development (Figure 5.12). On the other hand, genes from which transcripts accumulated towards stage 5 were associated with metabolic processes, as well as, cell wall biosynthesis and photosynthesis (Figure 5.13). These results are consistent with an organ development process, which is initially driven by cell division, and gradually transitions to a cell expansion and differentiation stage. Gene sets with peaks in stages 2, 3 and 4 were considerably smaller, therefore, not as many GO terms were associated with them. Genes involved in protein translation were over-represented in the gene set with expression peak in stage 2 (Figure 5.14), while, an association with steroid biosynthesis was found for genes peaking in stage 3 (Figure 5.15). No significant GO terms were identified for the gene set showing higher expression levels in stage 4.

Table. 5.1. Gene sets analysed in functional enrichment test.

Peak of expression	Clusters grouped	Total number of genes
Stage 1	1, 10, 18, 21	4,558
Stage 2	8, 14, 19	747
Stage 3	9, 15, 16, 17	559
Stage 4	7, 11, 20	453
Stage 5	2, 3, 4, 5, 6, 12, 13	5,801
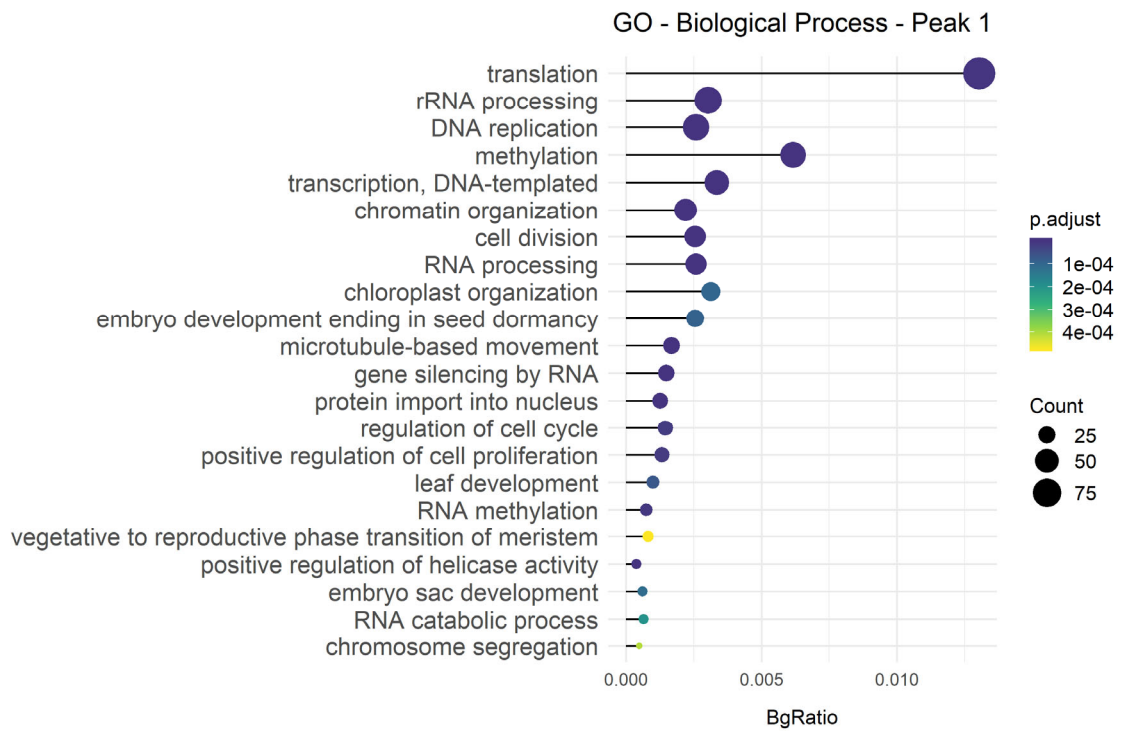
Figure 5.12. Biological processes associated with genes peaking in stage 1. Count refers to the number of DEGs in a GO term. Colour scale corresponds to the adjusted p-value. BgRatio is the ratio between the number of genes annotated in a GO term and the total expressed genes analysed (31,017 genes).
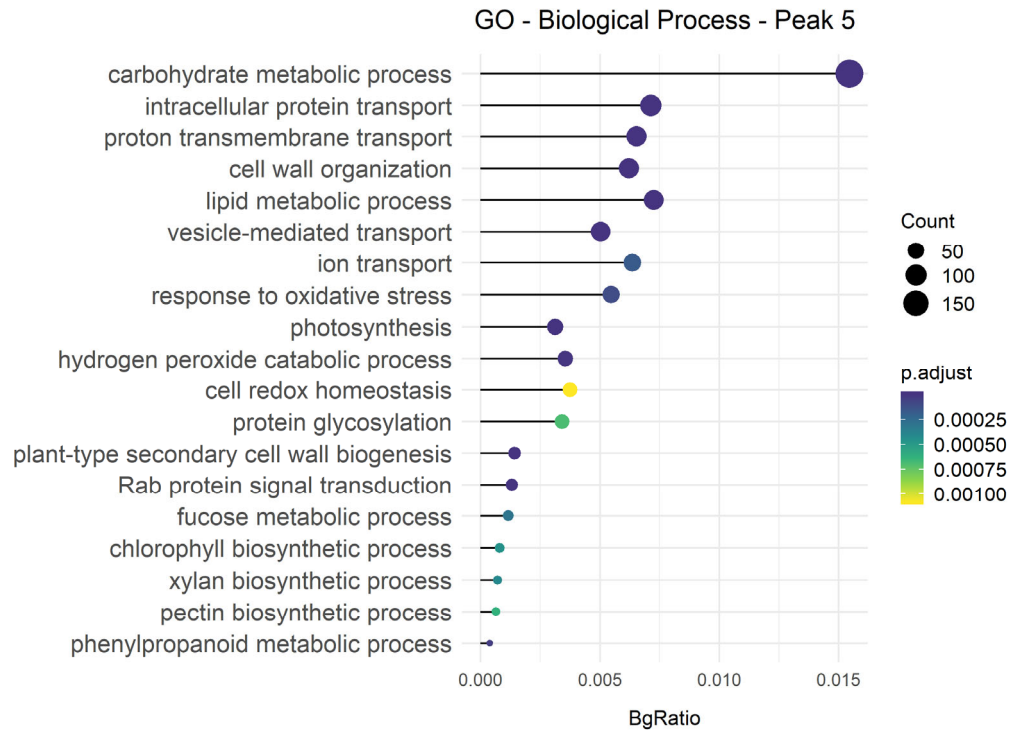
Figure 5.13. Biological processes associated with genes peaking in stage 5. Count refers to the number of DEGs in a GO term. Colour scale corresponds to the adjusted p-value. BgRatio is the ratio between the number of genes annotated in a GO term and the total expressed genes analysed (31,017 genes).
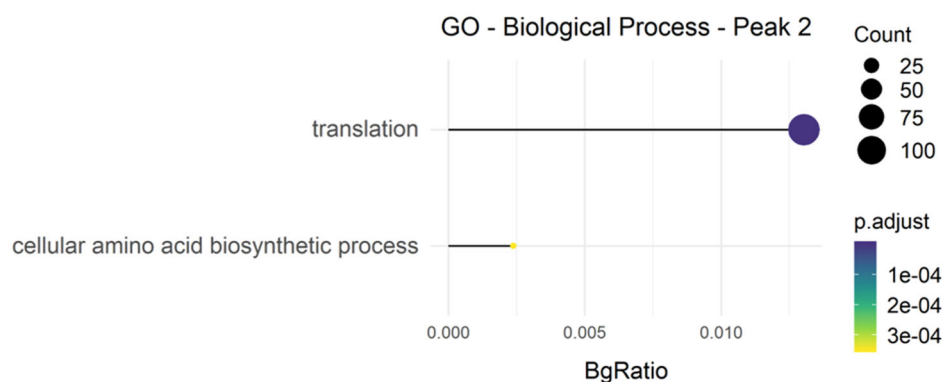
Figure 5.14. Biological processes associated with genes peaking in stage 2. Count refers to the number of DEGs in a GO term. Colour scale corresponds to the adjusted p-value. BgRatio refers to the ratio between the number of genes annotated in a GO term and the total expressed genes analysed (31,017 genes).
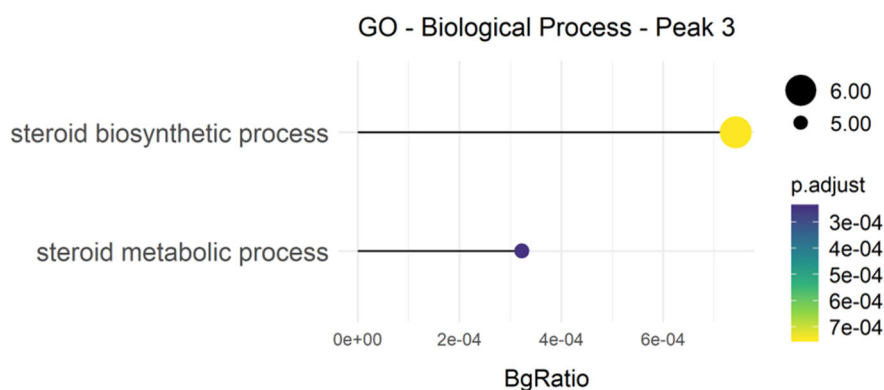
Figure 5.15. Biological processes associated with genes peaking in stage 3. Count refers to the number of DEGs in a GO term. Colour scale corresponds to the adjusted p-value. BgRatio is the ratio between the number of genes annotated in a GO term and the total expressed genes analysed.

5.2.5. Expression of stomatal genes in developing IR64 florets

- *Expression of stomatal development genes*

The expression of genes associated with stomatal development was analysed in the stages 1 to 5 of IR64 florets (Figure 5.16). The function of proteins encoded by the majority of genes investigated in this study had originally been identified in Arabidopsis and also previously studied in rice or other grasses (Table 5.2). From the 27 genes analysed, 20 were identified as DEGs across these samples in the likelihood ratio test. Overall, the expression patterns (Figure 5.16 and Figure 5.17) of these DEGs are consistent with the current knowledge of stomatal development in rice leaves. Genes important for stomatal lineage initiation, such as *OsSPCH1/2*, *OsSHR1/2*, *OsSCR1/2*, *OsICE1*, *OsSCRM2*, *OsCYCA2;1* showed highest expression levels at Stage 1. From these,

OsSHR1/2, *OsSCR1/2* and *OsICE1* probably also regulate other fate transitions during stomatal development (Wu et al., 2019), but here the expression levels of these genes were reduced towards the later stages analysed. *OsMUTE*, which is associated with the formation of SCs and maintenance of GMC identity (Wu et al., 2019), reached its highest expression in stage 3, falling dramatically in stage 4. In line with its role in GCs maturation (Liu et al., 2009), *OsFAMA* expression increased gradually, reaching its highest level at stage 5. Genes encoding for the signalling peptides OsEPF1/2 and OsEPFL9 accumulated in initial stages. In addition, transcript levels for the co-receptor TMM, were more abundant in stages 1 and 2, dropping substantially from stage 3. This was consistent with the TMM expression pattern in Arabidopsis, where *AtTMM* expression is highest in stomatal precursor cells, less abundant in young GCs and absent in mature GCs (Nadeau and Sack, 2002). The rice orthologs of the ERECTA family – *OsER*/*OsER2* (*AtER*) and *OsERL1* (*AtERL1*/*AtERL2*) – showed higher transcript levels in the initial stages, however, a marked decline in expression across the stages was observed in *OsER*. As ERECTA genes are known to regulate various processes, including in floral development (Cai et al., 2017; Pillitteri et al., 2007), this pattern also could be related to other functions. Finally, although very low read counts were associated with the subtilisin protease SDD1, *OsSDD1* seems to be most expressed in stages 1-3.

Figure 5.16. Heatmap of stomatal development genes. Row z-score of vst-transformed values across samples was plotted. Rows correspond to genes. Columns correspond to samples.

Table 5.2. Genes associated with stomatal development analysed in this study.

Rice gene id	Gene name	Adjusted p-value (LRT)	Role	Organism relevant role was shown	Reference
Os12g0502300	*OsCYCA2;1*	1.41E-24 *	Control of entry division	Rice	Qu et al. (2018)
Os04g0637300	*OsEPF1*	3.48E-08 *	Inhibition of stomatal development	Rice	Caine et al. (2019)
Os04g0457700	*OsEPF2*	1.99E-24 *	Inhibition of stomatal development	Rice	Lu et al. (2019)
Os09g0482660 [#]	*OsCRSP*	0.1538	Cleaves *AtEPF2*	Arabidopsis (*AtCRSP*)	Engineer et al. (2014)
Os01g0914400	*OsEPFL9*	6.89E-61 *	Positive regulation of stomatal development	Rice	Yin et al. (2017)
Os06g0203800	*OsER*	2.84E-44 *	Regulation of stomatal development	Arabidopsis (*AtER*)	Shpak et al. (2005); Mohammed et al. (2019)
Os02g0777400	*OsER2*	5.74E-34 *	Regulation of stomatal development	Arabidopsis (*AtER*)	Shpak et al. (2005); Mohammed et al. (2019)
Os06g0130100	*OsERL1*	0.0009 *	Regulation of stomatal development	Arabidopsis (*AtERL1*, *AtERL2*)	Shpak et al. (2005); Mohammed et al. (2019)
Os05g0586300	*OsFAMA*	1.53E-15 *	Differentiation of stomatal complex	Rice	Liu et al. (2009)
Os07g0627300	*OsFLP*	0.438807	Orientation of GMC division	Rice	Wu et al. (2019)
Os11g0523700	*OsICE1*	1.98E-132 *	Initiation of stomatal lineage, regulates SMC/SC and GMC/GCs transitions.	Rice	Wu et al. (2019)
Os03g0143800	*OsLPL2*	0.0001 *	Epidermal cell morphogenesis	Rice	Zhou et al. (2016)
Os08g0544500	*OsLPL3*	0.6088 *	Epidermal cell morphogenesis	Rice	Zhou et al. (2016)
Os05g0597000	*OsMUTE*	1.46E-38 *	GMC identity, SCs recruitment	Rice	Wu et al. (2019)
Os08g0506400 [#]	*OsPan1*	0.6428	Polarization of SMC	Maize (*ZmPan1*)	Cartwright et al. (2009)
Os07g0145400 [#]	*OsPan2*	0.6279	Polarization of SMC & SC morphogenesis	Maize (*ZmPan2*)	Sutimantanapi et al. (2014)
Os11g0124300	*OsSCR1*	9.78E-52 *	Initiation of stomatal lineage, SCs formation	Rice	Wu et al. (2019)
Os12g0122000	*OsSCR2*	7.55E-64 *	Initiation of stomatal lineage, SCs formation	Rice	Wu et al. (2019)
Os01g0928000	*OsSCRM2*	3.20E-199 *	Initiation and differentiation of stomata	Rice	Wu et al. (2019)
Os03g0143100 [(#)]	*OsSDD1*	0.0007 *	Negative regulation of stomatal development	Maize (*ZmSDD1*)	Liu et al. (2015)

Rice gene id	Gene name	Adjusted p-value (LRT)	Role	Organism relevant role was shown	Reference
Os07g0586900	*OsSHR1*	1.40E-53 *	Initiation of stomatal lineage, SCs formation	Rice	Wu et al. (2019)
Os03g0433200	*OsSHR2*	0.0001 *	Initiation of stomatal lineage, SCs formation	Rice	Wu et al. (2019)
Os06g0526100	*OsSPCH1*	2.25E-66 *	Initiation of stomatal lineage	Rice	Wu et al. (2019)
Os02g0257500	*OsSPCH2*	1.51E-12 *	Initiation of stomatal lineage	Rice	Wu et al. (2019)
Os01g0623000	*OsTMM*	2.27E-80 *	Regulation of stomatal development	Arabidopsis (*AtTMM*)	Nadeau and Sack. 2002), Mohammed et al. (2019)
Os04g0559800	*OsYDA1*	0.8619	Regulates cell fate post entry division	Brachypodium (*BdYDA1*)	Abrash et al. (2018), Peterson et al. 2010)
Os02g0666300	*OsYDA2*	0.8421	Unknown	Brachypodium (*BdYDA2*)	Abrash et al. (2018), Petterson et al. (2010)

[#] Gene id identified using Orthofinder. * Significant adjusted p-values (< 0.001) from LRT (likelihood ratio test) analysis in DESeq2, this analysis identified genes that showed changes in expression across stages 1 to 5 of IR64 florets.
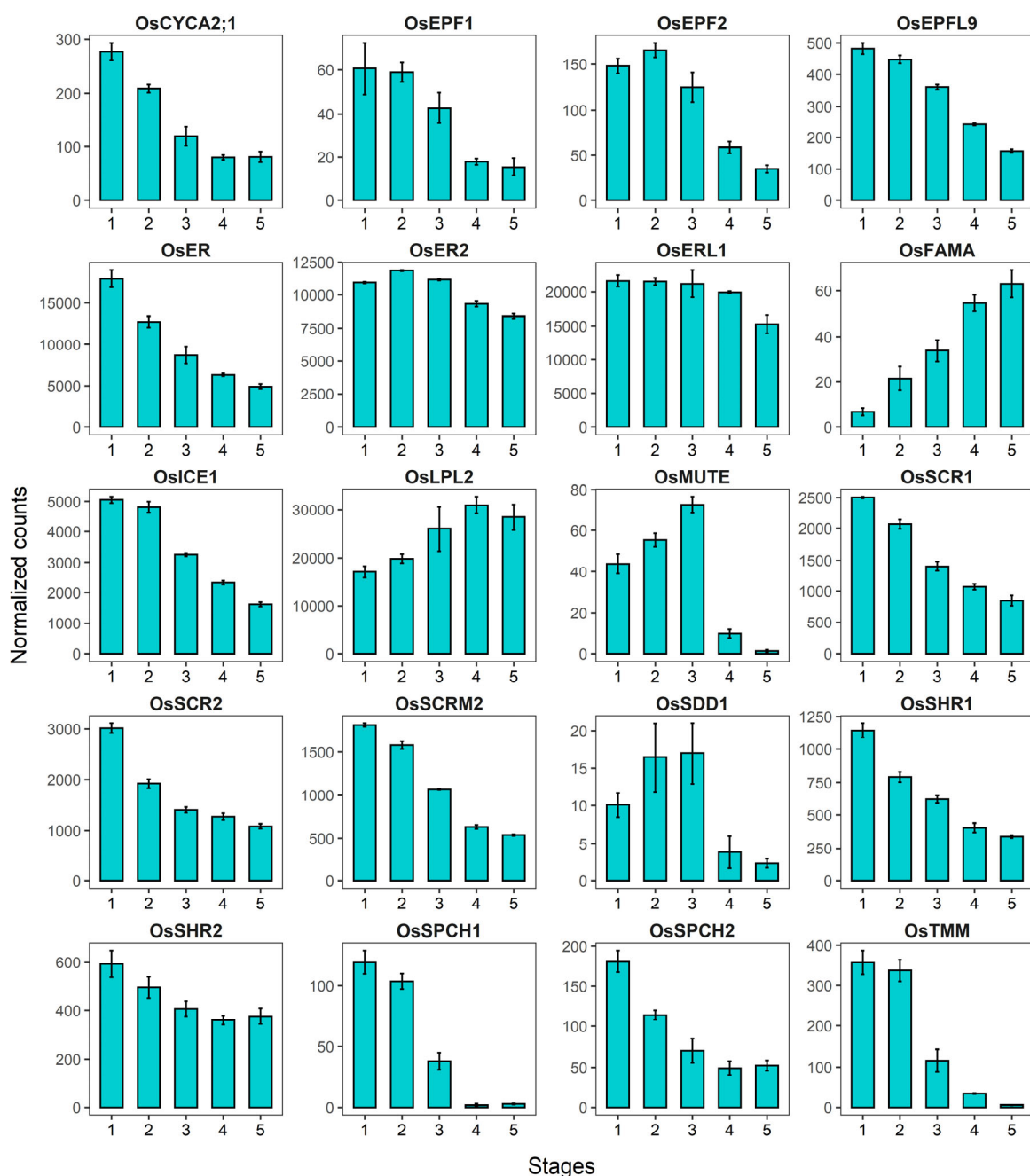
Figure 5.17. Transcript abundance of stomatal genes differentially expressed across stages 1 to 5 of IR64 florets (p-adjusted < 0.001, LRT in DESeq2). Each graph in the panel compares the normalized counts of a gene between each stage studied. Counts were normalized by size factor. Error bars show standard error of the mean.

Genes that did not show a significant variation in expression were: *OsCRSP*, *OsFLP*, *OsLPL3*, *OsPan1*, *OsPan2, OsYDA1* and *OsYDA2*. *OsFLP* is part of the MYB family of transcription factors and is involved in GMC symmetric division in rice (Wu et al., 2019). Its Arabidopsis orthologs, *AtFLP* and *AtMYB88*, function controlling GMC division, as well as reproductive development, being widely expressed in vegetative and reproductive organs (Lei et al., 2015). *OsLPL3* is part of the SCAR/WAVE complex in rice, showing

a role in the F-actin rearrangement associated with epidermal cells morphogenesis and stomatal patterning (Zhou et al., 2016). *OsPan1, OsPan2, OsYDA1, OsYDA2* and *OsCRSP* have not had their functions directly investigated in rice. *ZmPan1* and *ZmPan2* are receptor-like kinases, both associated with SMC division orientation in maize, with *ZmPan2* also accumulating a role in SCs morphogenesis (Cartwright et al., 2009; Nunes et al., 2019; Sutimantanapi et al., 2014). The MAPK kinase kinases BdYDA1 and BdYDA2 have been studied in *Brachypodium* (Abrash et al., 2018). *BdYDA1* appears to play a role in stomatal fate determination after asymmetric entry division, whilst the function of *BdYDA2* is not yet understood. Studies in Arabidopsis showed that *AtYDA* also acts in floral development (Meng et al., 2013), what could explain the expression pattern observed here. Moreover, *AtCRSP* encodes a peptidase which is activated in response to rise in CO_2 levels in Arabidopsis, and can cleave AtEPF2 to produce its active form (Engineer et al., 2014); however, the function of its ortholog in rice is yet to be investigated. Although the above-mentioned genes are not differentially expressed across the stomatal development series analysed here, their expression was detected in all stages (Figure 5.18).
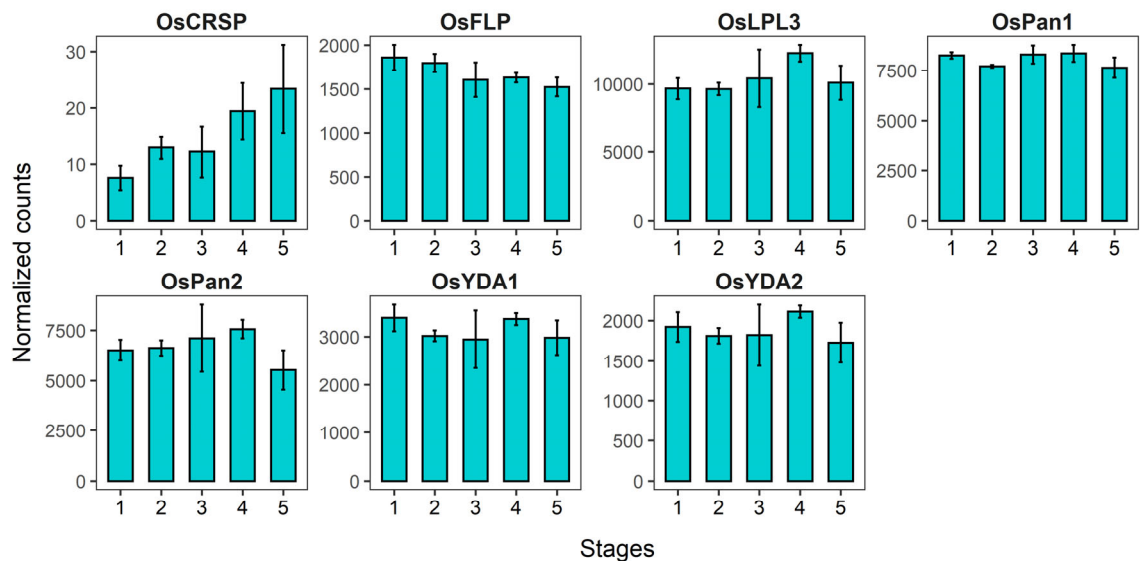
Figure 5.18. Transcript abundance of stomatal genes not differentially expressed across stages 1 to 5 of IR64 florets (p-adjusted > 0.001, LRT in DESeq2). Each graph in the panel compares the normalized counts for a gene between each stage studied. Counts were normalized by size factor. Error bars show standard error of the mean.

- *Expression of stomatal response genes*

Several genes with potential to affect the aperture of mature stomata in rice were also investigated. These included genes encoding signalling components (such as transcription factors and protein kinases), turgor regulators (such as anion and cation channels and a

proton pump-ATPase), as well as genes in the ABA biosynthesis and signalling pathway, among others. Out of the 23 genes analysed (Table 5.3), 15 showed a significant variation in transcript abundance across the stomatal development series in IR64 florets. The expression of most of these DEGs genes started to increase in the later developmental stages (Figures 5.19 and 5.20). Since these gene products are associated with stomatal opening and closure responses, this trend could be related to guard cell maturation, and subsequent ability to function. It is important to highlight, however, that the expression of many of these genes is not restricted to the cells of the stomatal lineage, being potentially also associated with other processes or under environmental regulation.

Table 5.3. Genes associated to stomatal function analysed in this study.

Rice gene id	Rice name	Molecular function	Reference	Adj. p-value
Os04g0656100	*OSA7*	H$^+$- ATPase	Toda et al. (2016)	1.42E-13 *
Os04g0448900	*OsABA1*	Zeaxanthin epoxidase (*OsZEP1*)	Oliver et al. (2007)	0.1680
Os03g0810800	*OsABA2*	Short-chain alcohol dehydrogenase	Liao et al. (2018)	1.40E-21 *
Os03g0281900	*OsABCG5*	ABA transporter	Matsuda et al. (2016)	1.64E-26 *
Os01g0859300	*OsABI5*	bZIP transcription factor	Zou et al. (2008)	0.1228
Os01g0583100	*OsABI-like1*	Protein Phosphatase 2C	Li et al. (2015)	0.5815
Os03g0688300	*OsCPK9*	Calcium-dependent kinase	Wei et al. (2014)	3.24E-12 *
Os10g0456800	*OsDCA1*	Transcriptional co-activator	Cui et al. (2015)	1.71E-10 *
Os03g0786400	*OsDST*	Transcription factor	Huang et al. (2009)	3.26E-14 *
Os06g0636600[#]	*OsHT1*	Protein kinase	Hashimoto et al. (2006)	0.015621
Os06g0250600	*OsK5.2*	Outward K+ channel	Nguyen et al. (2017)	0.2833
Os01g0210700	*OsKAT2*	Inward K+ channel	Hwang et al. (2013)	0.8531
Os02g0245800	*OsKAT3*	Inward K+ channel	Hwang et al. (2013)	1.50E-05 *
Os07g0154100	*OsNCED3*	9-cis-epoxycarotenoid dioxygenase	Oliver et al. (2007)	*NA* [1]
Os07g0448800	*OsPIP2;1*	Aquaporin	Lian et al. (2006)	3.69E-92 *
Os10g0573400	*OsPYL1*	ABA receptor	Miao et al. (2018)	0.9395
Os02g0255500	*OsPYL10*	ABA receptor	Kim et al. (2012)	8.02E-05 *
Os01g0827800	*OsPYL4*	ABA receptor	Miao et al. (2018)	1.33E-36 *
Os03g0297600	*OsPYL6*	ABA receptor	Miao et al. (2018)	1.62E-07 *
Os03g0610900	*OsSAPK10*	Protein kinase (*AtOST1* homolog)	Min et al. (2019)	0.0476
Os03g0764800	*OsSAPK8*	Protein kinase (*AtOST1* homolog)	Sun et al. (2016)	2.92E-06 *
Os04g0574700	*OsSLAC1*	S-type anion efflux channel	Kusumi et al. (2012)	3.49E-17 *
Os01g0639900	*OsβCA1*	Carbonic anhydrase	Chen et al. (2017)	9.79E-99 *

[#] Rice gene id was identified using Orthofinder. * Significant adjusted p-values (< 0.001) in LRT (likelihood ratio test) analysis in DESeq2, this analysis identified genes that showed changes in expression across stages 1 to 5 of IR64 florets. [1] Low count transcripts were filtered out of LRT analysis by default DESeq2 independent filtering.
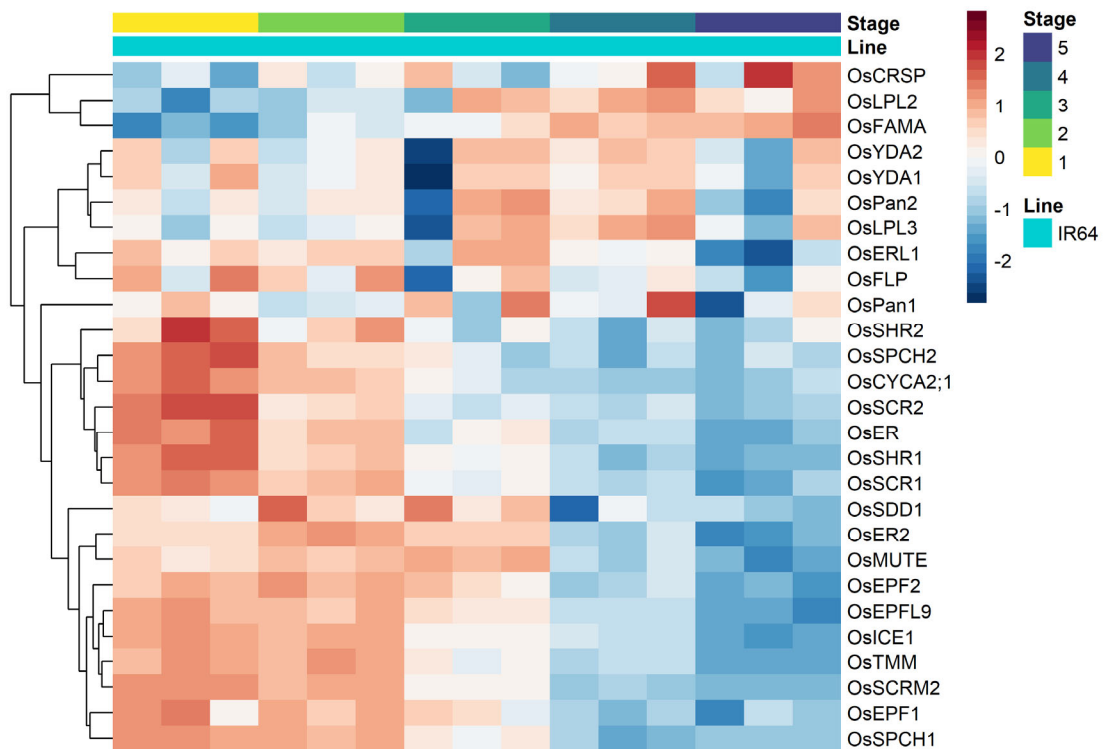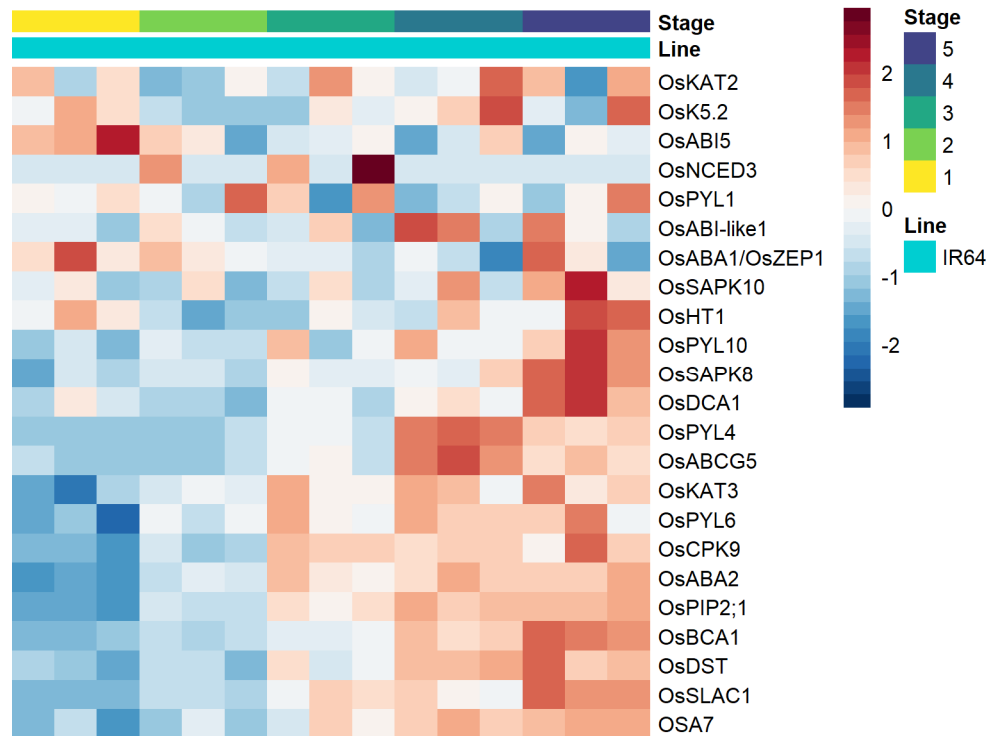
Figure 5.19. Heatmap of stomatal response genes. Row z-score of vst-transformed values across samples was plotted. Rows correspond to genes. Columns correspond to samples.

Several genes previously described as being preferentially expressed in GCs did not show a significant variation in expression across the stages. This was the case for *OsKAT2*, a potassium ion channel gene whose transcripts are predominantly found in rice GCs (Hwang et al., 2013), and *OsSAPK10*, which encodes a rice homolog of *AtOST1* (*OPEN STOMATA 1*) protein kinase that is highly expressed in rice stomata (Min et al., 2019). In the case of *OsSAPK10*, however, its expression pattern showed a trend towards increasing in line with stomatal development. The expression of *OsHT1*, encoding the ortholog of *AtHT1* (*HIGH LEAF TEMPERATURE 1*) a protein kinase that regulates *OST1* activity in Arabidopsis (Hashimoto et al., 2006), was variable across the development. *OsABI5* and *OsNCED3* had very low transcript counts through all the stages analysed. Other genes in the ABA pathway, such as *OsABA1*, *OsABI-like1* and *OsPYL1* were expressed in all stages, but with no significant variation. On the other hand, *OsABA2*, involved in ABA biosynthesis; the ABA receptors *OsPYL10*, *OsPYL4*, *OsPYL6* and the transporter *OsABCG5* showed significant variation in expression during the IR64 stomatal development (Figures 3.19 and 3.20).

Figure 5.20. Expression of genes associated to stomatal responses. Each graph in the panel compares the transcript abundance of a gene between each stage studied in the IR64 stomatal development series. * Significant DEGs, adjusted p-value < 0.001, LRT in DESeq2. NS, not significant. Counts were normalized by size factor. Error bars show standard error of the mean.

5.2.6. Effect of *OsEPF1* overexpression in floret development – Genotype-specific changes across stages 1 to 5

To investigate differences between the expression profile of developing florets in IR64 and OsEPF1-oe-S (a rice line with strongly reduced level of stomatal development, as shown in Chapter 3), a differential expression analysis was performed using the R package DESeq2 (Love et al., 2014). A likelihood ratio test (LRT) was used to identify genes that changed expression in a genotype-specific manner across the stages 1 to 5 of floret development (testing for genes with an expression pattern that is affected by the interaction between the factors genotype and stage). From a total of 31,813 genes included in this analysis, 845 were identified as differentially expressed, considering an adjusted p-value < 0.05 (Benjamini-Hochberg correction). A hierarchical clustering of the 250 most significantly impacted genes grouped florets stages 1 and 2 together, whilst stages 3, 4 and 5 formed a second group (Figure 5.21). Interestingly, samples from stage 5 of OsEPF1-oe-S did not cluster closely to IR64 stage 5 samples. Moreover, an analysis of the expression patterns of the 845 DEGs across the developmental series placed these genes in 14 significant clusters (Figure 5.22).

Figure 5.21. Hierarchical clustering analysis with the 250 most significant DEGs found in the LRT comparing IR64 and OsEPF1-oe-S floret developmental stages 1 to 5 (adjusted p-value < 0.05). Heatmap scale shows row z-score of vst-transformed counts across samples. Rows correspond to genes. Columns correspond to samples.
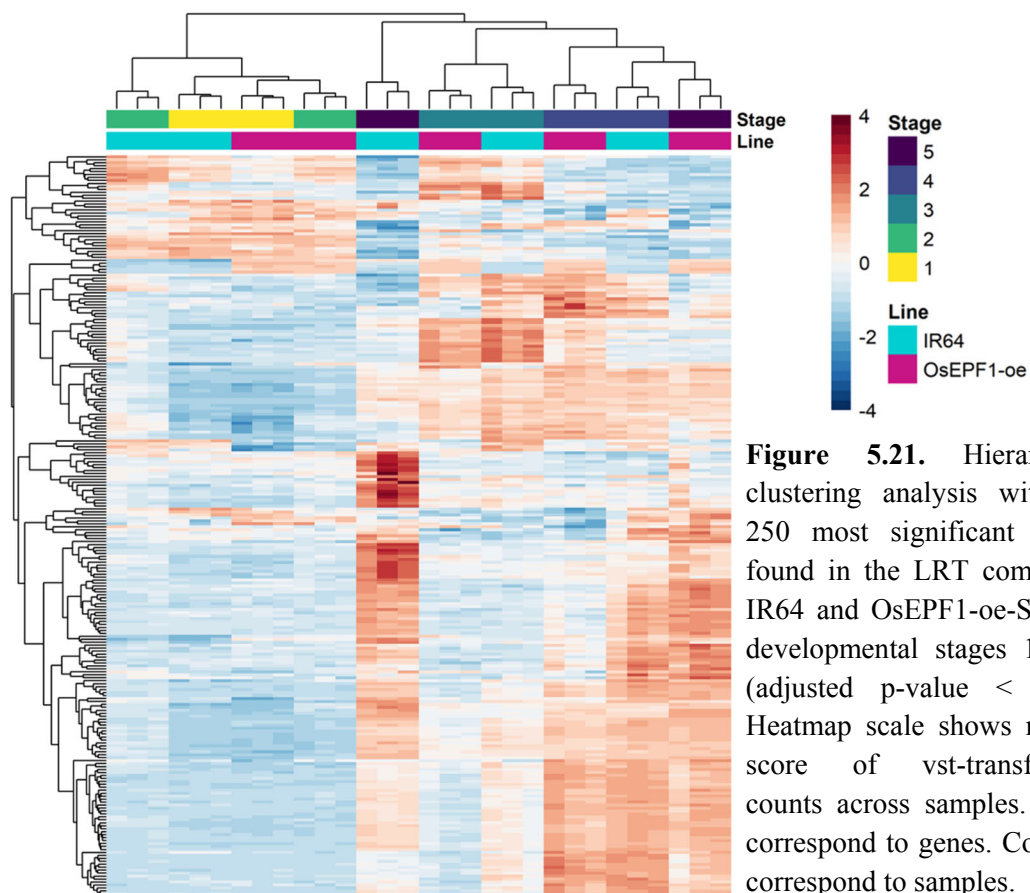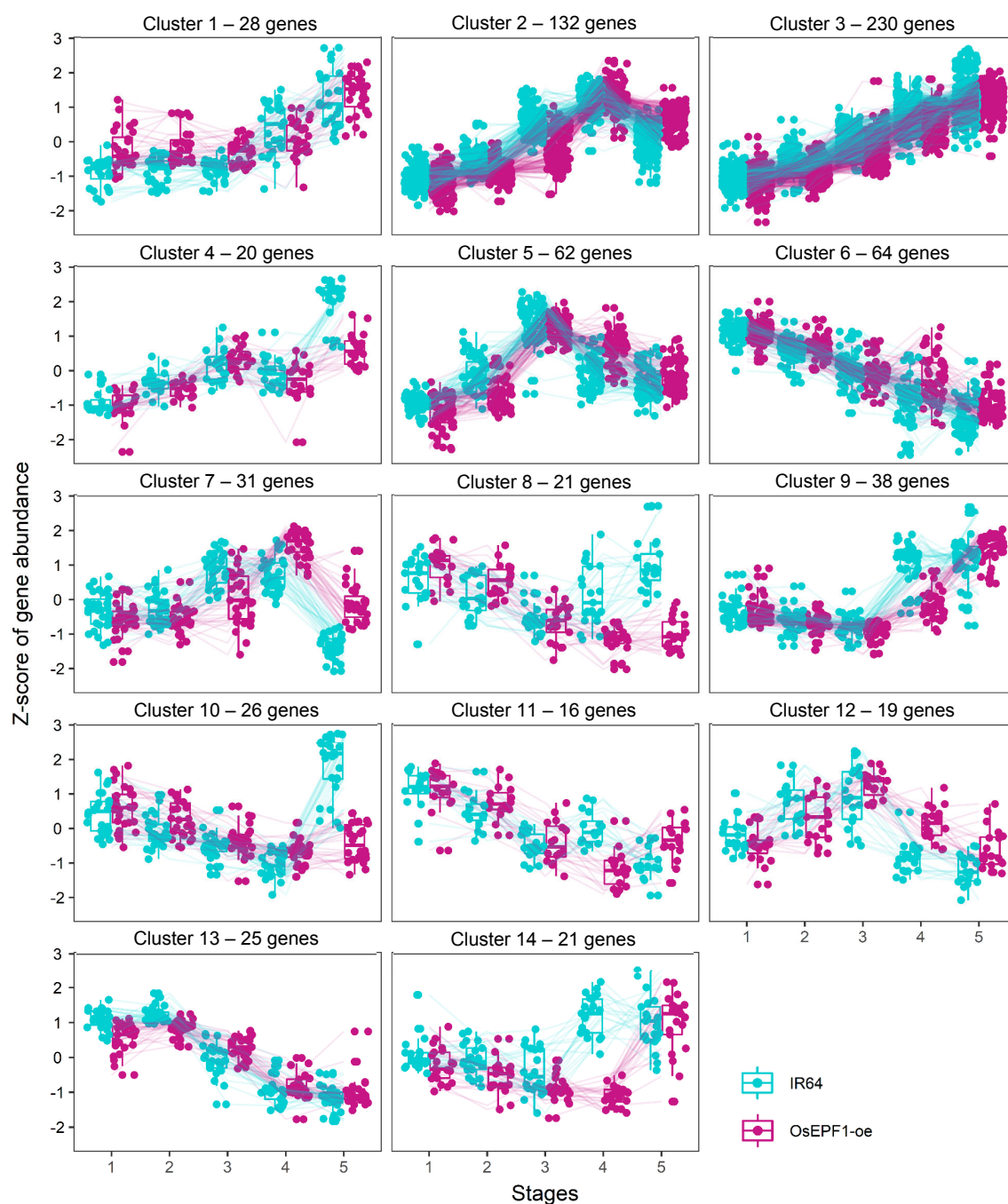
Figure 5.22. Expression patterns of genes differentially expressed in OsEPF1-oe-S developing florets in comparison to IR64. Genes were grouped in 14 significant clusters according to their expression patterns. A hierarchical clustering approach was applied.

- *Functional profile of DEGs – Genotype-specific changes across stages 1 to 5*

A GO term analysis revealed a small number of over-represented classes of genes in the DEGs dataset (Figure 5.23). The most significant terms found were "SCF-dependent proteasomal ubiquitin-dependent catabolic protein process" and "meiotic cell cycle", thus DEGs included in these classes were further investigated (lists of DEGs associated with each GO term can be found in Appendix A, Tables A2 to A10). The SCF complex is a multi-subunit E3 ligase (SKP1-CUL1-F-box protein) that catalyses ubiquitination of

proteins targeted for degradation by the ubiquitin 26S-proteassome, regulating a myriad of biological processes in plants (Magori and Citovsky, 2011; Mazzucotelli et al., 2006). Most of the DEGs linked to "SCF-dependent proteasomal ubiquitin-dependent catabolic protein process" (summarized in Table 5.4) were not associated to specific pathways in the annotation available on Ensembl Plants (https://plants.ensembl.org) and on RAP-DB (https://rapdb.dna.affrc.go.jp). Exceptions were, *OsCOI1b*, which functions in the jasmonic acid response signalling pathway (Lee et al., 2015), and *OsCUL1-3*, potentially linked to stress responses in rice (Kim et al., 2018). Moreover, *OSK19*, *OSK21* and *OSK22* are highly expressed during early anther development, according to He et al. (2016). Many of the DEGs in the SCF complex class were included in clusters 2 and 3, according to their expression patterns (Fig. 5.22), a more detailed comparison of their expression profile can be visualized in Figure 5.24.
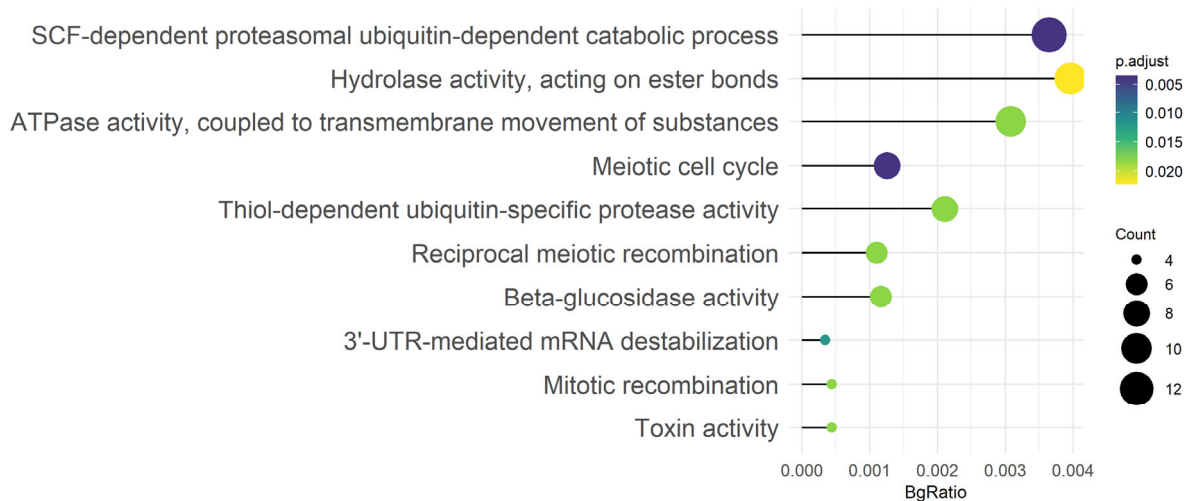
Figure 5.23. GO terms associated with DEGs found in OsEPF1-oe-S developing florets in comparison to IR64. Count refers to the number of DEGs in a GO term. Colour scale corresponds to the adjusted p-value. BgRatio stands for ratio between the number of genes in a GO term and the total genes analysed.

Table 5.4. DEGs belonging to the SCF-dependent proteasomal ubiquitin-dependent catabolic protein process GO term.

Gene id	Gene name	Cluster	Description (Ensembl Plants annotation)
Os07g0409500	*OSK21*	2	SKP1-like gene 21, BTB/POZ fold domain containing protein
Os07g0625500	*OSK22*	3	SKP1-like gene 22, similar to Fimbriata-associated protein
Os01g0369200	*OsCUL1-3*	5	Component of cullin-RING E3 ubiquitin ligase complex, salt/drought and cold stress response
Os07g0625600	*OSK19*	2	SKP1-like gene 19, fimbriata-associated protein
Os12g0594600	-	2	BTB/POZ fold domain containing protein
Os02g0281150	-	13	Similar to Leucine Rich Repeat family protein
Os07g0624900	*OSK17*	2	SKP1-like gene 17
Os10g0128600	*OsFbox518*	3	Cyclin-like F-box domain containing protein
Os07g0535700	-	12	F-box associated type 1 domain containing protein
Os12g0595600	-	2	Hypothetical conserved gene
Os10g0124700	*OsFbox508*	2	Cyclin-like F-box domain containing protein
Os05g0449500	*OsCOI1b*	3	Component of the SCF E3 ubiquitin ligase complex, jasmonate-regulated defense responses, regulation of leaf senescence
Os10g0148800	*OsF0711*	6	Similar to F-box domain containing protein
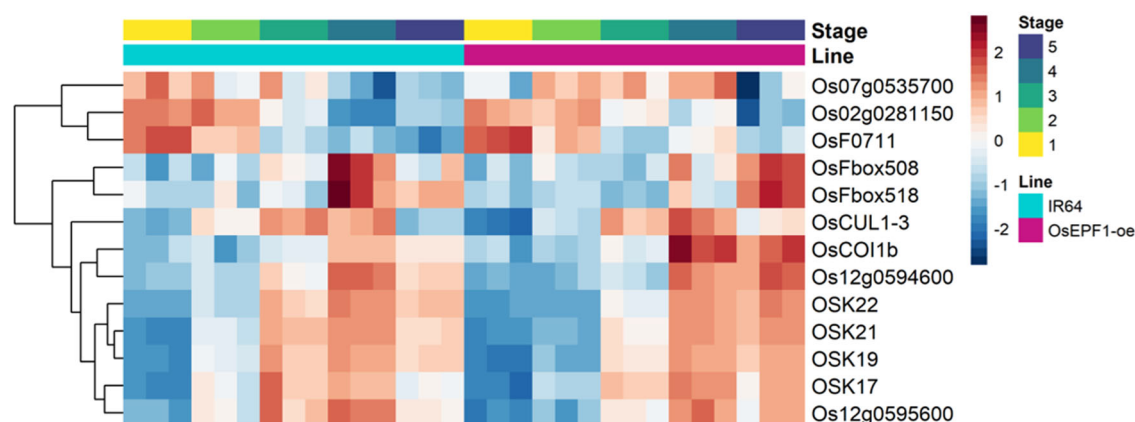
Figure 5.24. Heatmap of DEGs associated to SCF-dependent proteasomal ubiquitin-dependent catabolic protein process GO term. Scale shows row z-score of vst-transformed counts across samples. Rows correspond to genes. Columns correspond to samples.

Eight of the DEGs were associated to the GO term "meiotic cell cycle", with some of these genes being also included in the "reciprocal meiotic recombination" and "mitotic recombination" terms (Fig. 5.25), which were also found to be enriched (Fig. 5.23). Information on the genes identified in significant GO terms related to cell division processes were summarized in Table 5.5. According to annotation in Ensembl Plants, these genes function in chromosome pairing and recombination, being implicated in male

and female gamete formation. Their detailed expression profiles in IR64 and OsEPF1-oe-S florets are shown in Figure 5.26.
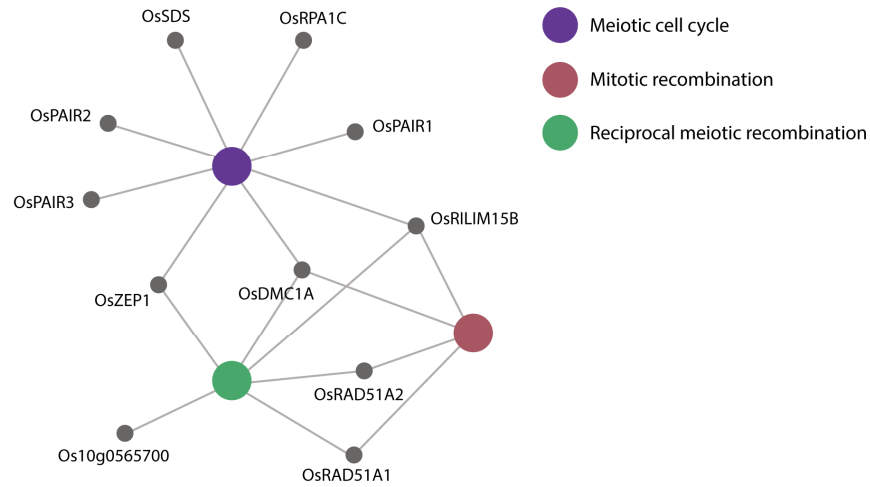
Figure 5.25. Genes identified in meiotic cell cycle GO term are also linked to other significant GO terms.

Table 5.5. DEGs associated to significant cell division-related GO terms.

Gene id	Gene name	Cluster	Description (Ensembl Plants annotation)
Os11g0146800	*OsRILIM15B/ DCM1B*	7	Meiosis-specific DNA recombinase, synaptonemal complex (SC) assembly
Os09g0506800	*OsPAIR2*	2	Similar to essential protein for meiotic synapsis
Os03g0225200	*OsSDS*	7	Cyclin, A/B/D/E domain containing protein
Os04g0452500	*OsZEP1*	2	Similar to H0505F09.1 protein
Os10g0565700	-	2	Similar to SNF2 family N-terminal domain containing protein
Os03g0106300	*OsPAIR1*	-	Coiled-coil protein, homologous chromosome pairing in meiosis
Os12g0497300	*OsRAD51A2*	11	DNA double strand break repair and homologous recombination
Os05g0111000	*OsRPA1C*	11	Replication protein A1c, similar to Gag polyprotein
Os12g0143800	*OsDMC1A*	2	Meiosis-specific DNA recombinase, synaptonemal complex (SC) assembly
Os11g0615800	*OsRAD51A1*	14	DNA repair protein RAD51, homologous pairing
Os10g0405500	*OsPAIR3*	6	Coiled-coil protein, homologous chromosome pairing and synapsis in meiosis
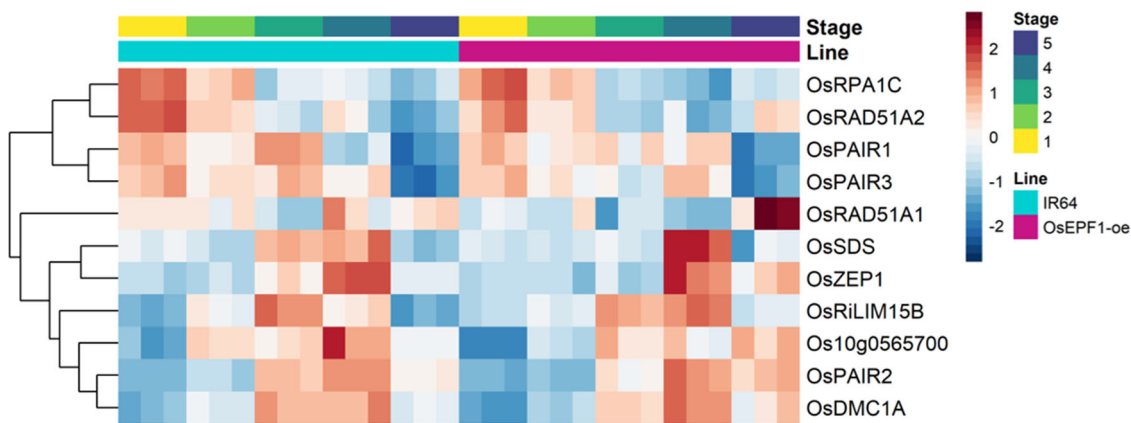
Figure 5.26. Heatmap of DEGs associated to cell division-related GO terms. Scale shows row z-score of vst-transformed counts across samples. Rows correspond to genes. Columns correspond to samples.

5.2.7. Effect of *OsEPF1* overexpression on floret development and mature flowers – Pairwise comparisons

To investigate differences in gene expression between OsEPF1-oe-S and IR64 in each floret developmental stage and in mature flowers, a second differential expression analysis was conducted using DESeq2 (Love et al., 2014). In this analysis, pairwise comparisons between each stage were performed to identify genes that were up or down-regulated in specific stages of OsEPF1-oe-S flowers in comparison to IR64. A null hypothesis of $\log_2$ fold change (LFC) equals 0 (no difference in expression) was tested using a Wald test, with an adjusted p-value cut-off of 0.05 (Benjamini-Hochberg correction). An overview of the results from each comparison can be visualized in Figure 5.27. From a total of 31,544 genes analysed, 380 were identified as DEGs in stage 1; 542 in stage 2; 701 in stage 3; 1,106 in stage 4; 943 in stage 5; and finally, 979 in mature florets (Figure 5.27). Notably, the number of DEGs with great differences in expression levels between genotypes was reduced in mature flowers compared to other stages, in which more genes show LFC higher than 1 or lower than -1 (Figure 5.27 A). Thirty-one of all DEGs were found to be in common across the stage comparisons (Table A11 in Appendix).

(A)

(B)

Figure 5.27. Genes up and down-regulated in OsEPF1-oe-S in comparison to IR64 in specific floret stages **(A)** Global view of DEGs in each stage. The shrunken LFC is plotted on y-axis and the mean of the counts normalized by size factor is shown on x-axis. Each gene is represented by a dot. DEGs are shown in red (adjusted p-value below 0.05). DEGs with LFC > 0 were up-regulated in OsEPF1-oe-S florets, whilst DEGs with LFC < 0 were down-regulated. **(B)** Proportion of up and down-regulated genes in each stage comparison.

- *Functional profile of DEGs*

Enrichment analyses of stage specific DEGs datasets reported a few over-represented GO terms at each stage, with exception of stage 1, where no over-represented terms were identified (Figure 5.28, gene lists per GO term can be found in Tables A12 to A23 in Appendix). Only the processes 'toxin activity' and 'synapsis' were related to the GO terms found in the previous analysis comparing OsEPF1-oe-S and IR64. Most of the DEGs annotated under 'toxin activity' were down-regulated in stage 2 (Figure 5.29 A). From a total of six genes, two have unknown function (Os03g0688000, Os03g0683500), and other four encode proteins containing a ribosome-inactivating domain (RIP). In stage

3, the DEGs annotated as 'synapsis' related (*OsPAIR2*, *OsPAIR3*, *OsSDS* and *OsZEP1*) were also identified in the genes described as 'meiotic cell-cycle' related in the previous analyses (Table 5.5 and Figure 5.26). Overall, there was little consistency between the GO terms found in each stage, except for groups of genes associated with 'thylakoid' and 'chloroplast thylakoid membrane'. These two groups together comprised 38 genes with various functions in chloroplast function and maintenance. Although these genes were down-regulated in stages 4 and 5 of OsEPF1-oe-S florets (Figure 5.29 B), they were not differentially expressed in mature flowers, where their transcripts were more abundant (not shown). Seven genes associated to the 'chloroplast nucleoid' term were found to be up-regulated in mature OsEPF1-oe-S flowers (Figure 5.29 C).
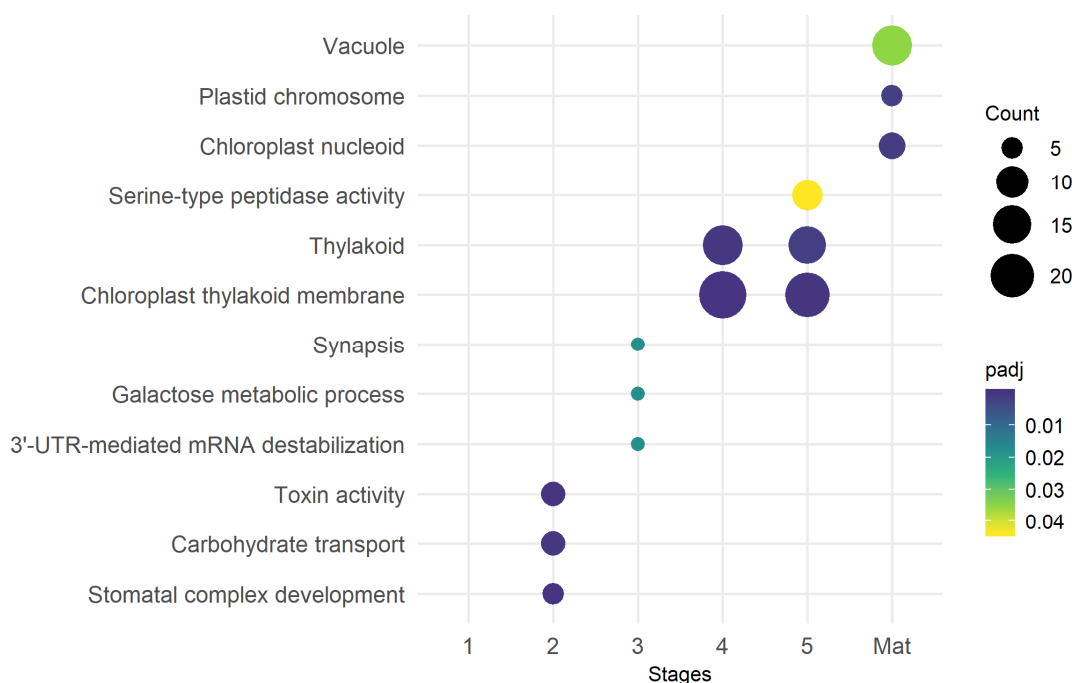
Figure 5.28. Functional enrichment analysis of DEGs in each floret stage. Y-axis shows GO terms and x-axis refers to each of the stage dataset analysed. Colour scale corresponds to the adjusted p-value. Count refers to the number of DEGs in a GO term.

To further examine the changes that were specific to each floret stage analysed, this study performed a functional enrichment analysis with the sets of genes that are differentially expressed exclusively in each stage, as well as with the DEGs that are shared by all stages analysed. The gene sets tested comprised: 124 genes for stage 1; 168 genes for stage 2; 235 for stage 3; 583 for stage 4; 482 for stage 5; 798 in mature florets; and 31 shared genes. Classes found for unique DEGs in stages 1, 2, 3 and 4 were already reported previously by the above analyses; however, for stage 5, mature flowers and the shared DEGs, distinct GO terms were identified (Figure 5.30). Most significant GO terms

identified were "pollen exine formation" and "lipid metabolic process". The genes associated with them were mostly down-regulated in stage 5 (gene lists per GO term are found in Appendix tables A14 to A33). In addition, in the shared dataset, only the term 'oxidoreductase activity' was reported as over-represented, with two genes found in this dataset. Both genes encoded proteins of unknown function (family DUF1637), and were up-regulated in OsEPF1-oe-S florets (not shown).
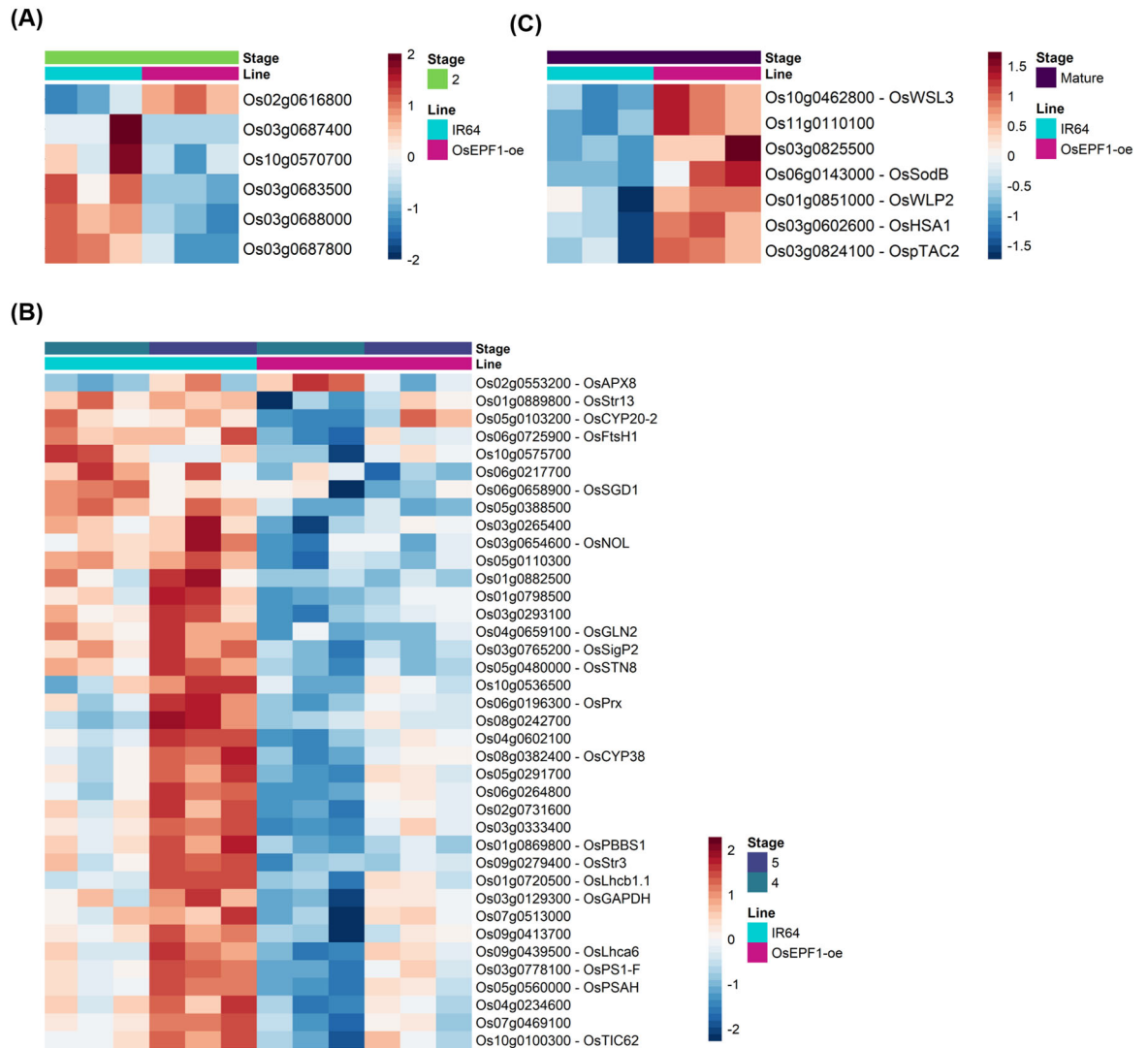
Figure 5.29. Heatmaps of DEGs associated to GO terms in enrichment analysis. **(A)** Toxin activity. **(B)** Chloroplast nucleoid. **(C)** Thylakoid and chloroplast thylakoid membrane. Scale shows row z-score of vst-transformed counts across samples. Rows correspond to genes. Columns correspond to samples.
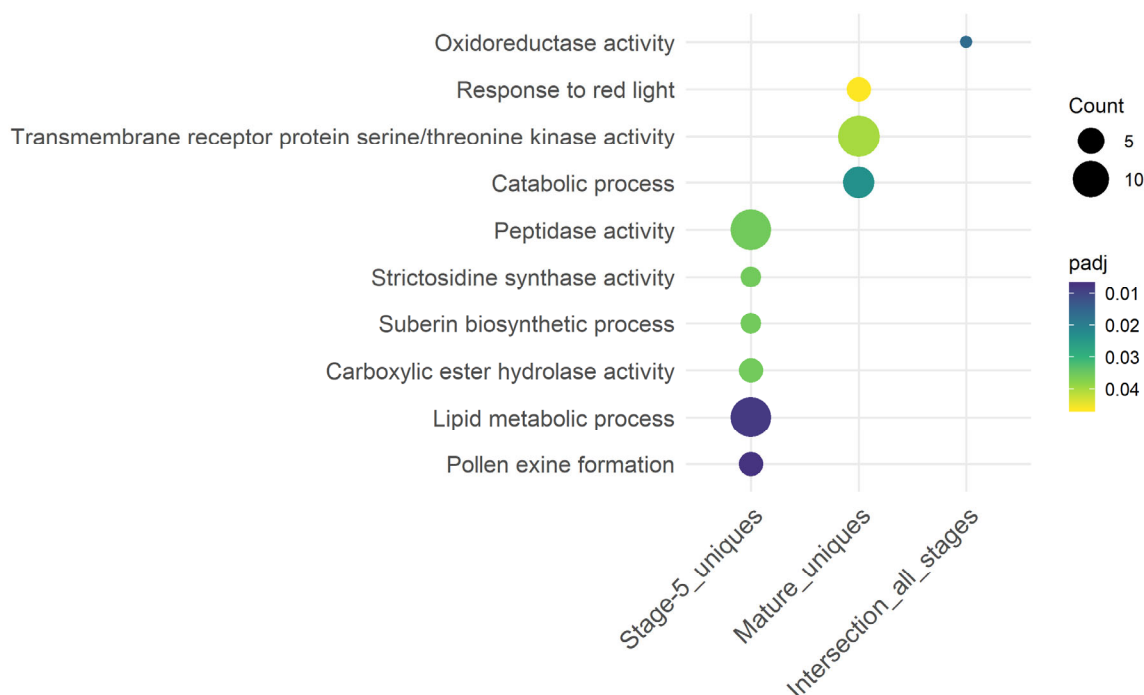
Figure 5.30. Distinct GO terms associated with genes exclusively differentially expressed in stage 5 and mature flowers, and with DEGs shared by all stages analysed. Y-axis shows GO terms and x-axis refers to the datasets analysed. Colour scale corresponds to the adjusted p-value. Count refers to the number of DEGs in a GO term.

5.2.8. Effect of *OsEPF1* overexpression on stomatal genes

- *Stomatal development genes*

The differential expression analyses comparing IR64 and OsEPF1-oe-S samples revealed that most of the genes with function in stomatal development investigated here (previously described in table 5.2) did not show a significant difference in transcript abundance between these two rice genotypes. However, the overexpression of *OsEPF1* led to changes in the expression pattern of several key stomatal transcription factors (Figure 5.31 and Figure 5.32). *OsMUTE*, *OsFAMA*, *OsICE1* and *OsSPCH1* transcription factor genes and *OsEPF2* signalling peptide gene were identified as DEGs in either the pairwise stage comparisons or in the genotype-specific comparison (development series, stages 1 to 5). *OsEPF2*, *OsFAMA* and *OsMUTE* were clearly down-regulated throughout stomatal development, whilst *OsICE1* and *OsSPCH1* showed a more evident drop in expression during the initial stages analysed (Figure 5.31 and 5.32). Interestingly, *OsEPFL9* signalling peptide gene and *OsER2* receptor component gene showed a trend to an increased expression in OsEPF1-oe-S florets, and *OsTMM* receptor component gene showed a reduction in transcript accumulation in initial stages, although these results were not statistically significant (Figure 5.32). In addition, *OsFAMA*, *OsICE1* and *OsSCRM2*

were identified as down-regulated in OsEPF1-oe-S mature florets, although their expression was much lower than detected in the previous stages analysed (Figure 5.32).
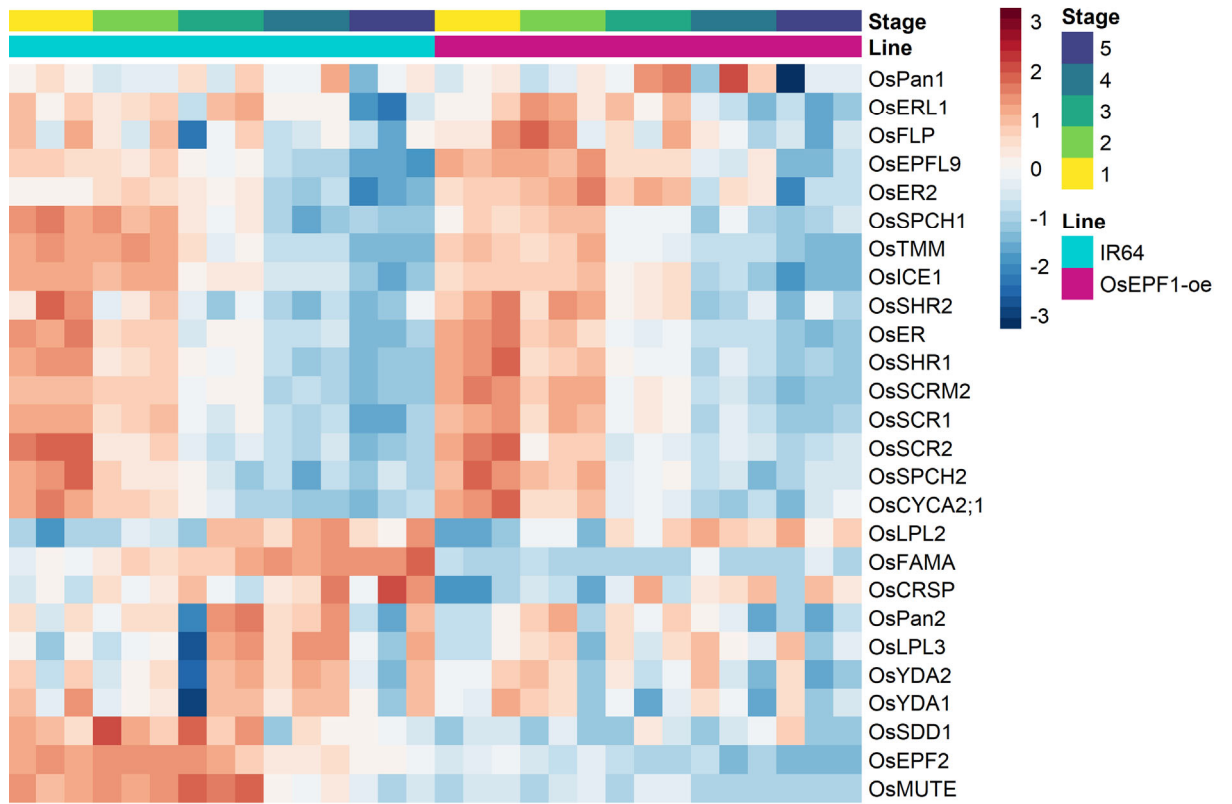
Figure 5.31. Heatmap showing the expression patterns of stomatal development genes during the floret development series (stages 1 to 5). Scale shows row z-score of vst-transformed counts across samples. Rows correspond to genes. Columns correspond to samples.
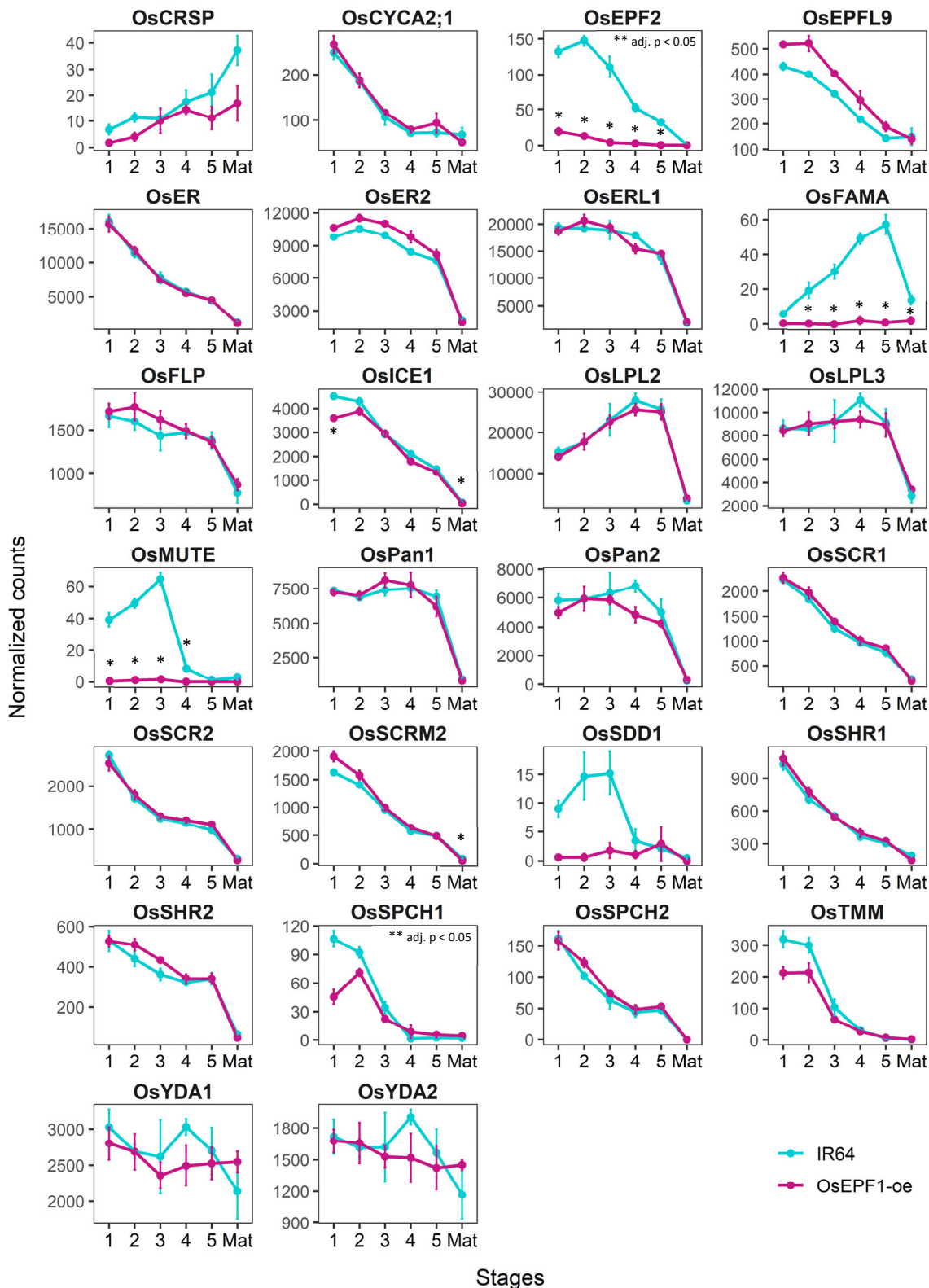
Figure 5.32. Transcript abundance of stomatal development genes in OsEPF1-oe-S and in IR64 florets. Each graph in the panel compares the normalized counts of a gene between lines in each floret developmental stage studied. Counts were normalized by size factor. Error bars show standard error of the mean. Genes identified as differentially expressed in specific developmental stages were: *OsEPF2*, *OsFAMA*, *OsICE1* and *OsSCRM2*; * Wald test adjusted p-value < 0.05 for a specific stage comparison. *OsSPCH1* showed an expression pattern significantly different in OsEPF1-oe-S floret development series, stages 1 to 5; ** LRT adjusted p-value < 0.05.

- Stomatal response genes

Similar analyses revealed that genes potentially associated with stomatal aperture responses in rice (previously described in table 5.3) have a very similar expression pattern between IR64 and OsEPF1-oe-S florets (Figure 5.33). Most of these genes showed higher expression in the mature florets of both genotypes, with exception of *OsKAT3*, *OsABCG5*, *OsABA2*, *OsPYL1* and *OsPYL4* (Figure 5.33). From the genes analysed, only *OsSLAC1*, *OsDCA1*, *OsKAT3*, *OsPIP2;1*, *OsABCG5* and *OsPYL4* had significant differences in transcript accumulation in OsEPF1-oe florets in comparison to IR64 (Figure 5.34).

Figure 5.33. Heatmap showing the expression patterns of stomatal response genes. Scale shows row z-score of vst-transformed counts across samples. Rows correspond to genes. Columns correspond to samples.
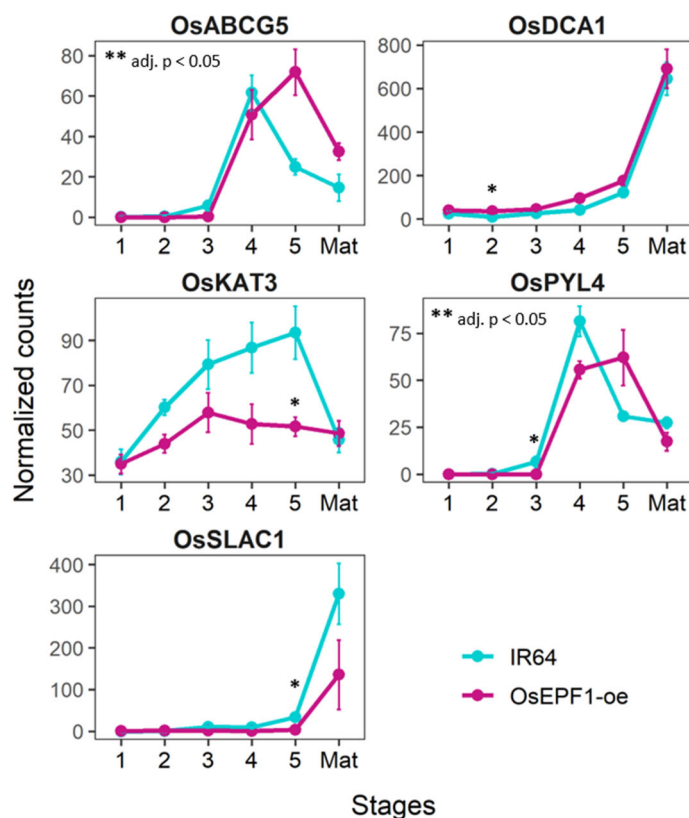
Figure 5.34. Expression of stomatal response genes that were differentially expressed in OsEPF1-oe-S florets in comparison to IR64. Each graph in the panel compares the normalized counts of a gene between genotypes in each floret stage studied. Counts were normalized by size factor. Error bars show standard error of the mean. * Wald test adjusted p-value < 0.05 for a specific stage comparison. ** LRT adjusted p-value < 0.05, comparison across stages 1 to 5 only.

5.2.9. Effect of *OsEPF1* on other developmental pathways

As suggested by the enrichment analyses, several genes associated with meiotic cell cycle, chloroplast, and pollen exine formation showed altered expression in OsEPF1-oe-S florets. To further understand these changes and to investigate if they are potentially impacting on other developmental pathways, this study examined in detail other genes known to be involved in anther/pollen development and in chloroplast development and photosynthesis.

- Anther and pollen development genes

The expression of 23 selected genes with known function in rice anther/pollen development was analysed (Table 5.6, Figure 5.35). First, by looking into the expression trends of these genes in IR64 florets, the 5 stages of floret-stomatal development series were correlated with the major anther development events (anther developmental stages 1 to 14, here designated Ant-1 to Ant-14, according to description in Zhang et al., 2011; Zhang and Wilson, 2009). Expression patterns of these selected genes in IR64 florets was

compared to information from the literature on their transcript levels during anther development, and also with data available on the RiceAntherNet (Lin et al., 2017). As the dataset analysed in this study comprised whole florets divided into stages that reflect stomatal development, the expression of individual genes was not always easily comparable to available data in specific anther stages. However, the global trends allowed the association of anther developmental windows to the different floret stages analysed here (Figure 5.36).

As indicated in Figure 5.35, *OsMSP1* and *OsMEL1* showed higher expression in floret stages 1-2. This was followed by the accumulation (from floret stage 3) of transcripts known to be highly expressed in the pre meiotic and early meiotic anthers, such as *OsUDT1*, *OsTDR*, and *OsEAT1*. These trends suggest that florets in stages 1-2 potentially include anthers around stages Ant-2 to Ant-5 (comprising events such as cell layer specification, and the formation of archesporial and sporogenous cells). In addition, it is likely that the transition from floret stages 2 to 3 is associated with anther developmental stage Ant-6 (microspore mother cell formation). The high expression of *OsUDT1* and *EAT1* in floret stage 3 is consistent with anthers in early meiosis (Ant-7). Later on, in stage 4, a peak of expression was identified for *OsDEX1, OsTIP2, OsTDR*, characteristic of stage Ant 8a-8b (meiosis). In floret stage 5, the steep increase in *OsCP1*, *OsPTC1* and *OsDPW* transcripts correlates with Ant-8b/9. Moreover, high expression of other genes related to pollen wall biosynthesis, such as *OsC4, OsRAFTIN, OsCYP703A3, OsCYP704B2*, and *OsDEX1*, further support a transition to Ant-9 (young microspores).

Regarding the differences in expression patterns between OsEPF1-oe-S and IR64 genotypes, 14 of the 23 selected genes associated with anther development were found to be differentially expressed (Figure 5.37). Changes were identified in various floret developmental stages, but there were no differences in mature flowers. In addition to previously described changes in expression of *OsPAIR1-3* genes, *OsPSS1*, which also functions in the meiotic cell cycle, had altered expression in OsEPF1-oe-S flowers. Changes in expression of genes related to pollen wall biosynthesis were particularly evident in later stages, with *OsC4, OsRAFTIN, OsCYP703A3, OsCYP704B2* and *OsDPW*, being down-regulated. Likewise, genes with function in tapetum development and programmed cell death, such as, *OsTIP2, OsEAT1, OsUDT1* and *OsTDR* were also found to be down-regulated in specific stages. These findings suggest that the overexpression of *OsEPF1* somehow impacted the pollen development pathway in OsEPF1-oe-S plants; however, previous evidence suggested that these plants had no fertility issues under standard growth room conditions (Chapter 3 and Caine et al., 2019).

Table 5.6. Selected genes with function in rice anther/pollen development.

Gene id	Gene name	Function	Reference
Os06g0181300	*OsAID1*	Anther dehiscence	Zhu et al. (2004)
Os08g0546300	*OsC4*	Pollen wall biosynthesis	Tsuchiya et al. (1994)
Os11g0582500	*OsC6*	Pollen wall biosynthesis	Zhang et al. (2010)
Os04g0670500	*OsCP1*	Tapetum PCD (programmed cell death)	Lee et al. (2004)
Os08g131100	*OsCYP703A3*	Pollen wall biosynthesis	Yang et al. (2014)
Os03g0168600	*OsCYP704B2*	Pollen wall biosynthesis	Li et al. (2010)
Os03g0825700	*OsDEX1*	Pollen wall biosynthesis	Yu et al. (2016)
Os03g0167600	*OsDPW*	Pollen wall biosynthesis	Shi et al. (2011)
Os04g0599300	*OsEAT1*	Tapetum PCD	Ono et al. (2018)
Os01g0812000	*OsGAMYB*	Tapetum and pollen wall development	Kaneko et al. (2004)
Os03g0800200	*OsMEL1*	Pre-meiotic mitosis and meiosis	Nonomura et al. (2007)
Os01g0917500	*OsMSP1*	Sporogenous cells development and anther wall specification	Nonomura et al. (2003)
Os03g0106300	*OsPAIR1*	Meiosis	Nonomura et al. (2004)
Os09g0506800	*OsPAIR2*	Meiosis	Nonomura et al. (2006)
Os10g0405500	*OsPAIR3*	Meiosis	Yuan et al. (2009)
Os08g0117000	*OsPSS1*	Meiosis and dehiscence	Zhou et al. (2011)
Os09g0449000	*OsPTC1*	Tapetum PCD and pollen wall synthesis	Li et al. (2011)
Os08g0496800	*OsRAFTIN*	Pollen wall biosynthesis	Wang et al. (2003)
Os05g0125000	*OsSIZ1*	Anther dehiscence	Thangasamy et al. (2011)
Os12g0472500	*OsTDL1*	Anther wall specification	Zhao et al. (2008)
Os02g0120500	*OsTDR*	Tapetum development/PCD, pollen wall	Li et al. (2006)
Os01g0293100	*OsTIP2*	Tapetum PCD	Ko et al. (2017)
Os07g0549600	*OsUDT1*	Tapetum development	Jung et al. (2005)
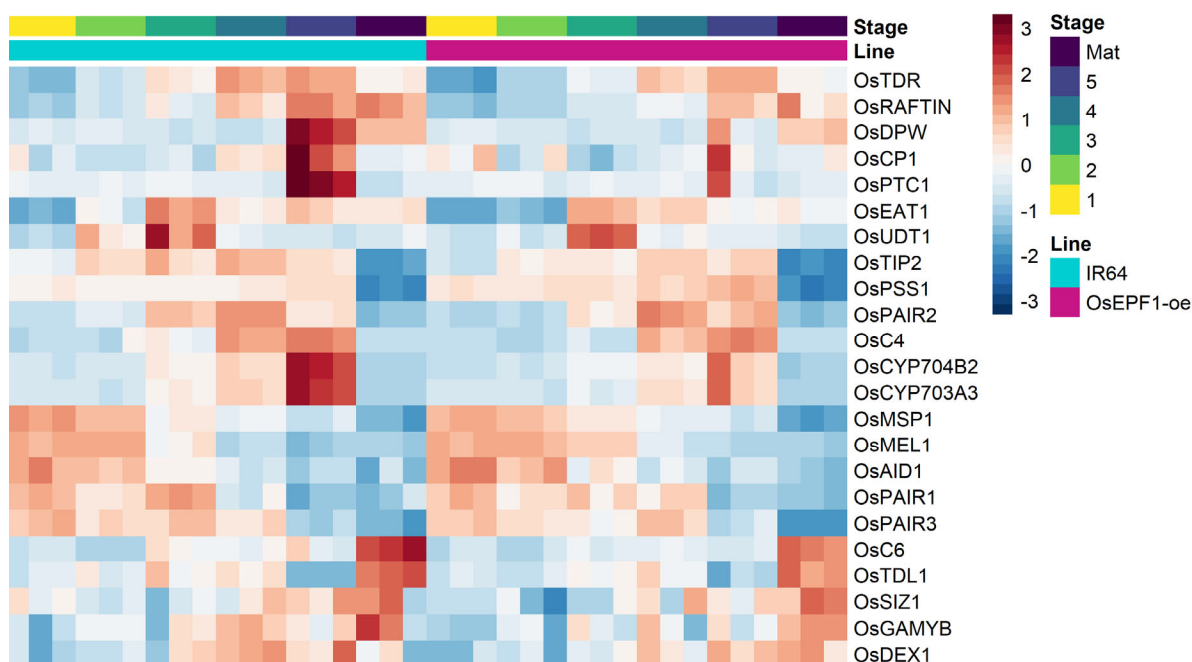
Figure 5.35. Heatmap showing the expression patterns of anther/pollen development genes. Scale shows row z-score of vst-transformed counts across all samples. Rows correspond to genes. Columns correspond to samples.
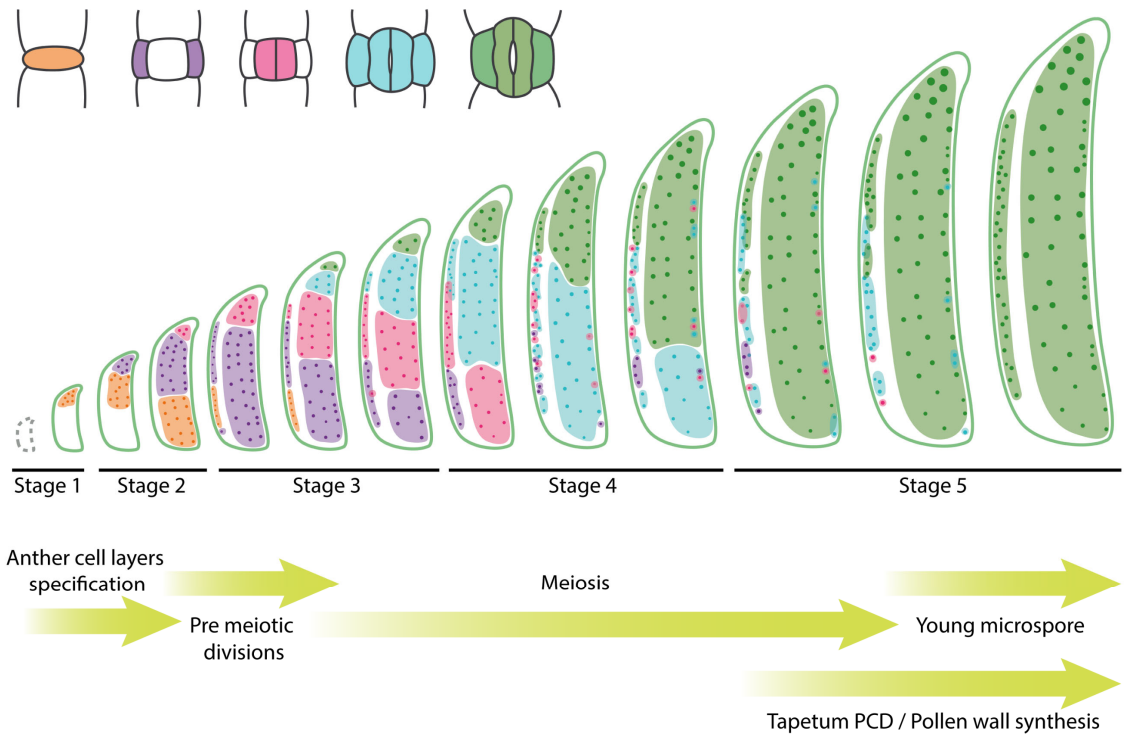
**Figure 5.36.** Diagram showing the different floret-stomatal development stages and the anther developmental events potentially associated to each of them.
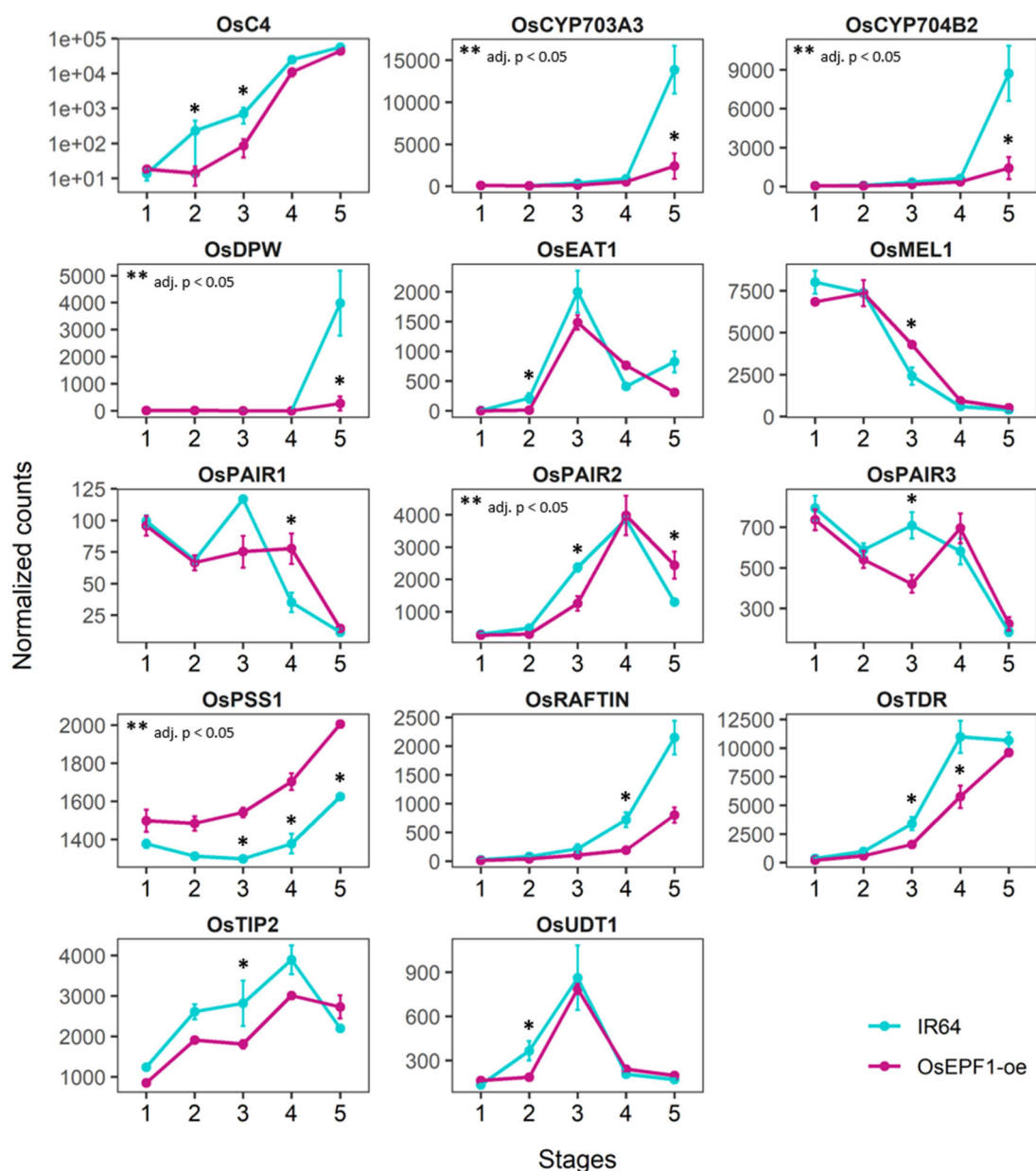
Figure 5.37. Expression of genes involved in anther development that were differentially expressed in OsEPF1-oe-S florets in comparison to IR64. Each graph in the panel compares the normalized counts of a gene between lines from stages 1 to 5 of floret development. Counts were normalized by size factor. Error bars show standard error of the mean. In *OsC4* plot y-axis shows $\log_{10}$ scale. * Wald test adjusted p-value < 0.05. ** LRT test adjusted p-value < 0.05.

- Photosynthetic development genes

The expression patterns of 26 rice genes known to be involved in photosynthetic development, previously summarized in van Campen et al. (2016), were also investigated (gene ids available in Appendix table A34). Overall, changes in expression over the different floret stages was very similar between IR64 and OsEPF1-oe-S (Figure 5.38). Although some genes showed a significant fold change in transcript abundance for specific stages in OsEPF1-oe florets in comparison to IR64 (Figure 5.39), these were

mostly modest changes. In mature flowers, *OsNUS1*, *OsSIG3*, and *OsRpoTp* were found to be up-regulated. In stage 4 of OsEPF1-oe-S florets, *OsRNRS1* showed a significant increase in transcript abundance, while *OsPAC* and *OsHsp70CP1* appeared to be down-regulated.
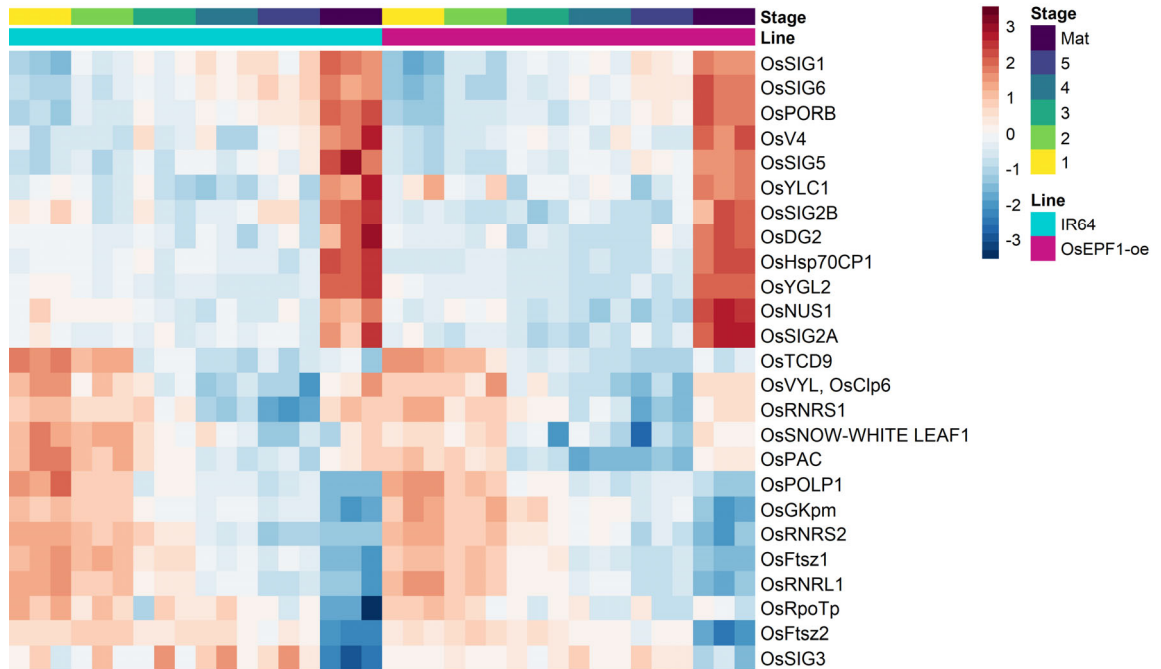
Figure 5.38. Heatmap showing the expression patterns of chloroplast development genes. Scale shows row z-score of vst-transformed counts across samples. Rows correspond to genes. Columns correspond to samples.
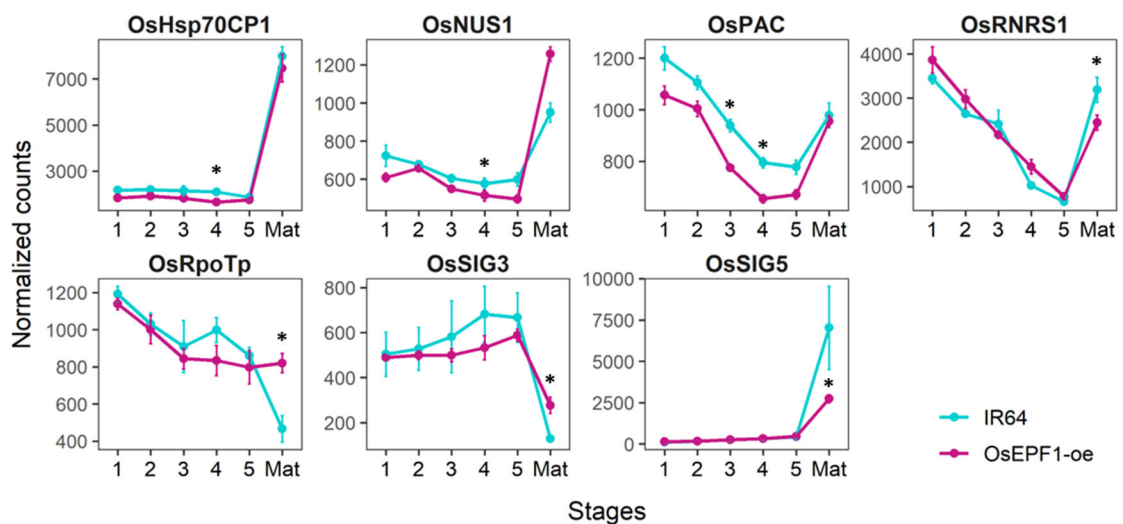
**Figure 5.39.** Expression of genes involved in photosynthetic development that were differentially expressed in OsEPF1-oe-S florets in comparison to IR64. Each graph in the panel compares the normalized counts of a gene between lines in each floret stage studied. Counts were normalized by size factor. Error bars show standard error of the mean. * Wald test adjusted p-value < 0.05.

5.2.10. Effect of *OsEPF1* overexpression on high temperature response genes

To investigate whether the absence of stomata on OsEPF1-oe-S florets and the reduction in stomatal densities on other aerial organs could impact on floret temperature regulation, and consequently lead to changes in the transcription of high temperature induced genes, the expression of known heat shock factors (HSFs) was analysed. Rice has 25 heat shock factors, which can be up-regulated in response to a variety of stresses, including heat stress. Several of these transcription factors are naturally highly expressed in some tissues, in particular in panicles and in developing seeds (Chauhan et al., 2011). In the dataset analysed here, the expression patterns of these 25 HSFs were very similar between OsEPF1-oe-S and IR64 florets (Figure 5.40). Only three HSFs were reported as differentially expressed in specific floret stages (Wald test, p-adjusted < 0.05). From these, two were down-regulated, whilst *OsHsfA1a* was up-regulated. Only *OsHsfA1a* showed an increase in transcript level in OsEPF1-oe mature flowers and this was modest (average 11.7%), suggesting that a potential distinct high temperature response was not triggered in OsEPF1-oe-S florets, at least not under the conditions that plants were grown for this study. To further verify this result, the transcript levels of 70 chaperones, including heat shock proteins (HSPs), that were previously shown to be induced by high temperature stress in panicles (Zhang et al., 2012) were analysed. From these, only a single gene encoding for a HSP, belonging to the HSP70 family, was up-regulated, specifically in floret stage 3 of OsPF1-oe plants (3-fold increase, data not shown).
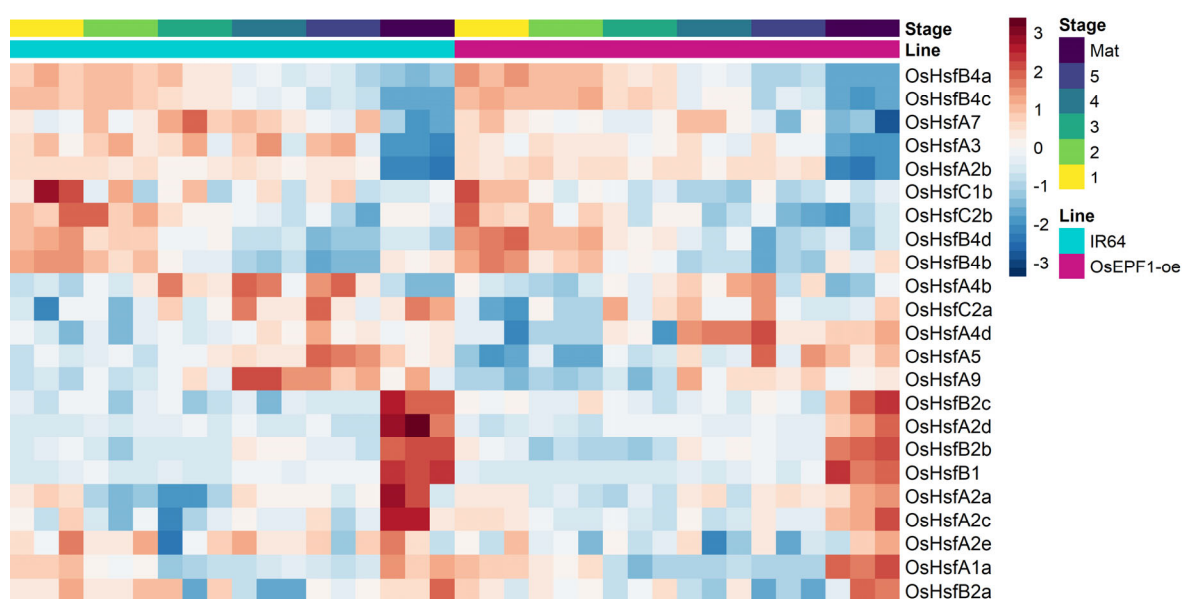
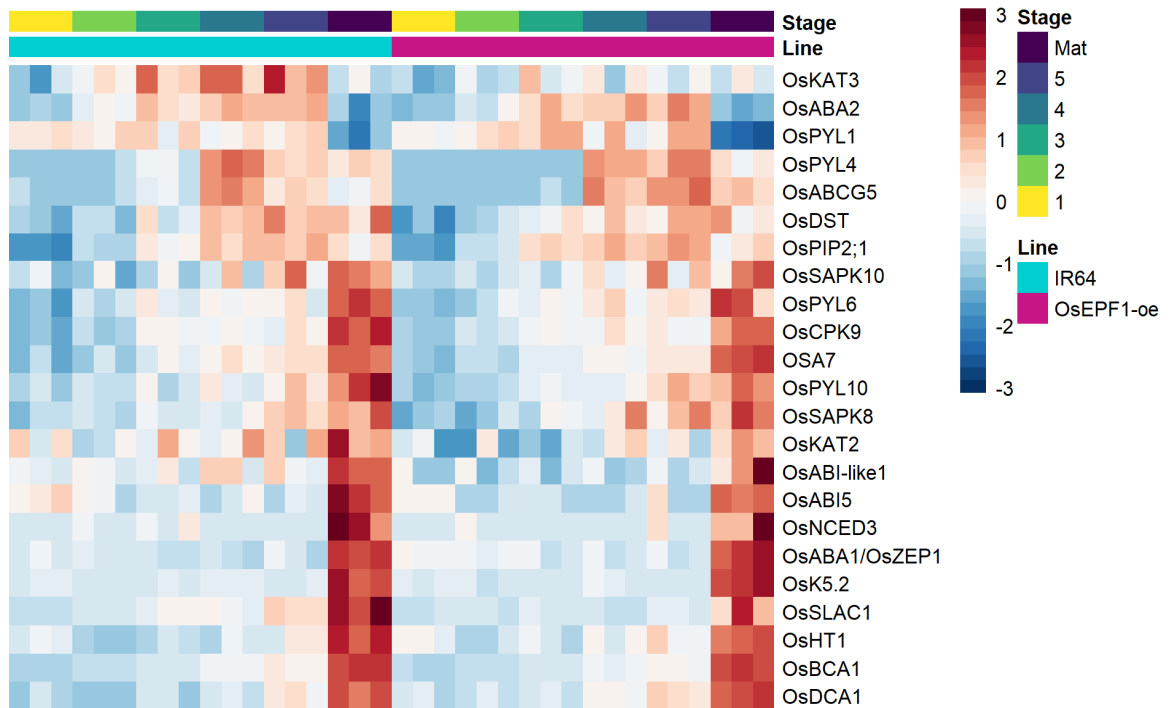**Figure 5.40.** Heatmap showing the expression patterns of HSFs. Scale shows row z-score of vst-transformed counts across samples. Rows correspond to genes. Columns correspond to samples.

5.3. Discussion

The presence of stomata on floral tissues has been reported in several plant species (Clement et al., 1997; Ebenezer et al., 1990; Teare et al., 1972; Wei et al., 2018; Zhang et al., 2018), however little attention has been paid to understanding how these stomatal pores develop. In this Chapter, the sequential events of stomatal development were studied in rice florets with a focus on lemma, a grass-specific bract-like organ. This was combined with a transcriptomic analysis, allowing the investigation of gene expression patterns during the stomatal development in rice florets. Additionally, a comparison between IR64 and OsEPF1-oe-S expression profiles was performed, resulting in the identification of processes that are potentially altered in the floret development of this transgenic line with reduced stomatal density.

5.3.1. Stomatal development is similar in rice flowers and leaves

Although the shape and spatial arrangement of stomatal complexes on the epidermis of mature IR64 florets were distinct from those observed in the rice leaves (as shown in Chapter 3), the investigation of developing lemma and palea indicated that, in these floral organs, stomatal development progresses in a similar manner to that described for leaves of rice and other grasses (Hepworth et al., 2018; Wu et al., 2019). To form mature stomatal complexes, undifferentiated cells in the young floret entered the stomatal lineage pathway and progressed through the same transitions as seen in the leaf epidermis, resulting in mature complexes formed of guard and subsidiary cells (as described in Figure 5.1). At the start of stomatal development in the floral organs, cells were arranged in noticeable rows, but as development progressed, pavement cells acquired an irregular shape, resulting in the less consistent spatial arrangement observed on the adaxial epidermis of lemma and palea. In addition, similarly to rice leaves, the stomatal development progressed as a spatiotemporal gradient, with earlier stages of the stomatal lineage being observed in the base of these floral organs and moving up as development of floret and stomata advanced (Figure 5.2).

Based on the stomatal lineage progression in the epidermis of lemma, and using floret length as a marker, developing IR64 florets were divided into 5 stages for a transcriptomic analysis. Each floret stage comprised a combination of stomatal lineage cells, being enriched with certain stomatal developmental stages (Figure 5.2). Expression pattern analysis of genes previously associated with stomatal development in leaves (as in table 5.2), suggested that most of these gene products might also be associated with stomatal

development in IR64 florets. Genes involved in grass stomatal lineage initiation *OsSPCH1/2*, *OsSHR1/2*, *OsSCR1/2*, *OsICE1*, *OsSCRM2* and *OsCYCA2;1* (Kamiya et al., 2003; Qu et al., 2018; Schuler et al., 2018; Wu et al., 2019) showed highest expression at stage 1 (when asymmetric entry divisions started), decreasing as stomatal development progressed (Figure 5.16). A similar pattern was observed for genes encoding the signalling peptides OsEPF1/2, OsEPFL9, and the co-receptor OsTMM, which are associated with stomatal patterning regulation (Caine et al., 2019; Lu et al., 2019; Yin et al., 2017). The expression of *OsMUTE* also agreed with its current proposed function in SCs formation and identity maintenance of GMCs in rice leaves (Serna, 2020; Wu et al., 2019). *OsMUTE* transcripts accumulated from the initial stages, reaching maximal expression in stage 3, and then showed a steep decrease in stage 4, when most SCs had already formed and GCs had divided. In contrast, the expression of *OsFAMA*, which is associated with stomatal complex maturation (Liu et al., 2009; Wu et al., 2019), gradually increased until stage 5, the last stage analysed here.

The coincidence of the expression of the genes described above with the stomatal lineage transitions in rice flowers is an expected outcome, although no studies have specifically investigated it before. Previous studies on leaves have suggested that the stomatal development pathway is regulated by the same group of transcription factors in widely different plant groups, producing a diversity of stomatal architectures (Caine et al., 2016; Chater et al., 2016; Liu et al., 2009; Raissig et al., 2016). Such a high degree of conservation would suggest that this same regulatory machinery would underlie the development of stomata on the flowers of rice. Indeed, the present study confirmed that at least two of these gene products function to regulate stomatal development in rice flowers. It was demonstrated here that stomatal patterning is altered in rice florets overexpressing either *OsEPFL9a* or *OsEPF1* (Chapter 3), and evidence from the literature supports that *AtICE1* is important for the development of stomata in Arabidopsis anthers (Wei et al., 2018).

Although rice flowers might employ the same gene regulatory networks as leaves to form stomata, other levels of regulation in this pathway might lead to the anatomical differences observed (such as differences in shape of guard and subsidiary cells). Further analysis of the RNA-seq dataset produced in this work in comparison to data on leaf development might elucidate further questions about the regulation at the transcriptional level. For instance, it is not known whether there are preferential splicing variants or specific isoforms of duplicated genes (e.g. *OsSPCH1/2*, *OsSHR1/2*) that function in each of these organs. The relative levels of expression of specific genes could also be compared

to test, for example, if a proportionally lower expression of genes involved in stomatal maturation, such as *OsFAMA,* lead to the more rounded stomatal shape observed in rice flowers.

5.3.2. The overexpression of *OsEPF1* affects the expression pattern of key stomatal development regulators in rice florets

OsEPF1 is a signalling peptide that acts as a negative regulator of stomatal development (Caine et al., 2019; Lu et al., 2019). Its ortholog in Arabidopsis (AtEPF2) also mediates stomatal development inhibition, by preventing stomatal lineage entry and amplifying divisions (Hara et al., 2007; Hunt and Gray, 2009; Lee et al., 2015a). In rice florets, the overexpression of *OsEPF1* led to alterations in expression of some key stomatal regulators (Figure 5.31). Genes encoding for transcription factors that act downstream of the asymmetric entry division, such as *OsMUTE* and *OsFAMA*, were downregulated as cells failed to enter the stomatal lineage. In addition, the expression of *OsEPF2*, also a negative regulator of stomatal development (Lu et al., 2019), was decreased in OsEPF1-oe-S florets. Interestingly, a trend was observed towards an increase in *EPFL9a* transcripts, encoding for the peptide that antagonises OsEPF1 (Lee et al., 2015a; Yin et al., 2017), and towards the decrease of *OsTMM* expression (EPF1-2/EPFL9 receptor), which could indicate an attempt to promote stomatal development in opposition to the *OsEPF1* overexpression. However, further investigations would be required to establish whether these changes in expression levels have any functional relevance.

It has been recently proposed that the early acting bHLH transcription factors OsSPCH1 and OsSPCH2 act redundantly to promote stomatal initiation in rice, with OsSPCH2 showing a major role in this process (Wu et al., 2019). However, not much is known about how SPCH1/2 transcription and function are regulated in grasses. In IR64 florets both genes showed higher expression in stages 1 and 2, decreasing in later stages. The overexpression of *OsEPF1* did not change the transcript levels of *OsSPCH2*. However, a downregulation of *OsSPCH1* was observed in stage 1, indicating a potential divergence in the expression regulation of these genes in rice florets. Similar to *OsSPCH1*, the expression of OsICE1, a potential binding partner of OsSPCH1/2 (Raissig et al., 2016; Wu et al., 2019), was significantly decreased in stage 1 of OSEPF1-oe-S florets. The analysis performed in the present study also showed that the expression of genes associated with the specification of stomatal files in grasses leaves, such as *OsSHR1/2*

and *OsSCR1/2* (Kamiya et al., 2003; Wu et al., 2019), was not altered in OsEPF1-oe-S florets. Recent evidence suggests that the transcription of OsSCR1 and OsSCR2 could be enhanced by OsMUTE in rice leaves (Wu et al., 2019), however, the expression patterns observed in OsEPF1-oe-S florets suggested that this might not be the case, at least not in florets. In this transgenic rice line *OsMUTE* was clearly downregulated, yet no impacts were reported in *OsSCR1/2* expression.

5.3.3. Expression of stomatal response genes did not change in OsEPF1-oe-S florets

Despite the strong reduction in the number of stomata in OsEPF1-oe-S floret epidermis, most of the genes which are believed to function in stomatal responses (i.e. opening and closing of the pore) investigated here did not show altered transcript levels in developing and mature florets (Figure 5.33). In both IR64 and OsEPF1-oe-S florets, transcripts for stomatal response genes were, in most cases, more abundant in the mature stages of development which is consistent with a role in guard cell functioning. The genes investigated included transcription factors, protein kinases and turgor regulators with reported roles in rice stomatal aperture control, in addition to genes in the rice ABA pathway (Table 5.3). From these, only *OsKAT3* (encoding a K^+ channel) and *OsSLAC1* (encoding an anion channel) were downregulated in OsEPF1-oe-S floret stages with mature stomata. *OsABCG5* and *OsPYL4* (encoding respectively an ABA transporter and an ABA receptor) also showed different expression patterns through the floret development in OsEPF1-oe-S. Although many of the genes analysed here are known to be expressed in either GCs or SCs of leaves, their expression is not restricted to the stomatal lineage (e.g. Hwang et al., 2013; Matsuda et al., 2016; Nguyen et al., 2017; Toda et al., 2016), which could explain why more substantial changes in their expression patterns were not detected in florets with reduced stomatal density. A comparison between florets and mature leaves could help in the interpretation of these results, since it is not known how the expression levels of the stomatal response genes in florets compare to those from a tissue with high density of fully functional stomata. It is possible that some of the genes analysed here have very reduced expression in florets of both IR64 and OsEPF1-oe-S, explaining why differences were not detected. Additionally, some of the genes in the ABA pathway (such as *OsNCED3* and *OsABI5*, Figure 5.20) could be downregulated in florets of stages 1 to 5 due to the high humidity environment provided by the flag leaf sheath protection (Pantin et al., 2013). It is also to be studied whether the

rice floral stomata indeed respond dynamically to changes in external and internal stimuli like leaf stomata. Evidence from the literature suggests that the stomatal pores on flowers show variation in their functional responses. In gerbera sepals, stomata change their aperture in response to light/dark and ABA treatments (Huang et al., 2018); in tulip petals, stomata respond to changes in temperature but not in ABA (Azad et al., 2007); while floral stomata in orchids seem to be non-responsive to these stimuli (Hew et al., 1980).

5.3.4. Impact of *OsEPF1* overexpression in rice floret expression profile

In addition to the analysis of genes associated with stomatal development and function, the RNA-seq datasets of IR64 and OsEPF1-oe-S florets were compared in order to identify other pathways with altered expression in the transgenic rice plants. Although the primary interest of this analysis was to investigate changes potentially associated with the strong reduction in stomatal density in OsEPF1-oe-S florets, it is important to acknowledge that this rice line ectopically overexpresses *OsEPF1*, producing leaves with stomatal density reductions and affecting plant water use (Caine et al., 2019). Therefore, changes in gene expression profile in OsEPF1-oe-S florets could also be related to either the overexpression itself or the physiological consequences of an overall stomatal density reduction. Despite *OsEPF1* being more expressed in the developmental stages comprising stomatal entry divisions and establishment of GMCs and SMCs (stages 1 and 2) in IR64 florets, differences in expression profile between IR64 and OsEPF1-oe-S were more pronounced in stages when stomata should be maturing or recently matured (stages 4 and 5) (Figures 5.21 and 5.27). In fully developed OsEPF1-oe-S florets fewer DEGs showed large fold change magnitudes (relative to IR64), indicating that mature florets were not as impacted as florets in the final stomatal development stages. From all DEGs reported, 31 genes were found to be consistently altered throughout floral development, being most likely related to a whole-plant effect due to the overall reduction in stomatal density or to the accumulation of OsEPF1. Unfortunately, there was little information available about these genes or their encoded products in the annotation database (table A11 in Appendix A).

5.3.5. The expression of genes involved in pollen development is affected in OsEPF1-oe-S florets

Genes associated with the meiotic cell cycle and pollen exine formation were overrepresented in sets of genes differentially expressed in developing OsEPF1-oe-S

florets in comparison to IR64. To understand to what extent anther and pollen development were affected, further analyses were performed on 23 genes with known functions in rice pollen development (Table 5.6). Fourteen of these genes were identified as differentially expressed in either floret stages 2, 3, 4 or 5. These stages most likely comprise pollen development events such as, pre-meiotic division (floret stages 2 and 3), meiosis (stages 3, 4 and 5), pollen wall biosynthesis and tapetum programmed cell death (stage 5) in IR64 florets (Figure 5.36).

Substantial changes were observed in genes associated with pollen wall biosynthesis in the transition from stage 4 to 5 of floret development, with *OsRAFTIN*, *OsCYP703A3*, *OsCYP704B2* and *OsDPW* being all strongly downregulated in stage 5. The pollen wall is a multi-layered structure that protects male gametophytes from various abiotic stresses. It is formed by a pectocellulosic intine and a sporopollenin-based exine (Shi et al., 2015; Wilson and Zhang, 2009). Rice with mutations in genes encoding OsCYP703A3, OsCYP704B2, OsDPW and OsRAFTIN exhibit defective sporopollenin biosynthesis, leading to male sterility (Li et al., 2010; Shi et al., 2011; Wang et al., 2003; Yang et al., 2014). Therefore, it is likely that a strong downregulation of these genes would lead to an altered composition of the pollen wall and reduced fertility rates. Nonetheless, plants overexpressing OsEPF1 did produce viable pollen (see to Chapter 3) and did not show obvious fertility problems neither here nor in previous studies (Caine et al., 2019).

The biosynthesis of the pollen wall is regulated by the developing microspores and also by the tapetum. During tapetum degeneration, lipidic precursors and components that will form the exine are secreted (Gómez et al., 2015; Shi et al., 2015; Zhang and Wilson, 2009). Therefore, timely tapetal PCD is important for the pollen wall biosynthesis process. Interestingly, the expression of basic bHLH transcription factors important for tapetal PCD (*OsTIP2*, *OsEAT1*, *OsUDT1* and *OsTDR*) was altered in OsEPF1-oe-S florets. The expression analysis for these pollen development genes suggested that their transcripts accumulated later during floral expansion in *OsEPF1* overexpressing plants than in IR64-control. *OsTDR*, for example, was initially downregulated in the transgenic florets in stages 3 and 4, but its expression increased later, to reach similar levels as observed in IR64 plants by stage 5. This gene product has a function in tapetal PCD and in regulating lipid metabolism, affecting the expression of *OsCYP703A3*, *OsCYP704B2*, *OsC6* and *OsRAFTIN* (Li et al., 2011; Shi et al., 2015; Zhang et al., 2008).

Similar to that observed for the tapetal PCD transcription factors, *OsC4* and *OsMEL1* seemed to have a slightly delayed expression in the OsEPF1-oe-S plants. This could also be the case for genes with a role in pollen wall biosynthesis that were strongly

downregulated in stage 5. However, as this study has not captured the events happening between stages 5 (before heading, 6 to 6.5 mm length) and the mature florets (after heading, 8.5 to 9.5 mm length), this could not be investigated. It is also important to acknowledge that samples analysed here were collected based on floret size according to the stomatal development stages in IR64 palea and lemma, and that the relationship between floret size and anther developmental events could be altered in OsEPF1-oe-S, although results in Chapter 3 suggest that there were not significant changes in floret size in this transgenic line. An investigation of how pollen development relates to floret size in IR64 and OsEPF1-oe could help to elucidate if the expression changes detected are an artefact of how florets were staged. In addition, the investigation of gene expression in later developmental stages, as well as analyses of pollen wall morphology, lipidic composition and germination rates would be beneficial to understand whether these potential alterations in the regulation of pollen development are having a negative effect on plant fertility. Although reduced seed set was not observed in OsEPF1-oe-S, a more detailed analysis, perhaps under different environmental conditions, might reveal eventual effects.

5.3.6. Other processes potentially affected by the overexpression of *OsEPF1*

Several functional classes (gene ontology, GO) were overrepresented in the datasets of genes differentially expressed between IR64 and OsEPF1-oe-S florets, however, the GO term annotations were not particularly informative when DEGs by stage were accessed. In general, only a small number of DEGs was associated with each functional class found, or even within a group of similar classes as well. This could indicate that the overexpression of *OsEPF1* did not lead to substantial changes in specific biological processes. However, some GO terms did stand out from these analyses and require additional investigation. That is the case for a group of genes associated with the chloroplast thylakoid, which were downregulated in stages comprising stomatal maturation (stages 4 and 5). Although the expression patterns of genes associated with rice photosynthetic development suggested that this process progresses in a similar way in IR64 and OsEPF1-oe-S florets, it is not known if these rice lines show any sub-cellular differences, for example a significant difference in density of chloroplasts. Further analyses are needed to elucidate the cause and the impact of the gene expression changes reported here. This may be of importance, since grass inflorescences are photosynthetically active after heading and are believed to actively contribute to grain yield (Araus et al., 1993; Chang et al., 2020; Molero and Reynolds, 2020). Additional

investigations are also needed to provide a better understanding of the changes associated with "SCF-dependent proteasomal ubiquitin-dependent catabolic protein process" GO term. The SCF ligase complex mediates polyubiquitination of proteins targeted for degradation, which is important in the regulation of diverse biological processes, including hormone signalling, responses to stress, cell division, morphogenesis, defence responses, and others (Vierstra, 2009). Transcripts of *OsCOI1b*, a gene involved in the jasmonic acid response signalling pathway (Lee et al., 2015b), were shown to accumulate to higher levels in stages 4 and 5 of OsEPF1-oe-S florets. However, most of the DEGs identified with this GO term are yet to be associated with specific pathways in the annotation databases. Furthermore, genes associated with the meiotic cell cycle could also impact ovule development, which was not investigated in this study.

5.3.7. Conclusions

The work described in this chapter provides a valuable addition to the paucity of knowledge concerning floral stomata, demonstrating that stomatal development in rice leaves and florets progresses in a similar way, following the same cell transitions regulated by the same group of key signalling components. Following this work, a more detailed analysis comparing the expression profiles of florets and leaves is required to investigate differences in the transcriptional regulation of this pathway, which could perhaps explain the differences in GCs and SCs shape. This could include, for example, the analysis of preferential isoforms and splicing variants. Additionally, this work reported biological processes that are potentially affected during floret development in rice plants with stomatal density reductions. In particular, it showed that the expression pattern of genes with functions in stomatal development and in pollen development are significantly altered or delayed in OsEPF1-oe-S plants. Additional work on the characterization of pollen development in OsEPF1-oe-S plants is required to understand what these changes in gene expression represent. Although it is possible that the absence of stomata or the overexpression of *OsEPF1* altered the expression pattern of genes involved in pollen and tapetum development, it is also possible that differences detected here were due to the sampling method, since florets were collected according to the progression of stomata development in IR64 lemma and palea rather than based on pollen or anther development.

Chapter 6. General Discussion

Stomata play a fundamental role in moderating plant-atmosphere gas exchange. By controlling their aperture size these microscopic pores dynamically balance the uptake of CO_2 for photosynthesis and water loss for transpiration, influencing water-use-efficiency (WUE) and plant temperature regulation. Likewise, changes to the density and size of stomata impact on plant gas exchange capacity and potentially on operational rates (reviewed in Bertolino et al. 2019; Dow and Bergmann, 2014; Lawson and Matthews, 2020). With the predicted rises in global average temperature and in the frequency of heat waves and droughts, targeting changes to stomatal traits might be an effective approach for improving plant tolerance to the future adverse climate conditions. This study specifically hypothesized that an increase in the stomatal density of rice leaves and flowers could enhance plant evaporative cooling capacity during the reproductive phase, therefore minimizing heat-induced yield losses. This modification could be particularly useful for rice grown under paddy fields and irrigated conditions, as sufficient water supply is a crucial factor for maintaining transpiration levels. Analyses performed here were conducted using genetically modified plants of the IR64 lowland rice cultivar overexpressing the gene *OsEPFL9a*, moreover, studies of floral stomatal distribution and development were carried out for IR64 and transgenic lines overexpressing either *OsEPFL9a* or *OsEPF1*. Although the main hypothesis of this work was not corroborated, the data produced provide a valuable addition into the study of the effects of altering stomatal development in crop species and will support further investigations.

6.1. Constrains to the increase of stomatal conductance in rice

The genetic manipulation of stomatal development leading to an increased number of stomata in rice leaf epidermis has been previously reported in the literature (Mohammed et al., 2019; Schuler et al., 2018). These studies have, nonetheless, limited their investigations to the early vegetative phase of the plant life cycle. By extending analyses to the reproductive phase, the work presented here suggests that engineering substantial increments to the stomatal density of flag leaves might be more challenging than previously thought. Results from Chapter 3 showed that the epidermis of IR64 flag leaves have a very high density of stomata, being possibly close to a maximum limit, and that plants overexpressing *OsEPFL9a* did not have a great increase in the number of stomata in these leaves. Whether this phenotype is observed on the flag leaves of other transgenic

rice with increased stomatal densities is still to be investigated. However, it is plausible to speculate that the development of additional stomata on flag leaves could be constrained by a spatial coordination with the development of veins, mesophyll airspace and also neighbouring stomata, ensuring that hydraulic capacity and stomatal function are kept in an optimal range (de Boer et al., 2016; Franks and Farquhar, 2007). Regardless of the cause, the limited changes in the number of stomata in flag leaves of OsEPFL9a-oe lines imposed an obstacle to the proposal of enhancing evaporative cooling during the reproductive phase of rice. This growth phase is the most sensitive to heat damage (Jagadish et al., 2015; Satake and Yoshida, 1978), and therefore was the focus of this study. Perhaps unsurprisingly the modest increments in flag leaf stomatal density (+ 10%) did not promote significantly higher levels of transpiration-mediated cooling in either normal or elevated temperature conditions.

Substantial improvements in evaporative cooling were also not observed at earlier plant growth stages. Although the overexpression of *OsEPFL9a* significantly promoted stomatal development in leaf 6 epidermis, resulting in a g_{smax} increase of ~23-29%, greater levels of water diffusion through stomatal pores were not consistently observed across the transgenic lines investigated. These results were similar to those from studies on japonica cultivars overexpressing *OsEPFL9a* and *ZmSHR1*, where no improvements in operational gas exchange were detected, despite comparable levels of stomatal density increase (Mohammed et al., 2019; Schuler et al., 2018). This suggests that an even greater g_{smax}, or a manipulation of guard cells responses, might be required for enhancing water loss and cooling in rice plants. Whilst in the current project the overexpression of *OsEPFL9a* did not successfully enable the desirable levels of stomatal conductance, in the future a combination of genes could be targeted to further manipulate stomatal development or behaviour. If this is to be attempted, the coordination of stomatal cavities with the underlying leaf anatomy should also be considered to assure proper stomatal functioning and sufficient hydraulic supply, sustaining potential high transpiration levels (de Boer et al., 2016; Matthews et al., 2020). Additionally, although the use of transgenic plants is adequate for a proof of concept research, such as this work, there are still challenges to the acceptance of GM crops in many countries. Therefore, the use of other technologies more likely to be accepted, such, as CRISPR, should be considered.

6.2. Targeting evaporative cooling of rice florets

Promoting elevated evaporative cooling levels might help plants to overcome damage caused by above optimum temperatures. However, this process can only be sustained

while water supply is not limited. During extended heat waves or when drought and heat conditions coincide an increased transpiration rate could result in depletion of soil water reserves (Urban et al., 2017). While heat stress will impact many agricultural areas, water availability is also expected to have major limiting effect on yields in the near future, therefore efforts have been made in terms of improving agricultural practices and crop varieties to ensure that water is used in more effective way (Campbell et al., 2014; Iglesias and Garrote, 2015). Although a whole-plant increase in stomatal density has been demonstrated in Arabidopsis to give an approximately 30% increase in photosynthetic assimilation rate at high light intensity (Tanaka et al., 2013), observed high levels of water loss might have substantial negative impacts on water-use efficiency (WUE) throughout a crop growing season. As reproductive processes are particularly sensitive to high temperatures, this study began to investigate whether increasing stomatal density in rice florets could be a possible route to enhancing evaporative cooling. This could offer an alternative to the whole-plant approach, allowing a targeted modification of stomatal development in the floral tissues, and minimizing losses in plant WUE. Unfortunately, results from this work suggested that the spatial distribution of floral stomata might not favour an improvement in evaporative cooling of the heat-sensitive floral organs. Most of the floral stomata in IR64 plants were found to be located in the inner epidermis of the palea and lemma. In the outer epidermis of these floral organs, stomata were restricted to the tips and lateral edges, and although the overexpression of *OsEPFL9a* did significantly increase the number of stomata that developed on florets, their spatial distribution was still restricted to the same areas. Indeed, no differences in floret temperature were observed between transgenic and control plants despite large differences in stomatal numbers. It is possible that increases in the stomatal density of the inner floral tissues might offer benefits during the flowering stage when the epidermis is exposed to the atmosphere, potentially promoting cooling or a more effective anther dehiscence. However, the results in Chapter 4 indicated that OsEPFL9a-oe plants did not have greater fertility rates after high temperature treatment, with yield being negatively impacted in a similar manner to the controls.

6.3. Advancing floral stomatal characterization

Little attention has been focused on how stomatal pores develop and function on floral organs. Nonetheless, these are fundamental questions for understanding whether stomatal traits can be altered in the reproductive tissues, and the consequences of such

manipulation. The characterization of floral stomata conducted in this study for IR64 rice established that these structures have a slightly different morphology in comparison to leaf stomata. However, in the palea and lemma their development followed the same cell lineage transitions as for rice leaves. RNA-seq analysis of a developmental time-course suggested that these cellular transitions are most likely regulated by the same genetic network, since genes essential for stomatal development in rice leaves showed expression patterns that coincided with their (leaf) roles as stomata developed in rice florets.

It was also shown that the differentiation of stomata was completed by the time that IR64 florets had grown to approximately 6.5 mm in length, when panicles were at booting stage. At this point the expression levels of several genes associated with the operation of guard cells became accentuated. This expression pattern indicates that these floral stomata might be functional even before panicle heading. Nevertheless, further work is needed to understand whether floral stomata in rice are functional at all in opening and closing, and if so, what their physiological function might be. Characterizing which stimuli floral guard cell respond to, and whether aperture response alter during floral development might help to identify the biological processes likely to be supported by gas exchange through floral stomata. These structures might, for instance, contribute to photosynthesis, water and nutrient load, maintenance of optimum humidity conditions for late pollen/ovule development, or in facilitating anther dehiscence (Clement et al., 1997; Keijzer et al., 1987; Lugassi et al., 2020; Roddy et al., 2016; Wei et al., 2018).

Although the rice lines OsEPFL9a-oe and OsEPF1-oe produced florets with substantial alterations in the number of stomata, their phenotypes did not impose any obvious disadvantage (or advantage) to plant reproduction. Plants produced viable pollen and neither fertilization nor seed development impairments were observed in the conditions tested. Naturally, further analyses on these transgenic rice lines are necessary to exclude potential overlooked negative effects. For instance, the presence of stomata on anthers has been thought to support timely anther dehiscence by assisting the final dehydration process in several species (Keijzer et al., 1987; Wei et al., 2018; Wilson et al., 2011). In rice, the initial anther dehiscence steps (septum rupture and initial stomium split) are driven by pressure from the swelling of pollen grains (Matsui, 1999), and the subsequent widening of the splits is caused by a desiccation process (Matsui et al., 1999). If rice floral stomata do contribute to this process, it is possible that changes in relative humidity, for example, could lead to a delayed or incomplete anther dehiscence when floral stomata are not present.

Investigations into the differences between expression profiles of IR64 and OsEPF1-oe-S florets (which are almost devoid of stomata) indicated that several biological processes were substantially altered in plants with near absence of floral stomata under optimal conditions. Notably, the expression of genes associated with pollen development and the chloroplast were affected. Photosynthesis in the reproductive tissues is considered an important contributor to grain filling in grasses, as panicles are photosynthetically active after heading (Araus et al., 1993; Chang et al., 2020), and changes in this process could impact on grain quality. Yet, the contribution of floral stomata to spikelet photosynthesis is not well understood in grasses (Araus et al., 1993; Brazel and Ó'Maoileídigh, 2019). Likewise, abnormal pollen development could directly affect plant fertility (Gómez et al., 2015). The analyses presented here suggested that OsEPF1-oe-S plants have an altered (potentially delayed) expression pattern of genes associated with tapetum PCD and pollen wall biosynthesis. As discussed in Chapter 5, further analyses are necessary to understand if these changes are a result of an alteration in the relationship between floret size and anther developmental stages in OsEPF1-oe plants, or if this difference in expression pattern could be the consequence of the absence of stomata. A detailed comparison of pollen development, pollen wall morphology and lipidic composition between IR64 and OsEPF1-oe plants could help to elucidate these questions.

Although most significant changes in gene expression were seen in the developmental stages when floral stomata were maturing or mature (stages 4 and 5) in IR64, it is important to consider that comparing IR64 with OsEPF1-oe-S might not be the most appropriate approach to assess the impact of specifically altering floral stomatal development on floret gene expression. Identified changes might indeed be a direct result of the manipulation of stomatal development in flowers, which could be associated with a disruption in the coordination/interaction between developmental networks or with the absence of stomatal function itself. However, as OsEPF1-oe-S plants have also a strong reduction in leaf stomatal density (Caine et al., 2019), these changes could perhaps be the consequence of a whole-plant stomatal density change, as well as an unexpected effect of the ectopic accumulation of OsEPF1. Results from these analyses, however, form a starting point for further investigations. For example, the RNA-seq datasets produced during this study, in either IR64 or OsEPF1-oe-S might support further studies on floral stomatal development or on the coordination between the development of stomata and other floral structures.

6.4. Conclusions and future directions

This study revealed that enhancing stomatal development through the overexpression of *OsEPFL9a* is not an effective approach to promote increases in rice evaporative cooling and alleviate yield losses caused by heat stress during the reproductive phase. The increase in stomatal density in flag leaves was limited in OsEPFL9a-oe lines, and although significant increases in floret stomatal density were observed, these were not beneficial to plant fertility under heat stress conditions. Indeed, the spatial distribution of floral stomata suggested that these structures were unlikely to favour greater evaporative cooling in rice. Although it is still possible that a higher increase in leaf stomatal density could be effective, a better understanding of how flag leaf epidermal space is allocated and of how the development of underlying structures are coordinated might be helpful for future studies into this subject. With regards to the stomata present on rice florets, although their precise function in the different reproductive organs is yet to be elucidated, this study produced a detailed description of the distribution of stomata in the different floral organs and of how these structures develop in the rice lemma and palea. This characterization, along with the transcriptomic datasets generated in this study provide the foundation for future work into the development and function of floral stomata. Further investigations comparing datasets on the development of stomata in florets and leaves could indicate differences in the regulation of the genetic network involved in stomatal development, helping to elucidate how reproductive and leaf stomata differ. Analyses of guard cell behaviour in IR64 florets at different stages of the reproductive and ripening growth could reveal whether rice floral stomata are able to adjust their aperture, and if so, when during the development they become responsive. Additionally, further studies of OsEPFL9a-oe and OsEPF1-oe plants, or of rice with changes in stomatal development that are specific to the floral tissues, might produce valuable insights into the importance of floral stomata in rice and other grasses. For instance, differences in anther dehiscence, grain composition, photosynthesis and pollen development could be investigated, which would also help in the understanding to the gene expression differences found between OsEPF1-oe and IR64 florets.

References

Abrash, E., Gil, M. X. A., Matos, J. L., and Bergmann, D. C. (2018). Conservation and divergence of YODA MAPKKK function in regulation of grass epidermal patterning. *Dev.* 145. doi:10.1242/dev.165860.

Araus, J. L., Brown, H. R., Febrero, A., Bort, J., and Serret, M. D. (1993). Ear photosynthesis, carbon isotope discrimination and the contribution of respiratory CO2 to differences in grain mass in durum wheat. *Plant. Cell Environ.* 16, 383–392. doi:10.1111/j.1365-3040.1993.tb00884.x.

Arshad, M. S., Farooq, M., Asch, F., Krishna, J. S. V., Prasad, P. V. V. V., and Siddique, K. H. M. (2017). Thermal stress impacts reproductive development and grain yield in rice. *Plant Physiol. Biochem.* 115, 57–72. doi:10.1016/j.plaphy.2017.03.011.

Assmann, S. M., and Jegla, T. (2016). Guard cell sensory systems: recent insights on stomatal responses to light, abscisic acid, and CO2. *Curr. Opin. Plant Biol.* 33, 157–167. doi:10.1016/J.PBI.2016.07.003.

Azad, A. K., Sawa, Y., Ishikawa, T., and Shibata, H. (2007). Temperature-dependent stomatal movement in tulip petals controls water transpiration during flower opening and closing: Research article. *Ann. Appl. Biol.* 150, 81–87. doi:10.1111/j.1744-7348.2006.00111.x.

Barnabás, B., Jäger, K., and Fehér, A. (2008). The effect of drought and heat stress on reproductive processes in cereals. *Plant, Cell Environ.* 31, 11–38. doi:10.1111/j.1365-3040.2007.01727.x.

Bergmann, D. C. (2004). Integrating signals in stomatal development. *Curr. Opin. Plant Biol.* 7, 26–32. doi:10.1016/j.pbi.2003.10.001.

Bertolino, L. T., Caine, R. S., and Gray, J. E. (2019). Impact of Stomatal Density and Morphology on Water-Use Efficiency in a Changing World. *Front. Plant Sci.* 10, 225. doi:10.3389/fpls.2019.00225.

Bort, J., Brown, R. H., and Araus, J. L. (1996). Refixation of respiratory CO 2 in the ears of C 3 cereals. *J. Exp. Bot.* 47, 1567–1575. doi:10.1093/jxb/47.10.1567.

Bolger, A. M., Lohse, M., and Usadel, B. (2014). Trimmomatic: A flexible trimmer for Illumina sequence data. *Bioinformatics.* 30, 2114–2120. doi:10.1093/bioinformatics/btu170.

Brazel, A. J., and Ó'Maoileídigh, D. S. (2019). Photosynthetic activity of reproductive organs. *J. Exp. Bot.* 70, 1737–1753. doi:10.1093/jxb/erz033.

Bridge, L. J., Franklin, K. A., and Homer, M. E. (2013). Impact of plant shoot architecture on leaf cooling: A coupled heat and mass transfer model. *J. R. Soc. Interface* 10. doi:10.1098/rsif.2013.0326.

Buckley, C. R., Caine, R. S., and Gray, J. E. (2019). Pores for thought: Can genetic manipulation of stomatal density protect future rice yields? *Front. Plant Sci.* 10, 1783. doi:10.3389/FPLS.2019.01783.

Cai, H., Zhao, L., Wang, L., Zhang, M., Su, Z., Cheng, Y., et al. (2017). ERECTA signaling controls Arabidopsis inflorescence architecture through chromatin-mediated activation of PRE1 expression. *New Phytol.* 214, 1579–1596. doi:10.1111/nph.14521.

Caine, R. S., Chater, C. C., Kamisugi, Y., Cuming, A. C., Beerling, D. J., Gray, J. E., et al. (2016). An ancestral stomatal patterning module revealed in the non-vascular land plant Physcomitrella patens. *Dev.* 143, 3306–3314. doi:10.1242/dev.135038.

Caine, R. S., Yin, X., Sloan, J., Harrison, E. L., Mohammed, U., Fulton, T., et al. (2019). Rice with reduced stomatal density conserves water and has improved drought tolerance under future climate conditions. *New Phytol.* 221, 371–384. doi:10.1111/nph.15344.

Campbell, B. M., Thornton, P., Zougmoré, R., van Asten, P., and Lipper, L. (2014). Sustainable intensification: What is its role in climate smart agriculture? *Curr. Opin. Environ. Sustain.* 8, 39–43. doi:10.1016/J.COSUST.2014.07.002.

Cartwright, H. N., Humphries, J. A., and Smith, L. G. (2009). PAN1: A receptor-like protein that promotes polarization of an asymmetric cell division in maize. *Science* 323, 649–651. doi:10.1126/science.1161686.

Casson, S., and Gray, J. E. (2008). Influence of environmental factors on stomatal development. *New Phytol.* 178, 9–23. doi:10.1111/j.1469-8137.2007.02351.x.

Chang, T. G., Song, Q. F., Zhao, H. L., Chang, S., Xin, C., and Qu, M. (2020). An in situ approach to characterizing photosynthetic gas exchange of rice panicle. *Plant Methods*. 1–14. doi:10.1186/s13007-020-00633-1.

Chater, C. C. C., Caine, R. S., Fleming, A. J., and Gray, J. E. (2017). Origins and Evolution of Stomatal Development. *Plant Physiol.* 174, 624–638. doi:10.1104/pp.17.00183.

Chater, C. C., Caine, R. S., Tomek, M., Wallace, S., Kamisugi, Y., Cuming, A. C., et al. (2016). Origin and function of stomata in the moss Physcomitrella patens. *Nat. plants* 2, 16179. doi:10.1038/nplants.2016.179.

Chauhan, H., Khurana, N., Agarwal, P., and Khurana, P. (2011). Heat shock factors in rice (Oryza sativa L.): Genome-wide expression analysis during reproductive development and abiotic stress. *Mol. Genet. Genomics.* 286, 171–187. doi:10.1007/s00438-011-0638-8.

Cheabu, S., Moung-Ngam, P., Arikit, S., Vanavichit, A., and Malumpong, C. (2018). Effects of Heat Stress at Vegetative and Reproductive Stages on Spikelet Fertility. *Rice Sci.* 25, 218–226. doi:10.1016/j.rsci.2018.06.005.

Chen, T., Wu, H., Wu, J., Fan, X., Li, X., and Lin, Y. (2017). Absence of OsβCA1 causes

a CO2 deficit and affects leaf photosynthesis and the stomatal response to CO2 in rice. *Plant J.* 90, 344–357. doi:10.1111/tpj.13497.

Clement, C., Mischler, P., Burrus, M., and Audran, J. C. (1997). Characteristics of the photosynthetic apparatus and CO2-fixation in the flower bud of Lilium. I. Corolla. *Int. J. Plant Sci.* 158, 794–800. doi:10.1086/297492.

Crawford, A. J., McLachlan, D. H., Hetherington, A. M., and Franklin, K. A. (2012). High temperature exposure increases plant cooling capacity. *Curr. Biol.* 22, R396–R397. doi:10.1016/J.CUB.2012.03.044.

de Boer, H. J., Eppinga, M. B., Wassen, M. J., and Dekker, S. C. (2012). A critical transition in leaf evolution facilitated the Cretaceous angiosperm revolution. *Nat. Commun.* 3, 1221. doi:10.1038/ncomms2217.

de Boer, H. J., Price, C. A., Wagner-Cremer, F., Dekker, S. C., Franks, P. J., and Veneklaas, E. J. (2016). Optimal allocation of leaf epidermal area for gas exchange. *New Phytol.* 210, 1219–1228. doi:10.1111/nph.13929.

Deryng, D., Conway, D., Ramankutty, N., Price, J., and Warren, R. (2014). Global crop yield response to extreme heat stress under multiple climate change futures. *Environ. Res. Lett.* 9, 034011. doi:10.1088/1748-9326/9/3/034011.

Dilcher, D., Boer, H. J. de, Dekker, S. C., Dilcher, D. L., Lotter, A. F., and Wagner-Cremer, F. (2000). Toward a new synthesis: Major evolutionary trends in the angiosperm fossil record. *Proc. Natl. Acad. Sci.* 97, 7030–7036. doi:10.1073/pnas.97.13.7030.

Dittberner, H., Korte, A., Mettler-Altmann, T., Weber, A. P. M., Monroe, G., and de Meaux, J. (2018). Natural variation in stomata size contributes to the local adaptation of water-use efficiency in Arabidopsis thaliana. *Mol. Ecol.* doi:10.1111/mec.14838.

Doheny-Adams, T., Hunt, L., Franks, P. J., Beerling, D. J., and Gray, J. E. (2012). Genetic manipulation of stomatal density influences stomatal size, plant growth and tolerance to restricted water supply across a growth carbon dioxide gradient. *Philos. Trans. R. Soc. Lond. B. Biol. Sci.* 367, 547–55. doi:10.1098/rstb.2011.0272.

Dow, G. J., and Bergmann, D. C. (2014). Patterning and processes: How stomatal development defines physiological potential. *Curr. Opin. Plant Biol.* 21, 67–74. doi:10.1016/j.pbi.2014.06.007.

Dow, G. J., Bergmann, D. C., and Berry, J. A. (2014a). An integrated model of stomatal development and leaf physiology. *New Phytol.* 201, 1218–1226. doi:10.1111/nph.12608.

Dow, G. J., Berry, J. A., and Bergmann, D. C. (2014b). The physiological importance of developmental mechanisms that enforce proper stomatal spacing in Arabidopsis thaliana. *New Phytol.* 201, 1205–1217. doi:10.1111/nph.12586.

Dow, G. J., Berry, J. A., and Bergmann, D. C. (2017). Disruption of stomatal lineage signaling or transcriptional regulators has differential effects on mesophyll

development, but maintains coordination of gas exchange. *New Phytol.* 216, 69–75. doi:10.1111/nph.14746.

Dunn, J., Hunt, L., Afsharinafar, M., Meselmani, M. Al, Mitchell, A., Howells, R., et al. (2019). Reduced stomatal density in bread wheat leads to increased water-use efficiency. *J. Exp. Bot.* doi:10.1093/jxb/erz248.

Engineer, C. B., Ghassemian, M., Anderson, J. C., Peck, S. C., Hu, H., and Schroeder, J. I. (2014). Carbonic anhydrases, EPF2 and a novel protease mediate CO2 control of stomatal development. *Nature*. 513, 246–250. doi:10.1038/nature13452.

Ebenezer, G., Amirthalingam, M., Ponsamuel, J., and Dayanandan, P. (1990). Role of palea and lemma in the development of rice caryopsis. *J. Indian Bot. Soc*, 245–250.

Endo, M., Tsuchiya, T., Hamada, K., Kawamura, S., Yano, K., Ohshima, M., et al. (2009). High Temperatures Cause Male Sterility in Rice Plants with Transcriptional Alterations During Pollen Development. *Plant Cell Physiol.* 50, 1911–1922. doi:10.1093/pcp/pcp135.

Fang, Z., Ji, Y., Hu, J., Guo, R., Sun, S., and Wang, X. (2020). Strigolactones and Brassinosteroids Antagonistically Regulate the Stability of the D53–OsBZR1 Complex to Determine FC1 Expression in Rice Tillering. *Mol. Plant.* 13, 586–597. doi:10.1016/j.molp.2019.12.005.

Fanourakis, D., Giday, H., Milla, R., Pieruschka, R., Kjaer, K. H., Bolger, M., et al. (2015). Pore size regulates operating stomatal conductance, while stomatal densities drive the partitioning of conductance between leaf sides. *Ann. Bot.* 115, 555–565. doi:10.1093/aob/mcu247.

Farquhar, G. D., and Sharkey, T. D. (1982). Stomatal Conductance and Photosynthesis. *Annu. Rev. Plant Physiol.* 33, 317–345. doi:10.1146/annurev.pp.33.060182.001533.

Feild, T. S., Chatelet, D. S., and Brodribb, T. J. (2009). Giant flowers of Southern magnolia are hydrated by the xylem. *Plant Physiol.* 150, 1587–1597. doi:10.1104/pp.109.136127.

Franks, P. J., and Beerling, D. J. (2009). Maximum leaf conductance driven by CO2 effects on stomatal size and density over geologic time. *Proc. Natl. Acad. Sci. U. S. A.* 106, 10343–7. doi:10.1073/pnas.0904209106.

Franks, P. J., and Casson, S. (2014). Connecting stomatal development and physiology. *New Phytol.* 201, 1079–1082. doi:10.1111/nph.12673.

Franks, P. J., Drake, P. L., and Beerling, D. J. (2009). Plasticity in maximum stomatal conductance constrained by negative correlation between stomatal size and density: An analysis using Eucalyptus globulus. *Plant, Cell Environ.* 32, 1737–1748. doi:10.1111/j.1365-3040.2009.002031.x.

Franks, P. J., and Farquhar, G. D. (1999). A relationship between humidity response, growth form and photosynthetic operating point in C3 plants. *Plant, Cell Environ.* 22, 1337–1349. doi:10.1046/j.1365-3040.1999.00494.x.

Franks, P. J., and Farquhar, G. D. (2001). The Effect of Exogenous Abscisic Acid on Stomatal Development, Stomatal Mechanics, and Leaf Gas Exchange in Tradescantia virginiana. *Plant Physiology*. 125, 935-942.

Franks, P. J., and Farquhar, G. D. (2007). The Mechanical Diversity of Stomata and Its Significance in Gas-Exchange Control. *Plant Physiol.* 143, 78–87. doi:10.1104/pp.106.089367.

Franks, P. J., W. Doheny-Adams, T., Britton-Harper, Z. J., and Gray, J. E. (2015a). Increasing water-use efficiency directly through genetic manipulation of stomatal density. *New Phytol.* 207, 188–195. doi:10.1111/nph.13347.

Gómez, J. F., Talle, B., and Wilson, Z. A. (2015). Anther and pollen development: A conserved developmental pathway. *J. Integr. Plant Biol.* 57, 876–891. doi:10.1111/jipb.12425.

GRiSP (Global Rice Science Partnership). 2013. Rice almanac, 4th edition. Los Baños (Philippines): International Rice Research Institute. 283 p.

Grossiord, C., Buckley, T. N., Cernusak, L. A., Novick, K. A., Poulter, B., Siegwolf, R. T. W., et al. (2020). Plant responses to rising vapor pressure deficit. *New Phytol.* 226, 1550–1566. doi:10.1111/nph.16485.

Gupta, S. C., Paliwal, G. S., and Gupta, M. (1965). The Development of Stomata in Vegetative and Reproductive Organs of Bupleurum tenue Buch.-Ham. ex D. Don. *Ann. Bot.* 29, 645–654. doi:10.1093/oxfordjournals.aob.a083978.

Hara, K., Kajita, R., Torii, K. U., Bergmann, D. C., and Kakimoto, T. (2007). The secretory peptide gene EPF1 enforces the stomatal one-cell-spacing rule. *Genes Dev.* 21, 1720–5. doi:10.1101/gad.1550707.

Hardke, J. T. (2018). *Rice production handbook*. University of Arkansas Division of Agriculture Cooperative Extension Service.

Harrison, E. L., Arce Cubas, L., Gray, J. E., and Hepworth, C. (2020). The influence of stomatal morphology and distribution on photosynthetic gas exchange. *Plant J.* 101, 768–779. doi:10.1111/tpj.14560.

Hashimoto, M., Negi, J., Young, J., Israelsson, M., Schroeder, J. I., and Iba, K. (2006). Arabidopsis HT1 kinase controls stomatal movements in response to CO2. *Nat. Cell Biol.* 8, 391–397. doi:10.1038/ncb1387.

He, Y., Wang, C., Higgins, J. D., Yu, J., Zong, J., Lu, P., et al. (2016). MEIOTIC F-BOX is essential for male meiotic DNA double-strand break repair in rice. *Plant Cell.* 28, 1879–1893. doi:10.1105/tpc.16.00108.

Hepworth, C., Caine, R. S., Harrison, E. L., Sloan, J., and Gray, J. E. (2018). Stomatal development: focusing on the grasses. *Curr. Opin. Plant Biol.* 41, 1–7. doi:10.1016/j.pbi.2017.07.009.

Hepworth, C., Doheny-Adams, T., Hunt, L., Cameron, D. D., and Gray, J. E. (2015). Manipulating stomatal density enhances drought tolerance without deleterious effect

on nutrient uptake. *New Phytol.* 208, 336–341. doi:10.1111/nph.13598.

Hetherington, A. M., and Woodward, F. I. (2003). The role of stomata in sensing and driving environmental change. *Nature* 424, 901–908. doi:10.1038/nature01843.

Hew, C. S., Lee, G. L., and Wong, S. C. (1980). Occurrence of non-functional stomata in the flowers of tropical orchids. *Ann. Bot.* 46, 195–201. doi:10.1093/oxfordjournals.aob.a085907.

Hiei, Y., and Komari, T. (2008). Agrobacterium-mediated transformation of rice using immature embryos or calli induced from mature seed. *Nat. Protoc.* 3, 824–834. doi:10.1038/nprot.2008.46.

Huang, X. Y., Chao, D. Y., Gao, J. P., Zhu, M. Z., Shi, M., and Lin, H. X. (2009). A previously unknown zinc finger protein, DST, regulates drought and salt tolerance in rice via stomatal aperture control. *Genes Dev.* 23, 1805–1817. doi:10.1101/gad.1812409.

Huang, X., Lin, S., He, S., Lin, X., Liu, J., Chen, R., et al. (2018). Characterization of stomata on floral organs and scapes of cut 'Real' gerberas and their involvement in postharvest water loss. *Postharvest Biol. Technol.* 142, 39–45. doi:10.1016/J.POSTHARVBIO.2018.04.001.

Hughes, J., Hepworth, C., Dutton, C., Dunn, J. A., Hunt, L., Stephens, J., et al. (2017). Reducing Stomatal Density in Barley Improves Drought Tolerance without Impacting on Yield. *Plant Physiol.* 174, 776–787. doi:10.1104/pp.16.01844.

Hunt, L., Bailey, K. J., and Gray, J. E. (2010). The signalling peptide EPFL9 is a positive regulator of stomatal development. *New Phytol.* 186, 609–614. doi:10.1111/j.1469-8137.2010.03200.x.

Hunt, L., and Gray, J. E. (2009). The Signaling Peptide EPF2 Controls Asymmetric Cell Divisions during Stomatal Development. *Curr. Biol.* 19, 864–869. doi:10.1016/J.CUB.2009.03.069.

Hwang, H., Yoon, J., Kim, H. Y., Min, M. K., Kim, J.-A., Choi, E.-H., et al. (2013). Unique Features of Two Potassium Channels, OsKAT2 and OsKAT3, Expressed in Rice Guard Cells. *PLoS One.* 8, e72541. doi:10.1371/journal.pone.0072541.

Iglesias, A., and Garrote, L. (2015). Adaptation strategies for agricultural water management under climate change in Europe. *Agric. Water Manag.* 155, 113–124. doi:10.1016/J.AGWAT.2015.03.014.

Ikeda, K., Sunohara, H., and Nagato, Y. (2004). Developmental Course of Inflorescence and Spikelet in Rice. *Breed. Sci.* 54, 147–156. doi:10.1270/jsbbs.54.147.

Ikeda, N., Bautista, N. S., Yamada, T., Kamijima, O., and Ishii, T. (2001). Ultra-Simple DNA Extraction Method for Marker- Assisted Selection Using Microsatellite Markers in Rice. *Plant Mol. Biol. Report. Int. Soc. Plant Mol. Biol.* 19, 27–32.

IPCC (2014). *Climate Change 2014: Synthesis Report. Contribution of Working Groups I, II and III to the Fifth Assessment Report of the Intergovernmental Panel on*

Climate Change. [Core Writing Team, R.K. Pachauri and L.A. Meyer (eds.)]. IPCC, Geneva, Switzerland, 151 pp.

Itoh, J.-I., Nonomura, K.-I., Ikeda, K., Yamaki, S., Inukai, Y., Yamagishi, H., et al. (2005). Rice Plant Development: from Zygote to Spikelet. *Plant. Cell. Physiol.* 46, 23–47. doi:10.1093/pcp/pci501.

Jagadish, S. V. K. (2020). Heat stress during flowering in cereals – effects and adaptation strategies. *New Phytol.* 226, 1567–1572. doi:10.1111/nph.16429.

Jagadish, S. V. K., Craufurd, P. Q., and Wheeler, T. R. (2007). High temperature stress and spikelet fertility in rice (Oryza sativa L.). *J. Exp. Bot.* 58, 1627–35. doi:10.1093/jxb/erm003.

Jagadish, S. V. K., Murty, M. V. R., and Quick, W. P. (2015). Rice responses to rising temperatures - challenges, perspectives and future directions. *Plant. Cell Environ.* 38, 1686–1698. doi:10.1111/pce.12430.

Jagadish, S. V. K., Muthurajan, R., Oane, R., Wheeler, T. R., Heuer, S., Bennett, J., et al. (2010). Physiological and proteomic approaches to address heat tolerance during anthesis in rice (Oryza sativa L.). *J. Exp. Bot.* 61, 143–156. doi:10.1093/jxb/erp289.

Janni, M., Gullì, M., Maestri, E., Marmiroli, M., Valliyodan, B., Nguyen, H. T., et al. (2020). Molecular and genetic bases of heat stress responses in crop plants and breeding for increased resilience and productivity. *J. Exp. Bot.* 71, 3780–3802. doi:10.1093/jxb/eraa034.

Jiang, S., Wang, D., Yan, S., Liu, S., Liu, B., Kang, H., et al. (2019). Dissection of the Genetic Architecture of Rice Tillering using a Genome-wide Association Study. *Rice*. 12, 1–11. doi:10.1186/s12284-019-0302-1.

Julia, C., and Dingkuhn, M. (2012). Variation in time of day of anthesis in rice in different climatic environments. *Eur. J. Agron.* 43, 166–174. doi:10.1016/j.eja.2012.06.007.

Julia, C., and Dingkuhn, M. (2013). Predicting temperature induced sterility of rice spikelets requires simulation of crop-generated microclimate. *Eur. J. Agron.* 49, 50–60. doi:10.1016/j.eja.2013.03.006.

Jung, K. H., Han, M. J., Lee, Y. S., Kim, Y. W., Hwang, I., Kim, M. J., et al. (2005). Rice Undeveloped Tapetum1 is a major regulator of early tapetum development. *Plant Cell.* 17, 2705–2722. doi:10.1105/tpc.105.034090.

Kamiya, N., Itoh, J. I., Morikami, A., Nagato, Y., and Matsuoka, M. (2003). The SCARECROW gene's role in asymmetric cell divisions in rice plants. *Plant J.* 36, 45–54. doi:10.1046/j.1365-313X.2003.01856.x.

Kanaoka, M. M., Pillitteri, L. J., Fujii, H., Yoshida, Y., Bogenschutz, N. L., Takabayashi, J., et al. (2008). SCREAM/ICE1 and SCREAM2 specify three cell-state transitional steps leading to Arabidopsis stomatal differentiation. *Plant Cell* 20, 1775–1785. doi:10.1105/tpc.108.060848.

Kaneko, M., Inukai, Y., Ueguchi-Tanaka, M., Itoh, H., Izawa, T., Kobayashi, Y., et al.

(2004). Loss-of-Function Mutations of the Rice GAMYB Gene Impair α-Amylase Expression in Aleurone and Flower Development. *Plant Cell* 16, 33–44. doi:10.1105/tpc.017327.

Kawahara, Y., de la Bastide, M., Hamilton, J. P., Kanamori, H., Mccombie, W. R., Ouyang, S., et al. (2013). Improvement of the oryza sativa nipponbare reference genome using next generation sequence and optical map data. *Rice.* 6, 3–10. doi:10.1186/1939-8433-6-4.

Keijzer, C. J., Hoek, I. H. S., and Willeemse, M. T. M. (1987). the Processes of Anther Dehiscence and Pollen Dispersal III. the Dehydration of the Filament Tip and the Anther in Three Monocotyledonous Species. *New Phytol.* 106, 281–287. doi:10.1111/j.1469-8137.1987.tb00143.x.

Khatun, S., and Flowers, T. J. (1995). The estimation of pollen viability in rice. *J. Exp. Bot.* 46, 151–154. doi:10.1093/jxb/46.1.151.

Kim, D., Langmead, B., and Salzberg, S. L. (2015). HISAT: A fast spliced aligner with low memory requirements. *Nat. Methods.* 12, 357–360. doi:10.1038/nmeth.3317.

Kim, H., Hwang, H., Hong, J.-W., Lee, Y.-N., Ahn, I. P., Yoon, I. S., et al. (2012). A rice orthologue of the ABA receptor, OsPYL/RCAR5, is a positive regulator of the ABA signal transduction pathway in seed germination and early seedling growth. *J. Exp. Bot.* 63, 1013–1024. doi:10.1093/jxb/err338.

Kim, S. H., Woo, O. G., Jang, H., and Lee, J. H. (2018). Characterization and comparative expression analysis of CUL1 genes in rice. *Genes and Genomics.* 40, 233–241. doi:10.1007/s13258-017-0622-8.

Ko, S.-S., Li, M.-J., Lin, Y.-J., Hsing, H.-X., Yang, T.-T., Chen, T.-K., et al. (2017). Tightly Controlled Expression of bHLH142 Is Essential for Timely Tapetal Programmed Cell Death and Pollen Development in Rice. *Front. Plant Sci.* 8, 1258. doi:10.3389/fpls.2017.01258.

Kostaki, K. I., Coupel-Ledru, A., Bonnell, V. C., Gustavsson, M., Sun, P., McLaughlin, F. J., et al. (2020). Guard cells integrate light and temperature signals to control stomatal aperture. *Plant Physiol.* 182, 1404–1419. doi:10.1104/PP.19.01528.

Kumar Jewaria, P., Hara, T., Tanaka, H., Kondo, T., Betsuyaku, S., Sawa, S., et al. (2013). Differential Effects of the Peptides Stomagen, EPF1 and EPF2 on Activation of MAP Kinase MPK6 and the SPCH Protein Level. *Plant Cell Physiol.* 54, 1253–1262. doi:10.1093/pcp/pct076.

Kusumi, K., Hirotsuka, S., Kumamaru, T., and Iba, K. (2012). Increased leaf photosynthesis caused by elevated stomatal conductance in a rice mutant deficient in SLAC1, a guard cell anion channel protein. *J. Exp. Bot.* 63, 5635–5644. doi:10.1093/jxb/ers216.

Lake, J. A., Quick, W. P., Beerling, D. J., and Woodward, F. I. (2001). Plant development: Signals from mature to new leaves. *Nature* 411, 154–154. doi:10.1038/35075660.

Lampard, G. R., MacAlister, C. A., and Bergmann, D. C. (2008). Arabidopsis stomatal initiation is controlled by MAPK-mediated regulation of the bHLH SPEECHLESS. *Science* 322, 1113–1116. doi:10.1126/science.1162263.

Lawson, T., and Matthews, J. (2020). Guard Cell Metabolism and Stomatal Function. *Annu. Rev. Plant Biol.* 71, 273–302. doi:10.1146/annurev-arplant-050718-100251.

Lee, J. S., Hnilova, M., Maes, M., Lin, Y. C. L., Putarjunan, A., Han, S. K., et al. (2015). Competitive binding of antagonistic peptides fine-tunes stomatal patterning. *Nature* 522, 439–443. doi:10.1038/nature14561.

Lee, S. H., Sakuraba, Y., Lee, T., Kim, K. W., An, G., Lee, H. Y., et al. (2015). Mutation of Oryza sativa CORONATINE INSENSITIVE 1b (OsCOI1b) delays leaf senescence. *J. Integr. Plant Biol.* 57, 562–576. doi:10.1111/jipb.12276.

Lee, S., Jung, K. H., An, G., and Chung, Y. Y. (2004). Isolation and characterization of a rice cysteine protease gene, OsCP1, using T-DNA gene-trap system. *Plant Mol. Biol.* 54, 755–765. doi:10.1023/B:PLAN.0000040904.15329.29.

Lei, Q., Lee, E., Keerthisinghe, S., Lai, L., Li, M., Lucas, J. R., et al. (2015). The FOUR LIPS and MYB88 transcription factor genes are widely expressed in Arabidopsis thaliana during development. *Am. J. Bot*. 102, 1521–1528. doi:10.3732/ajb.1500056.

Li, C., Shen, H., Wang, T., and Wang, X. (2015). ABA Regulates Subcellular Redistribution of OsABI-LIKE2, a Negative Regulator in ABA Signaling, to Control Root Architecture and Drought Resistance in Oryza sativa. *Plant Cell Physiol*. 56, 2396–2408. doi:10.1093/pcp/pcv154.

Li, H., Handsaker, B., Wysoker, A., Fennell, T., Ruan, J., Homer, N., et al. (2009). The Sequence Alignment/Map format and SAMtools. *Bioinformatics.* 25, 2078–2079. doi:10.1093/bioinformatics/btp352.

Li, H., Pinot, F., Sauveplane, V., Werck-Reichhart, D., Diehl, P., Schreiber, L., et al. (2010). Cytochrome P450 family member CYP704B2 catalyzes the v-hydroxylation of fatty acids and is required for anther cutin biosynthesis and pollen exine formation in rice. *Plant Cell.* 22, 173–190. doi:10.1105/tpc.109.070326.

Li, H., Yuan, Z., Vizcay-Barrena, G., Yang, C., Liang, W., Zong, J., et al. (2011). PERSISTENT TAPETAL CELL1 encodes a PHD-finger protein that is required for tapetal cell death and pollen development in rice. *Plant Physiol.* 156, 615–630. doi:10.1104/pp.111.175760.

Li, N., Zhang, D. S., Liu, H. S., Yin, C. S., Li, X. X., Liang, W. Q., et al. (2006). The rice tapetum degeneration retardation gene is required for tapetum degradation and anther development. *Plant Cell.* 18, 2999–3014. doi:10.1105/tpc.106.044107.

Lian, H. L., Yu, X., Lane, D., Sun, W. N., Tang, Z. C., and Su, W. A. (2006). Upland rice and lowland rice exhibited different PIP expression under water deficit and ABA treatment. *Cell Res.* 16, 651–660. doi:10.1038/sj.cr.7310068.

Liao, Y., Bai, Q., Xu, P., Wu, T., Guo, D., Peng, Y., et al. (2018). Mutation in rice abscisic

acid2 results in cell death, enhanced disease-resistance, altered seed dormancy and development. *Front. Plant Sci.* 9, 405. doi:10.3389/fpls.2018.00405.

Liao, Y., Smyth, G. K., and Shi, W. (2014). FeatureCounts: An efficient general purpose program for assigning sequence reads to genomic features. *Bioinformatics.* 30, 923–930. doi:10.1093/bioinformatics/btt656.

Lin, H., Yu, J., Pearce, S. P., Zhang, D., and Wilson, Z. A. (2017). RiceAntherNet: a gene co‑expression network for identifying anther and pollen development genes. *Plant J.* 92, 1076‑1091. doi:10.1111/tpj.13744.

Liu, T., Ohashi-Ito, K., and Bergmann, D. C. (2009). Orthologs of Arabidopsis thaliana stomatal bHLH genes and regulation of stomatal development in grasses. *Development* 136, 2265–2276. doi:10.1242/dev.032938.

Liu, Y., Qin, L., Han, L., Xiang, Y., and Zhao, D. (2015). Overexpression of maize SDD1 (ZmSDD1) improves drought resistance in Zea mays L. by reducing stomatal density. *Plant Cell. Tissue Organ Cult.* 122, 147–159. doi:10.1007/s11240-015-0757-8.

Lobell, D. B., and Field, C. B. (2007). Global scale climate–crop yield relationships and the impacts of recent warming. *Environ. Res. Lett.* 2, 014002. doi:10.1088/1748-9326/2/1/014002.

Lobell, D. B., Schlenker, W., and Costa-Roberts, J. (2011). Climate trends and global crop production since 1980. *Science* 333, 616–620. doi:10.1126/science.1204531.

Lobell, D., Burke, M., Tebaldi, C., Mastrandrea, M., Falcon, W., and Naylor, R. (2008). Needs for Food Security in 2030. *Science* 319, 607–610. doi:10.1126/science.1152339.

Love, M. I., Huber, W., and Anders, S. (2014). Moderated estimation of fold change and dispersion for RNA-seq data with DESeq2. *Genome Biol.* 15, 550. doi:10.1186/s13059-014-0550-8.

Lu, J., He, J., Zhou, X., Zhong, J., Li, J., and Liang, Y.-K. (2019). Homologous genes of epidermal patterning factor regulate stomatal development in rice. *J. Plant Physiol.* 234–235, 18–27. doi:10.1016/j.jplph.2019.01.010.

Lugassi, N., Kelly, G., Arad, T., Farkash, C., Yaniv, Y., Yeselson, Y., et al. (2020). Expression of Hexokinase in Stomata of Citrus Fruit Reduces Fruit Transpiration and Affects Seed Development. *Front. Plant Sci.* 11, 255. doi:10.3389/fpls.2020.00255.

Lundgren, M. R., Mathers, A., Baillie, A. L., Dunn, J., Wilson, M. J., Hunt, L., et al. (2019). Mesophyll porosity is modulated by the presence of functional stomata. *Nat. Commun.* 10, 2825. doi:10.1038/s41467-019-10826-5.

MacAlister, C. A., Ohashi-Ito, K., and Bergmann, D. C. (2007). Transcription factor control of asymmetric cell divisions that establish the stomatal lineage. *Nature.* 445, 537–540. doi:10.1038/nature05491.

Mackill, D. J., and Khush, G. S. (2018). IR64: a high-quality and high-yielding mega variety. *Rice.* 11:18. doi:10.1186/s12284-018-0208-3.

Magori, S., and Citovsky, V. (2011). Hijacking of the host SCF ubiquitin ligase machinery by plant pathogens. *Front. Plant Sci.* 2, 87. doi:10.3389/fpls.2011.00087.

Manigbas, N. L., Lambio, L. A. F., Madrid, L. B., and Cardenas, C. C. (2014). Germplasm innovation of heat tolerance in rice for irrigated lowland conditions in the philippines. *Rice Sci.* 21, 162–169. doi:10.1016/S1672-6308(13)60180-8.

Mathew, L., Shai, G. L. I., and Vidyanagax, V. (1981). Structure and ontogeny of stomata on the vegetafive and floral organs in nine species of Verbena. *Proc. Indian Acad. Sci.* (Plant Sci.) 90, 485–497.

Matsuda, S., Takano, S., Sato, M., Furukawa, K., Nagasawa, H., Yoshikawa, S., et al. (2016). Rice Stomatal Closure Requires Guard Cell Plasma Membrane ATP-Binding Cassette Transporter RCN1/OsABCG5. *Mol. Plant.* 9, 417–427. doi:10.1016/j.molp.2015.12.007.

Matsui, T. (1999). Rapid swelling of pollen grains in response to floret opening unfolds anther locules in rice (Oryza sativa L.). *Plant Prod. Sci.* 2, 196–199. doi:10.1626/pps.2.196.

Matsui, T., and Hasegawa, T. (2019). Effect of long anther dehiscence on seed set at high temperatures during flowering in rice (Oryza sativa L.). *Sci. Rep.* 9, 1–8. doi:10.1038/s41598-019-56792-2.

Matsui, T., Kobayasi, K., Yoshimoto, M., and Hasegawa, T. (2007). Stability of Rice Pollination in The Field Under Hot And Dry Conditions in The Riverina Region of New South Wales, Australia. *Plant Prod. Sci.* 10, 57–63. doi:10.1626/pps.10.57.

Matsui, T., Omasa, K., and Horie, T. (1999). Mechanism of anther dehiscence in rice (Oryza sativa L.). *Ann. Bot.* 84, 501–506. doi:10.1006/anbo.1999.0943.

Matsui, T., Omasa, K., and Horie, T. (2000). High Temperature at Flowering Inhibits Swelling of Pollen Grains, a Driving Force for Thecae Dehiscence in Rice (Oryza sativa L.). *Plant Prod. Sci.* 3, 430–434. doi:10.1626/pps.3.430.

Matsui, T., and Osama, K. (2002). Rice (Oryza sativa L .) Cultivars Tolerant to High Temperature at Flowering : Anther Characteristics. *Ann. Bot.,* 683–687. doi:https://doi.org/10.1093/aob/mcf112.

Matthews, J. S., Vialet-Chabrand, S., Lawson, T., and Evans, J. (2020). Role of blue and red light in stomatal dynamic behaviour. *J. Exp. Bot.* 71, 2253–2269. doi:10.1093/jxb/erz563.

Mazzucotelli, E., Belloni, S., Marone, D., De Leonardis, A., Guerra, D., Di Fonzo, N., et al. (2006). The E3 Ubiquitin Ligase Gene Family in Plants: Regulation by Degradation. *Curr. Genomics.* 7, 509–522. doi:10.2174/138920206779315728.

Medina, S., Vicente, R., Nieto-Taladriz, M. T., Aparicio, N., Chairi, F., Vergara-Diaz, O., et al. (2019). The plant-transpiration response to vapor pressure deficit (VPD) in

durum wheat is associated with differential yield performance and specific expression of genes involved in primary metabolism and water transport. *Front. Plant Sci.* 9, 1994. doi:10.3389/fpls.2018.01994.

McElwain, J. C., Yiotis, C., and Lawson, T. (2016). Using modern plant trait relationships between observed and theoretical maximum stomatal conductance and vein density to examine patterns of plant macroevolution. *New Phytol.* 209, 94–103. doi:10.1111/nph.13579.

McKown, K. H., and Bergmann, D. C. (2020). Stomatal development in the grasses: lessons from models and crops (and crop models). *New Phytol.*, nph.16450. doi:10.1111/nph.16450.

Meinzer, F. C. (1993). Stomatal control of transpiration. *Trends Ecol. Evol.* 8, 289–294. doi:10.1016/0169-5347(93)90257-P.

Meng, X., Chen, X., Mang, H., Liu, C., Yu, X., Gao, X., et al. (2015). Differential Function of Arabidopsis SERK Family Receptor-like Kinases in Stomatal Patterning. *Curr. Biol.* 25, 2361–2372. doi:10.1016/j.cub.2015.07.068.

Miao, C., Xiao, L., Hua, K., Zou, C., Zhao, Y., Bressan, R. A., et al. (2018). Mutations in a subfamily of abscisic acid receptor genes promote rice growth and productivity. *Proc. Natl. Acad. Sci. U. S. A.* 115, 6058–6063. doi:10.1073/pnas.1804774115.

Min, M. K., Choi, E. H., Kim, J. A., Yoon, I. S., Han, S., Lee, Y., et al. (2019). Two Clade A Phosphatase 2Cs Expressed in Guard Cells Physically Interact With Abscisic Acid Signaling Components to Induce Stomatal Closure in Rice. *Rice* 12, 37. doi:10.1186/s12284-019-0297-7.

Mohammed, U., Caine, R. S., Atkinson, J. A., Harrison, E. L., Wells, D., Chater, C. C., et al. (2019). Rice plants overexpressing OsEPF1 show reduced stomatal density and increased root cortical aerenchyma formation. *Sci. Rep.* 9, 1–13. doi:10.1038/s41598-019-41922-7.

Molero, G., and Reynolds, M. P. (2020). Spike photosynthesis measured at high throughput indicates genetic variation independent of flag leaf photosynthesis. *F. Crop. Res.* 255, 107866. doi:10.1016/j.fcr.2020.107866.

Mohanty S., Wassmann R., Nelson A., Moya P., and Jagadish S.V.K. (2013). Rice and climate change: significance for food security and vulnerability. *IRRI Discussion Paper Series.* No. 49. Los Baños (Philippines): International Rice Research Institute. 14 p.

Nadeau, J. A., and Sack, F. D. (2002). Control of stomatal distribution on the Arabidopsis leaf surface. *Science.* 296, 1697–1700. doi:10.1126/science.1069596.

Nelson, M. R., Band, L. R., Dyson, R. J., Lessinnes, T., Wells, D. M., Yang, C., et al. (2012). A biomechanical model of anther opening reveals the roles of dehydration and secondary thickening. *New Phytol.* 196, 1030–1037. doi:10.1111/j.1469-8137.2012.04329.x.

Nguyen, T. H., Huang, S., Meynard, D., Chaine, C., Michel, R., Roelfsema, M. R. G., et

al. (2017). A dual role for the OsK5.2 ion channel in stomatal movements and k+ loading into Xylem Sap. *Plant Physiol.* 174, 2409–2418. doi:10.1104/pp.17.00691.

Nonomura, K. I., Miyoshi, K., Eiguchi, M., Suzuki, T., Miyao, A., Hirochika, H., et al. (2003). The MSP1 gene is necessary to restrict the number of cells entering into male and female sporogenesis and to initiate anther wall formation in rice. *Plant Cell.* 15, 1728–1739. doi:10.1105/tpc.012401.

Nonomura, K. I., Morohoshi, A., Nakano, M., Eiguchi, M., Miyao, A., Hirochika, H., et al. (2007). A germ cell-specific gene of the ARGONAUTE family is essential for the progression of premeiotic mitosis and meiosis during sporogenesis in rice. *Plant Cell.* 19, 2583–2594. doi:10.1105/tpc.107.053199.

Nonomura, K. I., Nakano, M., Eiguchi, M., Suzuki, T., and Kurata, N. (2006). PAIR2 is essential for homologous chromosome synapsis in rice meiosis I. *J. Cell Sci.* 119, 217–225. doi:10.1242/jcs.02736.

Nonomura, K. I., Nakano, M., Fukuda, T., Eiguchi, M., Miyao, A., Hirochika, H., et al. (2004). The novel gene Homologous Pairing Aberration In Rice Meiosis1 of rice encodes a putative coiled-coil protein required for homologous chromosome pairing in meiosis. *Plant Cell* 16, 1008–1020. doi:10.1105/tpc.020701.

Nunes, T. D. G., Zhang, D., and Raissig, M. T. (2019). Form, development and function of grass stomata. *Plant J.*, tpj.14552. doi:10.1111/tpj.14552.

Ohashi-Ito, K., and Bergmann, D. C. (2006). Arabidopsis FAMA controls the final proliferation/differentiation switch during stomatal development. *Plant Cell* 18, 2493–2505. doi:10.1105/tpc.106.046136.

Okonechnikov, K., Conesa, A., and García-Alcalde, F. (2016). Qualimap 2: Advanced multi-sample quality control for high-throughput sequencing data. *Bioinformatics.* 32, 292–294. doi:10.1093/bioinformatics/btv566.

Oliver, S. N., Dennis, E. S., and Dolferus, R. (2007). ABA Regulates Apoplastic Sugar Transport and is a Potential Signal for Cold-Induced Pollen Sterility in Rice. *Plant Cell Physiol.* 48, 1319–1330. doi:10.1093/pcp/pcm100.

Ono, S., Liu, H., Tsuda, K., Fukai, E., Tanaka, K., Sasaki, T., et al. (2018). EAT1 transcription factor, a non-cell-autonomous regulator of pollen production, activates meiotic small RNA biogenesis in rice anther tapetum. *PLoS Genet.* 14. doi:10.1371/journal.pgen.1007238.

Pantin, F., Renaud, J., Barbier, F., Vavasseur, A., Le Thiec, D., Rose, C., et al. (2013). Developmental priming of stomatal sensitivity to abscisic acid by leaf microclimate. *Curr. Biol.* 23, 1805–1811. doi:10.1016/j.cub.2013.07.050.

Patiño, S., and Grace, J. (2002a). The cooling of convolvulaceous flowers in a tropical environment. *Plant. Cell Environ.* 25, 41–51. doi:10.1046/j.0016-8025.2001.00801.x.

Peng, S., Huang, J., Sheehy, J. E., Laza, R. C., Visperas, R. M., Zhong, X., et al. (2004).

Rice yields decline with higher night temperature from global warming. *Proc. Natl. Acad. Sci.* 101, 9971–9975. doi:10.1073/pnas.0403720101.

Peterson, K. M., Rychel, A. L., and Torii, K. U. (2010). Out of the mouths of plants: The molecular basis of the evolution and diversity of stomatal development. *Plant Cell.* 22, 296–306. doi:10.1105/tpc.109.072777.

Pfaffl, M. W. (2001). A new mathematical model for relative quantification in real-time RT-PCR. *Nucleic Acids Res.* 29, 45e – 45. doi:10.1093/nar/29.9.e45.

Pillitteri, L. J., Bemis, S. M., Shpak, E. D., and Torii, K. U. (2007). Haploinsufficiency after successive loss of signaling reveals a role for ERECTA-family genes in Arabidopsis ovule development. *Development* 134, 3099–3109. doi:10.1242/dev.004788.

Pillitteri, L. J., and Dong, J. (2013). Stomatal development in Arabidopsis. *Arab. B.* 11, e0162. doi:10.1199/tab.0162.

Pillitteri, L. J., Sloan, D. B., Bogenschutz, N. L., and Torii, K. U. (2007). Termination of asymmetric cell division and differentiation of stomata. *Nature* 445, 501–505. doi:10.1038/nature05467.

Qu, X., Peterson, K. M., and Torii, K. U. (2017). Stomatal development in time: the past and the future. *Curr. Opin. Genet. Dev.* 45, 1–9. doi:10.1016/j.gde.2017.02.001.

Qu, X., Yan, M., Zou, J., Jiang, M., Yang, K., and Le, J. (2018). A2-type cyclin is required for the asymmetric entry division in rice stomatal development. *J. Exp. Bot.* 69, 3587–3599. doi:10.1093/jxb/ery158.

Raissig, M. T., Abrash, E., Bettadapur, A., Vogel, J. P., and Bergmann, D. C. (2016). Grasses use an alternatively wired bHLH transcription factor network to establish stomatal identity. *Proc. Natl. Acad. Sci.* 113, 8326–8331. doi:10.1073/pnas.1606728113.

Raissig, M. T., Matos, J. L., Gil, M. X. A., Kornfeld, A., Bettadapur, A., Abrash, E., et al. (2017). Mobile MUTE specifies subsidiary cells to build physiologically improved grass stomata. *Science* 355, 1215–1218. doi:10.1126/science.aal3254.

Rang, Z. W., Jagadish, S. V. K., Zhou, Q. M., Craufurd, P. Q., and Heuer, S. (2011). Effect of high temperature and water stress on pollen germination and spikelet fertility in rice. *Environ. Exp. Bot.* 70, 58–65. doi:10.1016/j.envexpbot.2010.08.009.

Rao, A. N., Wani, S. P., Ramesha, M. S., and Ladha, J. K. (2017). "Rice Production Systems," in *Rice Production Worldwide*, eds. B. S. Chauhan, K. Jabran, and G. Mahajan (Springer, Cham), 185–205. doi:10.1007/978-3-319-47516-5.

Roddy, A. B., Brodersen, C. R., and Dawson, T. E. (2016). Hydraulic conductance and the maintenance of water balance in flowers. *Plant. Cell Environ.* 39, 2123–2132. doi:10.1111/pce.12761.

Rodriguez-Riano, T., and Dafni, A. (2000). A new procedure to asses pollen viability. *Sex. Plant Reprod.* 12, 241–244. doi:10.1007/s004970050008.

Rudall, P. J., Chen, E. D., and Cullen, E. (2017). Evolution and development of monocot stomata. *Am. J. Bot.* 104, 1122–1141. doi:10.3732/ajb.1700086.

Saichuk, J. (2009). *Louisiana Rice Production Handbook.* Louisiana State University Agricultural Center.

Sailaja, B., Subrahmanyam, D., Neelamraju, S., Vishnukiran, T., Rao, Y. V., Vijayalakshmi, P., et al. (2015). Integrated Physiological, Biochemical, and Molecular Analysis Identifies Important Traits and Mechanisms Associated with Differential Response of Rice Genotypes to Elevated Temperature. *Front. Plant Sci.* 6, 1044. doi:10.3389/fpls.2015.01044.

Sakai, H., Lee, S. S., Tanaka, T., Numa, H., Kim, J., Kawahara, Y., et al. (2013). Rice annotation project database (RAP-DB): An integrative and interactive database for rice genomics. *Plant Cell Physiol.* 54. doi:10.1093/pcp/pcs183.

Satake, T., and Yoshida, H. (1978). High Temperature-Induced Sterility in Indica Rices at Flowering. *Japanese J. Crop Sci.* 47, 6–17. doi:10.1626/jcs.47.6.

Schatz, M. C., Maron, L. G., Stein, J. C., Wences, A. H., Gurtowski, J., Biggers, E., et al. (2014). Whole genome de novo assemblies of three divergent strains of rice, Oryza sativa, document novel gene space of aus and indica. *Genome Biol.* 15, 506. doi:10.1186/s13059-014-0506-z.

Schuler, M. L., Sedelnikova, O. V, Walker, B. J., Westhoff, P., and Langdale, J. A. (2018). SHORTROOT-Mediated Increase in Stomatal Density Has No Impact on Photosynthetic Efficiency. *Plant Physiol.* 176, 757–772. doi:10.1104/pp.17.01005.

Serna, L. (2020). The Role of Grass MUTE Orthologues During Stomatal Development. *Front. Plant Sci.* 11, 55. doi:10.3389/fpls.2020.00055.

Shah, F., Huang, J., Cui, K., Nie, L., Shah, T., Chen, C., et al. (2011). Impact of high-temperature stress on rice plant and its traits related to tolerance. *J. Agric. Sci.* 149, 545–556. doi:10.1017/S0021859611000360.

Sheriff, D. W. (1984). Epidermal transpiration and stomatal responses to humidity: Some hypotheses explored. *Plant. Cell Environ.* 7, 669–677. doi:10.1111/1365-3040.ep11571796.

Shi, W., Li, X., Schmidt, R. C., Struik, P. C., Yin, X., and Jagadish, S. V. K. (2018). Pollen germination and in vivo fertilization in response to high-temperature during flowering in hybrid and inbred rice. *Plant Cell Environ.* 41, 1287–1297. doi:10.1111/pce.13146.

Shi, J., Cui, M., Yang, L., Kim, Y. J., and Zhang, D. (2015). Genetic and Biochemical Mechanisms of Pollen Wall Development. *Trends Plant Sci.* 20, 741–753. doi:10.1016/j.tplants.2015.07.010.

Shi, J., Tan, H., Yu, X. H., Liu, Y., Liang, W., Ranathunge, K., et al. (2011). Defective pollen wall is required for anther and microspore development in rice and encodes a fatty acyl carrier protein reductase. *Plant Cell.* 23, 2225–2246.

doi:10.1105/tpc.111.087528.

Shpak, E. D., McAbee, J. M., Pillitteri, L. J., and Torii, K. U. (2005). Plant science: Stomatal patterning and differentiation by synergistic interactions of receptor kinases. *Science*. 309, 290–293. doi:10.1126/science.1109710.

Stebbins, G. L., and Shah, S. S. (1960). Developmental studies of cell differentiation in the epidermis of monocotyledons. *Dev. Biol.* 2, 477–500. doi:10.1016/0012-1606(60)90050-6.

Streck, N. A. (2003). Stomatal Response To Water Vapor Pressure Deficit: an Unsolved Issue. *Rev. Bras. Agrociência* 9, 317–322. doi:10.18539/cast.v9i4.649.

Sugano, S. S., Shimada, T., Imai, Y., Okawa, K., Tamai, A., Mori, M., et al. (2010). Stomagen positively regulates stomatal density in Arabidopsis. *Nature* 463, 241–244. doi:10.1038/nature08682.

Sun, Y., Yan, F., Cui, X., and Liu, F. (2014). Plasticity in stomatal size and density of potato leaves under different irrigation and phosphorus regimes. *J. Plant Physiol.* 171, 1248–1255. doi:10.1016/J.JPLPH.2014.06.002.

Supek, F., Bošnjak, M., Škunca, N., and Šmuc, T. (2011). Revigo summarizes and visualizes long lists of gene ontology terms. *PLoS One*. 6, e21800. doi:10.1371/journal.pone.0021800.

Sutimantanapi, D., Pater, D., and Smith, L. G. (2014). Divergent roles for maize PAN1 and PAN2 receptor-like proteins in cytokinesis and cell morphogenesis. Plant *Physiol*. 164, 1905–17. doi:10.1104/pp.113.232660.

Taiz L, Zeiger E. 2010. Plant physiology. 5th edn. Sunderland, MA: Sinauer Associates, Inc., Publishers.

Tanaka, Y., Sugano, S. S., Shimada, T., and Hara-Nishimura, I. (2013). Enhancement of leaf photosynthetic capacity through increased stomatal density in Arabidopsis. *New Phytol.* 198, 757–764. doi:10.1111/nph.12186.

Tang, R. S., Zheng, J. C., Jin, Z. Q., Zhang, D. D., Huang, Y. H., and Chen, L. G. (2008). Possible correlation between high temperature-induced floret sterility and endogenous levels of IAA, GAs and ABA in rice (Oryza sativa L.). *Plant Growth Regul*. 54, 37–43. doi:10.1007/s10725-007-9225-8.

Teare, I. D., Law, A. G., and Simmons, G. F. (1972). Stomatal frequency and distribution on the inflorescence of Triticum aestivum. *Can. J. Plant Sci.* 52, 89–94. doi:10.4141/cjps72-011.

Teixeira, E. I., Fischer, G., van Velthuizen, H., Walter, C., and Ewert, F. (2013). Global hot-spots of heat stress on agricultural crops due to climate change. *Agric. For. Meteorol.* 170, 206–215. doi:10.1016/j.agrformet.2011.09.002.

Thangasamy, S., Guo, C.-L., Chuang, M.-H., Lai, M.-H., Chen, J., and Jauh, G.-Y. (2011). Rice SIZ1, a SUMO E3 ligase, controls spikelet fertility through regulation of anther dehiscence. *New Phytol*. 189, 869–882. doi:10.1111/j.1469-

8137.2010.03538.x.

Toda, Y., Wang, Y., Takahashi, A., Kawai, Y., Tada, Y., Yamaji, N., et al. (2016). Oryza sativa H+-ATPase (OSA) is Involved in the Regulation of Dumbbell-Shaped Guard Cells of Rice. *Plant Cell Physiol.* 57, 1220–1230. doi:10.1093/pcp/pcw070.

Tsuchiya, T., Toriyama, K., Ejiri, S. ichiro, and Hinata, K. (1994). Molecular characterization of rice genes specifically expressed in the anther tapetum. Plant *Mol. Biol.* 26, 1737–1746. doi:10.1007/BF00019488.

Urban, J., Ingwers, M. W., McGuire, M. A., and Teskey, R. O. (2017). Increase in leaf temperature opens stomata and decouples net photosynthesis from stomatal conductance in Pinus taeda and Populus deltoides x nigra. *J. Exp. Bot.* 68, 1757–1767. doi:10.1093/jxb/erx052.

van Campen, J. C., Yaapar, M. N., Narawatthana, S., Lehmeier, C., Wanchana, S., Thakur, V., et al. (2016). Combined Chlorophyll Fluorescence and Transcriptomic Analysis Identifies the P3/P4 Transition as a Key Stage in Rice Leaf Photosynthetic Development. *Plant Physiol.* 170, 1655–74. doi:10.1104/pp.15.01624.

Vierstra, R. D. (2009). The ubiquitin-26S proteasome system at the nexus of plant biology. *Nat. Rev. Mol. Cell Biol.* 10, 385–397. doi:10.1038/nrm2688.

Wahid, A., Gelani, S., Ashraf, M., and Foolad, M. R. (2007). Heat tolerance in plants: An overview. *Environ. Exp. Bot.* 61, 199–223. doi:10.1016/j.envexpbot.2007.05.011.

Wang, A., Xia, Q., Xie, W., Datla, R., and Selvaraj, G. (2003). The classical Ubisch bodies carry a sporophytically produced structural protein (RAFTIN) that is essential for pollen development. *Proc. Natl. Acad. Sci. U. S. A.* 100, 14487–14492. doi:10.1073/pnas.2231254100.

Wang, W., Mauleon, R., Hu, Z., Chebotarov, D., Tai, S., Wu, Z., et al. (2018). Genomic variation in 3,010 diverse accessions of Asian cultivated rice. *Nature.* 557, 43–49. doi:10.1038/s41586-018-0063-9.

Wang, Y., and Li, J. (2005). The plant architecture of rice (Oryza sativa). *Plant Mol. Biol.* 59, 75–84. doi:10.1007/s11103-004-4038-x.

Wang, Y., and Li, J. (2011). Branching in rice. *Curr. Opin. Plant Biol.* 14, 94–99. doi:10.1016/j.pbi.2010.11.002.

Wassmann, R., Jagadish, S. V. K., Heuer, S., Ismail, A., Redona, E., Serraj, R., et al. (2009). "Climate Change Affecting Rice Production. The Physiological and Agronomic Basis for Possible Adaptation Strategies" in *Advances in Agronomy* (Elsevier Inc.), 59–122. doi:10.1016/S0065-2113(08)00802-X.

Watson, L. (1962). The Taxonomic Significance of Stomatal Distribution and Morphology in Epacridaceae. *New Phytol.* 61, 36–40.

Weerakoon, W. M. W., Maruyama, A., and Ohba, K. (2008). Impact of Humidity on Temperature-Induced Grain Sterility in Rice (Oryza sativa L). *J. Agron. Crop Sci.* 194, 135–140. doi:10.1111/j.1439-037X.2008.00293.x.

Wei, D., Liu, M., Chen, H., Zheng, Y., Liu, Y., Wang, X., et al. (2018). INDUCER OF CBF EXPRESSION 1 is a male fertility regulator impacting anther dehydration in Arabidopsis. *PLOS Genet.* 14, e1007695. doi:10.1371/journal.pgen.1007695.

Wei, S., Hu, W., Deng, X., Zhang, Y., Liu, X., Zhao, X., et al. (2014). A rice calcium-dependent protein kinase OsCPK9 positively regulates drought stress tolerance and spikelet fertility. *BMC Plant Biol.* 14, 133. doi:10.1186/1471-2229-14-133.

Wilson, Z. A., Song, J., Taylor, B., and Yang, C. (2011). The final split: The regulation of anther dehiscence. *J. Exp. Bot.* 62, 1633–1649. doi:10.1093/jxb/err014.

Woodward, F. I. (1987). Stomatal numbers are sensitive to increases in CO2 from pre-industrial levels. *Nature* 327, 617–618. doi:10.1038/327617a0.

Woolfenden, H. C., Baillie, A. L., Gray, J. E., Hobbs, J. K., Morris, R. J., and Fleming, A. J. (2018). Models and Mechanisms of Stomatal Mechanics. *Trends Plant Sci.* 23, 822–832. doi:10.1016/j.tplants.2018.06.003.

Wu, C., Cui, K., Hu, Q., Wang, W., Nie, L., Huang, J., et al. (2019a). Enclosed stigma contributes to higher spikelet fertility for rice (Oryza sativa L.) subjected to heat stress. *Crop J.* 7, 335–349. doi:10.1016/j.cj.2018.11.011.

Wu, C., Tang, S., Li, G., Wang, S., Fahad, S., and Ding, Y. (2019b). Roles of phytohormone changes in the grain yield of rice plants exposed to heat: a review. *PeerJ.* 7, e7792. doi:10.7717/peerj.7792.

Wu, L., Guan, Y., Wu, Z., Yang, K., Lv, J., Converse, R., et al. (2014). OsABCG15 encodes a membrane protein that plays an important role in anther cuticle and pollen exine formation in rice. *Plant Cell Rep.* 33, 1881–1899. doi:10.1007/s00299-014-1666-8.

Wu, Z., Chen, L., Yu, Q., Zhou, W., Gou, X., Li, J., et al. (2019b). Multiple transcriptional factors control stomata development in rice. *New Phytol.* 223, 220–232. doi:10.1111/nph.15766.

Xu, M., Zhu, L., Shou, H., and Wu, P. (2005). A PIN1 family gene, OsPIN1, involved in auxin-dependent adventitious root emergence and tillering in rice. *Plant Cell Physiol.* 46, 1674–1681. doi:10.1093/pcp/pci183.

Yang, D., Peng, S., and Wang, F. (2020). Response of Photosynthesis to High Growth Temperature Was Not Related to Leaf Anatomy Plasticity in Rice (Oryza sativa L.). *Front. Plant Sci.* 11, 1. doi:10.3389/fpls.2020.00026.

Yang, X., Wu, D., Shi, J., He, Y., Pinot, F., Grausem, B., et al. (2014). Rice CYP703A3, a cytochrome P450 hydroxylase, is essential for development of anther cuticle and pollen exine. *J. Integr. Plant Biol.* 56, 979–994. doi:10.1111/jipb.12212.

Yeh, S.-Y., Chen, H.-W., Ng, C.-Y., Lin, C.-Y., Tseng, T.-H., Li, W.-H., et al. (2015). Down-Regulation of Cytokinin Oxidase 2 Expression Increases Tiller Number and Improves Rice Yield. *Rice.* 8, 36. doi:10.1186/s12284-015-0070-5.

Yi, H., Chen, Y., Wang, J. Z., Puri, V. M., and Anderson, C. T. (2019). The stomatal

flexoskeleton: how the biomechanics of guard cell walls animate an elastic pressure vessel. J. Exp. Bot. 70, 3561–3572. doi:10.1093/jxb/erz178.

Yin, X., Biswal, A. K., Dionora, J., Perdigon, K. M., Balahadia, C. P., Mazumdar, S., et al. (2017). CRISPR-Cas9 and CRISPR-Cpf1 mediated targeting of a stomatal developmental gene EPFL9 in rice. *Plant. Cell. Rep.* 36, 745–757. doi:10.1007/s00299-017-2118-z.

Yu, G., Wang, L. G., Han, Y., and He, Q. Y. (2012). ClusterProfiler: An R package for comparing biological themes among gene clusters. *Omi. A J. Integr. Biol.* 16, 284–287. doi:10.1089/omi.2011.0118.

Yu, J., Meng, Z., Liang, W., Behera, S., Kudla, J., Tucker, M. R., et al. (2016). A rice Ca2+ binding protein is required for tapetum function and pollen formation. *Plant Physiol.* 172, 1772–1786. doi:10.1104/pp.16.01261.

Yuan, W., Li, X., Chang, Y., Wen, R., Chen, G., Zhang, Q., et al. (2009). Mutation of the rice gene PAIR3 results in lack of bivalent formation in meiosis. *Plant J.* 59, 303–315. doi:10.1111/j.1365-313X.2009.03870.x.

Yoshida, S. (1981). Fundamentals of Rice Crop Science. Manila, Philippines: The International Rice Research Institute.

Yoshida, H., and Nagato, Y. (2011). Flower development in rice. *J. Exp. Bot.* 62, 4719–4730. doi:10.1093/jxb/err272.

Zhang, C., Li, G., Chen, T., Feng, B., Fu, W., Yan, J., et al. (2018). Heat stress induces spikelet sterility in rice at anthesis through inhibition of pollen tube elongation interfering with auxin homeostasis in pollinated pistils. *Rice*. 11, 14. doi:10.1186/s12284-018-0206-5.

Zhang, F.P., Carins Murphy, M. R., Cardoso, A. A., Jordan, G. J., and Brodribb, T. J. (2018). Similar geometric rules govern the distribution of veins and stomata in petals, sepals and leaves. *New Phytol.* 219, 1224–1234. doi:10.1111/nph.15210.

Zhang, D. B., and Wilson, Z. A. (2009). Stamen specification and anther development in rice. *Chinese Sci. Bull.* 54, 2342–2353. doi:10.1007/s11434-009-0348-3.

Zhang, D., Liang, W., Yin, C., Zong, J., Gu, F., and Zhang, D. (2010). OsC6, encoding a lipid transfer protein, is required for postmeiotic anther development in rice. *Plant Physiol.* 154, 149–162. doi:10.1104/pp.110.158865.

Zhang, D. S., Liang, W. Q., Yuan, Z., Li, N., Shi, J., Wang, J., et al. (2008). Tapetum degeneration retardation is critical for aliphatic metabolism and gene regulation during rice pollen development. *Mol. Plant.* 1, 599–610. doi:10.1093/mp/ssn028.

Zhang, D., Luo, X., and Zhu, L. (2011). Cytological analysis and genetic control of rice anther development. *J. Genet. Genomics*. 38, 379–390. doi:10.1016/j.jgg.2011.08.001.

Zhang, X., Li, J., Liu, A., Zou, J., Zhou, X., Xiang, J., et al. (2012). Expression Profile in Rice Panicle: Insights into Heat Response Mechanism at Reproductive Stage. *PLoS*

One. 7. doi:10.1371/journal.pone.0049652.

Zhao, X., De Palma, J., Oane, R., Gamuyao, R., Luo, M., Chaudhury, A., et al. (2008). OsTDL1A binds to the LRR domain of rice receptor kinase MSP1, and is required to limit sporocyte numbers. *Plant J.* 54, 375–387. doi:10.1111/j.1365-313X.2008.03426.x.

Zhao, C., Liu, B., Piao, S., Wang, X., Lobell, D. B., Huang, Y., et al. (2017). Temperature increase reduces global yields of major crops in four independent estimates. *Proc. Natl. Acad. Sci.* 114, 201701762. doi:10.1073/pnas.1701762114.

Zhao, C., Piao, S., Wang, X., Huang, Y., Ciais, P., Elliott, J., et al. (2016). Plausible rice yield losses under future climate warming. *Nat. Plants* 3. doi:10.1038/nplants.2016.202.

Zhou, S., Wang, Y., Li, W., Zhao, Z., Ren, Y., Wang, Y., et al. (2011). Pollen semi-sterility1 encodes a kinesin-1-like protein important for male meiosis, anther dehiscence, and fertility in rice. *Plant Cell.* 23, 111–129. doi:10.1105/tpc.109.073692.

Zhou, W., Wang, Y., Wu, Z., Luo, L., Liu, P., Yan, L., et al. (2016). Homologs of SCAR/WAVE complex components are required for epidermal cell morphogenesis in rice. J. Exp. Bot. 67, 4311–4323. doi:10.1093/jxb/erw214.

Zhu, Q. H., Ramm, K., Shivakkumar, R., Dennis, E. S., and Upadhyaya, N. M. (2004). The anther indehiscence1 gene encoding a single MYB domain protein is involved in anther development in rice. Plant Physiol. 135, 1514–1525. doi:10.1104/pp.104.041459.

Zinn, K. E., Tunc-Ozdemir, M., and Harper, J. F. (2010). Temperature stress and plant sexual reproduction: Uncovering the weakest links. *J. Exp. Bot.* 61, 1959–1968. doi:10.1093/jxb/erq053.

Zou, M., Guan, Y., Ren, H., Zhang, F., and Chen, F. (2008). A bZIP transcription factor, OsABI5, is involved in rice fertility and stress tolerance. *Plant Mol. Biol.* 66, 675–683. doi:10.1007/s11103-008-9298-4.

Zoulias, N., Harrison, E. L., Casson, S. A., and Gray, J. E. (2018). Molecular control of stomatal development. *Biochem. J.* 475, 441–454. doi:10.1042/BCJ20170413.

Appendix

Table A1. Summary of RNA-seq reads processing.

Sample Name	Stage	Million pairs (raw data)	Million pairs (after trimming)	Overall alignment rate	Uniquely mapped pairs
S1-1_IR64	1	55.2	53.6	94.17%	86.20%
S1-2_IR64	1	35.8	34.8	95.84%	88.55%
S1-3_IR64	1	33.1	31.7	95.99%	87.88%
S2-1_IR64	2	32.6	31.2	96.11%	88.29%
S2-2_IR64	2	39.4	37.8	96.13%	88.39%
S2-3_IR64	2	58.9	56.5	96.15%	87.69%
S3-1_IR64	3	40.4	38.8	96.08%	89.13%
S3-2_IR64	3	32.8	31.5	96.17%	88.04%
S3-3_IR64	3	79.4	76.1	96.06%	88.49%
S4-1_IR64	4	39.7	38.6	95.94%	88.20%
S4-2_IR64	4	38.9	37.8	95.85%	87.85%
S4-3_IR64	4	43.2	42	95.93%	87.91%
S5-1_IR64	5	39	37.8	95.76%	88.24%
S5-2_IR64	5	39.6	38.4	95.56%	88.86%
S5-3_IR64	5	33.7	32.7	95.74%	89.01%
S1-1_OsEPF1-oe	1	40.1	39	95.59%	88.93%
S1-2_OsEPF1-oe	1	34.8	33.9	95.61%	88.47%
S1-3_OsEPF1-oe	1	38.4	37.3	95.65%	88.55%
S2-1_OsEPF1-oe	2	42.5	41.3	95.81%	88.91%
S2-2_OsEPF1-oe	2	36.6	35.5	95.71%	89.00%
S2-3_OsEPF1-oe	2	32.4	31.5	95.67%	88.94%
S3-1_OsEPF1-oe	3	37.4	35.8	96.07%	89.60%
S3-2_OsEPF1-oe	3	34.5	33.1	95.90%	89.62%
S3-3_OsEPF1-oe	3	33.9	32.5	95.92%	88.81%
S4-1_OsEPF1-oe	4	35.9	34.3	96.02%	88.78%
S4-2_OsEPF1-oe	4	36.1	34.5	95.95%	89.29%
S4-3_OsEPF1-oe	4	35.9	34.3	95.94%	89.66%
S5-1_OsEPF1-oe	5	36.2	34.5	95.75%	89.02%
S5-2_OsEPF1-oe	5	31.7	30.4	95.79%	89.58%
S5-3_OsEPF1-oe	5	41.1	39.3	95.74%	89.13%
Mat-1_IR64	Mature	32.6	31.2	96.10%	89.00%
Mat-2_IR64	Mature	31.5	30.2	96.23%	88.51%
Mat-3_IR64	Mature	37.2	35.6	96.00%	88.63%
Mat-1_OsEPF1-oe	Mature	45.8	43.8	95.97%	88.04%
Mat-2_OsEPF1-oe	Mature	38.4	36.8	95.94%	87.91%
Mat-3_OsEPF1-oe	Mature	42.6	40.7	95.96%	88.14%

The following tables list DEGs found in the differential expression analyses comparing OsEPF1-oe-S and IR64 florets.

Table A2. Genes associated with the 'SCF-dependent proteasomal ubiquitin-dependent catabolic protein process' GO term.

Rice gene id	Gene name	Cluster	Description (Ensembl)	p-adjusted (LRT)
Os07g0409500	*OSK21*	4	SKP1-like gene 21, BTB/POZ fold domain containing protein	2.69E-22
Os07g0625500	*OSK22*	5	SKP1-like gene 22, similar to Fimbriata-associated protein	1.14E-12
Os01g0369200	*OsCUL1-3*	8	Component of cullin-RING E3 ubiquitin ligase complex, salt/drought and cold stress response	3.81E-10
Os07g0625600	*OSK19*	4	SKP1-like gene 19, fimbriata-associated protein	1.73E-05
Os12g0594600	-	4	BTB/POZ fold domain containing protein	0.000120304
Os02g0281150	-	19	Similar to Leucine Rich Repeat family protein	0.001564606
Os07g0624900	*OSK17*	4	SKP1-like gene 17	0.00249673
Os10g0128600	*OsFbox518*	5	Cyclin-like F-box domain containing protein	0.017312152
Os07g0535700	-	17	F-box associated type 1 domain containing protein	0.022145894
Os12g0595600	-	4	Hypothetical conserved gene	0.026803288
Os10g0124700	*OsFbox508*	4	Cyclin-like F-box domain containing protein	0.033543052
Os05g0449500	*OsCOI1b*	5	Component of the SCF E3 ubiquitin ligase complex, jasmonate-regulated defense responses, regulation of leaf senescence	0.039451762
Os10g0148800	*OsF0711*	9	Similar to F-box domain containing protein	0.040870438

Table A3. Genes associated with the 'Hydrolase activity, acting on ester bonds' GO term.

Rice gene id	Gene name	Cluster	Description (Ensembl)	p-adjusted (LRT)
Os03g0310000	*OsGELP46*	8	Lipase, GDSL domain containing protein	4.71E-12
Os01g0331100	*OsGELP16*	5	Similar to Alpha-L-fucosidase 2	1.06E-09
Os01g0329900	*OsGELP14*	5	Similar to Lipase homolog (Fragment)	9.66E-07
Os02g0290900	*OsGELP34*	4	Similar to GDSL-motif lipase/hydrolase family protein	1.90E-06
Os04g0652700		5	Similar to Nuclease PA3	1.65E-05
Os06g0156600	*OsGELP77*	5	Lipase, GDSL domain containing protein	0.001824358
Os08g0112900	*OsGELP95*	5	Lipase, GDSL domain containing protein	0.002659045

Rice gene id	Gene name	Cluster	Description (Ensembl)	p-adjusted (LRT)
Os12g0126100		5	Similar to GDSL-like Lipase/Acylhydrolase family protein, expressed	0.003956792
Os02g0110000	*OsGELP30*	-	Lipase, GDSL domain containing protein	0.009227732
Os06g0635300		9	Similar to gastric triacylglycerol lipase	0.012669681
Os03g0859100	*OsGELP55*	5	Esterase, SGNH hydrolase-type domain containing protein	0.014512826

Table A4. Genes associated with the 'ATPase activity, coupled to transmembrane movement of substances' GO term.

Rice gene id	Gene name	Cluster	Description (Ensembl)	p-adjusted (LRT)
Os01g0533900	*OsABCB2*	11	Similar to Multidrug resistance protein 1 homolog	1.13E-10
Os02g0323000	*OsABCB10*	8	Similar to Felis catus multi-drug resistance related (Fragment)	1.10E-07
Os01g0609200	*OsABCG35*	10	Similar to Pleiotropic drug resistance protein 3	1.87E-05
Os05g0120200	*OsABCG11*	5	Similar to ATPase, coupled to transmembrane movement of substances	0.000185567
Os01g0911300	*OsABCB24*	-	Similar to Transporter associated with antigen processing-like protein	0.000219248
Os03g0157400	*OsABCG4*	22	ABC transporter-like domain containing protein	0.003000705
Os03g0281900	*ABCG5*	5	ATP-binding cassette (ABC) transporter, Hypodermal suberization of roots, Salt stress tolerance	0.007410936
Os06g0589300	*OsABCA2*	2	ABC transporter-like domain containing protein	0.015431687
Os08g0398300	*OsABCA4*	22	ABC transporter-like domain containing protein	0.020511507
Os02g0211000	*OsABCA1*	22	Conserved hypothetical protein	0.021021271

Table A5. Genes associated with the 'Meiotic cell cycle' GO term.

Rice gene id	Gene name	Cluster	Description (Ensembl)	p-adjusted (LRT)
Os11g0146800	*OsRILIM15B*	10	Meiosis-specific DNA recombinase, Synaptonemal complex (SC) assembly	1.34E-10
Os09g0506800	*OsPAIR2*	4	Similar to Meiotic asynaptic mutant 1	1.90E-06

Rice gene id	Gene name	Cluster	Description (Ensembl)	p-adjusted (LRT)
Os03g0225200	*OsSDS*	10	Cyclin, A/B/D/E domain containing protein	0.000462028
Os04g0452500	*OsZEP1*	4	Similar to H0505F09.1 protein	0.000472419
Os03g0106300	*OsPAIR1*	-	Coiled-coil protein, Homologous chromosome pairing in meiosis	0.004717358
Os05g0111000	*OsRPA1C*	16	Similar to Gag polyprotein [Contains: Core protein p15 (Matrix protein); Core protein p24; Core protein p12]	0.015281112
Os12g0143800	*OsDMC1A*	4	Meiosis-specific DNA recombinase, Synaptonemal complex (SC) assembly	0.015351976
Os10g0405500	*OsPAIR3*	9	Coiled-coil protein, Homologous chromosome pairing and synapsis in meiosis	0.037291027

Table A6. Genes associated with the 'Thiol-dependent ubiquitin-specific protease activity' GO term.

Rice gene id	Gene name	Cluster	Description (Ensembl)	p-adjusted (LRT)
Os02g0521500	-	12	Peptidase C65, otubain domain containing protein	3.81E-10
Os04g0652600	-	12	Similar to OSIGBa0113E10.15 protein	2.38E-08
Os08g0528000	-	22	Peptidase C19, ubiquitin carboxyl-terminal hydrolase 2 family protein	2.83E-05
Os03g0589300	-	-	Ovarian tumour, otubain domain containing protein	6.09E-05
Os02g0521600	-	2	Ovarian tumour, otubain domain containing protein	6.10E-05
Os08g0527900	-	5	Peptidase C19, ubiquitin carboxyl-terminal hydrolase 2 family protein	0.001050783
Os08g0527300	-	4	Peptidase C19, ubiquitin carboxyl-terminal hydrolase 2 domain containing protein	0.004523598
Os04g0574600	-	16	Ankyrin repeat containing protein	0.015944512

Table A7. Genes associated with the 'Reciprocal meiotic recombination' GO term.

Rice gene id	Gene name	Cluster	Description (Ensembl)	p-adjusted (LRT)
Os11g0146800	*OsRILIM15B*	10	Meiosis-specific DNA recombinase, Synaptonemal complex (SC) assembly	1.34E-10
Os04g0452500	*OsZEP1*	4	Similar to H0505F09.1 protein	0.000472419
Os10g0565700	-	4	Similar to SNF2 family N-terminal domain containing protein	0.000585182

Rice gene id	Gene name	Cluster	Description (Ensembl)	p-adjusted (LRT)
Os12g0497300	*OsRAD51A2*	16	DNA repair protein RAD51, Homologous pairing, DNA double strand break (DSB) repair and homologous recombination	0.009371578
Os12g0143800	*OsDMC1A*	4	Meiosis-specific DNA recombinase, Synaptonemal complex (SC) assembl	0.015351976
Os11g0615800	*OsRAD51A1*	22	DNA repair protein RAD51, Homologous pairing, DNA double strand break (DSB) repair and homologous recombination	0.031302831

Table A7. Genes associated with the 'Beta-glucosidase activity' GO term.

Rice gene id	Gene name	Cluster	Description (Ensembl)	p-adjusted (LRT)
Os08g0111200		-	Beta-glucosidase, GBA2 type domain containing protein	2.97E-07
Os05g0365600	*Os5bglu19*	5	Similar to Hydroxyisourate hydrolase	0.000626115
Os04g0474900	*OsTAGG1*	12	Similar to Cyanogenic beta-glucosidase precursor (EC 3.2.1.21) (Linamarase) (Fragment)	0.009545049
Os05g0366600	*Os5bglu22*	5	Similar to Hydroxyisourate hydrolase	0.017686659
Os09g0491100	*Os9bglu30*	5	Similar to Beta-primeverosidase (EC 3.2.1.149)	0.021098564
Os10g0323500	*Os10bglu34*	5	Similar to Beta-glucosidase	0.044315265

Table A8. Genes associated with the '3'-UTR-mediated mRNA destabilization' GO term.

Rice gene id	Gene name	Cluster	Description (Ensembl)	p-adjusted (LRT)
Os08g0491700	*OsC3H57*	4	Putative zinc finger CCCH domain-containing protein 57	1.43E-16
Os07g0139000	*OsC3H48*	4	Putative zinc finger CCCH domain-containing protein 48	1.48E-07
Os03g0301500	*OsC3H21*	4	Zinc finger, CCCH-type domain containing protein	1.14E-06
Os05g0576300	*OsC3H39*	10	Zinc finger, CCCH-type domain containing protein	3.28E-05

Table A9. Genes associated with the 'Mitotic recombination' GO term.

Rice gene id	Gene name	Cluster	Description (Ensembl)	p-adjusted (LRT)
Os11g0146800	*OsRILIM15B*	10	Meiosis-specific DNA recombinase, Synaptonemal complex (SC) assembly	1.34E-10

Rice gene id	Gene name	Cluster	Description (Ensembl)	p-adjusted (LRT)
Os12g0497300	*OsRAD51A2*	16	DNA repair protein RAD51, Homologous pairing, DNA double strand break (DSB) repair and homologous recombination	0.009371578
Os12g0143800	*OsDMC1A*	4	Meiosis-specific DNA recombinase, Synaptonemal complex (SC) assembly	0.015351976
Os11g0615800	*OsRAD51A1*	22	DNA repair protein RAD51, Homologous pairing, DNA double strand break (DSB) repair and homologous recombination	0.031302831

Table A10. Genes associated with the 'Toxin activity' GO term.

Rice gene id	Gene name	Cluster	Description (Ensembl)	p-adjusted (LRT)
Os03g0688000	-	5	Hypothetical conserved gene	1.32E-13
Os03g0687800	-	4	Ribosome-inactivating protein domain containing protein	4.73E-08
Os03g0683500	-	5	Hypothetical conserved gene	0.000208731
Os03g0687400	-	5	Ribosome-inactivating protein family protein	0.016642293

Table A11. DEGs shared by all stage comparisons.

Gene_id	Gene name	Description (Ensembl)
Os04g0637300	*OsEPF1*	Similar to predicted protein
Os01g0956500	-	Conserved hypothetical protein
Os02g0640800	-	Similar to Carbonyl reductase 1
Os05g0501001	-	Hypothetical gene
Os03g0115800	-	Conserved hypothetical protein
Os11g0146950	-	Hypothetical conserved gene
Os03g0105500	-	Conserved hypothetical protein
Os05g0325200	-	Cyclin-related 2 domain containing protein
Os02g0492900	-	Similar to Ankyrin-like protein-like protein
Os06g0363000	-	Non-protein coding transcript
Os11g0306400	-	Similar to Herbicide safener binding protein
Os05g0124600	-	Ankyrin repeat domain containing protein
Os06g0265100	-	Hypothetical conserved gene
Os04g0538750	-	Conserved hypothetical protein
Os03g0842501	-	Hypothetical conserved gene
Os03g0668033	-	Hypothetical gene
Os04g0635100	-	Similar to H0315F07.12 protein
Os01g0303800	-	UspA domain containing protein
Os02g0580600	-	Similar to Dimethylaniline monooxygenase-like protein
Os02g0286891	-	Similar to OSIGBa0161P06.1 protein

Gene_id	Gene name	Description (Ensembl)
Os05g0418800	*ONAC087*	No apical meristem (NAM) protein domain containing protein
Os01g0318202	-	Hypothetical gene
Os01g0956700	*LCD*	Cadmium tolerance and accumulatio
Os02g0503700	-	Similar to Cytochrome P450 CYP81L6
Os12g0623600	-	Protein of unknown function DUF1637 family protein
Os11g0240800	-	Hypothetical conserved gene
Os12g0609050	-	Hypothetical conserved gene
Os05g0204600	*OsBBX14*	B-box zinc finger protein, Repressor of flowering under long and short-day condition
Os10g0148100	-	Protein of unknown function DUF1210 family protein
Os03g0619700	-	Conserved hypothetical protein
Os05g0592300	-	Protein of unknown function DUF1637 family protein

Table A12. Genes associated with the 'Stomatal development' GO term, in Stage 2.

Gene id	LFC	p-adjusted (Wald test)	Gene name	Description (Ensembl)
Os04g0637300	9.659247	0	*OsEPF1*	Similar to predicted protein
Os04g0457700	-3.5313	2.21E-21	*OsEPF2*	Similar to H0523F07.14 protein
Os05g0597000	-5.30837	1.05E-08	*OsMUTE*	Similar to DNA binding protein
Os11g0581700	0.482269	0.028471	*EPFL4/5*	Similar to EPIDERMAL PATTERNING FACTOR-like protein 4
Os05g0476400	0.273777	0.045567	*EPFL6*	Similar to allergen-related

Table A13. Genes associated with the 'Carbohydrate transport' GO term, in Stage 2.

Gene id	LFC	p-adjusted (Wald test)	Gene name	Description (Ensembl)
Os02g0513100	-2.00668	6.72E-08	*OsSWEET15*	Similar to MtN3 protein precursor
Os03g0363600	-1.69222	6.95E-05	-	Similar to Sugar transporter-like protein
Os08g0535200	-0.53184	0.024817	*xa13*	Similar to MtN3-like protein
Os03g0170900	1.28307	0.000356	*OsSUT1*	Sucrose transporter
Os07g0559700	-2.77035	0.005506	*OsMST6*	Similar to Monosaccharide transporter 3
Os01g0172100	0.846036	0.000445	*OsPPT3*	Similar to Triose phosphate/phosphate translocator, non-green plastid, chloroplast precursor (CTPT)

Table A14. Genes associated with the '3'UTR-mediated mRNA destabilization' GO term, in Stage 3.

Gene id	LFC	p-adjusted (Wald test)	Gene name	Description (ENsembl)
Os02g0616800	1.230925	0.000272	-	Ribosome-inactivating protein domain containing protein

Gene id	LFC	p-adjusted (Wald test)	Gene name	Description (ENsembl)
Os03g0688000	-4.76751	1.55E-18	-	Hypothetical conserved gene
Os03g0687400	-7.90916	8.09E-05	-	Ribosome-inactivating protein family protein
Os10g0570700	-3.35442	0.004293	-	Ribosome-inactivating protein family protein
Os03g0683500	-6.55903	3.72E-08	-	Hypothetical conserved gene
Os03g0687800	-4.40529	0.000314	-	Ribosome-inactivating protein domain containing protein

Table A15. Genes associated with the 'Carbohydrate transport' GO term, in Stage 3.

Gene id	LFC	p-adjusted (Wald test)	Gene name	Description (Ensembl)
Os07g0139000	-3.26007	2.23E-08	*OsC3H48*	Putative zinc finger CCCH domain-containing protein 48
Os03g0301500	-3.13638	2.03E-05	*OsC3H21*	Zinc finger, CCCH-type domain containing protein
Os08g0491700	-2.2748	5.41E-05	*OsC3H57*	Putative zinc finger CCCH domain-containing protein 57
Os07g0138400	-3.93636	0.002426	*C3H47*	CCCH-type zinc finger protein, Drought tolerance

Table A16. Genes associated with the 'Galactose metabolic process' GO term, in Stage 3.

Gene id	LFC	p-adjusted (Wald test)	Gene name	Description
Os04g0608100	0.369378	5.46E-05	*GalK2*	Ribosomal protein S5 domain 2-type fold domain containing protein
Os05g0595100	-1.43571	0.000349	*OsUGE1*	Uridine-diphospho-(UDP)-glucose 4-epimerase, Cell wall carbohydrate partitioning during nitrogen (N) limitation
Os09g0526700	-0.7995	0.000827	*OsUGE3*	Similar to UDP-glucose 4-epimerase (EC 5.1.3.2) (Galactowaldenase) (UDP-galactose 4-epimerase)
Os08g0129700	-0.33129	0.001704	-	NAD(P)-binding domain containing protein

Table A17. Genes associated with the 'Galactose metabolic process' GO term, in Stage 3.

Gene id	LFC	p-adjusted (Wald test)	Gene name	Description
Os04g0452500	-1.15791	0.001305	*OsZEP1*	Similar to H0505F09.1 protein
Os09g0506800	-0.91703	0.001839	*PAIR2*	Similar to Meiotic asynaptic mutant 1
Os03g0225200	-1.03945	0.002815	*OsSDS*	Cyclin, A/B/D/E domain containing protein
Os10g0405500	-0.74934	0.006718	*PAIR3*	Coiled-coil protein, Homologous chromosome pairing and synapsis in meiosi

Table A18. Genes associated with the 'Thylakoid and Chloroplast thylakoid membrane' GO terms, in Stage 4 (no redundancy).

Gene id	LFC	p-adjusted (Wald test)	Gene name	Description (Ensembl)
Os10g0575700	-0.6442	7.54E-06	-	Similar to plastid-lipid associated protein 3
Os01g0889800	-0.63456	3.44E-05	*OsStr13*	Rhodanese-like domain containing protein
Os03g0333400	-0.9555	0.000115	-	Similar to photosystem II 11 kD protein
Os05g0388500	-0.39041	0.000842	-	Similar to 50S ribosomal protein L1
Os04g0234600	-1.92546	0.001668	-	Similar to Sedoheptulose-1,7-bisphosphatase
Os10g0100300	-1.25558	0.003789	*TIC62*	NAD(P)-binding domain containing protein
Os03g0265400	-0.44554	0.00628	-	Similar to 50S ribosomal protein L4, chloroplast precursor (R-protein L4)
Os01g0869800	-0.85355	0.00654	*PSBS1*	22-kDa Photosystem II protein, Photoprotectio
Os03g0778100	-0.76372	0.0079	*OsPS1-F*	Similar to Photosystem-1 F subunit
Os03g0293100	-0.71368	0.011484	-	Conserved hypothetical protein
Os05g0560000	-0.78771	0.016465	*PSAH*	Photosystem I reaction center subunit VI, chloroplast precursor (PSI- H) (Light-harvesting complex I 11 kDa protein) (GOS5 protein)
Os07g0513000	-0.36212	0.017453	-	Similar to ATP synthase gamma chain, chloroplast (EC 3.6.1.34) (Fragment)
Os05g0480000	-0.62591	0.017536	*OsSTN8*	Serine/threonine protein kinase, Photosystem II (PSII) repair, Phosphorylation of PSII core protei
Os09g0439500	-1.02269	0.018618	*Lhca6*	Similar to Type II chlorophyll a/b binding protein from photosystem I precursor
Os02g0731600	-0.93273	0.0219	-	Similar to Threonine endopeptidase
Os06g0725900	-0.41477	0.023587	*OsFtsH1*	Similar to Cell division protein ftsH homolog, chloroplast precursor (EC 3.4.24.-) (DS9)
Os05g0291700	-0.66607	0.023985	-	Similar to PTAC16 (PLASTID TRANSCRIPTIONALLY ACTIVE18); binding / catalytic
Os03g0765200	-0.28511	0.025893	*OsSigP2*	Similar to Signal peptidase I family protein, expressed
Os07g0469100	-1.02266	0.032735	-	Similar to Thylakoid membrane phosphoprotein 14 kDa, chloroplast precursor
Os05g0110300	-0.25875	0.033731	-	Similar to NAD-dependent epimerase/dehydratase
Os02g0553200	0.305161	0.033754	*APX8*	Thylakoid membrane-bound ascorbate peroxidase, Tolerance

Gene id	LFC	p-adjusted (Wald test)	Gene name	Description (Ensembl)
				to bacterial blight, Response to NaCl
Os03g0129300	-0.65972	0.034762	*GADPH*	Similar to Glyceraldehyde-3-phosphate dehydrogenase (EC 1.2.1.13) (Fragment)
Os04g0659100	-0.43795	0.042049	*OsGLN2*	Chloroplastic glutamine synthetase, Reassimilation of the ammonia generated by photorespiration, Salt tolerance
Os05g0103200	-0.36714	0.042619	*OsCYP20-2*	Cyclophilin-like domain containing protein
Os06g0217700	-0.87905	0.043945	-	Conserved hypothetical protein
Os09g0413700	-0.27695	0.047168	-	Conserved hypothetical protein
Os06g0658900	-0.28112	0.049047	*OsSGD1*	Homogentisate phytyltransferase (HPT), Tocopherol (vitamin E) biosynthesis, Plant development, Cold tolerance

Table A19. Genes associated with the 'Serine-type peptidase activity' GO term, in Stage 5.

Gene id	LFC	p-adjusted (Wald test)	Gene name	Description (Ensembl)
Os01g0868900	-1.39155	3.02E-07	*OsSub11*	Peptidase S8, subtilisin-related domain containing protein
Os01g0767100	0.314207	0.002263	*OsProCP1*	Similar to Lysosomal Pro-X carboxypeptidase
Os03g0765200	-0.34762	0.00322	*OsSigP2*	Similar to Signal peptidase I family protein, expressed
Os06g0163200	0.27402	0.001088	*OsPOP11*	Esterase/lipase/thioesterase domain containing protein
Os09g0453700	-0.60611	0.008675	*OsPOP18*	Peptidase S9A, prolyl oligopeptidase family protein
Os12g0427600	-4.22187	0.043475	*OsSub63*	Similar to Subtilase
Os04g0543700	-3.6076	5.12E-09	*OsSub42*	Similar to Serine proteinase (Fragment)
Os03g0605300	-1.03121	7.69E-10	*OsSub30*	Similar to Subtilisin-like protease (Fragment)
Os02g0198700	-1.32002	0.025797	*OsSub12*	Similar to Subtilisin-like protease

Table A20. Genes associated with the 'Thylakoid and Chloroplast thylakoid membrane' GO terms, in Stage 5 (no redundancy).

Gene id	LFC	p-adjusted (Wald test)	Gene name	Description
Os08g0242700	-0.80176	7.30E-12	-	Similar to uridylyltransferase-related
Os01g0869800	-1.18892	1.04E-05	*PSBS1*	22-kDa Photosystem II protein, Photoprotectio
Os06g0196300	-0.6538	0.000145	*OsPrx*	Similar to Peroxiredoxin Q (Fragment)
Os05g0480000	-0.82765	0.000332	*OsSTN8*	Serine/threonine protein kinase, Photosystem II (PSII)

Gene id	LFC	p-adjusted (Wald test)	Gene name	Description
				repair, Phosphorylation of PSII core protein
Os01g0720500	-1.4637	0.000404	*Lhcb1.1*	Similar to Type I chlorophyll a/b-binding protein b (Fragment)
Os04g0602100	-0.51689	0.000644	-	Plant ascorbate peroxidase domain containing protein
Os06g0217700	-1.37298	0.000952	-	Conserved hypothetical protein
Os10g0536500	-2.49243	0.002592	-	Peptidase S10, serine carboxypeptidase, active site domain containing protein
Os03g0333400	-0.78944	0.002598	-	Similar to photosystem II 11 kD protein
Os03g0765200	-0.34762	0.00322	*OsSigP2*	Similar to Signal peptidase I family protein, expressed
Os04g0659100	-0.56761	0.003224	*OsGLN2*	Chloroplastic glutamine synthetase, Reassimilation of the ammonia generated by photorespiration, Salt toleranc
Os08g0382400	-0.54379	0.004331	*OsCYP38*	Peptidyl-prolyl cis-trans isomerase, cyclophilin-type domain containing protein
Os09g0279400	-0.63426	0.01169	*OsStr3*	Rhodanese-like domain containing protein
Os01g0882500	-2.12082	0.014276	-	Similar to NADH dehydrogenase I subunit N
Os03g0654600	-0.56287	0.020971	*NOL*	Similar to Myb-like DNA-binding domain, SHAQKYF class family protein, expressed
Os05g0291700	-0.67078	0.021996	-	Similar to PTAC16 (PLASTID TRANSCRIPTIONALLY ACTIVE18); binding / catalytic
Os06g0264800	-0.84564	0.026149	-	Similar to Threonine endopeptidase
Os01g0798500	-0.43534	0.0265	-	Similar to predicted protein
Os05g0388500	-0.30158	0.0265	-	Similar to 50S ribosomal protein L1
Os10g0100300	-0.99513	0.03071	*TIC62*	NAD(P)-binding domain containing protein
Os03g0293100	-0.63743	0.031927	-	Conserved hypothetical protein
Os04g0234600	-1.45089	0.03652	-	Similar to Sedoheptulose-1,7-bisphosphatase
Os03g0778100	-0.64312	0.042622	*OsPS1-F*	Similar to Photosystem-1 F subunit

Table A21. Genes associated with the 'Chloroplast nucleiod' GO term, in mature florets.

Gene id	LFC	p-adjusted (Wald test)	Gene name	Description (Ensembl)
Os03g0602600	0.886182	8.55E-05	*HSA1*	PfkB family fructokinase, WLP2 paralog, Chloroplast biogenesis and plant growth, Protection of chloroplasts under heat stres
Os03g0824100	0.773715	0.000829	*OspTAC2*	Pentatricopeptide repeat protein, Regulation of chloroplast developmen
Os10g0462800	0.446452	0.001354	*WSL3*	Component of the plastid-encoded plastid RNA polymerase (PEP), peripheral subunit of PEP complex, OsPAP1/OspTAC3, Early chloroplast developmen
Os06g0143000	0.347229	0.003374	*SodB*	Iron-superoxide dismutase (EC 1.15.1.1)
Os11g0110100	0.330806	0.011359	-	Similar to PTAC6 (PLASTID TRANSCRIPTIONALLY ACTIVE6)
Os01g0851000	0.469583	0.041971	*WLP2*	Carbohydrate/purine kinase domain containing protein
Os03g0825500	0.536725	0.046592	-	Transcription antitermination protein, NusG, N-terminal domain containing protein

Table A22. Genes associated with the 'Plastid chromosome' GO term, in mature florets.

Gene id	LFC	p-adjusted (Wald test)	Gene name	Description (Ensembl)
Os03g0824100	0.773715	0.000829	*OspTAC2*	Pentatricopeptide repeat protein, Regulation of chloroplast developmen
Os10g0462800	0.446452	0.001354	*WSL3*	Component of the plastid-encoded plastid RNA polymerase (PEP), peripheral subunit of PEP complex, OsPAP1/OspTAC3, Early chloroplast developmen
Os11g0110100	0.330806	0.011359	-	Similar to PTAC6 (PLASTID TRANSCRIPTIONALLY ACTIVE6)
Os05g0587200	0.328483	0.014022	*OsSET23*	Conserved hypothetical protein
Os03g0825500	0.536725	0.046592	-	Transcription antitermination protein, NusG, N-terminal domain containing protein

Table A23. Genes associated with the 'Plastid chromosome' GO term, in mature florets.

Gene id	LFC	p-adjusted (Wald test)	Gene name	Description (Ensembl)
Os02g0794500	-0.55312	1.43E-05	*OsSCP10*	Similar to Serine carboxypeptidase II precursor (EC 3.4.16.6) (Carboxypeptidase D) (Bri1 suppressor 1) [Contains: Serine carboxypeptidase II chain A; Serine carboxypeptidase II chain B]
Os01g0850900	-1.93881	3.91E-05	-	SOUL haem-binding protein domain containing protein

Gene id	LFC	p-adjusted (Wald test)	Gene name	Description (Ensembl)
Os05g0517500	-0.33535	9.67E-05	-	Similar to Gamma-glutamyl hydrolase precursor (EC 3.4.19.9) (Gamma-Glu-X carboxypeptidase) (Conjugase) (GH)
Os01g0559600	0.49155	0.005272708	*OsVPE2*	Similar to C13 endopeptidase NP1 precursor
Os03g0295800	-0.50881	0.008926044	-	Gamma interferon inducible lysosomal thiol reductase GILT family protein
Os06g0643900	0.20038	0.011421568	*OsPAP26*	Purple acid phosphatase (EC:3.1.3.2), Regulation of phosphate remobilization, Utilization of organic phosphoru
Os11g0522900	-0.65018	0.012327367	*OsSCP63*	Peptidase S10, serine carboxypeptidase family protein
Os01g0920000	-0.60684	0.018618467	*OsCBSCBS5*	Cystathionine beta-synthase, core domain containing protein
Os04g0396800	-0.54503	0.019770177	*OsSCP24*	Peptidase S10, serine carboxypeptidase family protein
Os02g0625000	0.40350	0.024855144	*OSCRY2*	Cryptochrome 2, blue light photoreceptor, Promotion of flowering tim
Os12g0429200	0.35814	0.026545068	*OsBgal13*	Similar to Relative to SR12 protein (Fragment)
Os11g0660000	-0.69073	0.028441739	*OsMHX*	Sodium/calcium exchanger membrane region domain containing protein
Os05g0567100	-0.24237	0.035890331	*Oryzasin*	Aspartic proteinase oryzasin 1 precursor (EC 3.4.23.-)
Os04g0650000	0.36257	0.042155121	*ocp**	Similar to Oryzain alpha chain precursor (EC 3.4.22.-)
Os04g0102700	0.25732	0.043506262	*FAAH*	Similar to N-acylethanolamine amidohydrolase
Os06g0136000	-0.33593	0.045417723	-	Similar to Hypersensitive-induced reaction protein 4

Table A24. Genes associated with the 'pollen exine' GO term, in Stage 5.

Gene id	LFC	p-adjusted (Wald test)	Gene name	Description (Ensembl)
Os03g0168600	-2.63415	1.05E-07	*CYP704B2*	Cytochrome P450 protein, Anther cutin biosynthesis and pollen exine formation
Os03g0263600	-2.52702	2.73E-07	*OsSTRL2*	Atypical strictosidine synthase, Regulation of anther development and pollen wall formation
Os08g0131100	-2.52353	5.75E-06	*CYP703A3*	Cytochrome P450 hydroxylase, Anther cuticle and pollen exine development
Os03g0167600	-3.84723	0.007145	*OsMS2*	Similar to Male sterility protein 2

Table A25. Genes associated with the 'lipid metabolic process' GO term, in Stage 5.

Gene id	LFC	p-adjusted (Wald test)	Gene name	Description (Ensembl)
Os08g0111200	-2.14965	5.58E-10	-	Beta-glucosidase, GBA2 type domain containing protein
Os11g0696200	-0.99416	5.58E-10	-	ATP citrate lyase beta (Fragment)
Os01g0300200	-0.67561	2.33E-09	-	Similar to ATP-citrate lyase subunit B
Os08g0298700	-3.31746	2.11E-08	-	Similar to male sterility protein 2
Os03g0118800	-0.40434	0.006538	-	Similar to Hydroxymethylglutaryl-CoA synthase
Os03g0167600	-3.84723	0.007145	*OsMS2*	Similar to Male sterility protein 2
Os02g0780700	-0.84574	0.018785	-	Lipase, class 3 family protein
Os05g0137400	-0.43748	0.023005	*OsAP1*	Similar to Aspartic protease precursor
Os07g0693800	-0.79047	0.023068	*FAD8*	Omega-3 fatty acid desaturase, Acclimation to low-temperature stress, Defense response
Os01g0660300	-0.31396	0.025133	-	Similar to Pyruvate kinase
Os04g0354600	-1.47922	0.030976	*OsCER4*	Similar to Acyl CoA reductase-like protein
Os02g0612100	0.450114	0.033629	-	Phospholipid methyltransferase family protein
Os12g0554500	0.430526	0.042622	-	Lipase, class 3 family protein

Table A26. Genes associated with the 'Carboxylic ester hydrolase activity' GO term, in Stage 5.

Gene id	LFC	p-adjusted (Wald test)	Gene name	Description (Ensembl)
Os07g0607400	-2.42608	0.003146	*OsPME20*	Pectin lyase fold/virulence factor domain containing protein
Os01g0892600	-0.88762	0.015328	-	Pectinacetylesterase family protein
Os02g0702400	0.486484	0.016718	-	Pectinacetylesterase family protein
Os04g0669700	0.923161	0.030846	-	Similar to H0818H01.9 protein

Table A27. Genes associated with the 'Suberin biosynthetic process' GO term, in Stage 5.

Gene id	LFC	p-adjusted (Wald test)	Gene name	Description (Ensembl)
Os08g0298700	-3.31746	2.11E-08	-	Similar to male sterility protein 2
Os03g0167600	-3.84723	0.007145	*OsMS2*	Similar to Male sterility protein 2
Os04g0354600	-1.47922	0.030976	*OsCER4*	Similar to Acyl CoA reductase-like protein

Table A28. Genes associated with the 'Strictosidine synthase activity' GO term, in Stage 5.

Gene id	LFC	p-adjusted (Wald test)	Gene name	Description (Ensembl)
Os03g0263600	-2.52702	2.73E-07	*OsSTRL2*	Atypical strictosidine synthase, Regulation of anther development and pollen wall formatio
Os03g0750700	-0.56091	0.001167	*OsSTRL3*	Six-bladed beta-propeller, TolB-like domain containing protein
Os11g0142400	-0.86521	0.026401	*OsSTRL20*	Similar to Strictosidine synthase family protein, expressed

Table A29. Genes associated with the 'Peptidase activity' GO term, in Stage 5.

Gene id	LFC	p-adjusted (Wald test)	Gene name	Description
Os03g0605300	-1.03121	7.69E-10	*OsSub30*	Similar to Subtilisin-like protease (Fragment)
Os04g0543700	-3.6076	5.12E-09	*OsSub42*	Similar to Serine proteinase (Fragment)
Os01g0886600	-0.89402	7.03E-05	*OsSTA38*	Similar to CLP protease regulatory subunit CLPX precursor
Os03g0589300	0.762417	9.82E-05	-	Ovarian tumour, otubain domain containing protein
Os09g0452800	-4.01067	0.00021	-	Peptidase A1 domain containing protein
Os03g0386700	-2.26701	0.000293	*OsSCP12*	Similar to serine carboxypeptidase
Os01g0332500	0.820994	0.001637	-	Similar to Serine carboxypeptidase II-like protein
Os02g0473200	-0.80708	0.006301	*OsAP19*	Peptidase aspartic, catalytic domain containing protein
Os04g0525700	-0.51454	0.014276	*OsSCP25*	Similar to Serine carboxypeptidase II precursor (EC 3.4.16.6) (Carboxypeptidase D) (Bri1 suppressor 1) [Contains: Serine carboxypeptidase II chain A; Serine carboxypeptidase II chain B]
Os05g0137400	-0.43748	0.023005	*OsAP1*	Similar to Aspartic protease precursor
Os02g0198700	-1.32002	0.025797	*OsSub12*	Similar to Subtilisin-like protease
Os11g0215400	-3.03384	0.040256	-	Peptidase aspartic, catalytic domain containing protein
Os12g0427600	-4.22187	0.043475	*OsSub63*	Similar to Subtilase

Table A30. Genes associated with the 'Catabolic process' GO term, in mature florets.

Gene id	LFC	p-adjusted (Wald test)	Gene name	Description
Os03g0252100	-1.06652	1.71E-07	-	Alpha/beta hydrolase fold-3 domain containing protein
Os09g0460300	-0.98615	0.009708	-	Alpha/beta hydrolase fold-3 domain containing protein

Os05g0407500	-0.35379	0.012948	*GID1*	Soluble gibberellin receptor, Gibberellin signalling
Os06g0214850	-0.66631	0.019565	-	Similar to gibberellin receptor GID1L2
Os09g0461900	-0.53501	0.026982	-	Alpha/beta hydrolase fold-3 domain containing protein
Os09g0462200	-0.48084	0.033163	-	Alpha/beta hydrolase fold-3 domain containing protein
Os06g0214800	-0.59382	0.043092	*GID1L2*	Alpha/beta hydrolase fold-3 domain containing protein

Table A31. Genes associated with the 'Transmembrane receptor protein serine/threonine kinase activity' GO term, in mature florets

Gene id	LFC	p-adjusted (Wald test)	Gene name	Description (Ensembl)
Os01g0384300	-0.80384	1.91E-05	-	Similar to RKF3 (RECEPTOR-LIKE KINASE IN IN FLOWERS 3); kinase
Os10g0533150	-0.9024	0.000282	-	Similar to BRASSINOSTEROID INSENSITIVE 1-associated receptor kinase 1
Os05g0398800	-0.7659	0.002588	-	Similar to Serine/threonine-protein kinase PBS1 (EC 2.7.1.37) (AvrPphB susceptible protein 1)
Os05g0436100	-0.6873	0.002677	-	Similar to predicted protein
Os11g0607200	0.916444	0.004054	*OsSERL1*	Protein kinase, core domain containing protein
Os03g0227900	-0.84486	0.00559	-	Serine/threonine protein kinase domain containing protein
Os02g0110600	-0.56268	0.007553	-	Similar to protein kinase
Os10g0516200	-0.84833	0.007673	*OsRLCK303*	Serine/threonine protein kinase domain containing protein
Os01g0936100	-0.558	0.02282	*OsRLCK55*	Similar to Protein kinase
Os07g0565400	-0.34295	0.0307	-	Similar to SRF8 (STRUBBELIG-RECEPTOR FAMILY 8)
Os02g0549200	-0.3551	0.03634	*OsRLCK73*	Similar to Ser Thr specific protein kinase-like protein
Os05g0319700	-0.592	0.038139	-	Similar to Protein kinase-like protein (Fragment)
Os05g0207700	-0.42711	0.046693	-	Similar to Serine/threonine-protein kinase PBS1 (EC 2.7.1.37) (AvrPphB susceptible protein 1)
Os04g0393900	-0.36053	0.047951	*OsRLCK149*	Similar to H0718E12.2 protein

Table A32. Genes associated with the 'Response to red light' GO term, in mature florets

Gene id	LFC	p-adjusted (Wald test)	Gene name	Description
Os02g0203000	-1.22	8.86E-05	*OsbZIP18*	Similar to transcription factor HY5
Os01g0174000	-0.91703	0.000327	*OsbZIP01*	Similar to BZIP transcription factor (Fragment)
Os06g0601500	-1.24199	0.005203	*OsbZIP48*	Similar to BZIP2
Os02g0260700	-0.89742	0.031706	-	Similar to GAMYB-binding protein (Fragment)

Table A33. Genes associated with the 'Oxidoreductase activity' GO term, found in all comparisons.

Gene id	Gene name	Description
Os12g0623600	-	Protein of unknown function DUF1637 family protein
Os05g0592300	-	Protein of unknown function DUF1637 family protein

Table A34. Gene ids corresponding to genes related to the photosynthetic development investigated in Chapter 5.

Gene_id	Gene_name
Os02g0606000	*OsDG2*
Os04g0665400	*OsFtsz1*
Os05g0443800	*OsFtsz2*
Os03g0320900	*OsGKpm*
Os05g0303000	*OsHsp70CP1*
Os03g0656900	*OsNUS1*
Os05g0393400	*OsPAC*
Os08g0175300	*OsPOLP1*
Os10g0496900	*OsPORB*
Os06g0168600	*OsRNRL1*
Os06g0257450	*OsRNRS1*
Os06g0127900	*OsRNRS2*
Os06g0652000	*OsRpoTp*
Os08g0163400	*OsSIG1*
Os11g0448400	*OsSIG2A*
Os03g0271100	*OsSIG2B*
Os05g0589200	*OsSIG3*
Os05g0586600	*OsSIG5*
Os08g0242800	*OsSIG6*
	OsSNOW-WHITE
Os04g0497900	*LEAF1*
Os09g0563300	*OsTCD9*
Os04g0475500	*OsV4*
Os03g0411500	*OsVYL, OsClp6*
Os06g0603000	*OsYGL2*
Os09g0380200	*OsYLC1*